Microcapsule internalization by cells *in vitro* caused by physical and biochemical stimuli

Weizhi Liu

Supervisor： Professor Gleb B. Sukhorukov

Professor Wen Wang

A thesis submitted to the University of London

for the degree of doctor of philosophy

School of Engineering and Materials Science

Queen Mary University of London, United Kingdom

2013

Abstract

There is a growing interest in micro sized vehicles with the function of storing, targeting and controlled releasing of substances during the past few decades. However, delivering the desired drugs inside micro containers to living cells is a particular challenging topic of material science. Microcapsules made of polyelectrolyte multilayers exhibit low- or non-toxicity, appropriate mechanical stability, variable degradation and can incorporate remotely addressable release mechanisms in responding to stimuli and external triggering, making them well suitable for targeted drug delivery to live cells. This study investigates interactions between microcapsules made of synthetic (i.e. PSS/PAH) or natural (i.e. DS/PArg) polyelectrolyte and cells, with particular focus on the effect of the glycocalyx layer on the intake of microcapsules by human umbilical vein endothelial cells (HUVECs). Neuraminidase cleaves N-acetyl neuraminic acid residues of glycoproteins and targets the sialic acid component of the glycocalyx on the cell membrane. Three-dimensional CLSM images reveal that microcapsules functionalized with neuraminidase can be internalized by endothelial cells, whereas ones without neuraminidase are blocked by the glycocalyx layer. Uptake of the microcapsules is most significant in the first 2 hours. Following their internalization by endothelial cells, biodegradable DS/PArg capsules rupture by day 5, however, there is no obvious change in the shape and integrity of PSS/PAH capsules within the period of observation. Results from the study support our hypothesis that the glycocalyx functions as an endothelium barrier to cross membrane movement of microcapsules. Neuraminidase-loaded microcapsules can enter endothelial cells by cleaving the glycocalyx in their close proximity with minimum disruption of the glycocalyx layer, therefore they have high potential to act as drug delivery carriers to pass through the endothelium barrier of blood vessels into the surrounding tissue.

Table of Contents

Figures:

Tables

List of Symbols and abbreviations

Letters

pKa pK_b	different dissociation constant
pKapp	apparent dissociation constant
a	the monomer size
Ree	end-to-end radius
N	number of monomers
K_{app}	an apparent equilibrium constant of acidity
α	the degree of dissociation
q_p	The persistence length
q_0	the steric length
q_e	the electrostatic contribution
l_B	Bjerrum length
K^{-1}	Debye length
l_{eff}	effective distance between charges
e	elementary charge
k_BT	the corresponding thermal energy
k_B	Boltzmann constant
T	absolute temperature in Kelvin
ε_R	dielectric constant of the medium
ε_0	vacuum permittivity
N_A	Avogadro's number
I	the ionic strength
Z_i	charge valency
C_i	molar concentration of the screening ions
θ	the degree of conversion
n	anionic groups number in solution
m	cationic number groups in solution
ζ	zeta-potential
υ_E	the mobility
ε_0	relative dielectric constant
ε_r	vacuum electrical permittivity
μ	solution viscosity

r	particle radius
k	Debye–Hückel parameter
u_{av}	given the average electro osmotic flow velocity
E_z	the applied electric field strength
I_0	light intensity entering the sample
I	the light intensity exiting the sample
C	the concentration of the sample
L	the light path length of the sample container
K	proportionality constant

Abbreviations

AFM	Atomic force microscope
BCA	bicinchoninic acid
BSA	bovine serum albumin
BSE	back scattered electrons
BSED	Back scattered electron detector
CA	citric acid
$CaCl_2$	calcium chloride
$CaCO_3$	Calcium carbonate
CLSM	confocal laser scanning microscopy
CO_2	carbon dioxide
cPAM	cationic polyacrylamides
DAPI	4',6-diamidino-2-phenylindole 2hci
DCSA	distributed cytoplasmic structural actin
DS	dextran sulfate sodium salt
DMSO	dimethyl sulfoxide
DNA	desoxyribonucleic acid
EDTA	ethylenediaminetetraacetic acid
ETD	Everhart-Thornley detector
$FeCl_2$	ferrous chloride
$FeCl_3$	ferric chloride
Fe_3O_4	ferroferric oxide
FIB	Focused ion beam
FITC	fluorescein isothiocyanate

FITC-PAH	fluorescein isothiocyanate-labeled PAH
GAG	Glycosaminoglycan
GNPs	Gold nanoparticles
HF	hydrogen fluoride
H_2O_2	hydrogen peroxide
HUVECs	The human umbilical vein endothelial cells
IR	infrared
KCl	Potassium Chloride
KCN	potassium cyanide
LbL	layer-by-layer
LMIS	liquid-metal ion source
MF	melamine formaldehyde
NaCl	sodium chloride
Na_2CO_3	sodium carbonate
$NaHCO_3$	Natrii Bicarbonas
N-DMF	N-Dimethylformamide
NH_3	Ammonia
NH_4Cl	ammonium chloride
NH_4OH	ammonium hydroxide
NH_4F	ammonium fluoride
PAH	poly(allylamine hydrochloride)
PArg	poly (L-arginine)
PBS	Phosphate Buffered Saline
PDADMAC	poly(diallyldimethylammonium chloride)
PLL	poly L lysine
PS	Polystyrene
PSS	poly(styrenesulfonate sodium salt)
SEM	scanning electron microscopy
SiO_2	silicon dioxide
SKL	sulfonated kraft lignin
SNARF	seminaphtho rhodafluor
TRITC	tetramethylrhodamine isothiocyanate
TRITC-BSA	Tetramethylrhodamine isothiocyanate–BSA
TRITC-dextran	Tetramethylrhodamine isothiocyanate–Dextran
UV	Ultraviolet

Acknowledgement

I would like to express my gratitude to all those staffs in SEMS department of Queen Mary University of London who contributed to the successful completion of this work.

I would like to acknowledge my supervisor Prof. Gleb Sukhorukov and Prof. Wen Wang for giving me the opportunity to prepare my experiments in the lab. Many thanks for their enlightening discussions, new ideas, support and encouragement in these years.

I would like to thank Dr. Denys Usov, who helped me in multilayer capsules fabrication and functionalization when I was starting the experiment. For conducting measurements, I would like to thank Dr. Zofia Luklinska help me with SEM and TEM. About endothelial cell culture, I would like to thank Ke Bai and Miao Lin in Wen's group.

Furthermore I am grateful to my family, they supported me in everything. Last but not least I would like to thank all the members of Gleb's and Wen's group over these years for the nice working atmosphere, support, and sharing the knowledge about capsules and cells.

1 Introduction

Various drug delivery systems have been developed over last several decades with numerous applications in biomedical science which are (De Cock, De Koker et al. 2010; De Koker, Lambrecht et al. 2011; Vergaro, Scarlino et al. 2011) reported in high impact publications. Modern drug delivery systems lead to a significant improvement in the research and pharmaceutical industry. Compared to the conventional drug delivery methods, modern drug delivery is more biocompatible and controllable.

When a polymer is combined with a drug or active agent which is mean the release from the bulk material is pre-designed, and controlled drug delivery becomes a reality. As the name implies, it is delivering a defined quantity of a therapeutic payload to a specific target site, at a controlled release rate, with or without external trigger (Langer and Tirrell 2004).

Nanometer- or micron-sized small particles are potent materials in the fields of bio-technology and bio-nanotechnology. When these particles penetrate into the living body, they are able to play various roles in biomedical and clinical applications. Some drugs have an advantage in intracellular target as they are enhancing the therapeutic efficiency while avoiding severe side effects, but disadvantages in cell uptake especially limited solubility in a soluble solution. There is a growing interesting in micro sized vehicles with the function of storing, targeting and controlled releasing of substances during the past few decades. But delivering the desired drugs inside micro containers to living cells is a particular challenging topic in material science.

A potential micro sized microcapsule as drug containing vesicles with controlled delivery and releasing to designated sites has been introduced over past decade (De Geest, Dejugnat et al. 2006; De Geest, Sukhorukov et

al. 2009). Polyelectrolyte multilayer materials have significantly affected the development of drug delivery due to its easily tunable properties such as biocompatibility, size, conformation and functionality. Microcapsules made from polyelectrolyte multilayers exhibit low- or non -toxicity, appropriate high mechanical stability, and variable degradation and stimuli responsive remotely addressable releasing mechanisms. Therefore, microcapsules are well suitable for targeting drug delivery to living cells.

A novel type of hollow microcapsules ranging in size from 60 nanometers to more than 10 micrometers is constructed using the Layer-by-Layer (LbL) technique. Figure 1 shows the fabrication of polyelectrolyte multilayer capsules using LbL technique. Oppositely charged substances such as proteins (Lvov, Ariga et al. 1995), polyelectrolytes (Decher 1997), nanoparticles (Caruso, Caruso et al. 1998), lipids (Moya, Donath et al. 2000), and nanotubes (Mamedov, Kotov et al. 2002) sequentially absorbed onto a charged template by electrostatic attraction, resulting in complex formation between polyanions and polycations (Sukhorukov, Donath et al. 1998). The hollow capsule is called polyelectrolyte multilayer microcapsule, and is obtained after decomposing the template core under certain conditions. The size and morphology of the capsules, the polyelectrolytes and thickness of the shell, the permeability properties as well as release activation mechanism (Sukhorukov, Rogach et al. 2007) can be well controlled with LbL method.

Several kinds of organic and inorganic materials have been used as colloidal template cores to fabricate hollow polyelectrolyte microcapsules. The main problems of the template core is that they are toxic, and hazardous solutions or chemicals are required during capsules fabrication (Gao, Moya et al. 2002). For example dissolution step of melamine formaldehyde (MF) oligomers formed capsules is biological incompatible. Therefore, encapsulation and core dissolution must be done under certain conditions

without extremely low or high pH, oxidizing agents, hydrofluoric acid, or organic solvents. Obviously, such conditions are able to influence the biological activities and damage sensitive biomolecules. Encapsulation of bioactive materials with a biocompatible template under appropriate conditions becomes a problem.

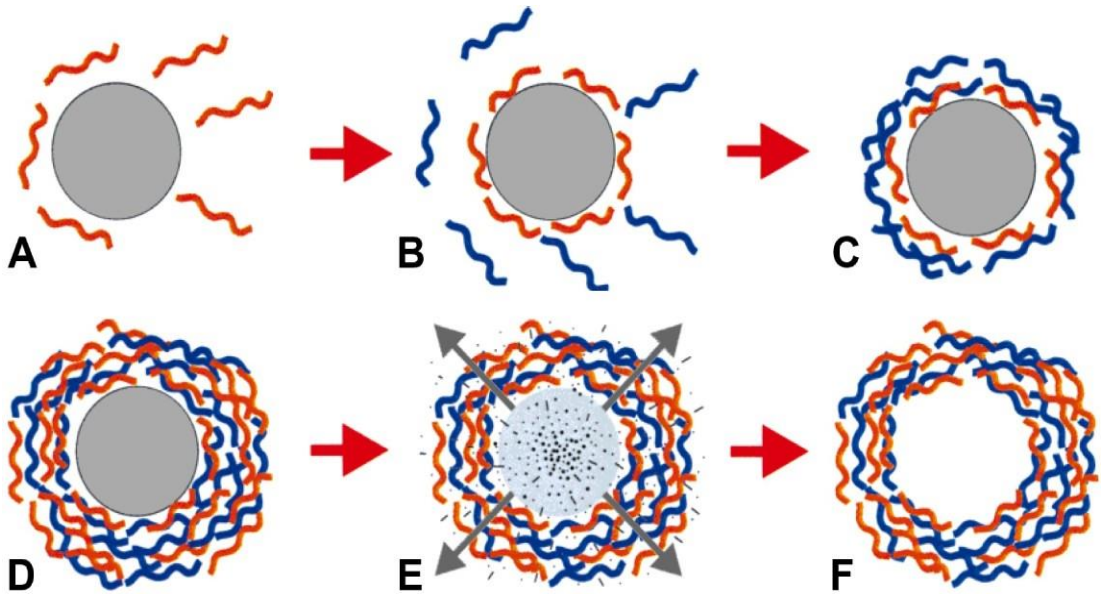

Figure 1: Schematic illustration of fabricate polyelectrolyte multilayer capsules with layer-by-layer technique

A) - D) These steps show consecutive formation of the polyelectrolyte layer film by repeated exposure of the template core (such as MF, $CaCO_3$ and PS) to polymers solution with alternating interactions. The unformed polymer is removed by 3 times of centrifugation and washing steps before exposure of the template cores to the next layer's polymer solution. E) After the desired numbers of polymer layers are deposited, the template cores are decomposed. F) After further washing steps, a suspension of hollow polyelectrolyte multilayer microcapsules are fabricated. (Donath, Sukhorukov et al. 1998)

Recently, nontoxic core of $CaCO_3$ colloidal templates have been used to produce hollow polyelectrolyte microcapsules. Core of $CaCO_3$ can be easily dissolved by 0.2 M ethylenediaminetetraacetic acid (EDTA). Most importantly, $CaCO_3$ particles are easily to be synthesized from Na_2CO_3 and $CaCl_2$

solution ($Na_2CO_3+CaCl_2=CaCO_3\downarrow+2NaCl$). They are able to fill with macromolecules up to a size of 40 nm due to their high porosity (Volodkin, Larionova et al. 2004).

The walls of microcapsule are established have semipermeable properties (Sukhorukov, Brumen et al. 1999). The permeability of the capsules has been studied using fluorescent dye as a release reagent (Antipov, Sukhorukov et al. 2001). The capsules permeability can be modified further using parameters, such as pH value (An, Möhwald et al. 2006), charge (Tong, Dong et al. 2005), salt concentration (Georgieva, Dimova et al. 2005), temperature (Köhler and Sukhorukov 2007) and ionic strength (Gao, Leporatti et al. 2003). The permeability of drug coated crystals is strongly influenced by the number of deposited multilayers. The temporal drug release rate is controlled by the layers, which can be tuned in the nanometer range. The composition of the capsules shell include innermost layer, outermost layer or between layers can additionally provide appropriate functionalities, for instance magnetic (Zebli, Susha et al. 2005), optical (Bédard, Skirtach et al. 2007), conductive, or targeting properties. After all, different kinds of biomaterials have been used to encapsulate, coat, and functionalize polyelectrolyte multilayer microcapsules.

In recent few years, numbers of natural polyelectrolytes and polypeptides have been used to fabricate biodegradable microcapsules. These biodegradable microcapsules are successfully internalized by several phagocytic cells like most cancer cells and immune cells (Sukhorukov, Rogach et al. 2005; De Geest, Vandenbroucke et al. 2006). The mechanisms of the living cells internalize microcapsules are not fully understood, however the natural endocytosis of the cells is one of believed to play an important role. So far, no report on microcapsules internalization and/or degradation by non-phagocytic cells has been published. The microcapsules could be

attracted, adhered and internalized by normal healthy cells result the delivery of drugs with an intracellular target.

The aim of this thesis consists in investigation of the interactions between microcapsules and cells. Functionalization of capsules is studied at the beginning. Capsules shell is modified with gold nanoparticles and magnetite nanoparticles for better contrast in SEM observation and external magnetic field, respectively. Investigation of interactions between magnetic microcapsules and epithelial cells is cooperated with Dr Maya Thanou (pharmacy department of King's College London). Capsules with and without magnetite nanoparticles are added to these cells with a magnet under the well. The capsules with magnetite are attracted to the bottom of the container by additional driving force. Confocal Laser Scanning Microscopy (CLSM) images show number of capsules adhered on the cells.

Chapter of introduction and literature review present scientific background for better understanding of the following works. Materials and methods used in the investigations are briefly introduced. The followed three chapters are results sections which show details of the research. Chapter 6 looks at the preparation of microcapsules. Fluorescent dyes, neuraminidase and DNA plasmids are encapsulated by $CaCO_3$ co-precipitation method. Capsules are prepared by “Layer-by-Layer” technique, and functionalized with colloidal gold nanoparticles or super paramagnetic iron nanoparticles.

The primary aim of this work is presented in chapter 7 and 8. In chapter 7, investigating interactions between epithelial cells (Caco-2 cell line) and capsules with magnetite nanoparticles is performed with physical method. After few minutes of magnet treatment, number of capsules with magnetite nanoparticles adhered by Caco-2 cells is much higher than control sample.

In chapter 8, interactions between capsules and human umbilical vein

endothelial cells are investigated with a chemical named neuraminidase. The main experiment is focus investigation of the role of the glycocalyx of Human Umbilical Vein Endothelial Cells (HUVECs) on trans-membrane transport of microcapsules *in vitro*. In order to stimulate capsule uptake, the microcapsules are functionalized with an enzyme namely neuraminidase, which has the ability to cleave N-acetyl neuraminic acid residues of glycoproteins and targets specifically the sialic acid component of the glycocalyx layer on the cell membrane surface. Neuraminidase is encapsulated by $CaCO_3$ co-precipitated method. After part of the glycocalyx is removed, channels that allowing the passage of capsules through the cell membrane becomes accessible. The neuraminidase encapsulation efficiency and release rate are investigated with UV visible spectrometer. Degradation rate of capsules after their internalization by HUVECs are observed up to 7 days. Four layered biodegradable DS/PArg capsules are observed to rupture into pieces by day 5, however, there is no obvious changes in the shape of PSS/PAH capsules within the period of time observed. Transfection of HUVECs by DNA plasmid and neuraminidase loaded capsules and commercial reagent Fugene 6 are also studied.

2 Literature review

This part of the report provides the scientific background to the reader for better understanding with the nature, functions and properties of the field investigated.

2.1 **Polyelectrolytes**

Polyelectrolytes are a group of macromolecules having both properties of polymers and electrolytes. In 1950s, Fuoss et al found complexes like precipitates can be formed between polycations and polyanions (Fuoss and Cathers 1947). Later, Michaels tested different types of polyelectrolytes, salt concentrations, and charge ratios to forming spherical complexes in nano-size range from 20 nm to 40 nm (Michaels 1965). Then, polyelectrolytes constructed layer conformations was discovered by Decher et al (Decher and Hong 1991a).

The term polyelectrolyte represents a polymer system that formed by macromolecule of charged or ionizable monomer units and low molecular weight counter ions, and maintain electrical neutrality (H. Dautzenberg 1994). Special structures of charged polymers play important roles in the forming of polypeptides, proteins, Glycosaminoglycans (GAG) and DNA in biological processes (Manning 1978). Two types of oppositely charged polyelectrolytes are polycations with positive charge and polyanions with negative charge. Because zwitterionic polymers can be varied between cationic and anionic forms, the special type of polyelectrolytes contains both negative and positive functional groups are called polyampholytes.

Polar solvents are composed of polar molecules like liquid ammonia. Because the dissociation of the ions from the charged groups, they are able to dissolve ionic compounds or ionize part of covalent compounds of

polyelectrolytes. Polyelectrolytes can be classified as weak or strong types. When a polyelectrolyte dissociates completely in an aqueous media for most reasonable pH values, it is classified as strong. Furthermore, their charge density is mostly independent on the solution pH. Compare with strong polyelectrolyte, the weak one is partially dissociated over a large pH range. Moreover, their charge is varied as the solution pH, counterions concentration, or ionic strength changing. In a dilute solution, an ionizable molecule under acid - base equilibrium is shown in equation 2.1, the ion pair *HA* could dissociate into cationic and anionic part, and the process could be reversed.

$$HA \leftrightharpoons H^+ + A^- \quad \text{(Eq. 2.1)}$$

For weak polyelectrolytes, the charge density depends on the strength of the poly-acid or poly-base. The dissociation behavior of each functional group along the chain is depend on the dissociation behavior of its nearest neighbors (Katchalsky and Spitnik 1947). Because slightly varying environments, each binding site exhibits a different dissociation constant pK_a or pK_b in the range of ~2 to ~10. It will be partially dissociated at intermediate pH. The apparent acidity of the weak polyacid decreases with progressive ionization of the polymer due to the difficulty deprotonation of the polymer chain (Burke and Barrett 2004). For a weak polyelectrolyte, an apparent equilibrium constant of acidity K_{app} can be described in equation 2.2.

$$\boldsymbol{K_{app}} = \frac{[\boldsymbol{H^+}][\boldsymbol{A^-}]}{\boldsymbol{HA}} \quad \text{(Eq. 2.2)}$$

And the degree of dissociation α can be easily obtained by equation 2.3

$$\boldsymbol{\alpha} = \frac{[\boldsymbol{A^-}]}{[\boldsymbol{A^-}] + \boldsymbol{HA}} \quad \text{(Eq. 2.3)}$$

As the *pKa* is defined as reflects the overall acid / base equilibrium of the

polyelectrolyte chains. Therefore, the acid / base equilibrium of the chains is defined by a modified version of the Henderson – Haselbalch equation. The equation takes the multifaceted dissociation behavior of polyion into account (n is depends on polymer charge density, which related to the extension of the chains):

$$\boldsymbol{logK_{app} = log\frac{[H^+][A^-]}{HA};\ logK_{app} = pKapp,\ log[H^+] = pH;}$$

$$\boldsymbol{pH = pK_{app} - nlog(\frac{1-\alpha}{\alpha})} \qquad \text{(Eq. 2.4)}$$

The properties of both polymers and electrolytes are maintained in polyelectrolytes. It is difficult to predict their structure in aqueous media may be using theoretical models. Because of long chains of polymers can acquire a large number of different conformations, their shape and size can only be described statistically. Freely - jointed - chain model and the Gaussian model are two frequently used models to describe the average conformation of flexible neutral polymers in aqueous media. Both of the models consider the mean - squared end - to - end radius *Ree* (in equation 2.5) is proportional to the number of monomers *N* in the polymer chain multiplied by the effective monomer size $\boldsymbol{a}$ (H. Dautzenberg 1994):

$$\boldsymbol{R^2_{ee} = Na^2} \qquad \text{(Eq. 2.5)}$$

Because *Ree* is quite smaller compare with the length of the extended polymer, the above equation only presents uncharged polymers. The persistence length q_p is used to present the stiffness and relative length of a charged polymer in solution. If the persistence length is longer than the polymer pieces, the molecule is similar as an elastic rod with more flexibility. If the persistence length is shorter, the molecule can only be described statistically, like a random walk in space. The persistence length of a polyelectrolyte is affected by the electrostatic interactions between monomer

and the counterions, and relate with the steric length q_0 and the electrostatic contribution q_e

$$\boldsymbol{q_p = q_0 + q_e} \quad \text{(Eq. 2.6)}$$

The q_e is described as

$$\boldsymbol{q_e = \frac{l_B}{4} (\frac{K^{-1}}{l_{eff}})^2} \quad \text{(Eq. 2.7)}$$

$\boldsymbol{l_B}$: Bjerrum length

$\boldsymbol{K^{-1}}$: Debye length

$\boldsymbol{l_{eff}}$: Effective distance between charges. (Fleer 1993)

Charges are electrically screened outside the Debye sphere with Debye length as radius. The Bjerrum length is the distance at which the magnitude of the electrostatic interaction between two elementary charges *e* is equal to the thermal energy ($\boldsymbol{k_B T}$).

$$\boldsymbol{l_B = \frac{e^2}{4\pi\varepsilon_0\varepsilon_R k_B T}} \quad \text{(Eq. 2.8)}$$

$\boldsymbol{k_B}$: Boltzmann constant

$\boldsymbol{T}$: Absolute temperature in Kelvin

$\boldsymbol{e}$: Elementary charge

$\boldsymbol{\varepsilon_R}$: Dielectric constant of the medium

$\boldsymbol{\varepsilon_0}$: Vacuum permittivity

For example two singly charged ions in water at room temperature using the equation 2.8, ε_R is ~ 80, *T* is 300 K, $4\pi\varepsilon_0$ equal to 1 at the Bjerrum length, so l_B can be calculated as 0.7 nm. When the charge distance is smaller than the Bjerrum length, electrostatic counterions can lower charge density of

polyelectrolyte by condense on its chain. In an electrolyte solution or a colloidal dispersion, by measuring the Debye length express symbol $\boldsymbol{k^{-1}}$ (Russel, Russel et al. 1992) the impact of ionic strength *I* on the electrostatic persistence length is shown below:

$$\boldsymbol{k^{-1}} = \sqrt{\frac{\varepsilon_0 \varepsilon_R k_B T}{2 N_A e^2 I}} \qquad \text{(Eq. 2.9)}$$

$\boldsymbol{N_A}$ is Avogadro's number and the ionic strength $\boldsymbol{I}$ is defined as:

$$\boldsymbol{I} = \frac{1}{2}\sum_i \boldsymbol{Z_i^2 C_i} \qquad \text{(Eq. 2.10)}$$

$\boldsymbol{Z_i}$: Charge valency

$\boldsymbol{C_i}$: Molar concentration of the screening ions

From the above equations, concentration of the screening ions is increased with Debye length and persistence length decreasing. The excess of electrolyte could make a coiled conformation easily when the conformation of the electrolyte becomes to be prolonged in aqueous media at relatively low ionic strength.

2.2 Polyelectrolyte complexes

Because of released counterions from the mixed solution of polyanions $(\text{├A}^- c^+)_n$ and polycations $(\text{├C}^+ a^-)_m$, interpolymer complexes $(\text{├A}^- C^+)_x$ can be self-formed. Polyacids and polybases with their neutralized metal and halogenide salts are able to cause complex formation. The basic process (H. Dautzenberg 1994) is shown in Figure 2.1.

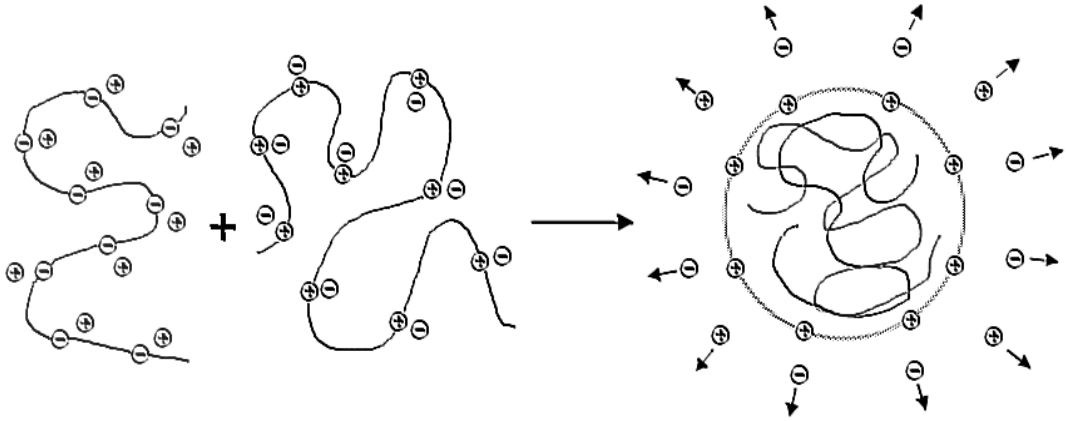

Figure 2.1: Schematic diagrams of the release of counterions upon polyelectrolyte complex formation

$$(\text{├A}^- c^+)_n + (\text{├C}^+ a^-)_m \leftrightharpoons [(\text{├A}^- C^+\text{┤})_x + (\text{├A}^- c^+)_{n-x} + (\text{├C}^+ a^-)_{m-x}] + xa^- + xc^+$$

A^- and C^+ are polyelectrolytes charged groups; a^- and c^+ are counterions; n and m are number of anionic groups and cationic groups respectively. The degree of conversion θ (= $\frac{x}{n}$ while n < m, or = $\frac{x}{m}$ while n > m) gives the idea of the component ions are all formed by the oppositely charged groups or part of the counterions (Thünemann, Müller et al. 2004).

The driving force of above process is gain in entropy due to release of low molecular counterions of a^- and c^+ which locate in the vicinity of the polyion chains. The main contribute to the complex formation is electrostatic interaction between the oppositely charged polyanions and polycations. Furthermore, the hydrogen bonding or hydrophobic interactions also play an

important role in complex formation. Michaels et al (Michaels and Miekka 1961) defined a theory of polyelectrolyte complex formation with two structures. The complex formation defined as ladder models at the molecular level, and with large number of particles in a chain as scrambled egg models. Figure 2.2 shows the ladder and scrambled egg models.

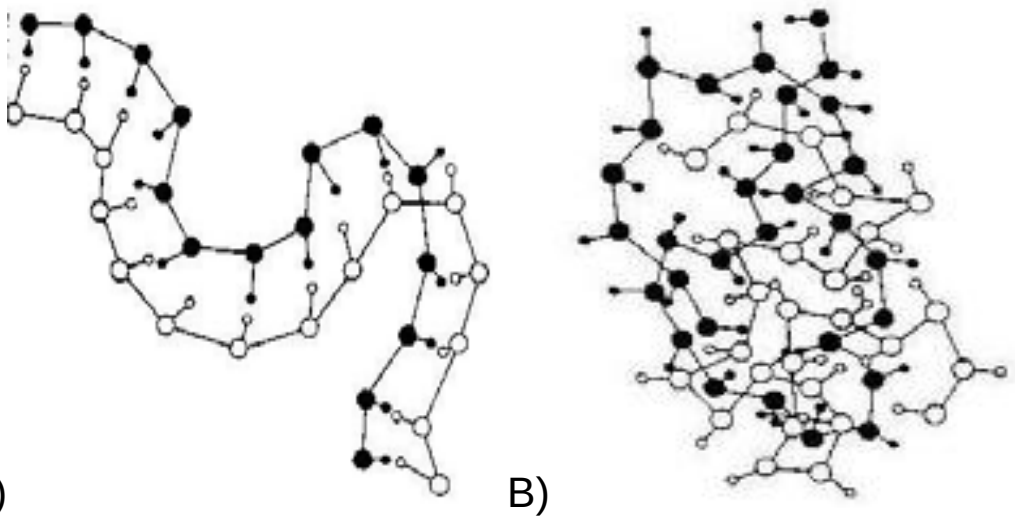

Figure 2.2: Images of the A) ladder and B) scrambled egg models.
Models are based on the polyelectrolyte complex structure theory of Michaels and Miekka. (H. Dautzenberg 1994)

The ladder like structure with fixed ionic crosslinks between two oppositely charged chains presents a complex reaction like a “zippering action”. Thus, the polyion close to the first reacted ones will be mostly reacted next. When the complex reaction is processing from more than one ions, a more cross linked structure is formed (Michaels 1965). Philipp et al (Philipp 1989) have been studied experimental structures between these two models. When the polyelectrolyte is close to another one, the restructuring complex is affected by the distance between charges, as well as the types of counterions present. The real structure of the complex is between the two models, but more favorite the scrambled egg structure with statistical charge compensation.

The polyelectrolyte structure formation mostly defined by the kinetics of

the process which usually less than 5 μs. Then, a slower step of chains redistribute to a conformation tend to equilibrium (Bakeev, Izumrudov et al. 1992). Structure formation is influenced by other parameters have been discussed recently, such as mixing procedure, medium conditions include concentration of salt and polyelectrolyte, polymer chain flexibility, molecular weight and linear charge density (Dragan and Schwarz 2004; Thünemann, Müller et al. 2004). When prepare the polyelectrolytes complexes, small difference of used polyelectrolytes results big difference on restructured complexes. Basically, there are three types of polyelectrolytes complexes structure which are water soluble, colloidally stable, and coacervate complexes. Main interaction forces such as Coulomb forces, hydrogen bonding, hydrophobic interactions, van der Waals forces, and charge transfer interaction are used to classify these three types (Tsuchida 1982).

2.2.1 Water-soluble polyelectrolyte complexes

Under appropriate salt conditions, water soluble polyelectrolyte complexes are obtained by mixing polyions with significantly different molecular weight. For example, a high molecular weight polyion (longer chain) as host is mixed with an oppositely charged lower molecular weight polyion (small chain) as guest in non-stoichiometric proportions; or by reacting oppositely charged macro-ions of comparable chain length at extremely low concentrations (Kabanov 2003). The structure of this complex basically looks like the ladder model, contains hydrophilic single stranded and hydrophobic double stranded segments (Kabanov and Zezin 1984). Figure 2.3 shows a sequentially water-soluble polyelectrolyte complex.

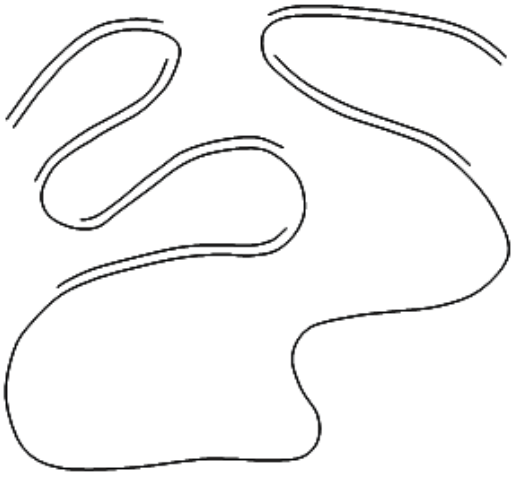

Figure 2.3: Image of a sequentially water-soluble polyelectrolyte complex.

Water-soluble polyelectrolyte complex could rearrangements in medium with low salt concentration, and tend to the thermodynamic equilibrium. Polyelectrolyte charges are shield and the complexes are shrunk with more salt present. Precipitation can be seen with higher concentration of salt in the medium. If the amount of long polycations is bigger than the short polyanions in polyelectrolyte complex, they cover the hydrophobic part of the conformation. Otherwise, polyelectrolyte complex becomes a micelle like structure (Kiriy, Yu et al. 2006).

2.2.2 Colloidally stable Polyelectrolyte complexes

Strong polyelectrolytes re-formed polyelectrolyte complexes lead to a highly aggregated or macroscopic flocculated system (Thünemann, Müller et al. 2004). In a medium with very low concentration of polyelectrolytes, the aggregation is suspended with spherical structure (size up to 100 nm) at a colloidal level. Macroscopic flocculation of the system occurs usually with a ratio of 1:1 stoichiometry for strong polyelectrolytes. However, the stoichiometry is influenced by the flexibility of polymer.

For instance, high stiffness polymer with non-uniform distribution in charge could leads to low capability of reconstruction. Thus, it tends to form

non-stoichiometric polyelectrolyte complexes. Moreover, branches of the polymer also make the reconstruction non-stoichiometric, due to the inner pieces of the molecules extremely hard to touch with the oppositely charged polyelectrolyte.

Polyelectrolytes form denser structures cause stoichiometry approach 1:1 ratio while adding salt to the medium (Vanerek and Van De Ven 2006). Complexation stoichiometry as a function of salt concentration has investigated many years before by Cundall et al (Cundall, Lawton et al. 1979). In pure water polyelectrolyte complexes formation is mostly affected by the kinetics during the complexes forming, result a frozen structures with non-thermo dynamic equilibrium.

Polyelectrolyte complexes colloids are in a stable distribution with non-stoichiometric solution while its concentration is lower than 1 g/ml. Once colloids molar mass reduced, secondary aggregation starts. This happens while the molar mixing ratio closes to 1:1. Appropriate charge density in strong polyelectrolytes could result the colloidal particles seriously swelling due to unmatched charge densities (Thünemann, Müller et al. 2004).

Salt significantly influences the polyelectrolyte complexes formation. Complexes are rapidly swelling or shrinking with varied ionic strength, but the coagulation speed is slower, depend on the colloidal particles concentrations (Dautzenberg and Rother 2004). During polyelectrolyte complexes conformation, the aggregation is suddenly reduced by adding salt. Higher ionic strengths lead to the secondary aggregation and macroscopic flocculation with the mixing ratios less than 1:1. It is caused by the screening of the electrostatically stabilizing shell of the major component around the polyelectrolyte complexes particles (Dautzenberg 1997).

Furthermore, the univalence or divalent salt ions such as Li^+, Na^+, and K^+

are all determine the interactions between the polyelectrolytes (Sukhishvili, Kharlampieva et al. 2006).

2.2.3 Coacervate Polyelectrolyte complexes

Oppositely charged polyelectrolytes are entangled with low charge density to form the coacervate complexes. It has the feature of liquid-like, electrophoretic mobility, and the structure reversibility (Biesheuvel and Stuart 2004a).

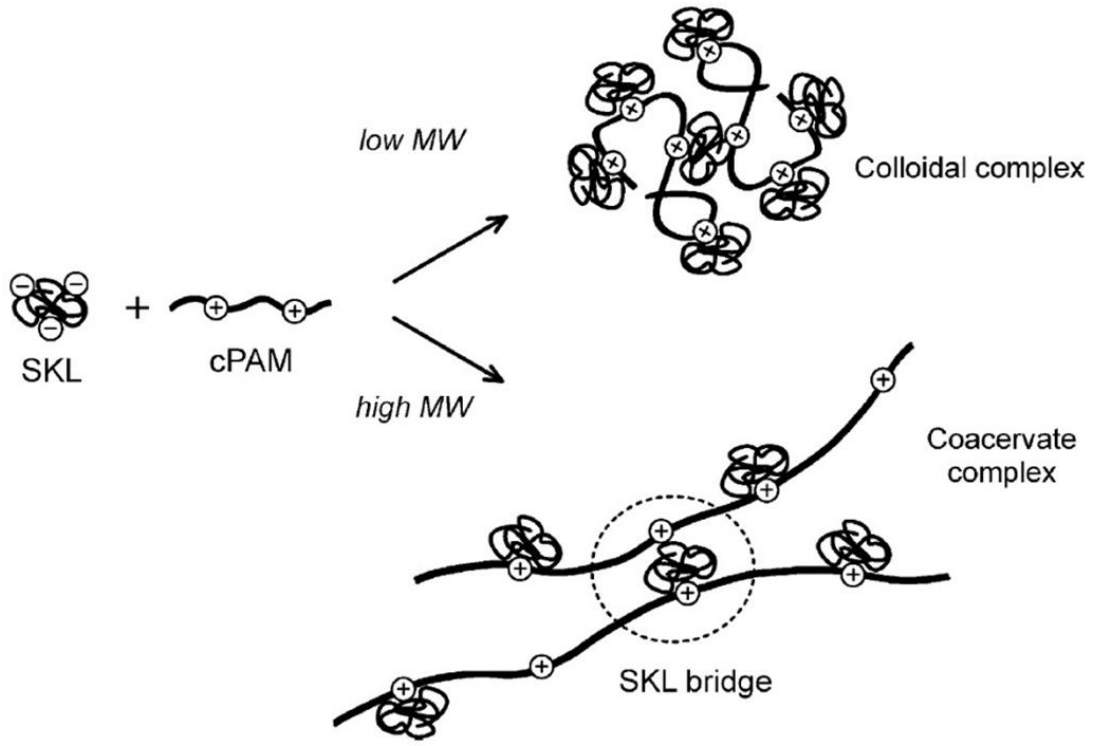

Figure 2.4: Schematic illustration of the effect of molecular weight on the formation of colloidal and coacervate complexes.

Low molar mass cPAM forms primary colloidal complexes while high molar mass cPAM forms mostly coacervate complexes with sulfonated kraft lignin (SKL) (Vanerek and Van De Ven 2006).

Figure 2.4 shows the effect of molecular weight on the formation of colloidal and coacervate complexes. Because the short chain is more favor to a precipitate coiled conformation, lower molecular weight of the mixed

polyelectrolytes is the main factor. Water soluble, colloid and coacervate of polyelectrolytes complexes are able to be formed at the same time. Biesheuvel et al design a mathematical model to investigate formation of coacervate complexes with different electrostatic free energy. In the model, several parameters such as distance between charges, salt concentrations and molar mixing ratios can be modified to determine the form of coacervate complexes (Biesheuvel and Stuart 2004b).

2.3 Polyelectrolyte Multilayers

Absorption of polyelectrolytes at surfaces is affected by many parameters, such as the polymers charge density, molecular weight and conformation. Moreover, other factors also influence the interface of polyelectrolytes absorption, like solvent's pH value, and ionic strength. More details will discuss in the following sections.

2.3.1 Polyelectrolyte absorption on a solid surface

The absorption of polyelectrolytes at interfaces is more like complex formation. The film structure fabricated by the absorption is mostly affected by the polyelectrolytes structure and the ionic strength. For polyelectrolyte with a non-twisted structure, the thin film is more easily deposited with low ion concentration. In this condition, nearly all charges of the polyelectrolyte are combined with the opposite ones at the surface along the polymer chains. Otherwise, polyelectrolyte with twisted structure is difficult to deposit entire pieces on the template surface. Therefore, the structure contains absorbed polymer chain called trains and non-absorbed chains like loops, and tails are shown in Figure 2.5.

Meaning of Tails and loops of the polymer chains just like their names. Tails are the end section of the polymer, and loops are parts of polymer chain which are not on the substrate surface. The main reason for forming the tails and loops structure is re-conformation speed of the coiled polymer much slower than the absorption speed on the substrate surface. Furthermore, electrostatic repulsion and steric effects prefer to attract only some part of the polyelectrolyte as train segments also affect the structure of tail and loop.

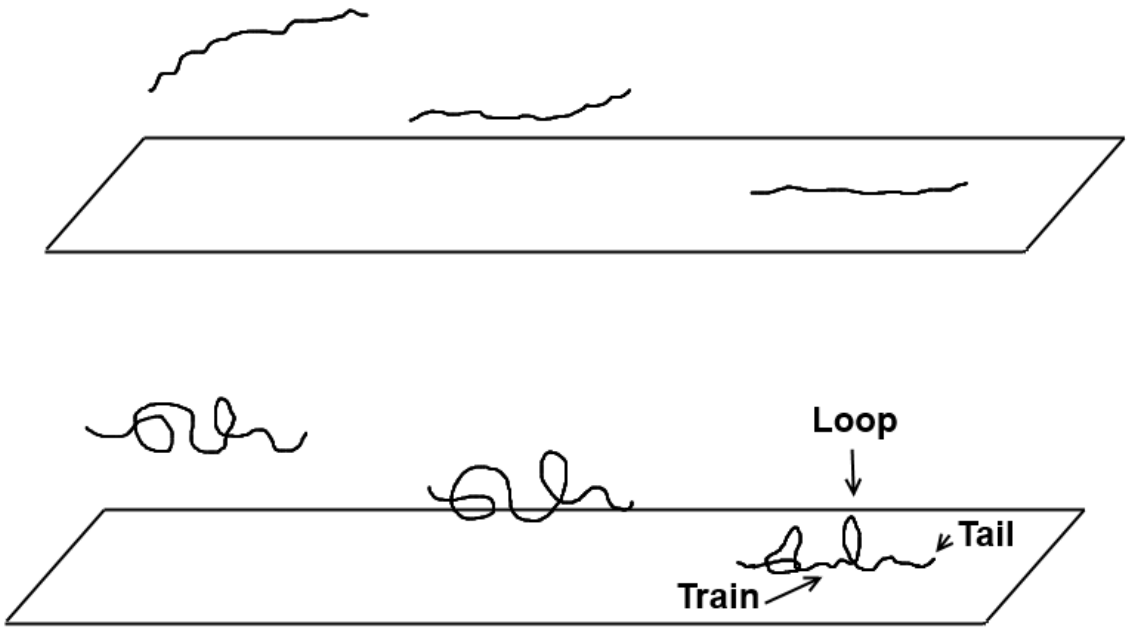

Figure 2.5: Schematic illustration of polyelectrolyte's absorption at an oppositely charged surface.

Polyelectrolytes are in a rod-like formation (top) and in a coiled conformation (bottom). After the deposition, polymer sections of loops and tails are not blinding on the substrate surface lead to charge overcompensation.

Beltran et al discovered that tails are favored at low degrees of chain ionization, while trains prefer high degrees of ionization. The number of adsorbed chain sections is increased with increasing charge density of surface and decreasing ionic strength in solution (Beltran, Hooper et al. 1991). As deposited film is formed by great numbers of polymers, the tail structure could also occur when one polymer is mostly absorbed, but the area of substrate surface for end of the polymer is already taken by the next polymer chain.

Because tails and loops exist in the deposited polyelectrolyte on the substrate surface, the charge of the polymer film is opposite to the substrate. It is called "charge overcompensation" which is the primary condition to make multilayer systems using the Layer-by-Layer technique.

2.3.2 The Layer-by-Layer technique

In the 1990s, Decher and Hong used complex formation of polyionic and polycationic compounds to produce organized multilayered thin films (Decher and Hong 1991a; Decher and Hong 1991b; Decher, Hong et al. 1992). This electrostatic layer-by-layer (LbL) assembly has been first investigated by Iler (Iler 1966). In the experiment, charged solid substrate is added into aqueous solutions of polyelectrolyte with positive charge and followed negative charge. For each layer of absorption, the polyelectrolyte molecules are attracted by the oppositely charged surface until fully covered film formed.

In the process of film forming, entropically driven by the release of counterions, restrict by electrostatic repulsions. Followed by the surface saturation, and then solid substrate is washed to remove the uncoated polymer that suspended in the solution. During LbL assembling, each adsorption step reverses the surface charge. So far, no number of layers is limited with this technique, Lenahan et al successfully fabricated a number of 1000 layers film (Lenahan, Wang et al. 1998).

Figure 2.6 shows a typical LbL process: a substrate with positive charge on the surface is immersed into a polyelectrolyte solution contains polyanions and appropriate concentration of salt. Salt helps polymers form a coiled structure. The polyelectrolytes distribute in the solution, some of them close to the substrate are attracted by the opposite charges.

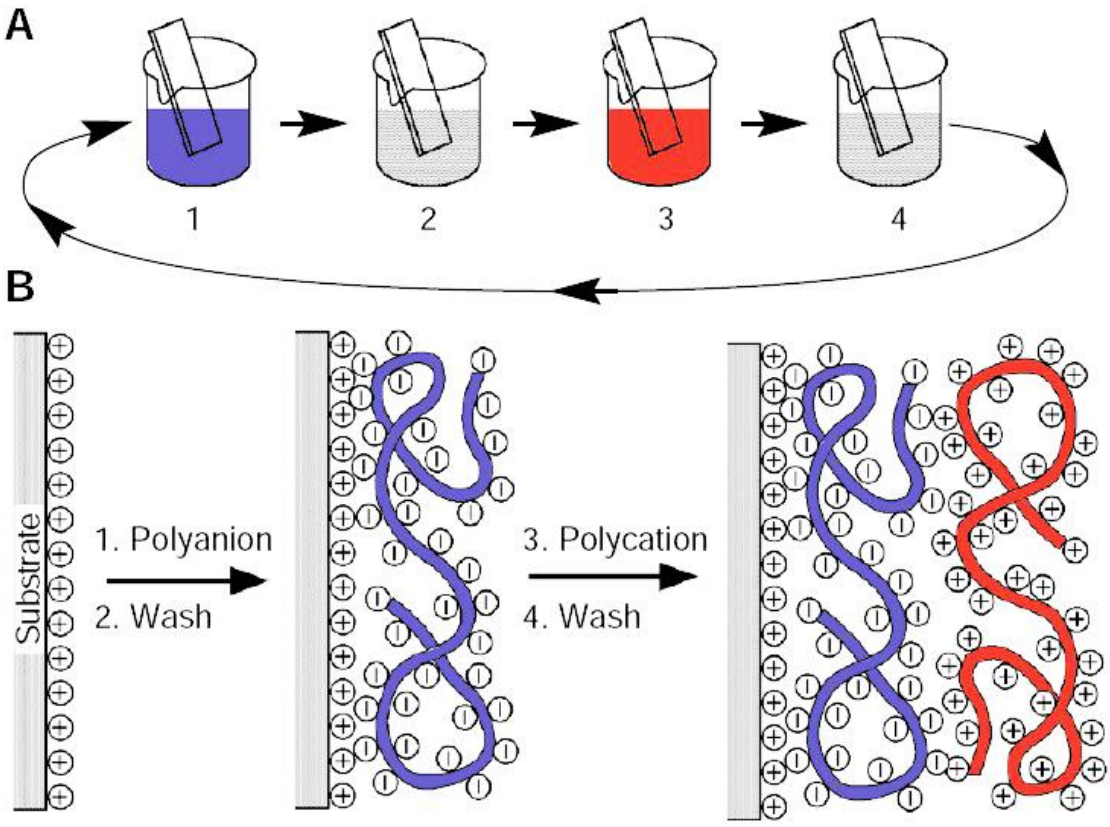

Figure 2.6: The electrostatic layer-by-layer (LbL) assembly.

(A) The mainly methods in experiment. (B) Theory explanation (Decher 1997).

After a certain time, most charges of the polymer chain are paired with the charges on the substrate. Thus, a layer of polyelectrolyte is formed on the substrate with a stretched conformation. Because loops and tails structures of polymer exist in the layer, charge overcompensation is approached. Then, the substrate with negative charge at the outmost layer is washed with water to remove excess polymer. The following layer is coated by immerse the substrate into polyelectrolyte solution with polycations and salt. After these steps, the thermodynamically stable polyelectrolyte bilayer is constructed on the substrate.

The process of a template with the polyanions /wash /polycations /wash steps could be repeated many times until a desired number of layers are coated. The thickness of one layer is from several angstroms to few

nanometers depends on the deposition conditions. Therefore, thickness of the film is able to be varied with an exactly numbers in the angstrom range. Under the LbL technique, multilayers on macroscopic substrates are able to be fabricated by spraying (Schlenoff, Dubas et al. 2000; Izquierdo, Ono et al. 2005) or spin coating (Chiarelli, Johal et al. 2001) which reduces the preparation time significantly.

LbL technique based on electrostatic interactions between oppositely charged polyelectrolyte is variety used for polyelectrolyte complex fabrication. The multilayer films are able to be assembled by differently functionalized synthetic polyelectrolytes (Baur, Kim et al. 1998; Jaber and Schlenoff 2005); charged biopolymers such as proteins (Lvov, Ariga et al. 1994; Lvov, Ariga et al. 1995; Onda, Lvov et al. 1996; Caruso, Furlong et al. 1998); nucleic acids (Lvov, Decher et al. 1993; Sukhorukov, Möhwald et al. 1996); lipids (Georgieva, Moya et al. 2000; Tiourina, Radtchenko et al. 2002); bolaamphiphiles (Saremi, Maassen et al. 1995; Saremi, Tieke et al. 1997; Dreja, Kim et al. 2000; Jung, Hong et al. 2002); viruses (Lvov, Ariga et al. 1994); metallo-supra molecular polyelectrolytes (Kurth, Schütte et al. 2002); inorganic nanoparticles like gold colloids (Cant, Critchley et al. 2003); quantum dots (Gao, Lesser et al. 2000); fullerenes (Guldi, Luo et al. 2002); carbon nanotubes (Mamedov, Kotov et al. 2002; Rouse and Lillehei 2003); dendrimers (Kim and Bruening 2003; Li, Mitamura et al. 2003); and multivalent organic ions such as dyes (Ariga, Lvov et al. 1997; Laschewsky, Wischerhoff et al. 1997).

This multi-function allows the high speed and uncomplicated preparation of surface covered layer depositing or free standing thin films with many properties, such as chemical, biological, optical, electronic, magnetic, anti-bacterial, or perm-selective, which make the applications suitable in a widely filed (Bertrand, Jonas et al. 2000).

2.3.3 Stabilizing interactions within multilayers

The driving force for polyelectrolyte layer deposition is electrostatic interactions, and the layer thickness is affected by the electrostatic repulsions of polyelectrolytes charge. Polyelectrolytes need have a minimum charge density for attracting with the charged surface of substrate (Steitz, Jaeger et al. 2001). Schoeler et al found a special case that a polyelectrolytes deposition has been discovered below the minimum charge density (Schoeler, Poptoshev et al. 2003), and propose the strength of the electrostatic interaction is more important than the charge density limitation.

The ions exist in the polymer solution is required to reach the charge overcompensation for depositing the following layer. After each polyelectrolytes deposition step, several times of wash step is used to remove the uncoated polymer. This step also washes the ions which connected with the polyion of the coated layer. Thus, high electrostatic interactions in a high compact layer lead to multilayers swelling (Sukhorukov, Schmitt et al. 1996).

The layers keep stable with enough number of polyion pairs exist. But high concentration of salt presents in the solution is able to cause the over screening within the layers, and disassemble the film. The ionic strength influences polyelectrolyte ion pairs of the film under the following equation. It shows the polyion pairs in an electrostatic bond with added ions a^+ and b^- in the solution (Dubas and Schlenoff 2001).

$$(\vdash A^+ B^- \dashv)_n + n a^+ + n b^- \leftrightharpoons (\vdash A^+ b^-)_n + (a^+ B^- \dashv)_n$$

Electrostatic interactions are reduced as high salt concentration present, result the polyion abandon thermodynamically favored conformation and back to the bulk solution. Thus, the electrostatic contribution is a very

important parameter of film stability. Besides electrostatic, other weak interactions are also contribute to a successful LbL deposition, for example hydrogen bonding (Stockton and Rubner 1997; Pontes, Raposo et al. 1999); hydrophobic interactions between polyelectrolytes (Dubas and Schlenoff 1999); charge transfer and π-π stacking, Van der Waals interactions (Kotov 1999); even polyelectrolyte with same charge, the hydrogen bonding formed multilayers could also be possible (Wang, Wang et al. 1997).

2.3.4 Growth and structure

When construct the multilayers, different polyelectrolytes result different thickness increments after every layer. For strong polyelectrolytes formed films, the thickness is more linearly as the number of layers increasing, and the mass of each polyelectrolyte layer is almost same (Ruths, Essler et al. 2000; McAloney, Sinyor et al. 2001). Some weak polyelectrolytes show an exponential increase on mass with the number of film layer increasing. The reason is one of used polyelectrolyte diffuse through the film raising the mass of last deposited layer (Picart, Lavalle et al. 2001; Lavalle, Picart et al. 2004).

Ladam et al (Ladam, Schaad et al. 2000) proposed a zone model for the multilayer film structure. The model can be divided into three zones named zone 1, 2 and 3 with defined properties respectively. Figure 2.7 shows zone model of the growth of polyelectrolyte multilayers. In zone 1, the first polyelectrolyte layer contact with the substrate. Conformation of the layer is directly determined by the solid support, and thickness of the layer usually less than the following layer in Zone 2. Zone 2 refers to the internal part of the film that between Zone 1 and 3. Therefore, Zone 2 determines most permeability and mechanical stability of LbL films. Polymer layer in Zone 3 exposes to the solution and contains excess charge is the last layer covers the multilayers (R. v. Klitzing 2002). Furthermore, Zone 3 more likes the diffusion depth is called a penetration length, through which polyion can pass

Zone 3 and spread to the layers of above zones (Schlenoff and Dubas 2001; Salomäki, Vinokurov et al. 2005; Porcel, Lavalle et al. 2006).

At the beginning of multilayer fabrication, only Zone 1 and 3 present in the film. As the deposition continues, the layers thickness is increasing, so Zone 2 is growing. In this LbL assembling, every layer will switch the transition area between Zone 2 and Zone 3. Thicknesses of the first and last layer are mostly determined by the used polyelectrolyte pair and the deposition conditions.

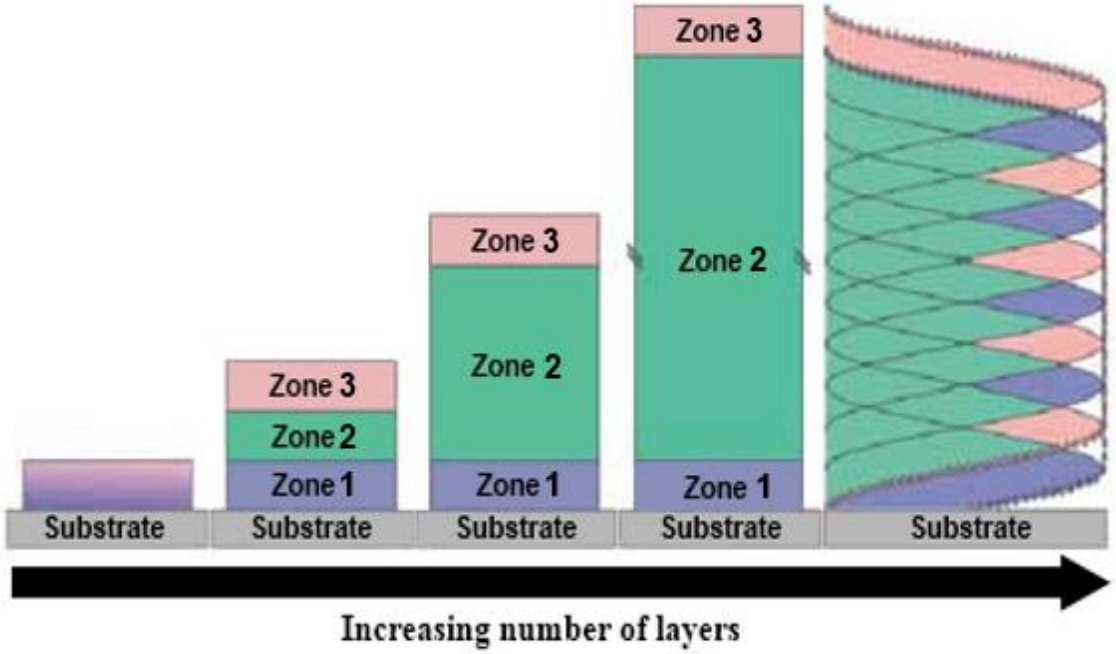

Figure 2.7: Zone model shows the growth of polyelectrolyte multilayers.

From left to right, shows the progressive evolution of the three different zones, and on the right a concentration profile for a multilayer composed of 10 layers shows the strong overlap between adjacent layers (Decher and Schlenoff 2003)

The growth of first layer in Zone 1 is mostly affected by the substrate surface. Thickness and mass growth of other layers with layer number increasing can be divided as exponential and linear growth. In exponential growth case, penetration depth is increased with thickness of Zone 3

increasing. Polymers penetrate Zone 3 and deposit in Zone 2 until the polyions are no longer diffuse through the diffusion depth. At this point, the Zone 3 reaches a critical thickness and Zone 2 stop growing. If the penetration depth of Zone 3 is fixed, the amount of polymer deposit every two layers is constant, which change the exponential growth to linear type.

In case of polyelectrolytes Poly (Allylamine Hydrochloride) (PAH) and Poly (Styrene Sulfonate) (PSS) formed pairs in a low ionic strength solution at room temperature; Zone 3 is a linear growth after the first deposited layer of Zone 1. For some polyelectrolyte such as poly (L-lysine) and hyaluronic acid, the polyions are able to penetrate deeply into the Zone 2 layer, cause the linear growth only be discovered after 25 or even more layers deposited (P. Lavalle 2004).

Moreover, the growth of polyelectrolyte multilayer is influenced by many parameters, for instance: ionic strength, polymer concentration (Lösche, Schmitt et al. 1998; Dubas and Schlenoff 1999; Steitz, Leiner et al. 2000; Steitz, Jaeger et al. 2001); charge density of the polymer (Glinel, Moussa et al. 2002; Schoeler, Kumaraswamy et al. 2002); molecular weight of the polyion (Dubas and Schlenoff 2001; Sui, Salloum et al. 2003); different kinds of salt in solution (Salomäki, Tervasmäki et al. 2004); different pH value (Shiratori and Rubner 2000; Choi and Rubner 2005); different solvent (Poptoshev, Schoeler et al. 2004); temperature (Tan, Meredith et al. 2003; Poptoshev, Schoeler et al. 2004; Gopinadhan, Ahrens et al. 2005) and time for deposition (Lvov, Decher et al. 1993). In conclusion, the ionic strength and temperature increased result formed film thickness increasing and exponential growth area prolonging.

In Zone 2, counterions density of polymer layers is less than polyion monomer density. Because present charged polyelectrolyte parts are paired by oppositely charged polyion parts (Klitzing and Moehwald 1995; Schlenoff,

Ly et al. 1998). Reconstruction of polymer chains is blocked by multiple ionic bonds as the polymers are firmly combined with each other. Because the charge overcompensation, polymer contains many counterions in Zone 3, and less densely formed than the polymer in Zone 2. Thus, the inside of polymer multilayers even has hydrophobic property may contains fifty percent of water (Estrela-Lopis, Leporatti et al. 2002); and ten to twenty percent of water been detected in dried state of the film (Farhat, Yassin et al. 1999).

The permeability of the multilayers for small molecules has been well known (Klitzing and Möhwald 1996; Regine v. Klitzing* and Möhwald 1996), which is determined by the film thickness, different types of the deposition polyelectrolytes and the solvent conditions. Moreover, the film with bipolar conformation has a property of selective differently charged ions or polar and non-polar compounds. Thus, the multilayers film attractive as separation membranes for ions, gases, and solutes (Krasemann and Tieke 1999; Krasemann and Tieke 2000; Krasemann and Tieke 2000; v. Klitzing and Tieke 2004; Jin, Toutianoush et al. 2005).

2.3.5 Stimuli-responsive properties of supported multilayers

The growth of polyelectrolyte multilayers is affected by many parameters, the films after deposition are also influenced by in the environment changes, for example: humidity (Kügler, Schmitt et al. 2002; Wong, Rehfeldt et al. 2004); solvent (Müller, Heinen et al. 2001); pH (Hiller and Rubner 2003; Zhai, Nolte et al. 2004); ionic strength (Dubas and Schlenoff 2001; McAloney, Dudnik et al. 2003) and temperature (Steitz, Leiner et al. 2002). Moreover, the dried multilayers films swell in water, or in a humidity environment, and become three times larger than the original thickness (Ahrens, Büscher et al. 2004). Figure 2.8 shows the changed temperature affects capsules shrinking and swelling. If the multilayers film contains one weak polyion, it only affected by changed pH value. Therefore, the charge balance in the multilayer varies

due to additional acid or base, and result a network re-conformation. Except continuous or discontinuous transitions of swelling and shrinking, wetness and roughness of the film surface changes; morphology and porosity of the multilayer have been investigated (Yoo, Shiratori et al. 1998; Mendelsohn, Barrett et al. 2000; Hiller, Mendelsohn et al. 2002).

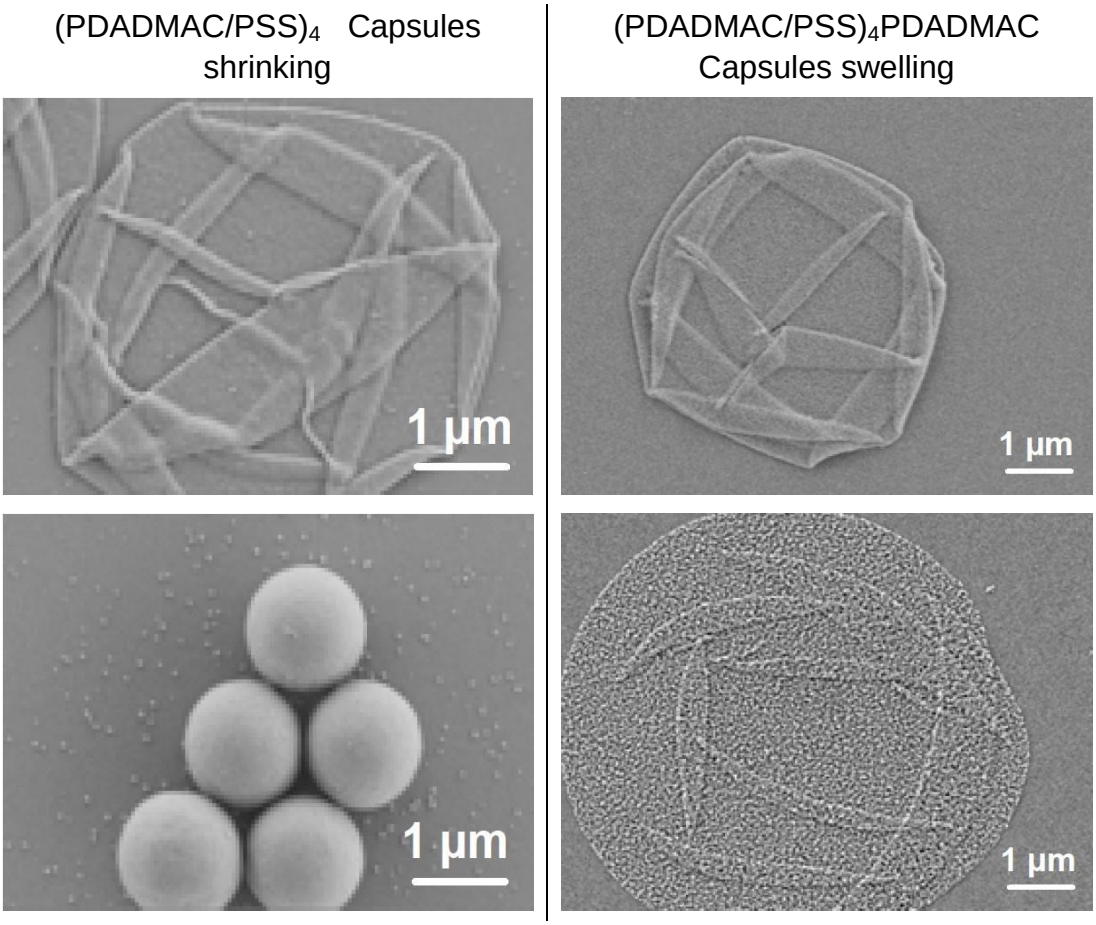

Figure 2.8: SEM micrographs of capsules shrinking and swelling.

Top images are initial capsules, bottom capsules are treated with heating. Thermally shrunk of $(PDADMAC/PSS)_4$ capsules (left) and thermally swollen of $(PDADMAC/PSS)_4PDADMAC$ capsules (right). (Köhler 2006)

Because the multilayers films are formed mostly by the electrostatic interactions, the ionic strength of the solution is more important to its conformation. Salt ions could increase the re-conformation of the polyion due to screening of the charges which result the polymer chains become smooth and inter-diffusion (McAloney, Dudnik et al. 2003). The conformation is also

determined by the salt type, the polyion bonding strength and the interactions, for instance hydrophobic and ionic strength lead to the beginning of the reconstruction (Dubas and Schlenoff 2001). Typically, the multilayers films swell with additional salt present, but for some polyelectrolyte film such as PSS/PDADMAC shows shrinkage and decomposition while a strong ionic strength exist. For study of multilayers affected by temperature change, many groups focus on the temperature response of the thermo sensitive films, only few experiments about no functionalized multilayers such as PAH/PSS film (Ahrens, Büscher et al. 2004).

2.4 Polyelectrolyte multilayer capsules

Multilayer films are made from sequentially absorb the oppositely charged polyelectrolytes on a substrate surface, and this method was first reported by Iler (Iler 1966). Decher et al investigated a self-assembly process using electrostatic interaction (Decher and Hong 1991a). Multilayer films are fabricated from electrostatic self-assembly method are suitable for most of charged substrate and better than other well established deposition techniques. At the interface of the substrate and polymer, the driving force of electrostatic interaction makes an excessed surface charge also called charge overcompensation. Electrostatic self-assembly technique could also produce multilayer films on a substrate with a non-flat surface known as Layer-by-Layer (LbL) technique (Sukhorukov, Donath et al. 1998).

The particle template in a micron size with a porosity property can be coated with multilayer films using LbL technique. If the polyelectrolyte film is stable after fabrication and even after template dissolution, the free standing membrane formed capsule with inside hollow structure is obtained (Donath, Sukhorukov et al. 1998; Sukhorukov, Donath et al. 1998). Polymer microcapsules preparation and fabrication, also substances encapsulation have been investigated many years before (Chang 1964).

Polyelectrolyte microcapsules under LbL process are much better than other micro containers such as micelles, liposomes, inorganic hollow shells. Especially in capsules mechanical properties with various factors changed on the multilayered films, for example: the layers composition, thickness, stiffness, roughness, density, hydration, diameter and permeability.

2.4.1 Polyelectrolyte multilayer capsules preparation

In 1998, hollow capsules on colloidal particles with non-planar surfaces was successfully formed by LbL assembly (Sukhorukov, Donath et al. 1998). Therefore, a charged surface is the only required condition for a substrate as template for capsules preparation, any shapes, morphology and composition are not problems. Some parameters of the solution have to be modified to a certain value, such as pH, ionic strength and polyion concentration. Therefore, polyelectrolyte aggregation is blocked and maintains a uniform coating.

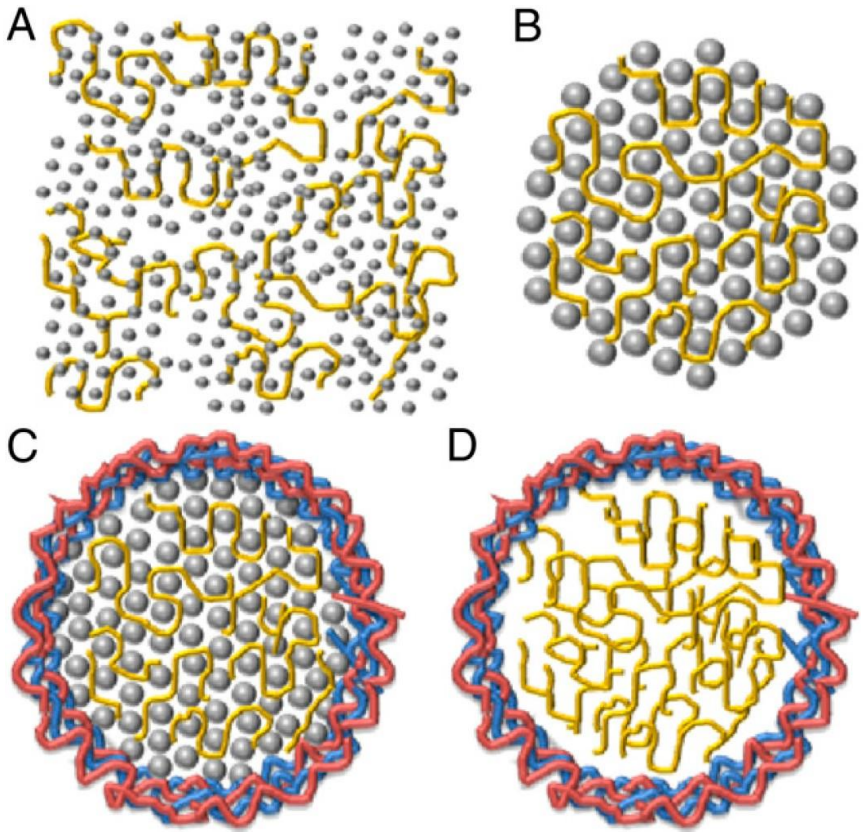

Figure 2.9: Substance encapsulation and hollow microcapsule fabrication.
Substance is mixed (A) and co-precipitated (B) with $CaCO_3$, and then covered by oppositely charged polyelectrolytes (C). Hollow capsules are obtained after core dissolution (D) (De Koker, Naessens et al. 2010).

Figure 2.9 shows general encapsulation of substance and fabrication of hollow microcapsule. After the required number of layers is coated, the

templates used for multilayers films deposition are dissolved. Two main conditions are required in dissolution step. One is polymer complexes remain stable during templates removing, and another one is most of the decomposed templates can pass the semipermeable shell. After all, the free standing multilayer films constructed hollow polymer shells are produced.

Microcapsules are conformed in aqueous media under the self-assembly process. After each deposition step, centrifugation step is used to separate the colloid templates from the supernatant (Sukhorukov, Donath et al. 1998); or a micro filtration is using for supernatant removing (Voigt, Lichtenfeld et al. 1999). Plenty of washing is important to remove loosely bond and uncoated polyelectrolytes. This step prevents polyelectrolytes complexes constructing in the solution without template and cause the solution milky-like and impurity.

The exact amount of polyelectrolyte needed to fully cover the template surface can be calculated theoretically assuming flat surface of template. Otherwise, the surface area is not possible to calculate for colloid particles in suspended solution. Thus, the overdose of polyelectrolyte solution should be added for each polymer layer coating (Peyratout and Dähne 2004). LbL process has been used to produce capsules size ranging from 15 nm (Schneider and Decher 2004) to 20 μm (Shenoy, Antipov et al. 2003).

Generally, shell component materials to form polymer microcapsules are required to containing minimum one polyion. Any charged polymer can meet the requirement, no matter synthetic polyelectrolytes or biomolecules. Small or low charge density molecules pair with oppositely charged polyions is easily neutralizing the surface charge, not reversing the charge. Thus, the following layer cannot be coated, and using these molecules for multilayer films self-assembling is difficult. But chemical cross‐linking (Tong, Gao et al. 2005; De Geest, McShane et al. 2008; Wang, Bansal et al. 2008) and click

chemistry (De Geest, Van Camp et al. 2008; Connal, Kinnane et al. 2009) have been reported recently, which successfully use small molecules or same charge materials to form multilayer complexes.

2.4.2 Template core dissolution

Many different types of template have been used for fabricating polyelectrolyte microcapsules, such as solid particles, liquid droplets and micro bubbles (Shchukin, Köhler et al. 2005; Fernandes, Tzvetkov et al. 2008; Gedanken 2008). But the liquid droplets and micro bubbles as the template core are not stable during the LbL process. Therefore, we focus on the template of solid particle. There are variety types of solid templates, such as organic particles like latexes (Sukhorukov, Shchukin et al. 2004); gel beads (Shenoy and Sukhorukov 2005; De Geest, Dejugnat et al. 2006); inorganic particles with size from nanometer to microns like silica (Bédard, Braun et al. 2008; Bedard, Munoz-Javier et al. 2009) and calcium carbonate (Sukhorukov, Volodkin et al. 2004; Volodkin, Larionova et al. 2004; Volodkin, Petrov et al. 2004); also living cells (Moya, Dähne et al. 2001; Neu, Voigt et al. 2001).

Microcapsules can be produced with size ranging from nanometers to microns. The limitation of the capsules minimum diameter is the stability decrease of depositing polymers on small particles cores. Maximum diameter of capsule is limited by osmotic pressure that leads to the large core particles decomposition (De Geest, Van Camp et al. 2008; De Geest, Van Camp et al. 2008).

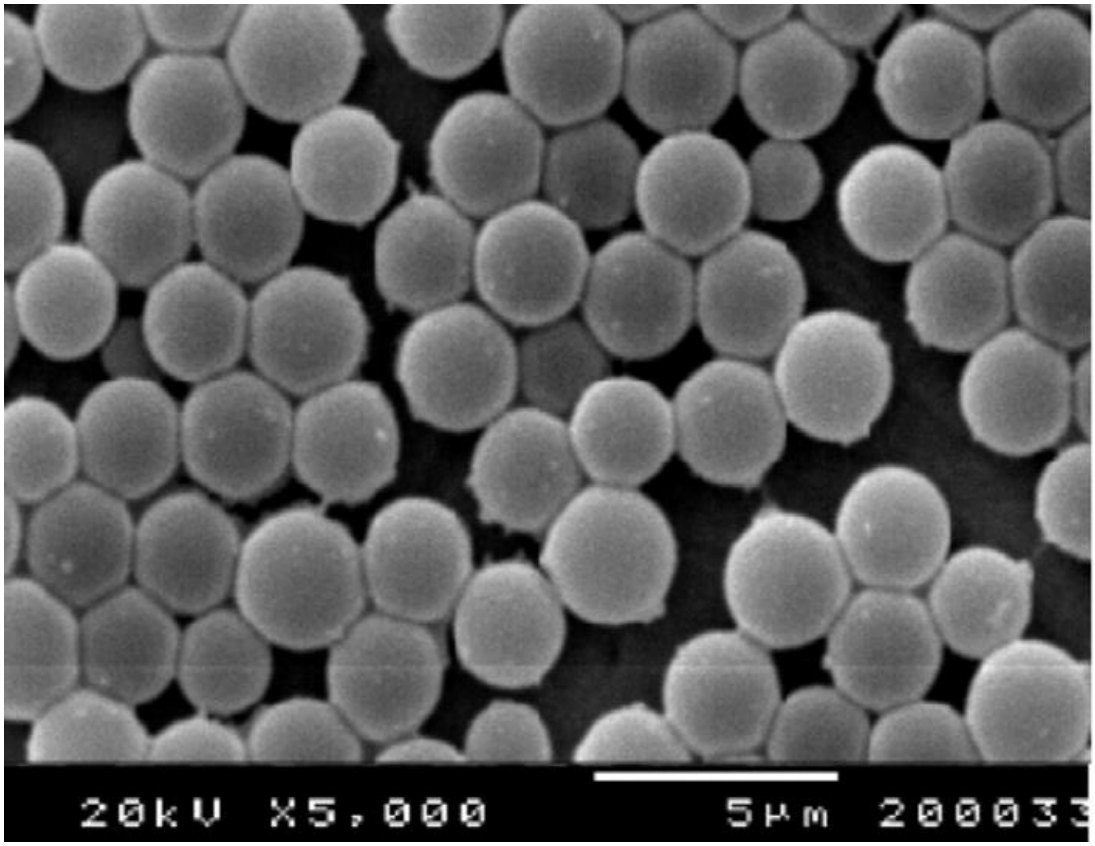

Figure 2.10: SEM images of the melamine formaldehyde microspheres prepared at pH=6.0. (Cheong, Shin et al. 2004)

Melamine formaldehyde (MF) micro particles (Figure 2.10) with properties of mono disperse and weakly cross-link has been mostly used as template core for capsule fabrication. MF particles are easily and quickly decomposed by acidic hydrolysis with HCl in a less than 1.6 pH value or some polar solvents like N,N-Dimethylformamide (DMF). The molecular weights of MF oligomers in the region from 4 to 14 kDa are not easy decomposed. Because decomposed MF particles pass the polymer shell is slower than the speed of MF particles reforming. Thus, capsules can be damaged or even ruptured during MF decomposition step (Gao, Moya et al. 2001). Moreover, the un-dissolved MF template and residual decomposed particles still leave inside the capsules or remain in the shell, which may cause the capsules properties out of control (Gao, Moya et al. 2002).

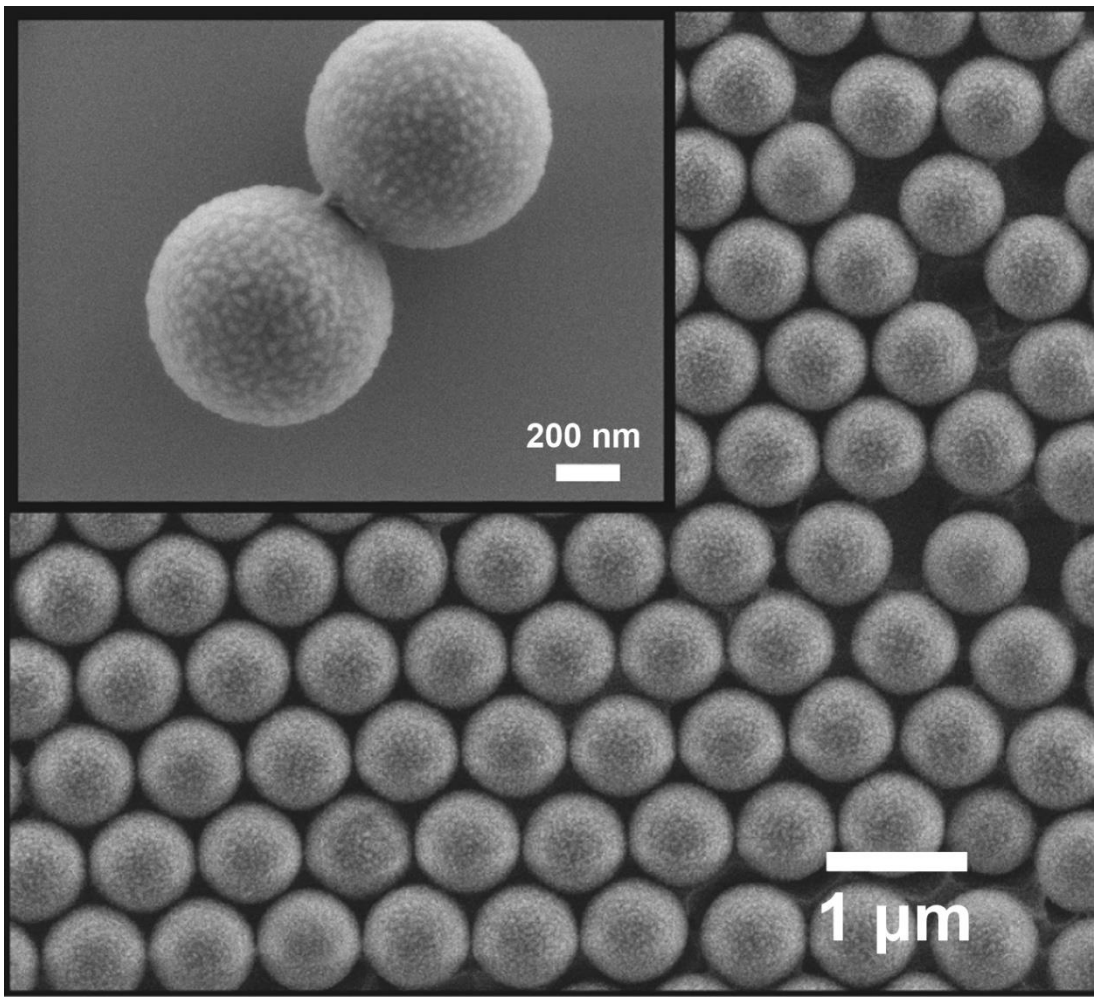

Figure 2.11: SEM images of PS particles prepared by surfactant-free emulsion polymerization.

(Telford, Pham et al. 2013)

Polystyrene (PS) (Figure 2.11) and poly (lactic acid) (PLA) are soluble in organic solvent, and are used extensively. But the completely removal of the PLA template is difficult and some residual of the decomposed PLA may remain inside capsules (Déjugnat and Sukhorukov 2004). Because the polymer films are in a glassy state, the morphology of capsules produce from LbL technique is mostly depends on the template core. Thus, to determine which type of cores is used for encapsulation is important.

Compared with organic template, inorganic cores can be completely decomposed and removed from capsules, such as manganese carbonate, silicon oxide, cadmium carbonate and calcium carbonate can be dissolved

into low molecular weight ions and carbon dioxide (Antipov, Shchukin et al. 2003). Thus, the decomposed cores are able to pass the polymer multilayer shell easily. Carbonate cores are able to be dissolved under a slightly acidic conditions or in ethylenediaminetetraacetic acid (EDTA) solution (Borodina, Markvicheva et al. 2007). Furthermore, due to the porosity of calcium carbonate, the polyelectrolytes could penetrate core surface in deposition step which lead to a complex network constructing of capsules interior (Volodkin, Petrov et al. 2004).

Compare with carbonate templates, silicon oxide has more smooth surface and spherical shape, but these particles are dissolved in hazardous and aggressive solutions such as ammonium fluoride (NH_4F) or hydrogen fluoride (HF). These solvents are able to make the capsules aggregation, specially for the weak polyelectrolytes capsules (Adalsteinsson, Dong et al. 2004; Itoh, Matsusaki et al. 2004). Mono-dispersed gold particles with nanometers size have to be dissolved in a more dangerous solution of potassium cyanide (KCN) (Schneider and Decher 2004). Because inorganic templates can be completely removed and only few or no influence on polymer multilayer films structure, they are preferred template and well used for microcapsules preparation.

2.4.3 Stimulus-free encapsulation and release methods

Polyelectrolyte microcapsules have ability of trapping substances in the capsules cavity performs important property for its applications. Therefore, a large number of encapsulation methods have been studied. The desired materials with low solubility can be coated by polyelectrolyte for controlled and released. The disadvantage of this method is require the materials have appropriate sizes and shapes like crystals, particles aggregated or in nano-size (Lu, Möhwald et al. 2007; Prouty, Lu et al. 2007). Two typical methods are well used for substance encapsulation. One is combining the

desired substance with the template before polyelectrolyte deposition step, and another one is diffusing the substance through the microcapsules shell after hollow capsules fabrication.

Substances are encapsulated with carbonated particles template before capsules fabrication. The desired substance are pre-mixed with the chemical solution and then forming the template particles (Petrov, Volodkin et al. 2005; Borodina, Markvicheva et al. 2007); or immersing the template particles into the substance solution which is diffusing into carbonate porous structure (Sukhorukov, Volodkin et al. 2004).

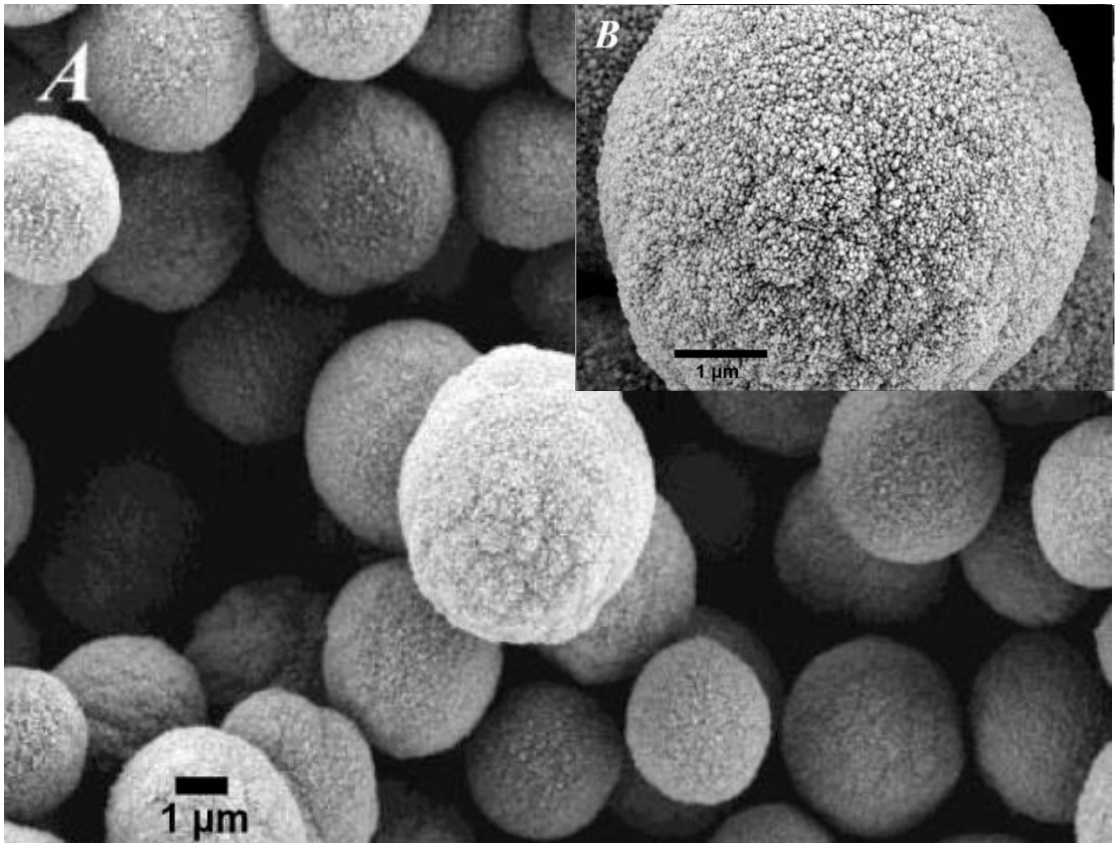

Figure 2.12: SEM images of $CaCO_3$ particles.
(A) overview of $CaCO_3$ particles and (B) porosity of $CaCO_3$ (Volodkin, Petrov et al. 2004)

Calcium carbonate particles as template are suitable for both pre- and after-loading encapsulation methods. After core dissolution the desired substance are encapsulated within the hollow polyelectrolyte microcapsules.

For size of desired substance is too big to pass through the polymer multilayers shell, or substance is affected by the conditions during LbL assembly process, the pre-loading method is better than after-loading method. (Kreft, Javier et al. 2007). An SEM image of $CaCO_3$ particles with a size of ~ 4 μm is shown in Figure 2.12 and the pores are clearly visible in the high magnification image.

Recently Kreft et al use this co-precipitation method to fabricate capsule in capsule, and each capsule contains different substance. The first desired material α is co-precipitated with $CaCO_3$ and absorbs a polymer layer shell. Then these capsules contain material α are co-precipitated with larger $CaCO_3$ particles with the second desired material β solution. Then, capsules are produced using LbL process (Kreft, Skirtach et al. 2007). EDTA is added to dissolve all $CaCO_3$ template cores, thus shell in shell microcapsules contains material β with an inside capsule contains material α are obtained.

Encapsulated substance releasing, capsules deformation and mechanical properties of capsules have been investigated (Cordeiro, Coelho et al. 2004). Atomic Force Microscope (AFM) is used for microcapsules shear stress and compression test (Lulevich, Radtchenko et al. 2003). Furthermore, certain enzymes change the permeability or degrade the shell of biological polyelectrolyte capsules, so the encapsulated materials are released (Kreft, Skirtach et al. 2007). Small molecules substance have also been studied by labeling on other materials and then encapsulated method (Gao, Donath et al. 2002).

2.4.4 Nanoparticles functionalized capsules

This part describes attachment of functionalized nanoparticles to the growth of multilayer films forming polyelectrolyte / nanoparticle layer. The formation of multilayer films depends on electrostatic interactions between

alternate layers of opposite charge. It was first introduced by Iler (Iler 1966) and developed by Decher (Decher and Schlenoff 2003). The composition of capsule shells can be tailored with metal nanoparticles. Therefore, these capsules are potential delivery vesicles in drug delivery system (Skirtach, Dejugnat et al. 2005).

2.4.4.1 Magnetite nanoparticles

Metal and metal oxide nanoparticles lead themselves to a variety of applications to the formation of polymer / nanoparticles composite films. Magnetite nanoparticles have small sizes varying from few nanometers to tens of nanometers. Property of magnetite nanoparticles obey Coulomb's law is very interesting. Therefore, an external magnetic field gradient is able to manipulate these particles. Furthermore, delivery substances or drugs with these particles are able to target a desired region.

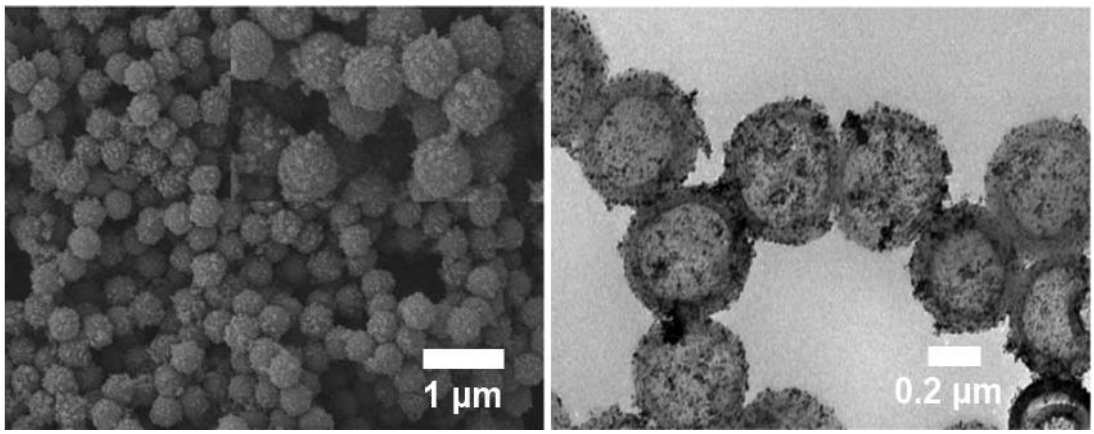

Figure 2.13: Images of capsules with magnetite nanoparticles.
SEM (left) and TEM (right) images show capsules with magnetite nanoparticles (Zhang, Zhou et al. 2013).

Figure 2.13 shows magnetic chitosan / poly (N-isopropylacrylamide) microcapsules. Magnetite nanoparticles are resonantly responding to a magnetic field, and absorb energy from the exciting field. (Pankhurst, Connolly et al. 2003). With magnetite nanoparticles, the drug is able to be

transferred to a targeted region under an external magnetic field and the release rate of the drug can be controlled under an external environment.

2.4.4.2 Gold colloid nanoparticles

Same as magnetite nanoparticles, Gold colloid Nanoparticles (GNP) can be incorporated with capsules shell by electrostatic interactions. Images of GNPs incorporated microcapsules are shown in Figure 2.14. These gold nanoparticles labeled capsules are sensitive to high temperature. Therefore, GNPs are used as trigger for encapsulated substance releasing near infrared in biomedical applications (Bédard, Braun et al. 2008). Better than visible or UV light, near infrared is able to penetrate deeper in living tissues. Remotely release the encapsulated substance at desired region is important in drug delivery.

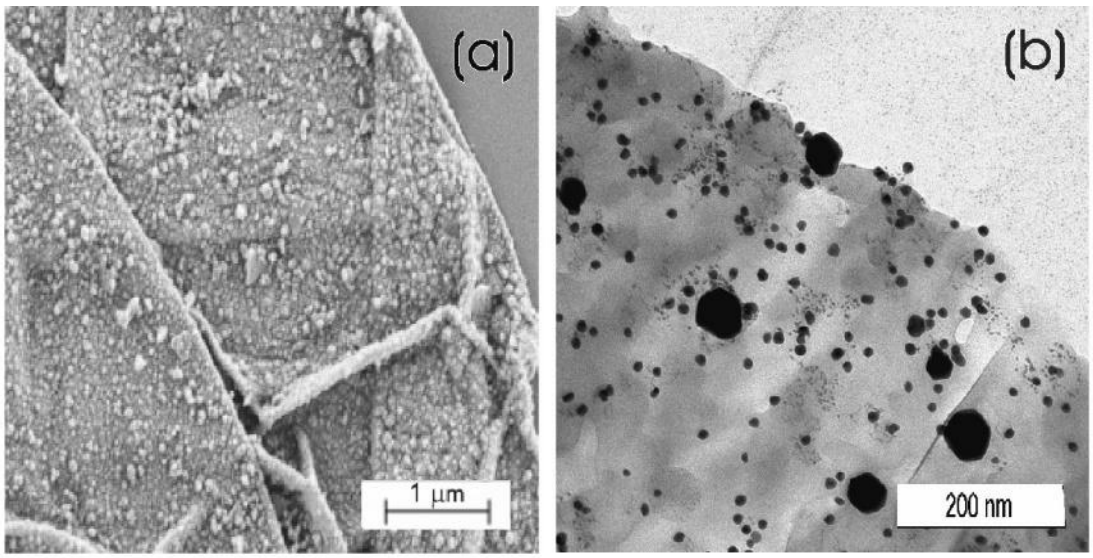

Figure 2.14: Images of GNPs incorporated capsules.
(a) SEM and (b) TEM images of (PAH/PSS) microcapsules contain GNPs in the shell. 10 nm non-aggregated gold nanoparticles and 20 to 50 nm gold sulfide core / gold shell nanoparticles can be seen in image b). (Skirtach, Dejugnat et al. 2005)

Gorin et al have fabricated biocompatible capsules with both magnetite and gold nanoparticles. These capsules are optically addressable and

susceptible to magnetic field (Gorin, Portnov et al. 2008). Moreover, GNPs always accompanied with stimulus responsive release method.

2.4.5 Stimulus-responsive encapsulation and release methods

Targeted delivery and controlled release of microcapsules contain desired substance play a very important role in investigation of microcapsules field. Most small ions as well as water molecules can easily pass the semi-permeable shell of the capsules (Klitzing and Moehwald 1995), but larger molecules are too big to pass the smaller pore size (Dong, Ferri et al. 2005). It depends on deposited polyelectrolyte, the conditions of the coating solution, the thickness of the shell and the template core used for capsule fabrication (Antipov, Sukhorukov et al. 2002).

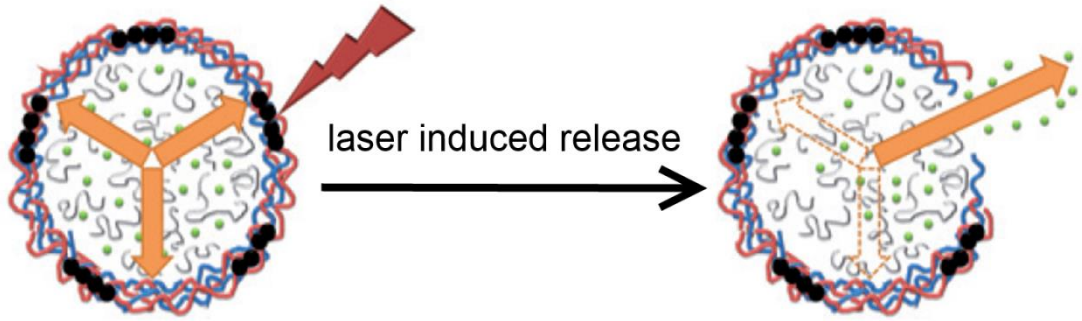

Figure 2.15: Schematic illustration of the laser induced opening of a capsule at a desired area.

(Bedard, De Geest et al. 2009)

For this encapsulation method, the release of the materials inside the microcapsule always accompanied triggers (De Geest, Sanders et al. 2007). Proximal and external are two types of triggers. Proximal trigger has to work within the solvent or present an interaction with the capsules such as appropriate pH, temperature and ionic strength (Gao, Leporatti et al. 2003; Déjugnat and Sukhorukov 2004; Georgieva, Dimova et al. 2005). External trigger directly works on the capsules with few or no influence on the solution, such as radiation, light, ultrasound, magnetic field and microwaves(Dalecki

2004; Kreft, Skirtach et al. 2007; Skirtach, Karageorgiev et al. 2008; Pavlov, Saez et al. 2011). Therefore, polyelectrolyte microcapsules are able to be remotely opened by these triggers to release encapsulated substances are very attractive for *in vitro* and *in vivo* experiments in drug delivery system.

2.5 Epithelial cells

Epithelial cells are firmly bounded cell layers cover internal and external surfaces of organs, also the primary component in human skin. These cells are very densely packed together without hardly any intercellular space. Epithelial cells are able to construct continuous layers that are connected the neighbors at many locations through several types of interactions, such as adherens junctions, tight junctions and desmosomes (Marieb and Hoehn 2007). Epithelial cells play a very important role at interfaces between the internal and external environments of the body. Because substances going in and out of the body have to pass through epithelium, the epithelial cells form an excellent biological barrier for drug delivery is of great interest to scientists.

2.5.1 Structure of epithelial cell

Figure 2.16 shows components of epithelial cells and characteristics of epithelial cell junctions. Epithelial cells are polarized and exhibit specific domains which are apical region, lateral region and basal region.

Apical region locates at the top of epithelial cell and faces the lumen or outside of the organ. Thus, apical region is also named free surfaces due to no connections between it and other cells or tissues. The free surfaces are the interface between epithelial cells and external environment. Apical region contains microvilli, cilia and the glycocalyx. Microvilli are tiny brush like plasma membrane evaginations of the apical surface. It significantly increased the absorptive capacity of epithelial cells. Cilia are also plasma membrane and locate in the tips of apical surface similar as microvilli. Moreover, cilia are motile and longer, thicker than microvilli (William and Krause 2005).

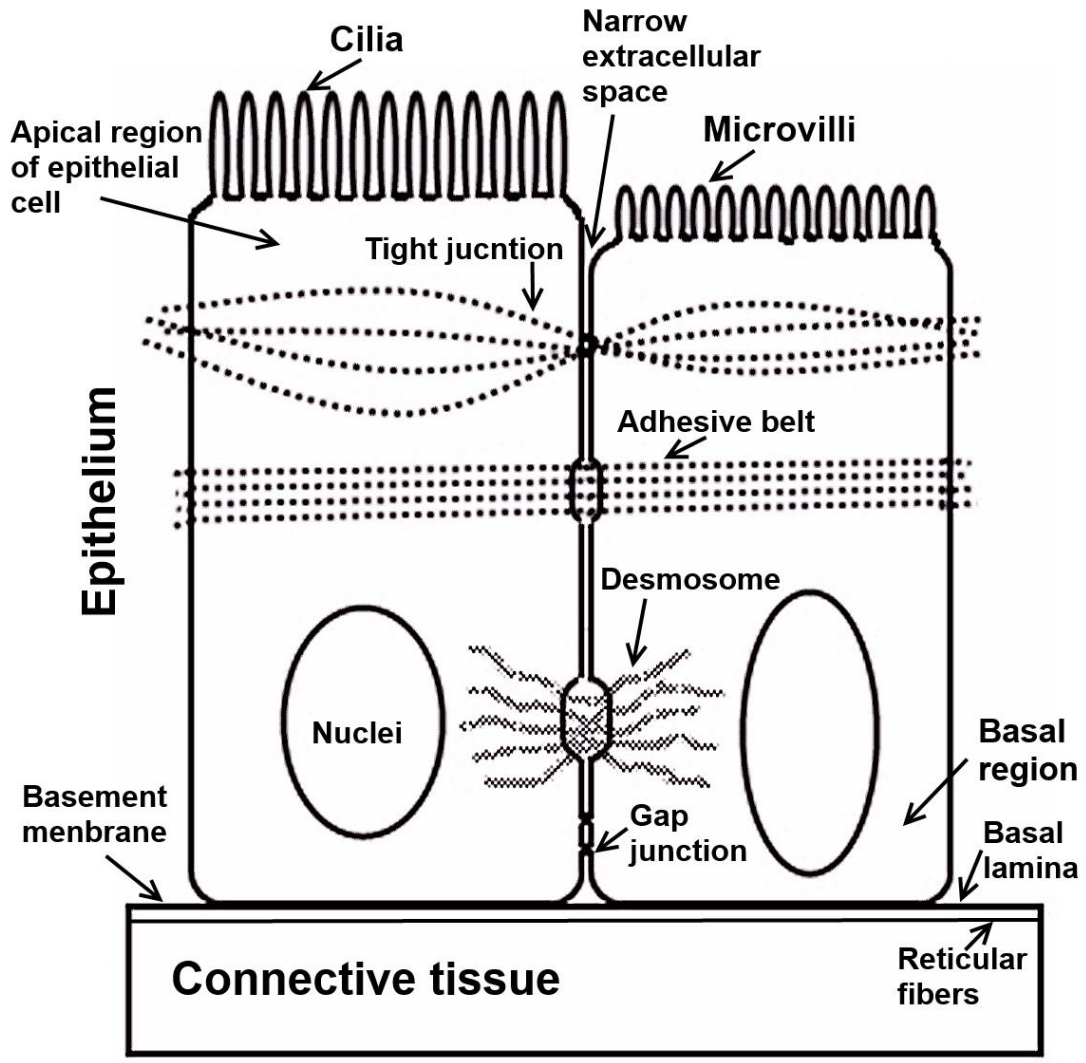

Figure 2.16: Characteristics of epithelial cell junctions.

Lateral region is most important functional surface in epithelial cells. It facing and connecting neighboring epithelial cells by junctional complexes. The lateral surfaces are the interfaces between epithelial cells, and contain tight junctions, adhering junctions, desmosome and gap junctions.

Tight junction is closest junctions in epithelium locates just beneath the apical surface, and firmly associates cells membrane and forms almost impermeable barrier to fluid. Thus, substances enter or exit the epithelial layer have to penetrate the cell membranes not the intercellular gaps between cells. Adhering junction is belt like junctions at the top of epithelial cells locates below tight junctions. There is a 15 to 20 nm wide space

between adjacent cell membranes. Desmosomes have elliptical shape construct spot like adhesions of attachment between cells lateral sides of plasma membranes. The intercellular space is up to 30 nm wide. A huge amount of desmosomes exist in stratified squamous epithelial cells. Gap junction (also named nexus) is a junctional area between adjacent cells and permits intercellular passage of ions, amino acids, and other small molecules. (William and Krause 2005)

Basal region locates at bottom of epithelial cells, faces the basal lamina adjacent to underlying connective tissue and blood vessels. Basement membrane is a thin layer supports epithelial cell, and formed by basal lamina and the reticular lamina. Basal lamina is an extracellular matrix layer produced by epithelial cell. The reticular lamina is formed by reticular fibers produced by the underlying connective tissues, and linked with Basal lamina by anchoring fibrils. Moreover, the nucleus of the epithelial cell is located around the basal region not the apical region.

2.5.2 Classification of epithelial cells

Glandular or lining are the two types of epithelium. Glandular epithelial cells adapted specifically for secretion constitute the glands. Lining epithelial cells protect the organs by covering and lining all body surfaces. Lining epithelial cells can be classified as simple and stratified epithelial cells. Simple epithelial cell has a single layer of cells, and the stratified one contains multiple cell layers.

Due to the geometric shapes of the epithelial cells, they can be classified into three types: squamous, cuboidal and columnar. Thus, they are further divided as simple squamous, simple cuboidal and simple columnar; also three stratified types. Figure 2.17 shows these types of epithelial cells.

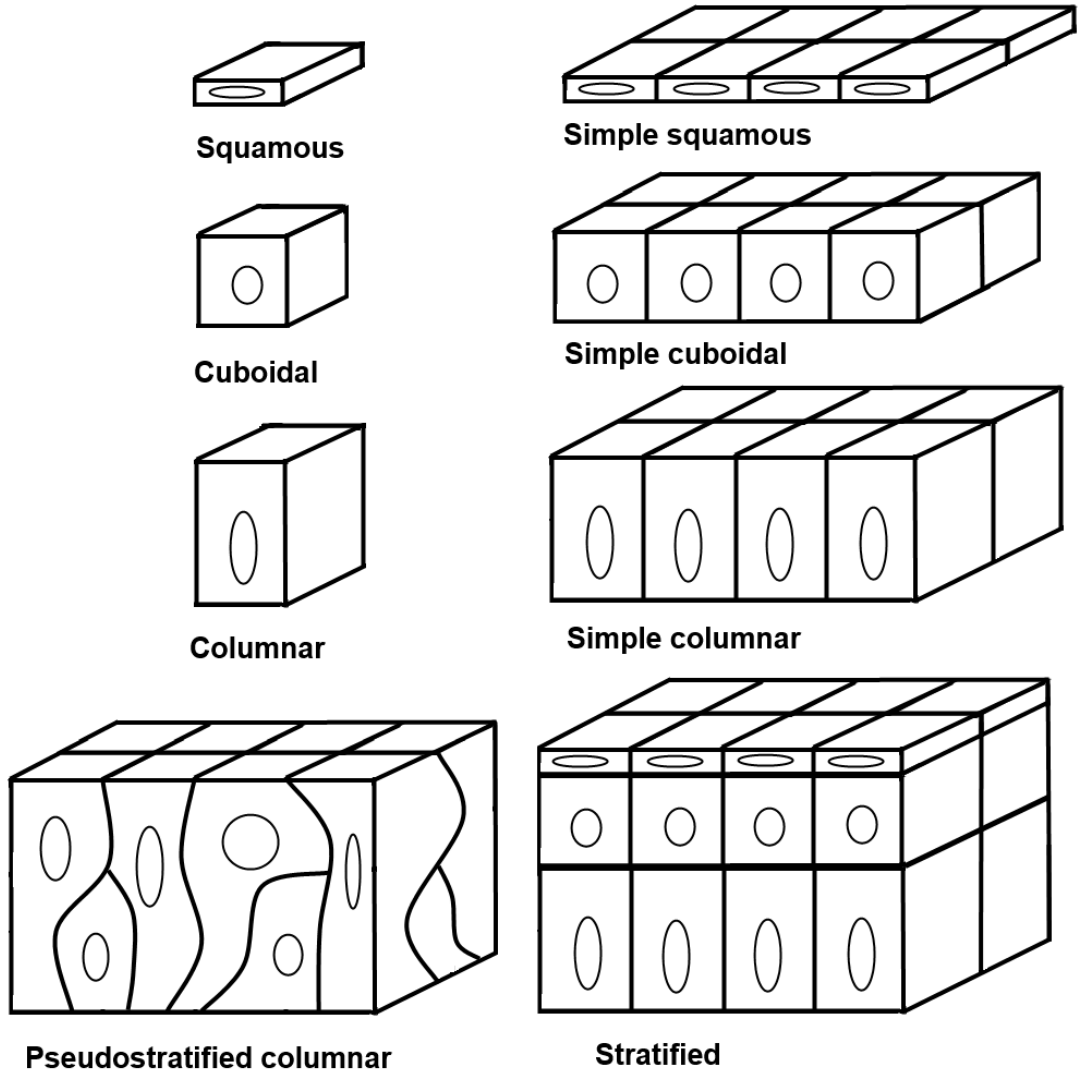

Figure 2.17: Classification of epithelial cell.

Simple squamous is a monolayer of thin, flattened and scale like cells. Squamous shape generates large surface area that touches with lumen and basement membrane. The nucleus of this cell is large and with elliptically shape. Due to one cell thickness layer, small molecules are easily penetrating the membrane and pass the cell. Simple cuboidal is a monolayer of cells has length similar as width. It has large and spherical nuclei that usually at the central of the cell. Simple columnar epithelial cells are a monolayer of cells that are taller than width. This cell with taller property gives a great protection with a single layer. Molecules cannot pass this thick layer by diffusion, and can be absorbed by active transport to pass the layer.

Pseudo-stratified columnar epithelium in left corner of Figure 2.17 is the fourth type of simple epithelial cells. It is formed by more than one type of simple epithelial cell with nuclei at different levels. All the cells in pseudo-stratified columnar type are directly touching with the base membrane, but not all cells reach the free surface. Stratified Epithelium in right corner of Figure 2.17 is constructed by minimum two layers of cells, but only the bottom layer is attached to the base membrane. Thus, stratified epithelial cells are thicker and provide more protection than the simple types.

2.6 Vascular endothelial cells

Luminal surface of blood and lymphatic vessels are fully covered by vascular endothelial cells. It has various functions in vascular biology, such as tissue homeostasis, fibrinolysis and coagulation, blood-tissue exchange, vascular regulation, the vascularization of various tissues, and blood cell activation and migration during physiological and pathological processes (Risau 1995).

2.6.1 Glycocalyx layer

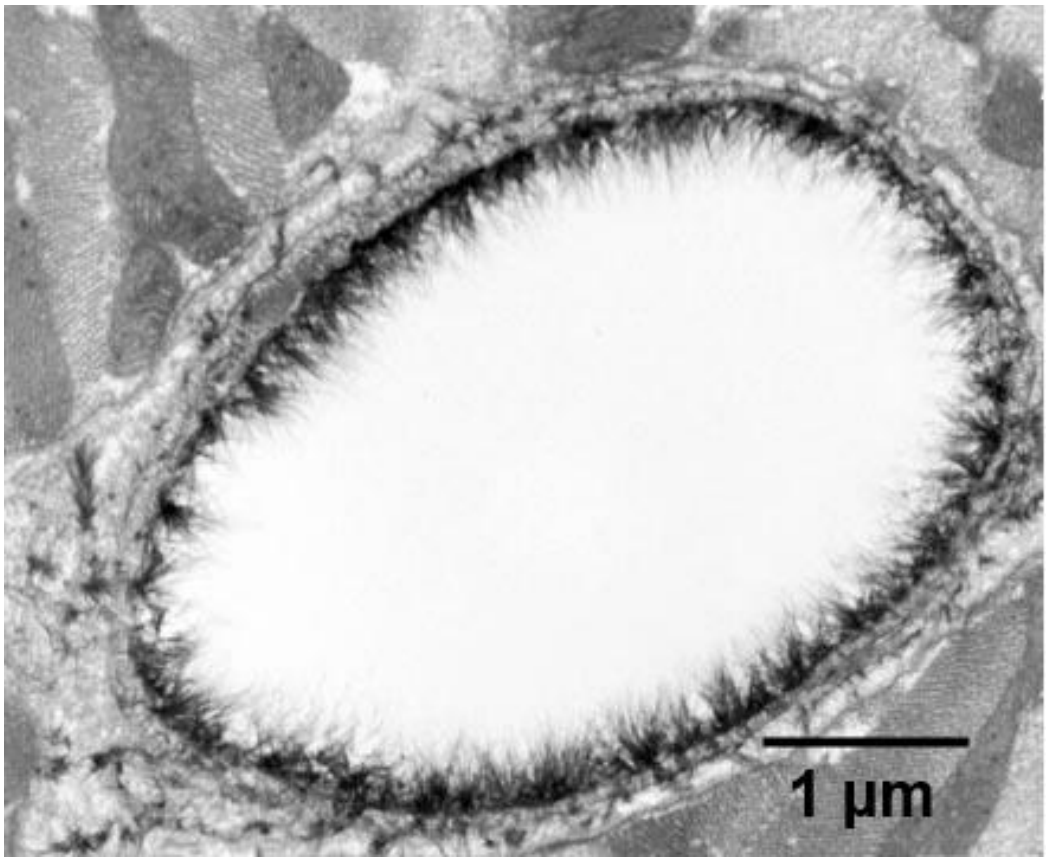

Figure 2.18: Electron microscopy image of coronary endothelial glycocalyx.
(van den Berg, Vink et al. 2003)

An endo-capillary layer has been found on endothelial cells by Luft (Luft 1966). This layer is un-informing with a fluffy structure is shown in Figure 2.18.

Figure 2.18 shows the shape of glycocalyx has a brush like conformation, and locates on the luminal surface of the endothelial cells. It has a negative charge and formed by a matrix of proteoglycans, glycolsaminoglycans, and glycoproteins. The shape and size of endothelial glycocalyx layer are affected by blood plasma proteins and molecules (Pries, Secomb et al. 2000).

Furthermore, ionic strength, pH value of plasma and other factors in the micro environment have significantly influence the glycocalyx layer shape (Seog, Dean et al. 2005; van Haaren, VanBavel et al. 2005). Squire et al propose glycocalyx on cell membrane layer with is linked to actin cytoskeleton (Squire, Chew et al. 2001).

Image (A) of Figure 2.19 shows complex distributed cytoplasmic structural actin (DCSA) network connect with apical and basal cell membranes physically. DCSA network is a signaling pathway from membrane to nucleus and able to transfer mechanical forces through the cells (Satcher, Dewey Jr et al. 1997). The glycocalyx is located on the luminal surface of the cell which connects the underlying endothelial cell cortical cytoskeleton.

In Figure 2.19 (B), this model gives a definition of the endothelial glycocalyx which are formed by the matrix of macromolecules. Squire et al suggest the thickness of endothelial glycocalyx layer to be around 200 nm. The gap between paralleled fibrous of the glycocalyx layer is approximate 20 nm, located perpendicular to the cell surface (Squire, Chew et al. 2001).

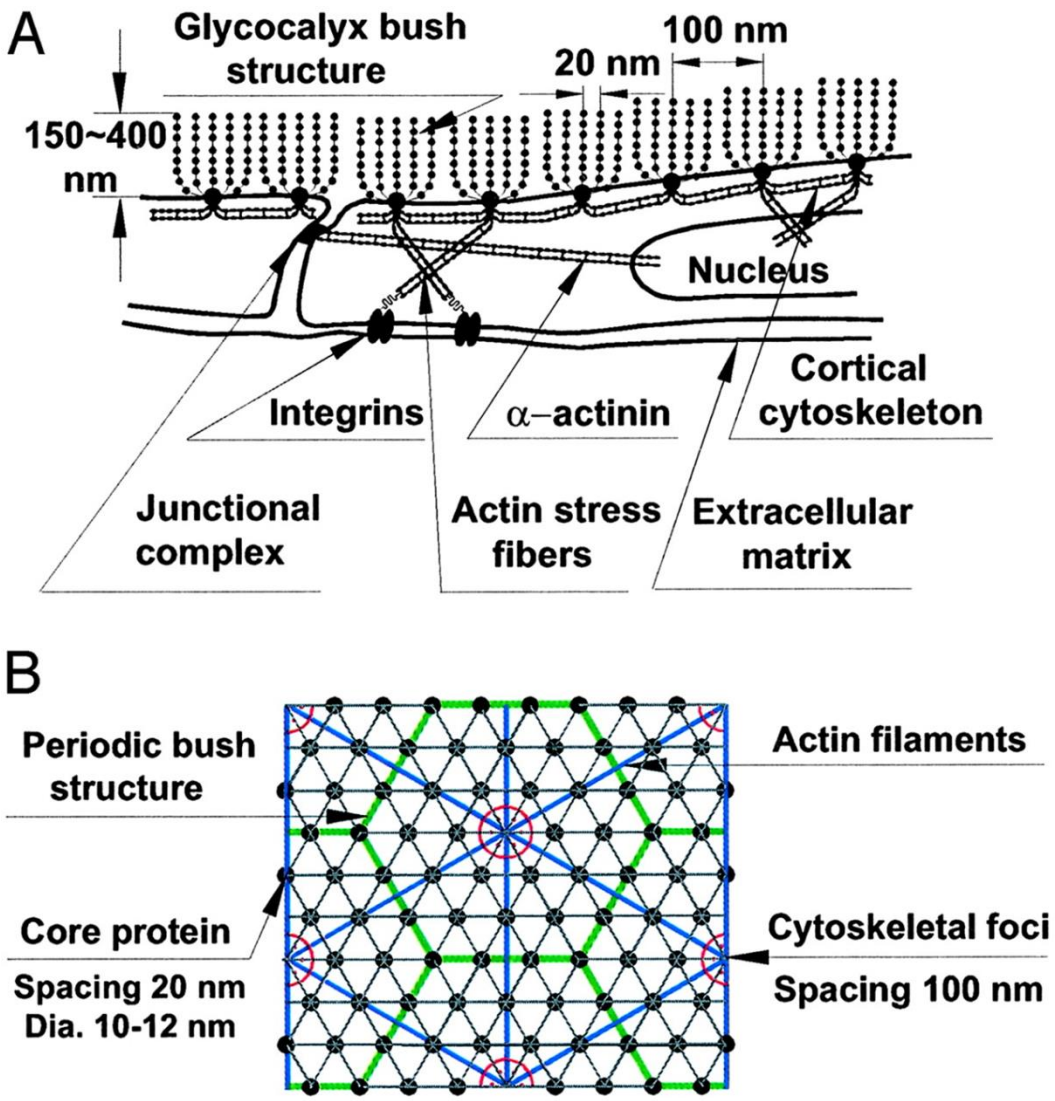

Figure 2.19: Endothelial glycocalyx layer model

A) Schematic illustration of Endothelial glycocalyx layer model presenting core protein arrangement and spacing of scattering centers along core proteins and their relationship to actin cytoskeleton as proposed by Squire. B) Idealized model for core protein clusters and cluster foci and their relationship to hexagonal actin lattice in cortical cytoskeleton (Weinbaum, Zhang et al. 2003).

2.6.2 Composition of glycocalyx

The endothelial glycocalyx with layer structure contains large amount of carbohydrate, form a line on the vascular endothelium which are connected with backbone molecules. Most of the molecules are proteoglycans and

glycoproteins, as well as some soluble molecules. A dynamic equilibrium exists between this layer of complex and the flowing blood, and continuously influences the glycocalyx thickness and components. Therefore, the glycocalyx is in a static condition, thus its components cannot be viewed and geometry is difficult to present (Lipowsky 2005).

2.6.2.1 Proteoglycans

The major functional backbone molecules of glycocalyx are formed by one of the most important component named proteoglycans which is *O*-glycosyl linkage c glycoproteins. Proteoglycans are found on the surface of endothelial cells and in the extra cellular matrix. It is affected by several growth factors such as fibroblast growth factor (Presta, Statuto et al. 1992), platelet-derived growth factor (Raines and Ross 1992) and transforming growth factor (Segarini PR 1989).

Proteoglycans are formed by covalently banded core protein of carbohydrate polymers with long and un-branched structure which are known as glycosaminoglycans (Pries, Secomb et al. 2000). Different core proteins attached by different glycosaminoglycan chains which contain different size, number and properties. Some of the core proteins are bounded to the cell membrane while others are not, and these core proteins form different proteoglycan. There are six groups of core protein which are classified as: syndecan, glypican, perlecan, versican, mimecan and biglycan. The first three types of core protein are main proteins of endothelial cells. Moreover, syndecan and glypican proteins are connected with the cell membrane; perlecan is not directly incorporated to the cell membrane.

2.6.2.2 Classification of Proteoglycans

Syndecans have a firm connection to the cell membrane via a membrane

spanning domain (syndecans) (Carey 1997). Its tail penetrate inside the cell cytoplasm and connect with the endothelial cytoskeleton, leads to assisting in reorganization of the cytoskeleton (Yoneda and Couchman 2003). Endothelial cells contain three types of syndecan, each of them with three glycosaminoglycan attachment sites which are usually occupied by heparan sulphate (Rosenberg, Shworak et al. 1997).

Glypican incorporate with the cell membrane via a glycosylphosphatidylinositol anchor (glypicans), and contains three or four glycosaminoglycans attachment sites which are only can be occupied by heparan sulphate (Fransson, Belting et al. 2004). The heparan sulphate chains attached on glypicans are typically combined with plasma membrane regions where contain caveolin-1 (Deurs, Roepstorff et al. 2003).

Perlecan is secreted by endothelial cells and interacts with collagens, laminin, and other components within the membrane of the basement (Murdoch, Dodge et al. 1992). Except these main core proteins, other proteoglycans exist as the soluble element of the glycocalyx, such as mimecan and biglycan. These soluble proteoglycans stay in the glycocalyx or spread into the blood flow (Reitsma, Slaaf et al. 2007).

2.6.2.3 Glycosaminoglycan chains

Glycosaminoglycan chains are linear polysaccharides in the extracellular matrix that contain characteristic disaccharide unit (Jackson, Busch et al. 1991). For endothelium glycocalyx, heparan sulphate, chondroitin sulphate, dermatan sulphate, keratan sulphate, and hyaluronan are five types of glycosaminoglycan chains that have been discovered yet (Reitsma, Slaaf et al. 2007).

Among these glycosaminoglycan chains, heparan sulfate proteoglycans

are estimated 50 - 90 % of the total proteoglycans within the glycocalyx (Ihrcke, Wrenshall et al. 1993). 15 - 24 % of the proteoglycans are formed by chondroitin sulphate proteoglycans which locate on the cell surface (Rapraeger, Jalkanen et al. 1985). Most of both largest glycosaminoglycan chains are attached on core proteins of trans-membrane syndecans and membrane bound glypicans (Pries, Secomb et al. 2000). The number of glycosaminoglycan chains attached to the core proteins are influenced by many factors, such as physiological state and the location of the tissue (Geary, Koyama et al. 1995; Li, Brown et al. 1997).

2.6.2.4 Glycoproteins

Compare with proteoglycans, glycoproteins are also known as primary backbone molecules and contain long linear side chains which connect with the glycocalyx to the endothelial cell membrane. These endothelial glycoproteins typically contain adhesion molecules and components of the coagulation and fibrinolysis system. (Reitsma, Slaaf et al. 2007). Changing of glycoproteins present on the endothelial cell membrane depend on cell activation or stimulation.

Sialic acid distributes widely in glycoproteins. It is a monosaccharide with a nine-carbon backbone and derivative of neuraminic acid (Varki, Cummings et al. 2009). High density of glycoproteins contain large amount of sialic acid form a negative charge on cell membranes and generate repulsion between cells (Fuster and Esko 2005). Most of the endothelial glycocalyx layers components are summarized in Figure 2.20

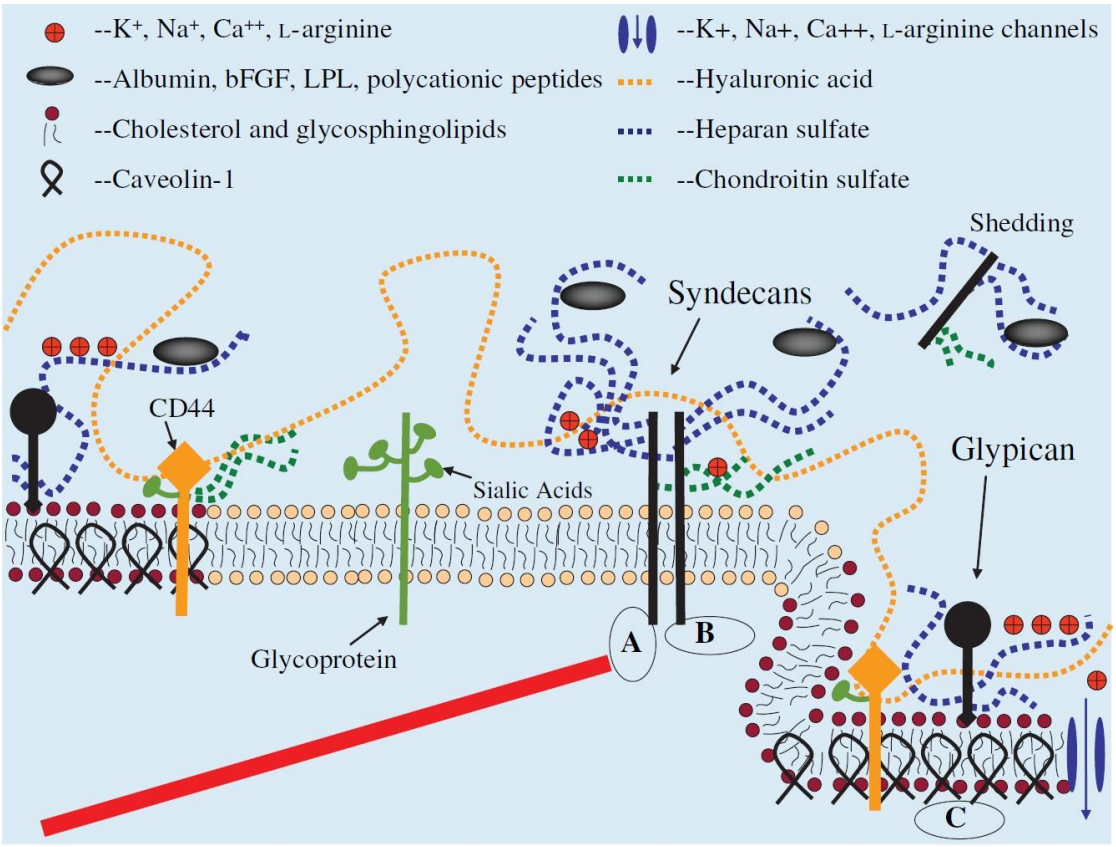

Figure 2.20: Schematic illustration of endothelial glycocalyx
It contains proteoglycans and glycoproteins on the luminal surface of endothelial cells.

Caveolin-1 forms as a tilted α shape connects with regions in the membrane where are located of glypicans with heparin sulphate chains. Trans-membrane syndecans contain both heparin sulphate and chondroitin sulphate chains are present as clusters. A glycoprotein contains short oligosaccharide branched chains and attached sialic acids are marked in the Figure. Hyaluronic acid is a long glycosaminoglycan chains weaves into the glycocalyx and binds with the cell membrane receptor CD44 which stay with caveolin. The cytoplasmic domains of syndecans could combine with molecules which connect to cytoskeletal elements (red line). (Tarbell and Pahakis 2006).

2.7 Interactions between microcapsules and cells

In recent years, progress have been developed in understanding the delivery mechanism of microcapsules into cells *in vitro* and *in vivo* (Sukhorukov, Rogach et al. 2007; Muñoz Javier, Kreft et al. 2008; An, Kavanoor et al. 2009; De Koker, De Geest et al. 2009; Rivera-Gil, De Koker et al. 2009; Vergaro, Scarlino et al. 2011). Internalization of microcapsules by cells was first reported by Gleb et al in 2005 (Sukhorukov, Rogach et al. 2005). Diameter of 5 μm polyelectrolyte capsules and breast cancer cells of the cell line MDA-MB-435s used in the report. Figure 2.21 shows a successful internalization of capsules by breast cancer cells.

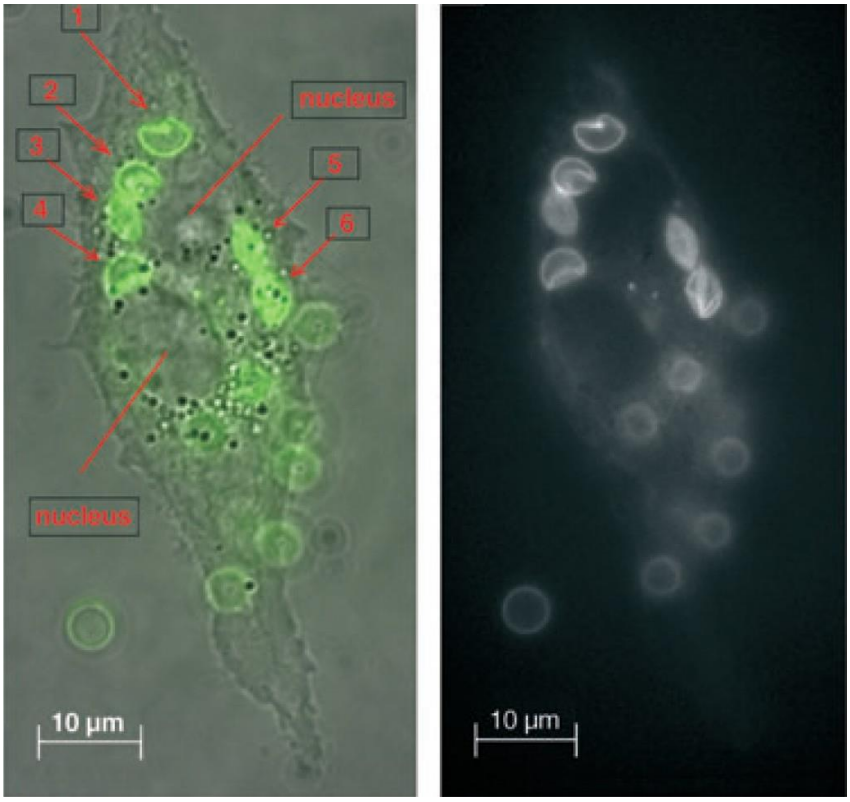

Figure 2.21: Images of human breast cancer cell with internalized capsules.
Left image is overlay of phase contrast and fluorescence image, and right image is fluorescence image. Capsules are coated with negatively charged fluorescent CdTe QDs (Sukhorukov, Rogach et al. 2005).

Internalized capsules with a non-spherical shape locate around the nuclei of cell. Non-internalized capsules are however still remaining in their original shape. After 48 hours capsules / cells co-incubation time, more than 95 % of cells contain capsules observed by CLSM. They also demonstrated a single cell is able to internalize up to 40 capsules. To further determine whether capsules are internalized by cells or not, pH-sensitive fluorescent seminaphtho rhodafluor 1 dye (SNARF1-1) is introduced.

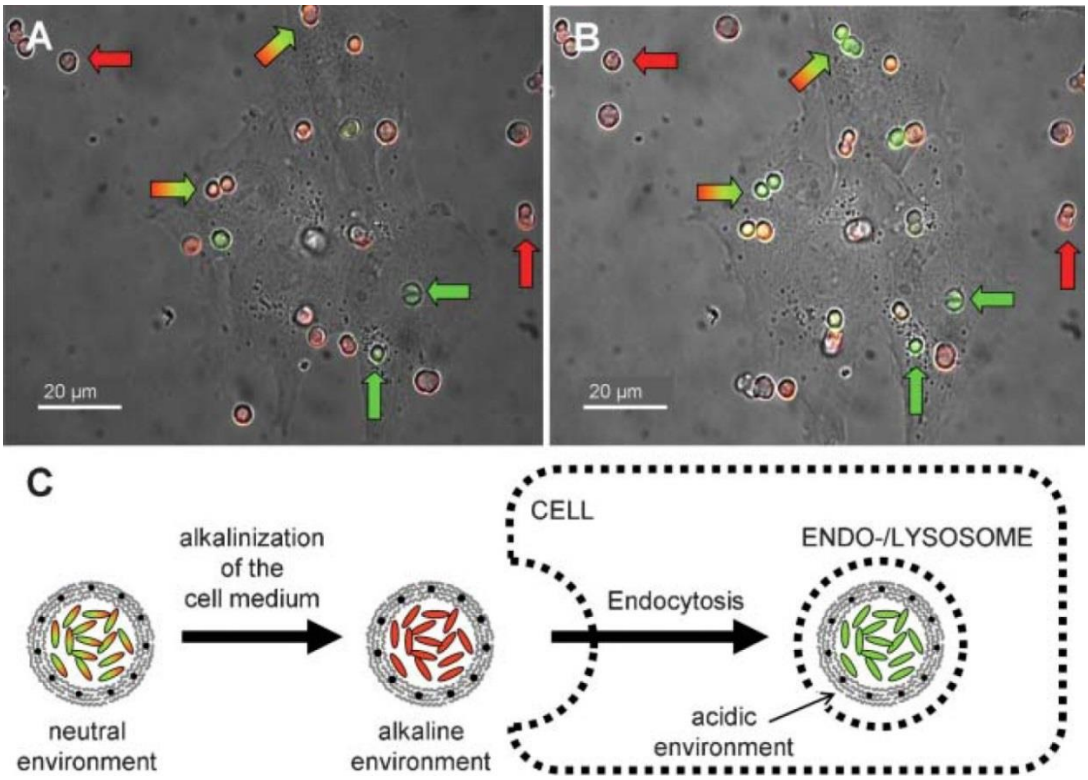

Figure 2.22: SNARF loaded capsules internalized by breast cancer cells.

Image (A) and (B) are CLSM images; (C) is general process of the test. (Kreft, Javier et al. 2007)

Kreft et al presented interactions between SNARF loaded capsules and breast cancer cells. After 5 hours of capsules / cells co-incubation time, culture medium is changed to an alkaline condition of pH 9.5. SNARF dye presents red colour in alkaline condition, and green colour in acidic environment of endosome. Image (B) of Figure 2.22 is the same cells in image (A) after another 30 min of co-incubation. The colour of capsules

changed from red to green proves they are internalized by the cell within 30 min.

Koker et al published intracellular delivery of biodegradable microcapsules formed by Dextran Dulphate (DS) and Poly-L-arginine (PArg) to dendritic cells in 2007 (De Koker, De Geest et al. 2007). MTT assay is used to test cytotoxicity of DS/PArg capsules. They demonstrate moderate number of capsules is not significantly affect cells viability. Biocompatibility of these capsules is tested *in vivo*. 4 layers capsules are subcutaneous injected into mice, after 30 days, inflammation remains local and no necrosis is observed.

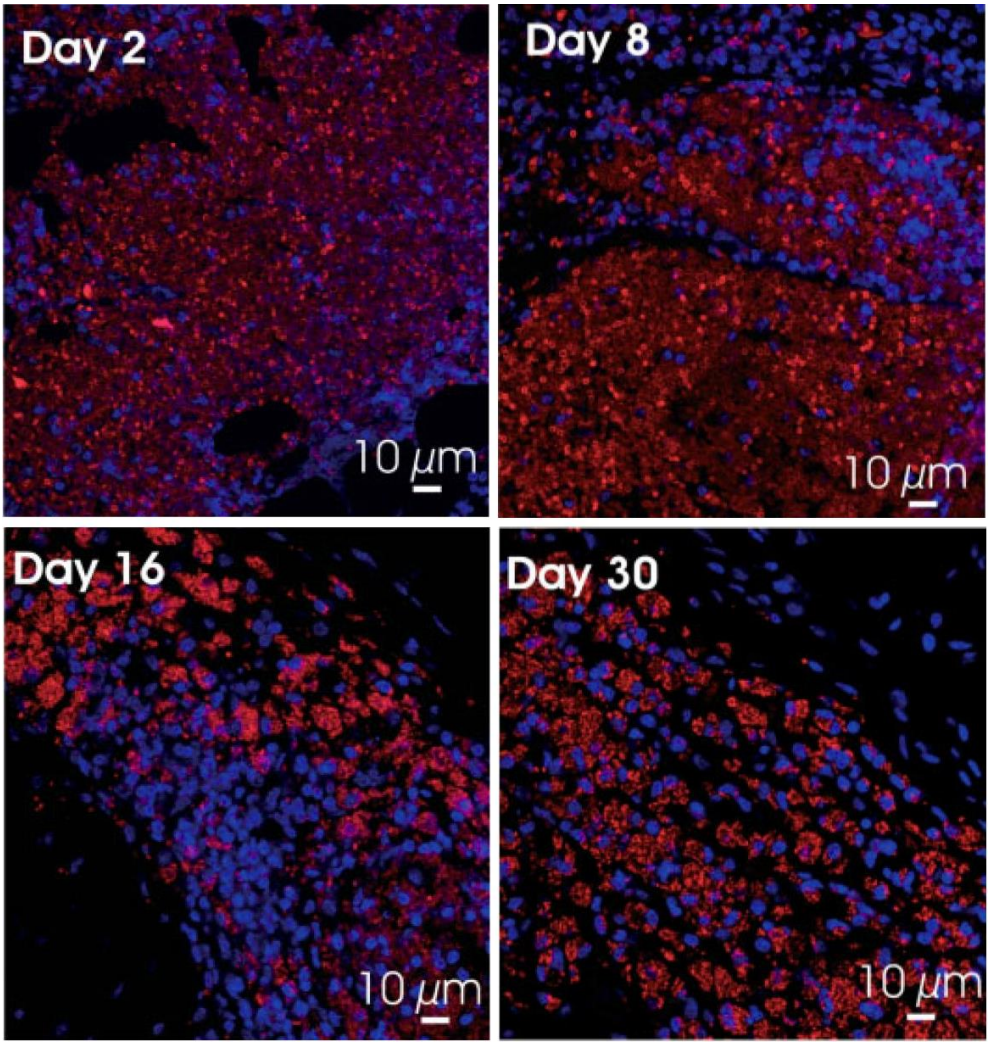

Figure 2.23: CLSM images of tissue sections after injection of microcapsules.

(De Koker, De Geest et al. 2007).

Figure 2.23 shows a large area of the injection site as an overlay of DS/PArg capsules (red) and nuclei (blue). Capsules with deformed and shrunk shape are internalized by cells; while non-internalized capsules remaining the same shape as injection. Moreover, internalization of capsules by cells always last for long time.

SEM images of capsules internalization by B50 rat neuronal cells has been reported by Pavlov et al in 2011 (Pavlov, Saez et al. 2011). In Figure 2.24, a capsule with intact $CaCO_3$ particle is internalized by the cell is shown. Focused ion beam milling is used in Figure 2.24 (b), in upper corner, rigid particle of $CaCO_3$ to provide a strong contrast.

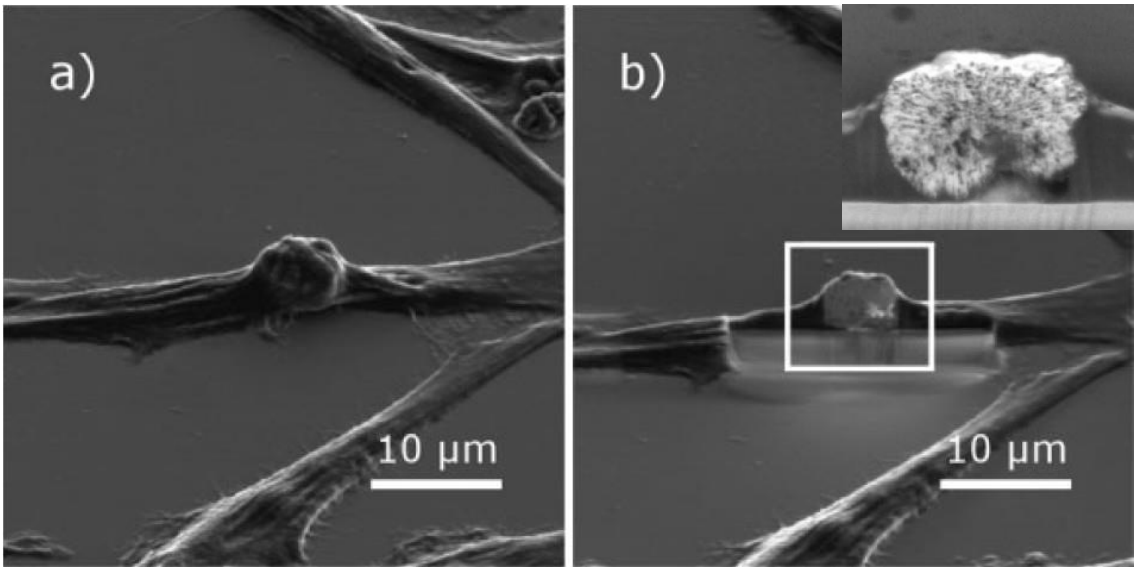

Figure 2.24: SEM images of a micro particle inside a neural cell.
(a) a cell contains a capsule, (b) focused ion beam milling at the bulge area, magnified region of (b) in upper corner showing porous $CaCO_3$ core (Pavlov, Sapelkin et al. 2011).

The above cells are all phagocytic cells, such as cancer cell. Internalization of capsules by non-phagocytic cells has not been published yet. Therefore, investigation of interactions between capsules and non-phagocytic cells becomes a great challenge.

3 Objectives and Approach

Microcapsules are suitable vehicle for various applications, most importantly as drug delivery. Thus, the aim of this project is to investigate the interactions between microcapsules and two types of cells namely epithelial and endothelial cells. The interactions of microcapsules and the cells are investigated by physical and biochemical stimuli.

First, the fabrication and characterization of microcapsules are carried out. Two typical types of microcapsules are fabricated through Layer-by-Layer (LbL) assembly technique. One is constructed by synthesis polyelectrolytes of PSS/PAH, and another is formed by biodegradable polyelectrolytes of DS/PArg or DS/PLL. Capsules are functionalized with super paramagnetic nanoparticles or gold nanoparticles. Fluorescent dyes and/ or enzyme are encapsulated for designed experiments.

The interactions between capsules with magnetite nanoparticles and epithelial cells are performed by physical means. Magnetite nanoparticles modified DS/PLL-FITC capsules are prepared and co-incubated with epithelial cells. A magnet is placed under the cell container to provide magnetic field. Capsules with magnetite nanoparticles are attracted to the well bottom by the magnet. DS/PLL-FITC microcapsules are prepared as control sample. Due to cancer cells are able to internalize microcapsules in hours spontaneously (Sukhorukov, Rogach et al. 2005; De Koker, De Geest et al. 2007; De Cock, De Koker et al. 2010), 5 and 10 minutes are chosen as co-incubation time of both capsules with magnetite nanoparticles and control capsules. The comparison of capsules number and location in both samples is observed using CLSM.

The main part of this thesis focuses on investigation of interactions between capsules and non-phagocytic cell of Human Umbilical Vein

Endothelial cells (HUVECs). Discover the role of the glycocalyx of HUVECs on trans-membrane movement of microcapsules *in vitro*. Toxicity analysis of the polyelectrolytes is checked by co-incubation of sterilized PSS/PAH capsules and HUVECs. These capsules are treated by autoclaving procedure at 126 ^{o}C for 40 minutes, and then incubated with HUVECs for up to 14 days. Then, characterization of capsules affected by the culture medium is studied.

The biochemical method of investigating interactions between HUVECs and capsules is performed by encapsulation of an enzyme named neuraminidase. Neuraminidase enzyme is able to cleave the neuraminic acid component of the glycocalyx on endothelial cells, such as sialic acid residues and N-acetyl-D-glucosaminyl residues of glycoproteins. Encapsulation efficiency and the release rate of neuraminidase in 4 layers capsules are analyzed. Samples of neuraminidase loaded capsules and HUVECs co-incubation and control samples are prepared for CLSM observation. Research of biological degradation of DS/PArg capsules in HUVECs is performed by distribution analysis of encapsulated TRITC-dextran in cytoplasm. Investigation of HUVECs transfection using co-incubation of cells with neuraminidase and DNA plasmid loaded capsules are also carried out. Green fluorescence protein expression of transfected HUVECs are checked by CLSM. Commercial transfection reagent Fugene 6 is tested as control.

The mechanisms of uptake of microcapsules by living cells are not fully understood and are still under investigation. The internalization and degradation of microcapsules by non-phagocytic cells had been not yet published. Therefore, the main experiment is aiming better performance of microcapsules with normal healthy cells in drug delivery system.

4 Materials

4.1 Materials

4.1.1 Polyelectrolytes for Capsule Preparation

All polyelectrolytes used for microcapsules fabrication are shown in Table 4.1. Two typical microcapsules were prepared from PSS/ PAH and degradable DS/ PArg (PLL) respectively. Figure 4.1 shows the chemical structural of the polyions. All the polyelectrolytes were purchased from Sigma Aldrich and used without further purification.

Polyelectrolyte	MW(kDa)	Abbreviation
Poly (styrenesulfonate sodium salt)	*70*	PSS
Poly (Allylamine hydrochloride)	56	PAH
Dextan sulfate sodium salt	100	DS
Poly (l-arginine) hydrochloride	15 - 70	PArg
FITC-labelled poly-L-Lysine	15 - 30	FITC - PLL

Table 4. 1: Overview of polyelectrolytes used for capsule preparation

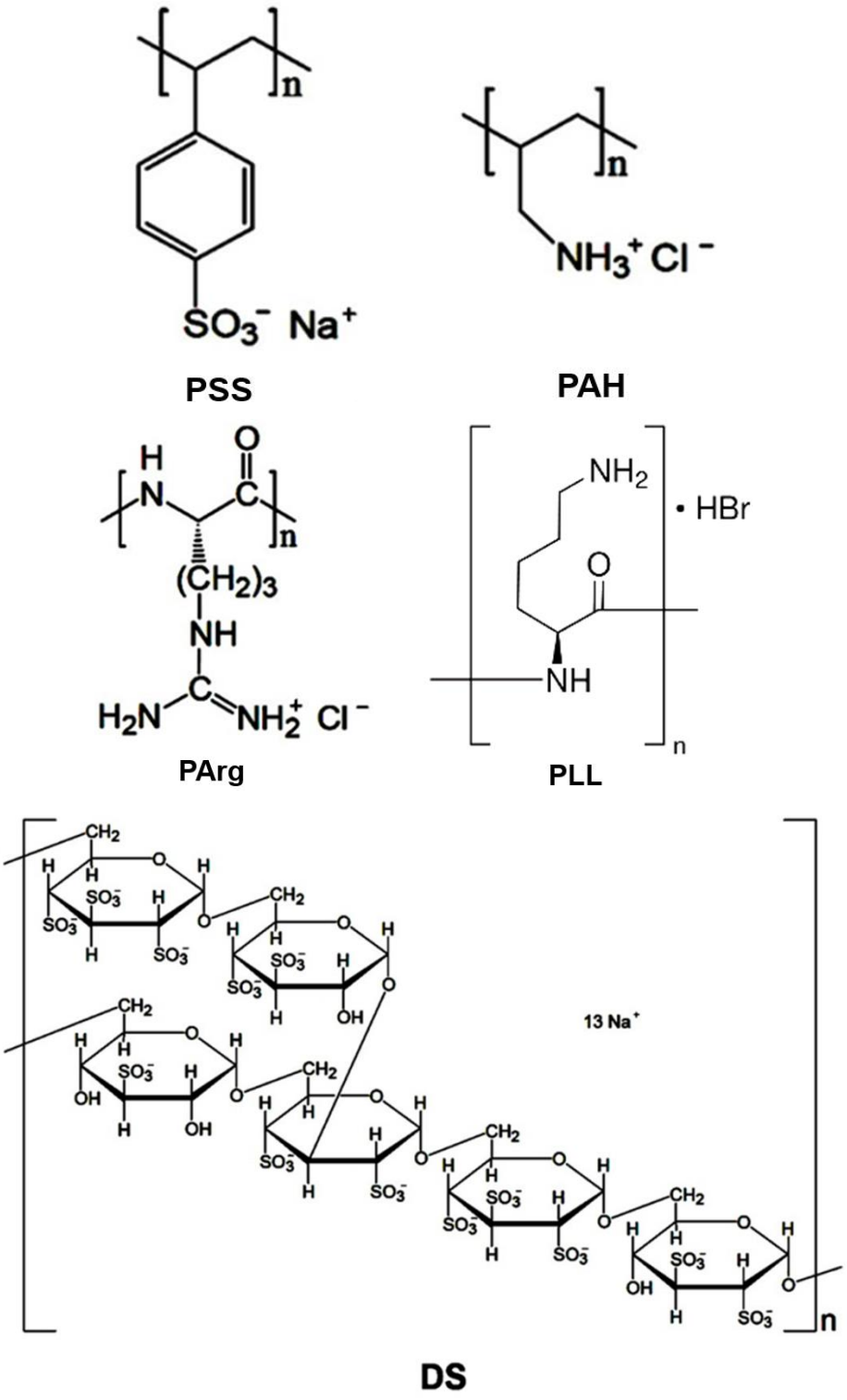

Figure 4.1: Structural formulas of polyelectrolytes for capsule preparation.

4.1.2 Fluorescent dyes and labeling

Fluorescent dyes of TRITC and FITC w used for encapsulation or labeling. Molecular weights of both dyes are given in Table 4.2 as well as TRITC labeled dextran sulfate and BSA. The chemical structure of FITC and TRITC are shown in Figure 4.2.

Reagent	Mw(Da)	Abbreviation
Fluorescein isothiocyanate isomer I	389.38	FITC
Tetramethylrhodamine isothiocyanate mixed isomers	443.52	TRITC
Tetramethylrhodamine isothiocyanate–Dextran	65 – 85 k	TRITC-dextran
Tetramethylrhodamine isothiocyanate–BSA	66 k	TRITC-BSA

Table 4.2: Overview of fluorescent dyes used for encapsulation or labeling.

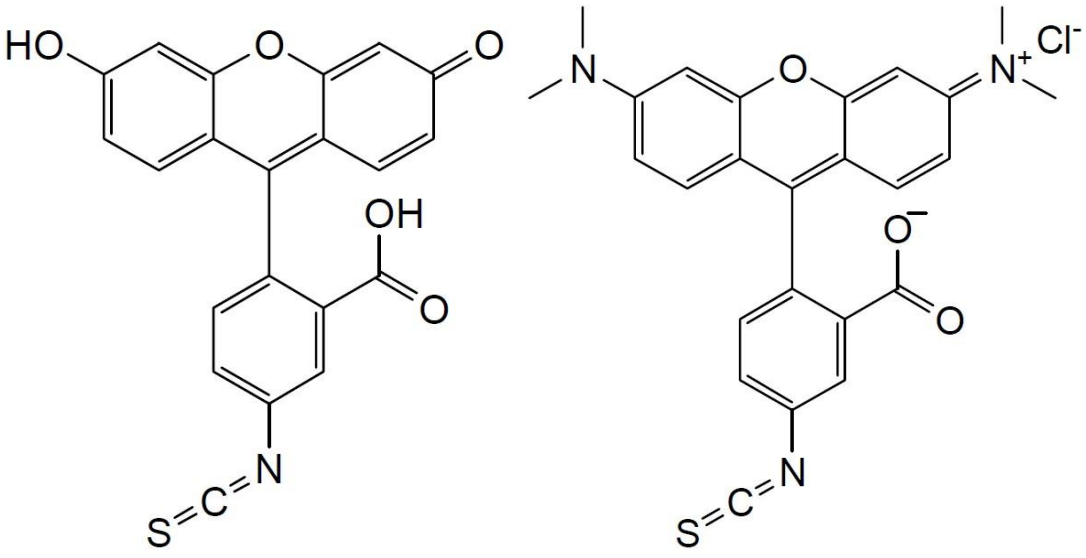

Figure 4.2: Structural formulas of fluorescent dyes.
Structure of FITC (left) and TRITC (right).

A general protocol for the modification of proteins, particularly immunoglobulin with TRITC (Hermanson 1996) is given below:

1: Protein solution of DS or BSA was prepared at concentration of 2 mg/ml in 0.1M sodium carbonate with pH 9.0.

2: In a dark environment, TRITC was dissolved in dry dimethyl sulfoxide (DMSO) at concentration of 1mg/ml. The solution was protected from light.

3: TRITC solution (step 2) was added into the protein solution (step 1) with the ratio of 0.05:1. The number of fluorochrome molecules per protein molecule is defined as the F/P ratio. For TRITC labeled protein, the ratio is controlled in the range from 0.3 to 0.7.

4: The solution was continuously stirred for 8 hours at 4 °C in the dark environment.

5: Dialysis process was applied to remove the unlabeled TRITC. The solution was moved into the dialysis bags (*MW* cut-off 14 kDa) and immersed in Milli-Q water for one week. The water was changed twice every day, until no fluorescence was detectable in the external solution.

The general reaction mechanism of TRITC and amine-containing molecules shows in Figure 4.3

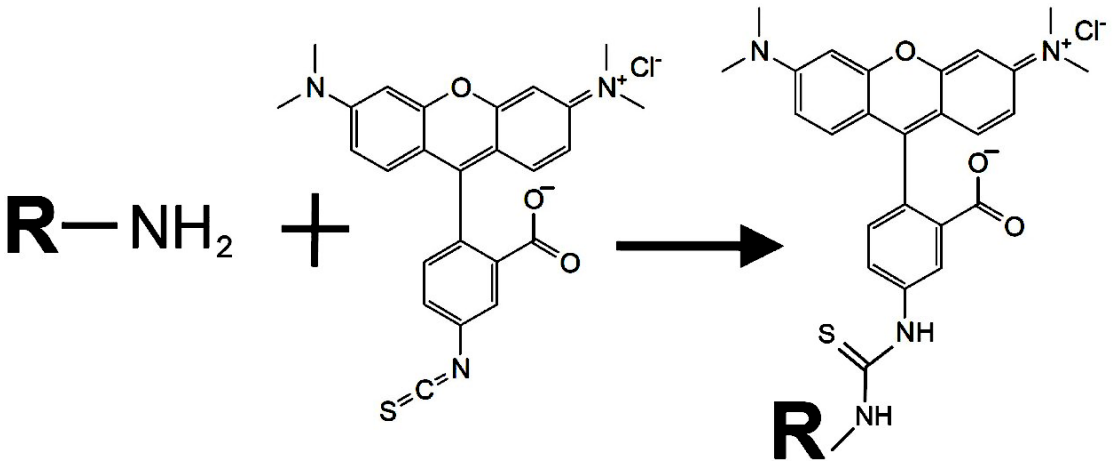

Figure 4.3: TRIT reacts with amine-containing molecules to create an isothiourea linkage.

The materials used for preparation of fluorescent dyes were purchased from Sigma Aldrich

4.1.3 Super paramagnetic (Fe_3O_4) nanoparticles

These super paramagnetic nanoparticles are used for capsules functionalization. A magnetic field can be used to manipulate the motions of these magnetite nanoparticles. A stable aqueous solution of super paramagnetic (Fe_3O_4) nanoparticles were prepared by functionalizing the surface with tri-carboxylic citric acid using a well-established Massart's co-precipitation method (Massart 1981), the general procedure are listed below:

1: In a typical reaction, 0.86 g $FeCl_2$ and 2.35 g $FeCl_3$ were placed into a flask with three necks, and then 40 ml MilII-Q water was added. The reaction was carried out under argon protection. The three necks of the flask were sealed with temperature senor probe, incoming argon gas and water cooling system respectively.

2: The solution was then heated to 80 ^oC, and then 5 ml of ammonium hydroxide (NH_4OH) was injected using a syringe. The solution was continuously stirred and maintained at a constant temperature. The reaction mechanism is shown below:

$$FeCl_2 + FeCl_3 + NH_3 \rightarrow Fe_3O_4 \downarrow + NH_4Cl$$

3: After 30 minutes heating, 1 g of Citric Acid (CA) in 2 ml of water was added to the mixture. The temperature was then increased to 95 ^oC for another 90 minutes.

4: The solution and resultant products were moved into dialysis bag (*Mw* cut-off 14 kDa) after cool down to room temperature. The bag was immersed

in Milli-Q water to remove the excess unbound CA for 3 days. The water was changed twice every day. The magnetite nanoparticles surface consisted of adsorbed citric acid layer present electrically charged with size range from 10 to 20 nanometers were obtained.

The materials used for synthesis of Fe_3O_4 nanoparticles were purchased from Sigma Aldrich.

4.2 Human umbilical vein endothelial cells culture

4.2.1 Culture medium preparation

The human umbilical vein endothelial cells (HUVECs) purchased from Lonza, was cultured at 37 °C in 5 % CO_2 incubator. Culture medium was changed every 2 or 3 days. The culture medium was prepared with several reagents and M199 medium. Typically 500 ml culture medium made from 500 ml M199 medium and several reagents are given in Table 4.3.

Reagent	Concentration
Foetal bovine serum	10 %
β-endothelial cell growth factor	1 ng/ml
Endothelial cell growth supplement from bovine neural extract	3 µg/ml
Thymidine	1.25 µg/ml
Heparin	10 U/ml
penicillin	100 U/ml
streptomycin	100 µg/ml

Table 4.3: Components of culture medium.

Chemicals for the M199 medium and the foetal bovine serum were purchased from Invitrogen, and the remaining chemicals were purchased from Sigma Aldrich.

Mixed solution was further sterilized by filtering through a 0.22 µm pore sterile filter (from Millipore). The sterilized medium was stored in a fridge at 8 ^{o}C for future use.

4.2.2 Trypsinization, cryopreservation and reawakening of HUVECs

After HUVECs reached 80 % confluence, trypsin (0.25 % trypsin-EDTA) is used for cells subculture. Culture medium was washed using PBS buffer (3 - 5 ml) for 10s. 2 ml of trypsin was added in the flask, and the flask was gently shaken. Cells morphology was checked using an optical microscopy. After the cells became rounded and detached from the flask, 5 ml culture medium was added to stop the trypsinization. The cells were centrifuged for 5 minutes at 1500 rpm. Then cells were washed with PBS buffer. Thus the cells were re-suspended in a pretreated flask at concentration of 5000 cells/ml. After 10 passages, the cells were discarded. To prepare the cell flasks or cover slips, cell culture flasks were coated with collagen type I (5 - 10 µg/ml) at 37 ^{o}C for 1 hour. Then flasks were gently washed using Phosphate Buffered Saline (PBS).

For future use, HUVECs were preserved in liquid nitrogen. After trypsinization and centrifugation steps, the cells were re-suspended in a medium which contains 20 % FBS, 70 % HUVECs culture medium and 10 % Dimethyl sulphoxide (DMSO). Then cells were put into cryo-vials and placed into a cryo-box (Nalgene freezing container, Nalgene, Hereford UK) stored in a freezer at - 80 ^{o}C overnight. Then the vials were transfered into a liquid nitrogen cryo-bank for long term storage.

To reawakening HUVECs, the vial was moved from liquid nitrogen and placed into 37 ^{o}C water bath. The medium was centrifuge for 5 minutes at 1500 rpm. Cells were re-suspended in 5 ml of HUVECs culture medium. Then the cells were placed in a collagen pre-coated culture flask at concentration of 5000 cells/cm^2, and transferred into an incubator with 37 ^{o}C and 5 % CO_2.

All chemical were purchased from Sigma Aldrich.

4.2.3 Immuno-fluorescent staining

As the HUVECs is cultured on a collagen pre-coated glass slide, the staining process of the cells *in vitro* (Bai and Wang 2012) is performed as followed:

1: All mediums and chemicals were pre-heated to 37 ^{o}C. The sample was washed with serum free M199 medium.

2: Lectin Wheat Germ Agglutinin (WGA) (Sigma Aldrich) was used to stain β-(1-4)-N-acetly-D-glucosamine and N-acetylneuraminic of glycocalyx. Cells were incubated with WGA at the concentration of 10 μg/ml for 15 minutes.

3: Sample was washed 3 times with serum free M199 medium to remove WGA solution. Then cell tracker red CMTPX (Invitrogen) at 0.5 μM was added for cytoplasm staining for 15 minutes.

4: Sample was washed 3 times with serum free M199 medium to remove cell tracker red CMTPX solution. 5 μg/ml of hochest 33342 (Invitrogen) was added to stain nucleus for 10 minutes.

5: After all these staining steps, the sample was washed with serum free M199 medium, and cell culture medium was added.

Then cells were ready for CLSM observation.

4.2.4 Function of neuraminidase

According to the product information from Sigma Aldrich, neuraminidase enzyme belongs to hydrolase enzymes. It plays an important role in influenza virus releasing and virus spreading. In this study, neuraminidase is used to

cleave the neuraminic acid component of the endothelial cells glycocalyx, such as sialic acid residues and N-acetyl-D-glucosaminyl residues of glycoproteins.

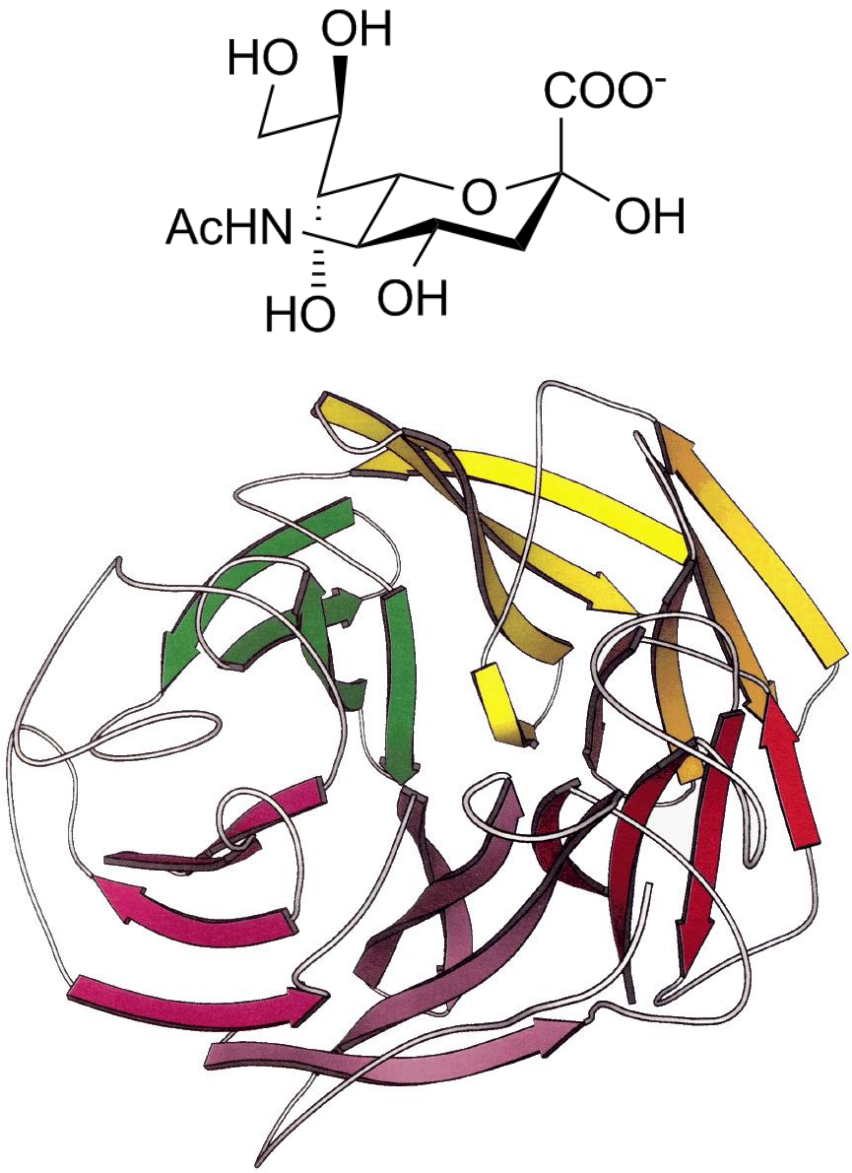

Figure 4.4: Structure of neuraminidase.
Neuraminidase of influenza virus (Colman 1994).

The chemical structural of neuraminidase is shown in Figure 4.4. The neuraminidase contains single polypeptide chain with six conserved polar amino acids, followed by hydrophilic, variable amino acids and a hydrophobic trans-membrane region that provides the anchor for the stalk and the head

domains (Varghese, McKimm‐Breschkin et al. 1992; Gouda, Aly et al. 2011).

The neuraminidase monomer mass is ~ 50 - 60 kDa, most often as 64 -66 kDa. It has highest activity in pH range from 5.0 to 5.5. While at pH 7.0 in phosphate buffer, its activity reduce to 30 - 50% (Cassidy, Jourdian et al. 1965). Neuraminidase from Clostridium perfringens (C. welchii) Type V, lyophilized powder was purchased from Sigma Aldrich without any further purification.

4.3 RCA cleaning

Silicon wafers, glasses and beakers were cleaned by RCA-1 process to remove any potential organic contaminants. The general procedure (Kern 1970) is followed.

1: Isopropanol and water were mixed at ratio of 1:1. Substrates were placed into the solution and sonicated for 5 minutes.

2: Water, ammonium hydroxide (NH_4OH) and hydrogen peroxide (H_2O_2) were mixed at ratio of 5:1:1. Substrates were washed with Milli-Q water, and then immersed into the solution.

3: The solution was heated to 75 ^{o}C for 15 minutes in water bath. Any organic materials were degraded in this step.

4: The substrates were washed with plenty of Milli-Q water after cooled to room temperature.

Now the substrates were ready to use for capsules preparation. Chemical used for RCA-1 process were purchased from Sigma Aldrich.

4.4 Pierce BCA protein assay

In 1985, Smith et al (Smith, Krohn et al. 1985) discovered a biochemical assay named Bicinchoninic Acid (BCA) assay. It is able to measure the protein's total concentration within the range from 0.5 µg/ml to 1.5 mg/ml. The colour of protein changes from green to dark purple as the concentration increasing. There are two primary reactions in the BCA assay. One is Cu^{2+} ions in cupric sulfate are reduced by protein's peptide bonds to Cu^{+}. Thus the amount of reduced Cu^{2+} is affected by the amount of protein exist in the solution. Another one is two molecules of BCA chelate with one cupric ion. A purple coloured component is created by the second reaction, and has a strong light absorption at wavelength of 562 nm. At this wavelength, a series concentration of proteins are nearly linear over a broad working range (Olson BJ 2007).

Peptide bonds of protein prefer high temperatures from 37 to 60 ^{o}C to form the reaction complex. Therefore, BCA assay is incubated in this temperature range to raise assay sensitivity. Protein concentrations are measured and recorded with reference to standards of Bovine Serum Albumin (BSA). A series of BSA dilutions of known concentration were prepared as calibration (Olson BJ 2007).

1: BCA working reagent was prepared by mixing reagent A and reagent B of Pierce BCA protein assay kit at ratio of 50:1.

2: 25 µL of series BSA dilutions were pipetted into 24 well micro plates in the working range between 20 – 2000 µg/ml.

3: 200 µL of the BCA working reagent was added to each well. Then the micro plate was gently shaken for 30 seconds.

4: The micro plate was incubated at 37 ^{o}C for 30 minutes.

5: The absorbance wavelengths of solutions were measure in each well at 562 nm using spectrophotometer.

The unknown concentrations of samples were measured with same method and calculated using the calibration curve of standard BSA. Pierce BCA protein assay kit was purchased from Thermo Scientific.

4.5 Laboratory equipment

Device	Type
Centrifuges	Eppendorf, centrifuge 5417c and 5418.
Shaker	IKA Vortex genius 3.
Ultrasonic bath	Elma S 15 H, Elmasonic.
Hot plate stirrer	IKA-Werke RET basic C + ETS-D4 fuzzy.
Autoclave	Prestige Medical, classic.
Electronic balance	Ser.No; 2905662. A&D company. Limited
Dialysis bag	Carl Roth GmbH + Co. KG, Dialysis membranes *Mw* cut-off 14 kDa.
pH paper	Sigma Aldrich, pH 1 - 11 Triple colour chart.
Tubes	Eppendorf, Standard micro test tube
Disposable cuvettes Plastibrand, polymethylmethacrylat	Carl Roth GmbH + Co. KG, PMMA: 300 - 900 nm
24 amplification plates	Nunc ^{TM}, made in denmark

5 Methods

5.1 Zeta potential measurements

The electro kinetic potential in colloidal systems is called zeta potential. Distribution of ion in the medium is affected by the presenting particle surface net charge. Concentration of counterions is higher in the region that closes to the particle. In this region, an electrical double layer of the particle liquid interface is formed. Stern layer is inner region and Gouy-Chapman layer is outer region. They are classified by the variation in electrical potential as a function of distance from a charged substrate. Figure 5.1 shows zeta potential and Zetasizer Nano cells.

Ions in Stern layer are strongly bounded and not affected by thermal motion. The thickness of Stern layer is a single hydrated ionic layer. While ions in Gouy-Chapman layer also called diffuse layer are less bounded, and its distribution depends on electrostatic forces and thermal motion. When particle moves, ions inside the boundary of electrical double layer are moved with the particle. Outside the boundary, ions are not bounded and moved with the particle. This boundary is called slipping plane, and the electric potential at this plane between the double layer and the surrounding medium is called zeta potential.

Zeta potential is determined by the effective charge on the particle and influences the electrostatic repulsion between the particles. Thus, zeta potential is directly affecting the stability of colloidal dispersion. Particles with high value of zeta potential remain non-aggregate dispersion and electrical stability. Otherwise, colloid particles with low zeta potential become coagulated, due to attraction is higher than repulsion between the particles.

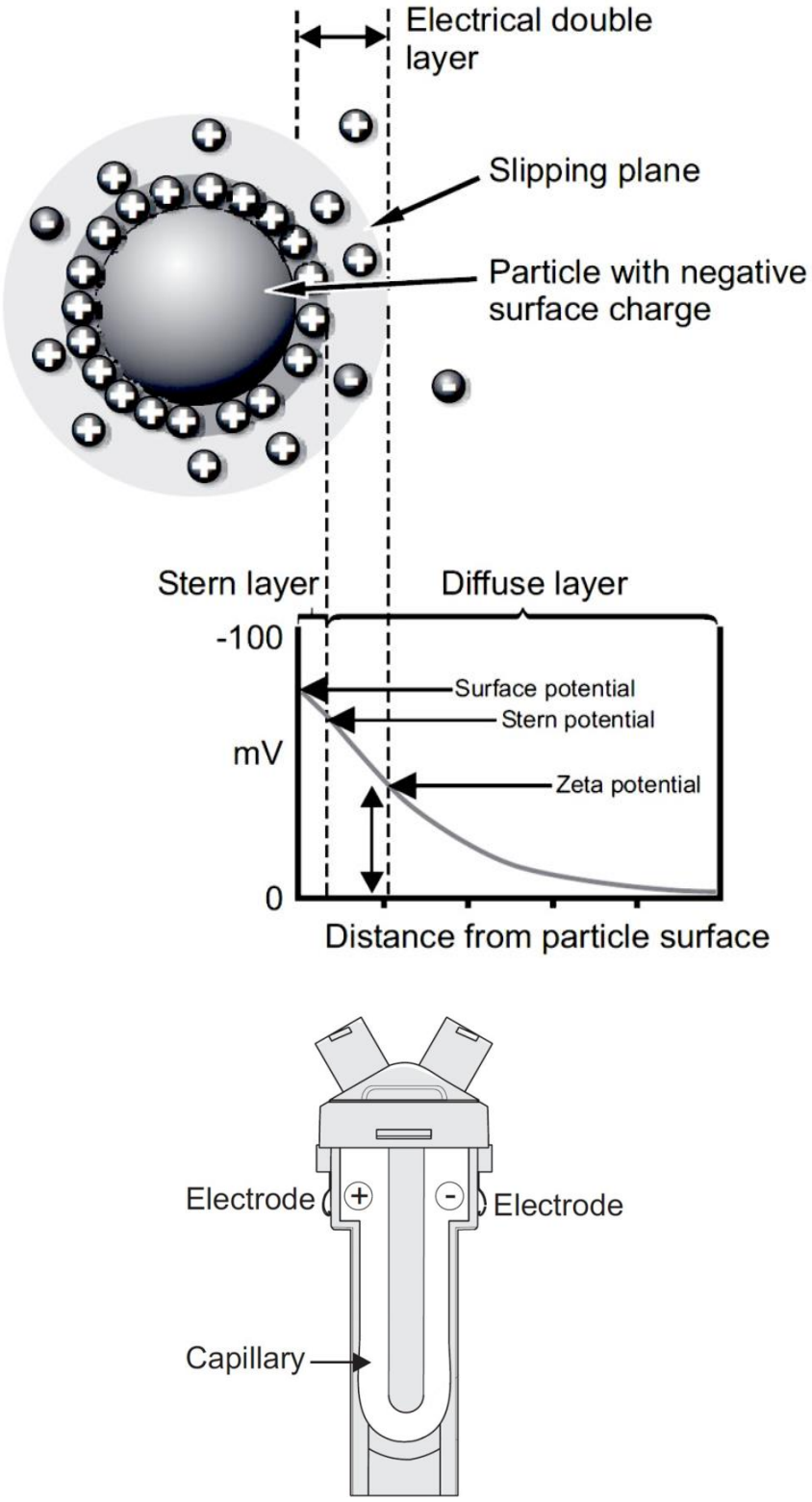

Figure 5.1: Schematic representation of zeta potential and Zetasizer Nano cells.

In colloid system, difference of ionic concentration and potential are used as a function of distance from the charged surface of a particle (Instruments 2004).

The charged surface of colloidal particle is able to prevent particle precipitation in solution. The charge can be determined by measuring its electrophoretic mobility in an electrical field. Zeta potential represents ions mobility of particles surround with electric field at slipping plane. Therefore, the actually potential of particle surface cannot be measured, due to ions in Stern layer are not able to move. Smoluchowski equation shows the relationship between zeta potential ζ at the interface and the electrophoretic mobility υ_E (Hunter 1981).

$$\boldsymbol{\upsilon_E = 4\pi\varepsilon_0\varepsilon_r \frac{\zeta}{6\pi\mu}(1 + kr)} \qquad \text{Eq. 5.1}$$

ε_0: relative dielectric constant.

ε_r: vacuum electrical permittivity.

μ: solution viscosity.

r: particle radius.

k: Debye–Hückel parameter.

Zeta Potential measurements of particles and capsules were using Zetasizer Nano (Malvern Instruments, Germany). The values of measured potential are averaged from 5 measurement cycles, each of the measurement have 10 single measurements. Disposable folded capillary cells is shown in Figure 5.1 with volume of 750 μm were purchased from Malvern Instruments.

5.2 Fluorescence spectroscopy

Fluorescence spectroscopy also known as fluorometry or spectro-fluorometry is an electromagnetic spectroscopy which is able to measure and analysis fluorescence of substance. After photon adsorption, an electron or atom is in an excited state, emission of photons brings them back to the ground state. The process is called luminescence which is simply defined as emission of light from substance.

Figure 5.2 shows a typical fluorescence spectroscopy. Xenon lamp has high intensity at wavelengths above 250 nm, and provides source of exciting light. The monochromators are performed to select the wavelengths of excitation and emission. Shutters are used to remove the exciting light or shut off the emission channel. The excitation light is reflected to a reference cell that contains a stable reference fluorophores by beam splitter. Photomultiplier tubes are working as a detector for fluorescence. The results are generally presented in graphical form stored digitally (Lakowicz 2006).

Fluorescence measurement is used to determine encapsulation and releasing efficiency of encapsulated fluorescent substance. Intensities of fluorescence are mostly linear with increasing concentrations of dye. Therefore, series of known concentrations of dye are measured as calibration. Supernatants are collected during capsules fabrication.

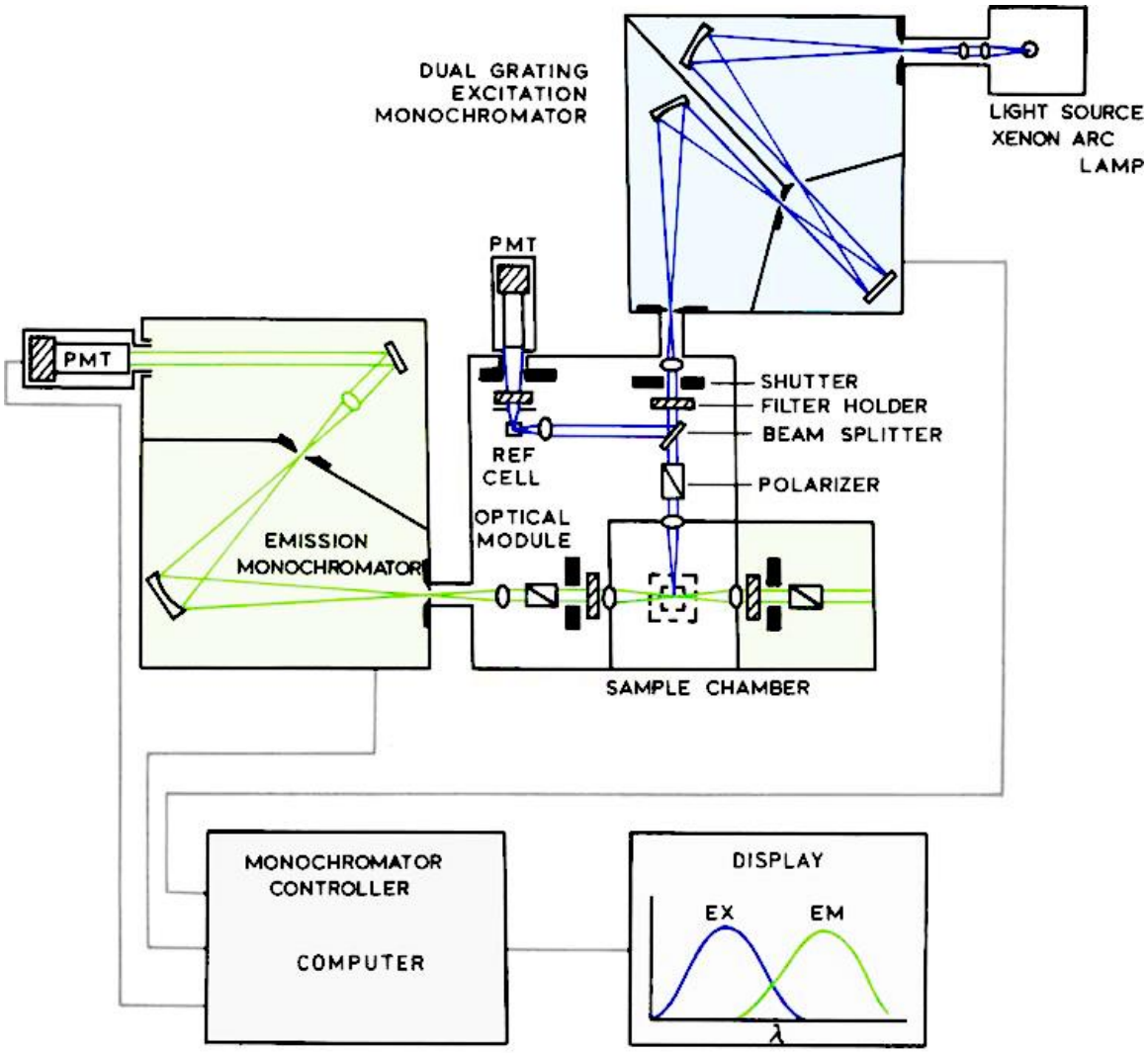

Figure 5.2: Schematic illustration of a general fluorescence spectroscopy. (Lakowicz 2006).

FluoroMax and Perkin-Elmer LS55 fluorescence spectrophotometers were using for fluorometry measurements. Disposable 4.5 ml and 1.5 ml cuvettes for fluorometry measurements were purchased from Roth.

5.3 Spectrophotometer

Two solutions with same material but different colour, normally the deeper colour one is considered with higher concentration. Colorimeter is defined as intensity measurement of visible light in a wide wavelength range of the given sample. Principle theory of spectrophotometer is measuring the concentrations of substances with colours. The measurement is based on light radiation absorption of solution at certain wavelength. At the wavelength, sample has maximum light absorption and minimum light transmission.

The term of transmittance is defined as the ratio of transmitted light of sample to incident light. The transmission is affected by the path length of the light passed. Light absorption is increased with the path length increasing and results light transmission decreasing. Therefore, the relationship among absorbance of light, concentration of substance and path length are summarized in Beer-Lambert Law:

$$\boldsymbol{A = log\frac{I_0}{I} = KCL,} \qquad \mathbf{T} = \frac{\boldsymbol{I}}{\boldsymbol{I_0}} = \mathbf{10}^{-\boldsymbol{KCL}} \quad \text{Eq. 5.2}$$

I_0 is the incident light and I is the transmitted light; C is concentration of the sample and L is the length of light path through the solution; K is proportionality constant named molar extinction coefficient or molar absorptivity with unit of liter / (mol×cm).

The major function of spectrophotometer is selectively tests the intensity of transmitted radiation. Figure 5.3 shows the basic components of the typical instrument.

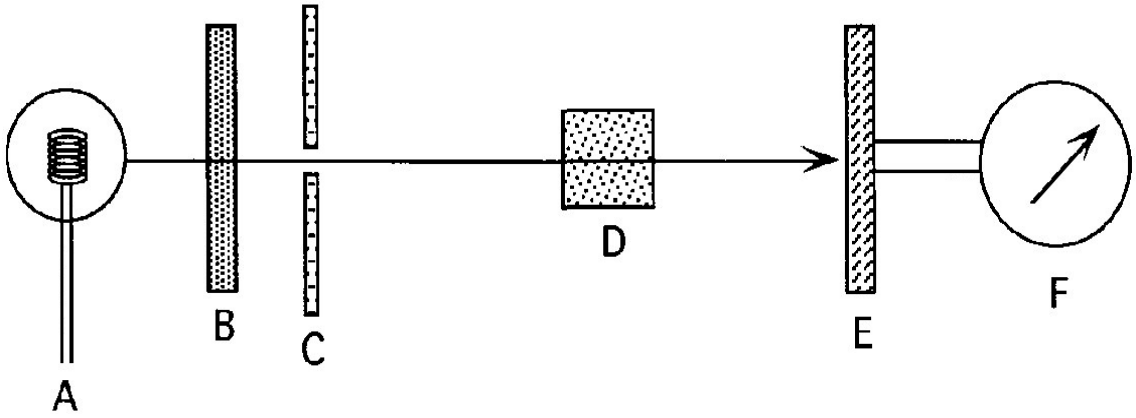

Figure 5.3: The basic components of colorimeters and spectrophotometers.

A: source of radiant energy; B: means of spectral isolation; C: adjustable diaphragm or amplification stage; D: cuvette as sample container; E: radiant energy detector; F: output system (Varcoe 2001).

Light radiation as a stable and continues spectrum from 200 to 1000 nm is supplied by energy source. Spectral Isolation is used to filter out the unrequired wavelengths. Adjustable diaphragm modifies the light intensity to regulation. For sample container, glass cuvettes can be used in the range of wavelength between 320 and 1000 nm. However, only quartz cuvettes can be used for wavelength below 320 nm.

In the experiment, samples were prepared with Pierce BCA protein assay kit from Thermo Scientific. The instrument used to measure the absorbance at the wavelength of 562 nm is Multiskan ascent with mode of 354 from Thermo life sciences.

5.4 Confocal laser scanning microscopy

Confocal Laser Scanning Microscopy (CLSM) is a non-destructive imaging technique, used for visualization and three-dimensional reconstruction with high resolution of biological samples. CLSM has better performance than conventional optical microscopy in imaging technology. Such as controllable depth of field imaging, elimination of background information from the focal plane, and sequential scanning of the sample with thickness up to 100 μm (N. S. Claxton 2006). There are three modes of confocal microscope which are fluorescence, transmission and reflection.

In 1957, the principle of confocal microscopy was first introduced by Marvin Minsky (Minsky 1961). However, the limitation of traditional microscopy techniques results low resolution images. In 1974, a laser scanning process was created by Thomas and Christoph Cremer (Cremer and Cremer 1974). With this technique, 3D structure of sample can be scanned point by point with the focus laser beam and reconstructed by electronic instrument.

Figure 5.4 shows optical pathway and typical components in CLSM. Excitation source system provides coherent light such as laser. The emitted laser passes through a pinhole aperture, and then is reflected by a dichromatic mirror to the sample. The dichromatic mirror is able to reflect the trapping laser into the optical path of the microscope and transmit the illuminative light (Neuman and Block 2004). While laser hits and scans across the sample in a pre-set focal plane, the scanned points emit secondary fluorescence. The lights reflected or emitted by the sample pass back through the dichromatic mirror and are focused as a confocal point at the detector pinhole aperture (N. S. Claxton 2006).

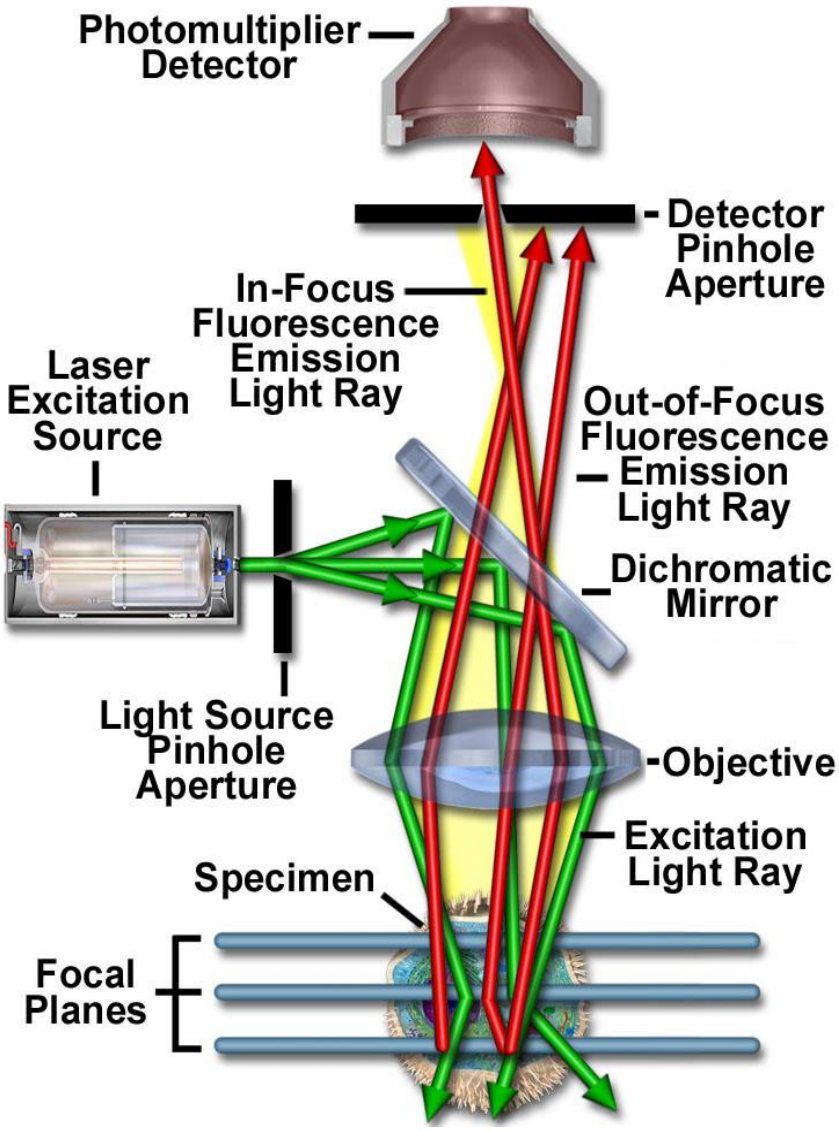

Figure 5.4: Schematic illustration of components in confocal laser scanning microscopy. (N. S. Claxton 2006).

Fluorescence emission occurs at points on the sample only in focus plane can pass through the detector pinhole aperture. In Figure 5.4, out of focus fluorescence emission light rays emitted above and below the focus plane are all eliminated. After passing detector pinhole aperture, the laser is collected by photomultiplier and transformed to data spot by computer.

Sample is scanned at the focal plane by a process named fly-back. Two oscillating mirrors of CLSM are used to control the focused laser beam scan a

desired part of sample in a raster pattern. Laser beam is moved from left to right along x - axis by one mirror, and along y – axis by another mirror. After scanning the sample along x - axis, the laser beam return to the initial position of the single scan and shift along y - axis to start a new single scan along x - axis (Webb 1996). The image of sample is point by point reconstructed from emission photon signals. Photons at each scanned point are collected by photomultiplier detector and transferred from an electrical signal to pixels.

A stepper motor controlled by computer is used to move microscope stage up and down and determines the focal plane. Image of the sample at z - axis can be recorded by continues moving the stage along z - axis after each x - y axis scanning. These data are converted into x - z and y - z plane, include x - y plane, the three dimensional reconstruction of the specimen are presented. This imaging process of CLSM is called sequential scanning and the minimum depth along z - axis is several nanometers.

Generally, a modern confocal fluorescence microscope contains several laser source systems for fluorophores excitation. Therefore, samples with more than one staining fluorophores can be imaged and presented in multiple colours. This function of CLSM is very important for cells with capsules studies, due to labeled dyes of sample up to 3 colours.

CLSM used to measure the aqueous samples is Leica TCS SP2 inverted confocal microscope system (Leica, Germany) equipped with a 63x oil immersion objective having a numerical aperture of 1.20. Laser of Ar - ion (488 nm) and a He - Ne (543 nm) as well as ultraviolet visible infrared (350 nm) are used as excitation sources to the fluorophore stained in the sample.

5.5 Scanning electron microscopy (SEM)

SEM is one of the electron microscopes with a focused beam of high energy electrons to scan the sample and generate images. Interactions between electrons and atoms of sample are transferred to signals, and then present information such as morphology, composition and electrical conductivity of the sample.

5.5.1 Principles of SEM

Figure 5.5 shows components of SEM. A typical SEM contains electron column, scanning system, detectors, display, vacuum system and electronics controls. Energy between 0.2 keV and 40 keV of thermionically electron beam is emitted by an electron gun. Then the beam is focused by condenser lens or electromagnetic lens to a spot with diameter in a range from 0.4 nm to 5 nm. The electron beam follows a vertical path through scanning coils in the electron column, and is deflected by the final lens in x - axis and y - axis. Therefore images of a rectangular area on the surface of specimen can be scanned in a raster fashion.

Because continue random scattering and absorption of the specimen, energy of electrons is lost while electron beam hits the specimen. The energy loss from electron beam and gain to the specimen causes reflection of high energy electrons, emission of secondary electrons and the emission of electromagnetic radiation. Signals are amplified by electronic amplifiers, and transferred to image with different brightness in output system. Thus the final image obtained by the computer is distribution map of the emitted signals intensity from the scanned area of the sample.

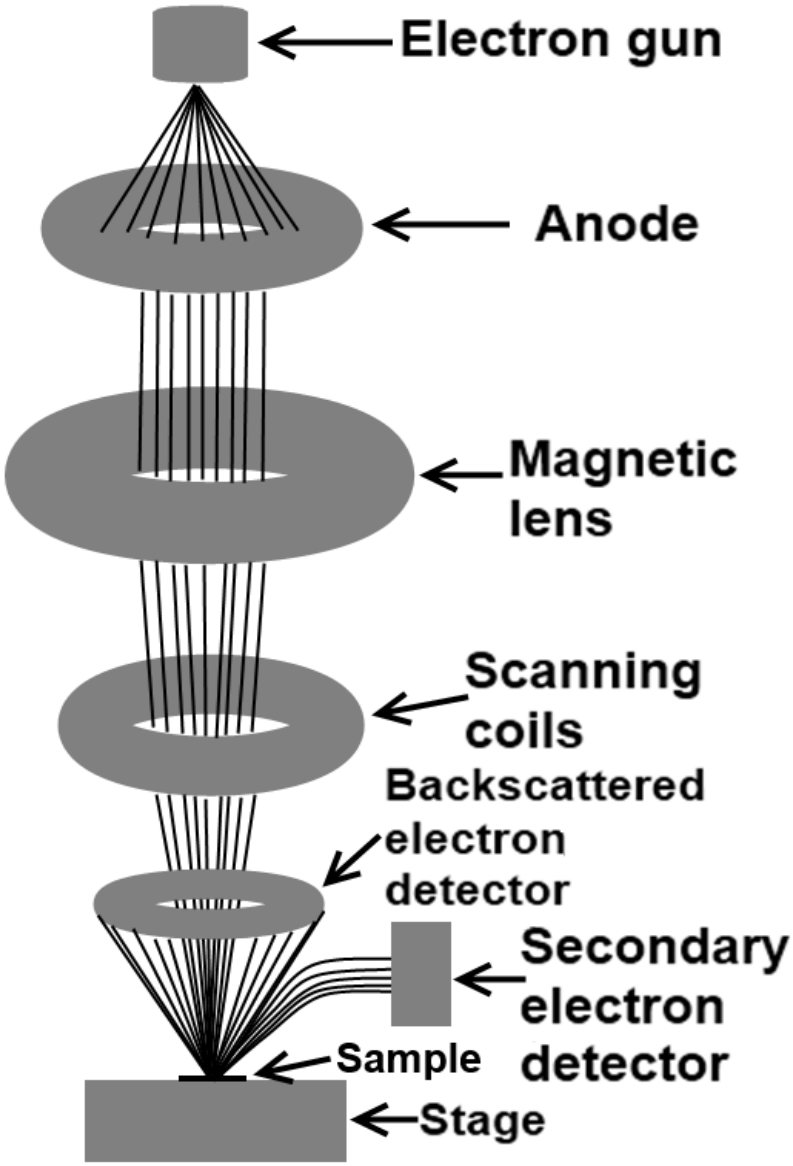

Figure 5.5: Schematic illustration of typical scanning electron microscopy components

There are several signal detectors of SEM, two typical signal detectors are Secondary Electron Detector (SED) and Back Scattered Electron Detector (BSED). SED is able to present the morphology and topography of the specimen. Low energy (less than 50 eV) secondary electrons are emitted from atoms on the surface of specimen by inelastic scattering interactions with beam electrons.

The secondary electrons are detected by an Everhart-Thornley detector (Everhart and Thornley 1960). The number of secondary electrons collected

by the detector affects brightness of the signal. Generally, steep surfaces and edges are brighter than flat surfaces of the specimen. SEM has narrow electron beam which leads to a large depth of field. Thus, secondary electrons are able to generate high resolution images of specimen, and present details in 1 nm size.

BSED collects electrons reflected by the specimen, and intensity of the signal generated from the scanned area is depended on the atomic number. Area with high average atomic number appears brighter than area with low atomic number. Therefore, BSED is well used to present contrasts of composition in multiphase samples.

5.5.2 Focused ion beam

The Focused Ion Beam also known as FIB technique was developed in 1980s. A typical FIB contains ion column, work chamber, vacuum system and the gas system. Similar as SEM work with a focused electron beam, the FIB system work with a focused ions beam instead. Low beam currents of FIB systems are used for sample imaging, while high beam currents are used for sample sputtering or milling.

Figure 5.6 shows the components of the FIB column. The chamber of FIB system is similar as SEM, requires a vacuum of 1×10^{-7} mbar. The ion beam is generated from a liquid metal ion source. Generally, the energy and currents of the beam are varied from 10 keV to 50 keV and 1 pA to 10 nA, respectively.

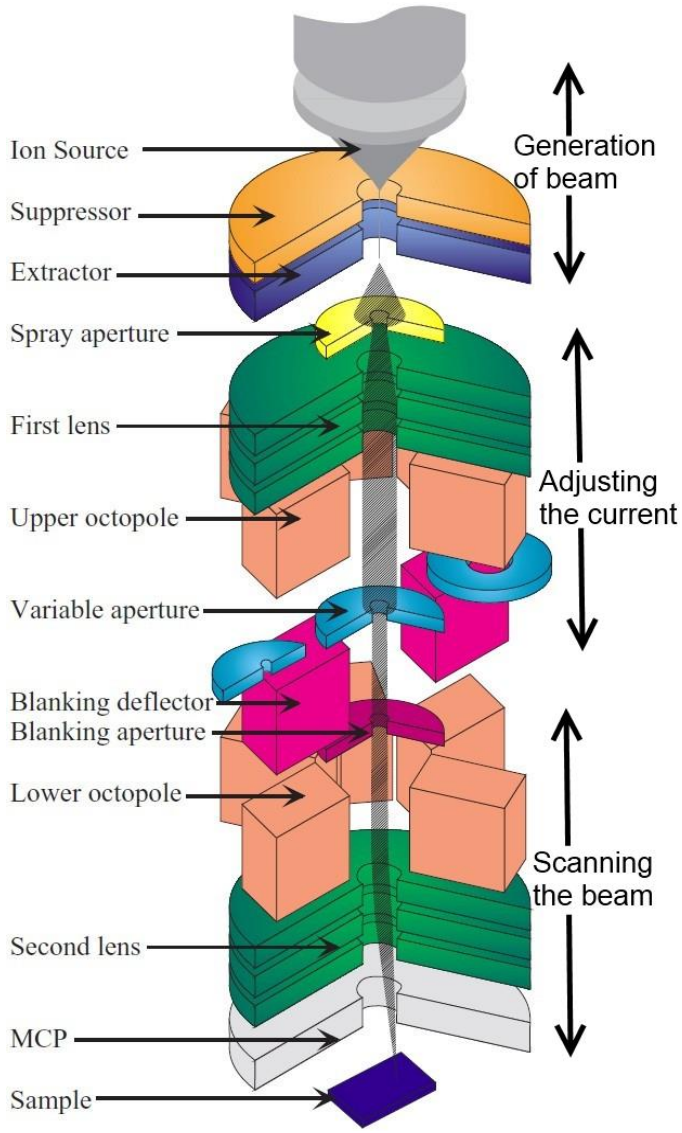

Figure 5.6: Schematic diagram of components in an ion column.
(Reyntjens and Puers 2001).

After passing spray aperture, the ion beam is condensed in the first electrostatic lens and adjusted by upper octopole. Blanking deflector and blanking aperture are used for blanking the ion beam. Lower octopole is used for raster scanning of the desired area on specimen. The second electrostatic lens focuses the ion beam to a fine spot for high resolution imaging. Secondary particles such as neutral atoms, ions and electrons are collected by multichannel plate and converted to image (Reyntjens and Puers 2001).

Because ions are larger and heavier than electrons, it cannot easily penetrate atoms of the sample. Ion beam with high current can be used to removal of sample material. Figure 5.7 shows physical sputtering of sample material. A desired rectangle etching shape on the sample obtained by continues scanning with the high current ion beam in the pre-set area. The milling depth from surface of the specimen can be varied from few nanometers to micrometers with different beam energy. The milling depth also depends on the material of the specimen as well as the angle between the ion beam and sample surface.

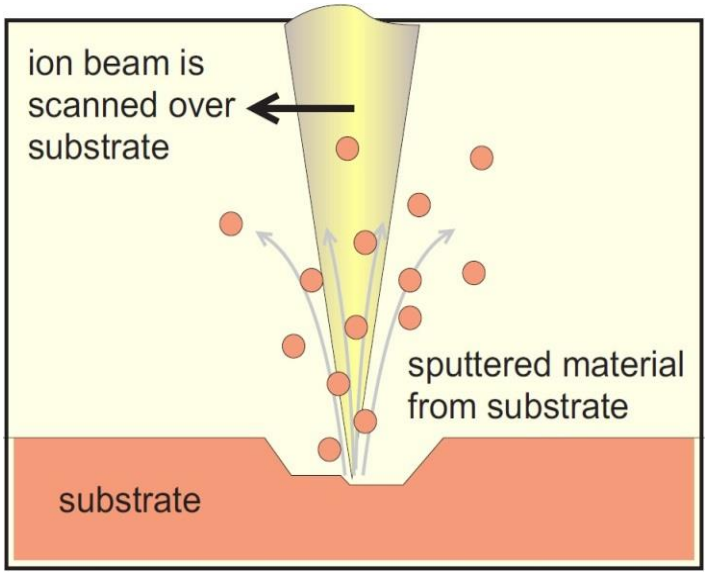

Figure 5.7: General milling process on a substrate with focused ion beam.
(Reyntjens and Puers 2001)

In this report, biological samples of endothelial cells with microcapsules were investigated by the scanning electron microcopy with focused ion beam of FEI Quanta 3D FEG, Dual Beam FIB-SEM instrument system equipped with Oxford Instruments.

5.5.3 SEM samples preparation.

Working chamber of SEM and FIB is high vacuumed, thus samples placed in the chamber must be completely dried. Otherwise, the chamber may loss the vacuum during observation of sample. Samples must be electrically conductive at the surface and electrically grounded to avoid the accumulation of electrostatic charge at the surface.

No further preparation for electrically conductive samples. However, many biological and materials specimens are insulators. Therefore, ultrathin layer of electrically conducting material coating is performed for non-conductive samples. A standard method for preparing non-conducting or poorly conducting specimens for SEM is performed by sputter coater. It is working in vacuum chamber with an electric field and argon gas. A thin layer of conducting material cover the specimen surface is produced by sputter deposition process. Both capsules and cells samples were coated before SEM imaging.

Biological samples are pre-treated by fixation and dehydration process to preserve their native structure before SEM observation. Fixation is a process of stop any ongoing biochemical reactions and avoids autolysis or putrefaction of the biological tissues. One of the most used chemical for fixation of biological samples is formalin. It is a crosslinking fixative and able to form covalent chemical bonds between proteins. Endothelial cells were fixed by fully immersed with 5 % formaldehyde for 10 minutes and then washed with PBS buffer. After fixation process, cell samples were stored in PBS medium in fridge at 4 ^{o}C.

Dehydration is defined as a process of losing water from tissues or cells. It can be processed by heating or dehydrating agents. A typical dehydration process is followed by sequentially wash the biological samples in methanol

with increased concentrations. Biological sample is first washed with concentration of 20 %, 40 % and 60 % methanol for 5 minutes of each washing step. Then raise the concentration of methanol to 80 % wash the sample for 3 minutes. At last 100 % methanol is used to wash the sample for 30 seconds. Remove the methanol and leave the sample in dry seal vacuum desiccator with calcium chloride anhydrous for drying.

In this report, samples of gold coating were using Agar auto sputter coater from Agar Scientific Elektron Technology UK Ltd, and carbon coating were using Balzers CED 030 carbon evaporator. Conductive carbon cement from Plano GmbH of Germany was used to fix the sample on a SEM metal holder.

5.6 Transmission electron microscopy

Transmission electron microscopy (TEM) is able to provide information about the inner structure of the sample. The electrons are transmitted through the sample, and an image is generated onto an imaging device or to be detected by a sensor.

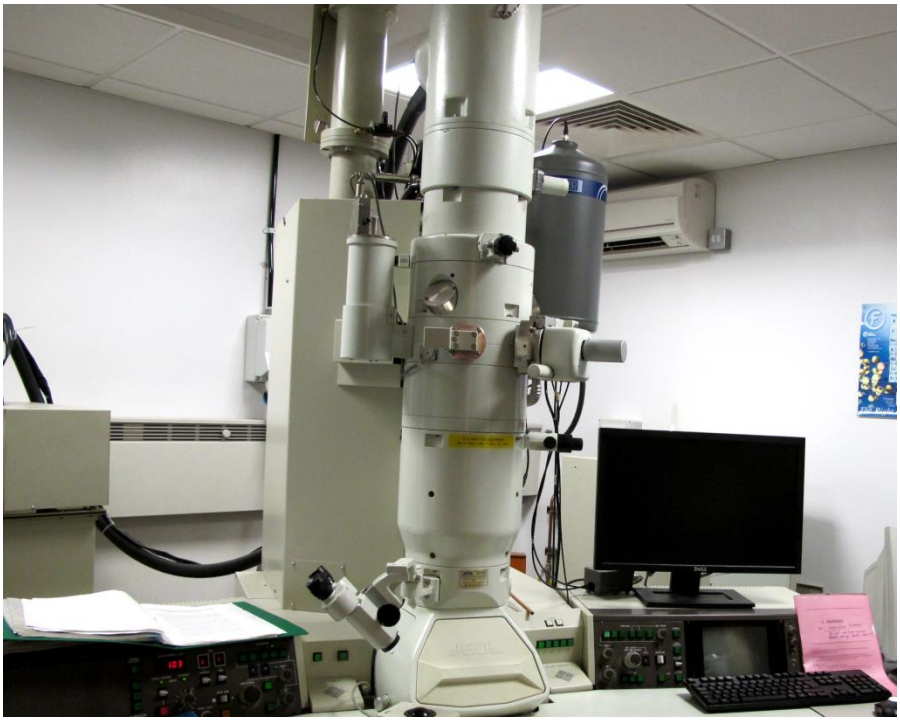

Figure 5.8: Photograph of transmission electron microscopy.

TEM was used to investigate the aggregation of gold nanoparticles in the shell of microcapsules. The contrast of the TEM image is affected by the different densities between metal nanoparticles and polyelectrolytes. One drop (about 5 μL) of capsules solution was pipetted onto a carbon coated copper grid and investigated using JEOL JEM 2010 transmission electron microscope (Figure 5.8) at acceleration voltage of 200 kV.

6 Microcapsules preparation and functionalization

This section provides details of capsules preparation and functionalization for the following experiments. All polyelectrolyte microcapsules are produced with $CaCO_3$ template cores. Capsules modified with magnetite nanoparticles are used for physical treatment with epithelial cells. Capsules contain neuraminidase and labeled with gold nanoparticles (GNPs) are prepared for biochemical treatment with endothelial cells. The GNPs are specific need for investigation by Scanning electron microscopy with focused ion beam.

6.1 Preparation of $CaCO_3$ micro particles

Calcium carbonate micro particles with porosity, uniform, almost spherical shape and narrow size distribution are fabricated from supersaturated solution by colloidal crystallization. There are two steps of $CaCO_3$ formation, first step is simultaneous and rapid nucleation, and the second step is growth also called aging and agglomeration (Otakar Söhnel 1992). Metastable precursor of calcite is the reason to form amorphous calcium carbonate, and the number of the growing spherical particles as well as the mass density remains constant after a short nucleation period. Figure 6.1 shows overview image, spherical and cubic shape of $CaCO_3$ cores. Due to calcite is the only thermodynamically stable modification of all $CaCO_3$ formations, amorphous $CaCO_3$ becomes crystal cubic structure after a certain time (Bolze, Peng et al. 2002).

The process is started by mixing calcium chloride and sodium carbonate with equal concentration and volume. The mixed solution is placed on the magnetic stirrer with continues stirring. While mix the two solutions, the amorphous precipitate appeared instantly, but the micro particles with 4µm diameter are formed more slowly. The size of the micro particles increase

with time, and the diameter could form up to 10 µm with the same particle morphology (Sukhorukov, Volodkin et al. 2004).

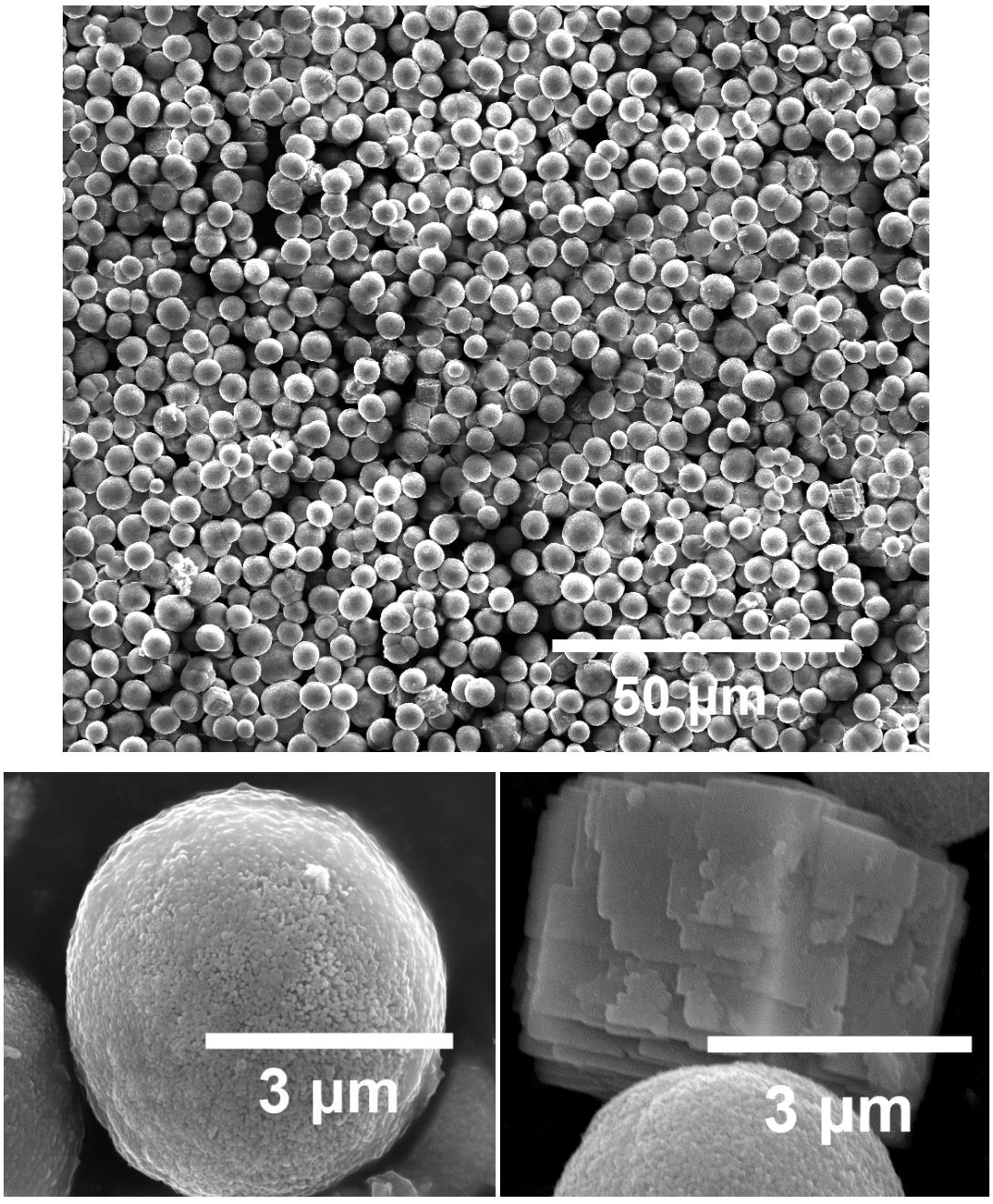

Figure 6.1: SEM images of $CaCO_3$.

Overview of uniform $CaCO_3$ cores (top image), spherical shape (bottom left) and cubic shape (bottom right) of $CaCO_3$ cores.

In a typical experiment, the template core of $CaCO_3$ was fabricated by mixing 0.33 M $CaCl_2$ and equal volume of 0.33 M Na_2CO_3 solution into a beaker with stirring for 30 seconds at room temperature (Sukhorukov, Volodkin et al. 2004). Subsequently, the solution was collected into tubes and applied three centrifugation and washing steps with MilII-Q water to remove residual salts and unreacted pieces. Spherical shaped $CaCO_3$ microparticles with a rather uniform average ~4 μm diameter were obtained. The porosity of $CaCO_3$ particles provides a large surface area and has the ability to capture macromolecules effectively. For long term dry storage, the micro particles were rinsed with ethanol and dried. For short term storage, the suspension was kept at 4 ^{o}C in fridge.

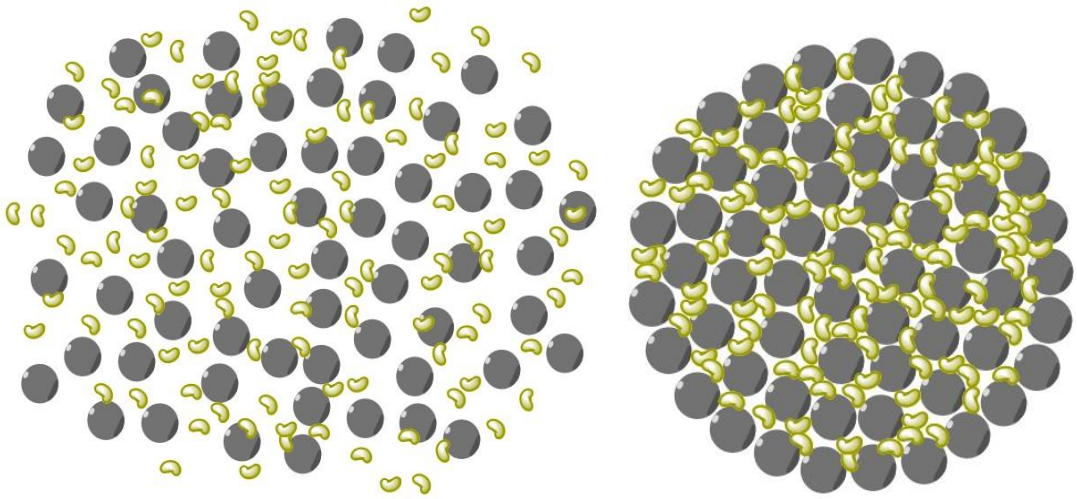

Figure 6.2: Preloading TRITC-dextran/ neuraminidase into $CaCO_3$ core.

Synthesis of neuraminidase (and, or TRICT-dextran) loaded $CaCO_3$ microparticles by co-precipitating $CaCl_2$ and Na_2CO_3 in the presence of neuraminidase.

Calcium carbonate microparticles are more biocompatible than other templates for LbL encapsulation of proteins and enzymes (Petrov, Volodkin et al. 2005). Figure 6.2 shows a method of pre-loading (see (Petrov, Volodkin et al. 2005) for details) was performed for TRICT-dextran encapsulation. 0.5 mg/mL of TRICT-dextran (red stain for visualization purpose) was premixed with $CaCl_2$ or Na_2CO_3 aqueous solutions; protein was captured by growing

$CaCO_3$ microspheres in the process of their formation named co-precipitation process. For neuraminidase-loaded microcapsules, 2 mg/ml neuraminidase was also encapsulated by the pre-loading method. Pre-loaded TRITC-dextran is for observing capsules with CLSM, and neuraminidase is for cleaving glycocalyx of endothelial cells.

6.2 Capsule preparation

Preparation of microcapsules with different shell materials requires different strategies such as core pretreatment, polyelectrolyte coating, and core dissolution. The alternating adsorption of polyelectrolytes onto the surface of $CaCO_3$ particles was produced by immerse the particles into 2 mg/ml oppositely charged polymer solutions with 0.5 M sodium chloride at a pH between 5 and 7. The polyelectrolyte absorption time required at least 15 minutes with continues shaking to fully cover the core particles surface. After each layer had been absorbed, core particles were centrifuged and washed with Milli-Q water for three times to remove the uncoated polymer. Figure 6.3 shows the capsules preparation and functionalization with nanoparticles.

Core particles aggregation may appear after several layers of polyelectrolyte was coated, depending on the size of the particles. 10 seconds ultrasonic bath was introduced to reduce the aggregation of the particles. After the desired number of capsule layers had been coated, $CaCO_3$ template core particles were dissolved by adding 0.2 M EDTA at pH 7 for three times. The capsules were then centrifuged and washed 3 times with Milli-Q water. They were seen to have rather uniform size and shape, with the average diameter of ~4 μm.

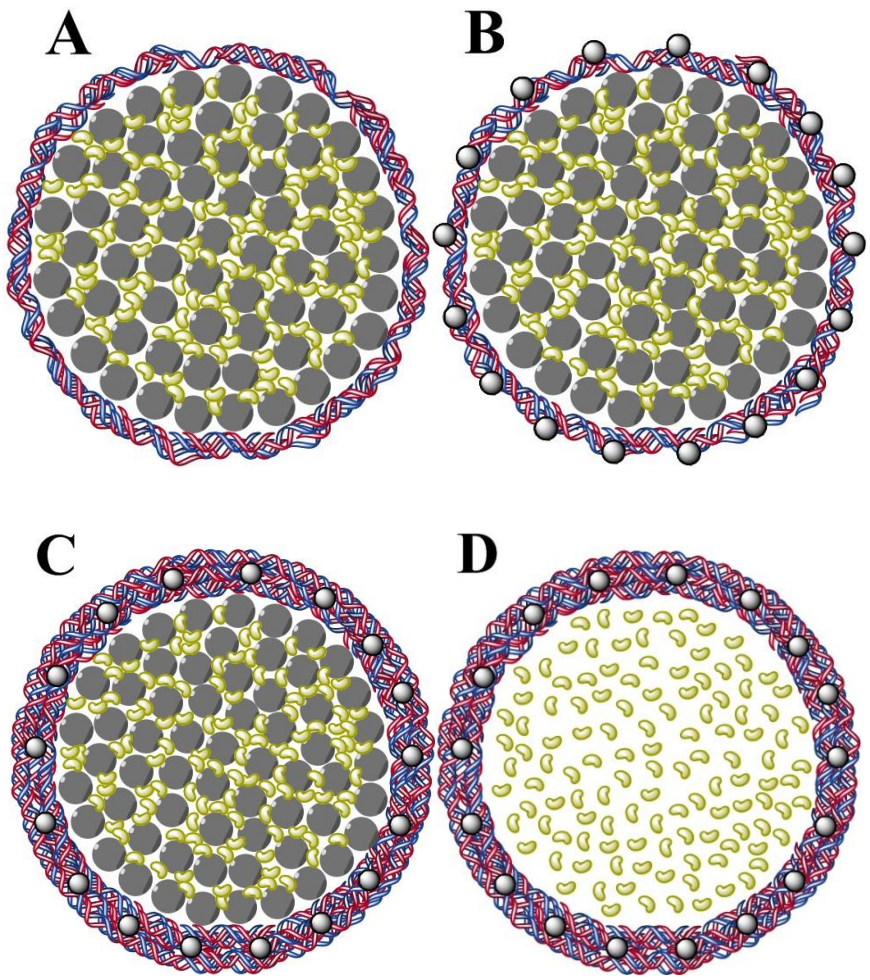

Figure 6.3: Capsules preparation and functionalize with nanoparticles.

(A) At least 2 layers of polyelectrolytes cover $CaCO_3$ particle which contains pre-loaded substance; (B) Modify capsule with nanoparticles; (C) Desired number of layers coated; (D) Hollow capsule obtained after $CaCO_3$ dissolution.

Find out the zeta potential at interface between solid and liquid are very important for polymer applications (Werner, König et al. 1999). As a solid presents in aqueous medium, at the interface, free ions are rearranged to form a region with certain charge density. Charges of the capsules each layer as well as the $CaCO_3$ core were measured using Zetasizer Nano and shown in Figure 6.4. Zeta potential measurement is carried out by adding 40 µL of capsules solution into the Zetasizer cuvette and filled with Milli-Q water with pH at 7. From Figure 6.4, zeta potential value changes from positive to

negative and repeat the changing during polyanionic and polycationic layers deposition. The potential values for each even or odd layer are similar. The reversed zeta potentials also prove charge overcompensation after every successful polymer layer deposition.

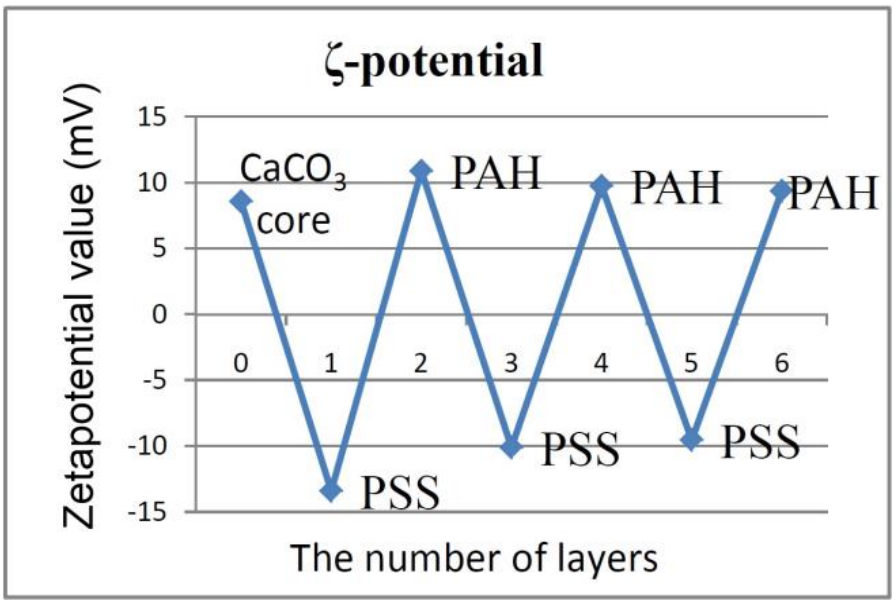

Figure 6.4: Schematic illustration of Zeta potential of capsules during LbL process.

Zeta potentials of samples are measured in Milli-Q water with pH at 7.

Capsules work with biological cells is better to be biocompatible and bio friendly. Negatively charged Dextran sulfate sodium salt (DS) and positively charged poly-L-lysine (PLL) as well as poly-L-arginine (PArg) are biodegradable polyelectrolytes used for capsules preparation. Poly (styrene sulfonate sodium salt) (PSS) with negative charge and Poly (allylamine hydrochloride) (PAH) with positive charge are used for synthetic capsules formation for some control samples.

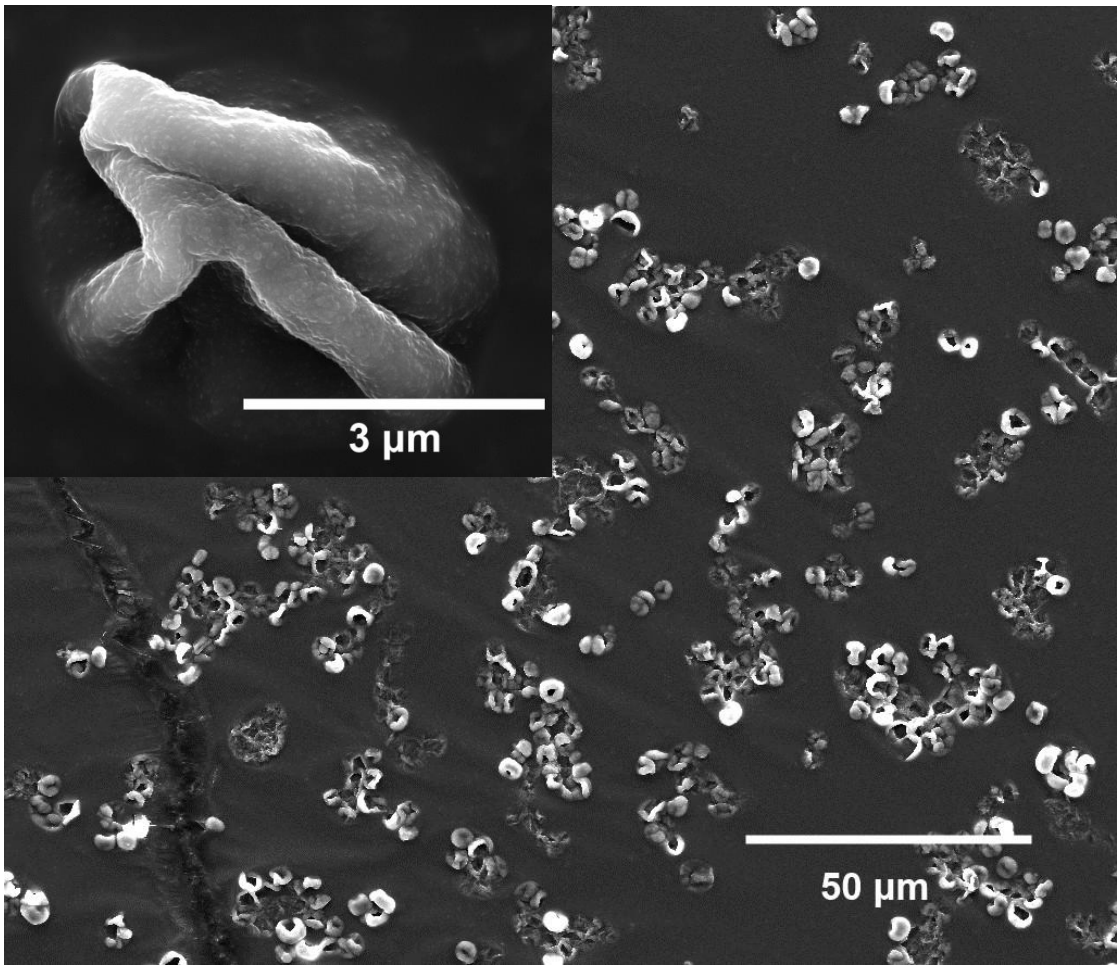

Figure 6.5: SEM image of dried hollow microcapsules with diameter around 4 µm.

Microcapsules morphology and size were checked using SEM after fabrication. SEM sample were prepared by pipet one drop (about 5 to 10µL) of hollow capsules solution on a SEM metal holder with a standard carbon conductive adhesive tab on the surface. Then, the sample was leaved in dry seal vacuum desiccator with calcium chloride anhydrous overnight. The sample was completely dried in the next day. In Figure 6.5, SEM image shows the capsule with a diameter around 4 µm obtained after core dissolution. Without the spherical template, capsules are collapsed. Gold nanoparticles and iron nanoparticles incorporated as layer constituents do not affect capsules morphology in dried status.

6.3 Capsules functionalized by gold nanoparticles

Gold nanoparticles (GNPs) have several advantage properties such as high charge density, small size, and light absorption. These characteristics of GNP make it well to functionalize polyelectrolyte microcapsules. GNPs can be coated by simply immerse the capsules into a mixed solution with water and nanoparticles with continues stirring. Because charge of gold nanoparticles is negative, it can be coated as a layer after positively charged layer. With a certain concentration of GNPs, it cannot fully cover the surface of previous layer. Thus, to achieve charge overcompensation, coating additional layer of previous polymer is needed. Therefore, the nanoparticles are coated in microcapsules shell.

There are two types of GNPs which are aggregated and non-aggregated GNPs. Aggregates of GNPs are premixed gold colloid solution with certain amount of NaCl for few seconds. GNPs can incorporate with positively charged polyelectrolytes solution, then deposit as a positively charged layer. In this case, no additional positively charged layer is required, and the following negatively charged polymer can be directly coated. Because polyelectrolyte solution contains ~0.5 M NaCl, after incorporate with polyelectrolyte, GNPs change to aggregated GNPs.

Figure 6.6: images of non- aggregated (left) and aggregated (right) 20 nm GNPs.

Non-aggregated colloid gold nanoparticles present red colour in solution show in left image of Figure 6.6. In the right image of Figure 6.6, because additional ions present in the solution, colour of aggregated gold

nanoparticles is changed from red to blue or purple. The phenomenon of aggregation or flocculation of gold colloid particles in solution is formed by “cross-linking” agent. Ligands with single charge affect GNPs assemble slowly to string structures. While ligands with multiple charges can force the GNPs form cluster structures (Olivier and Sorensen 1990). There is no obvious difference between aggregated and non-aggregated GNPs modified capsules with cells samples under SEM investigation. Figure 6.7 shows the TEM image of capsules contain non-aggregated GNPs. The black dots in the gray colour capsule are GNPs.

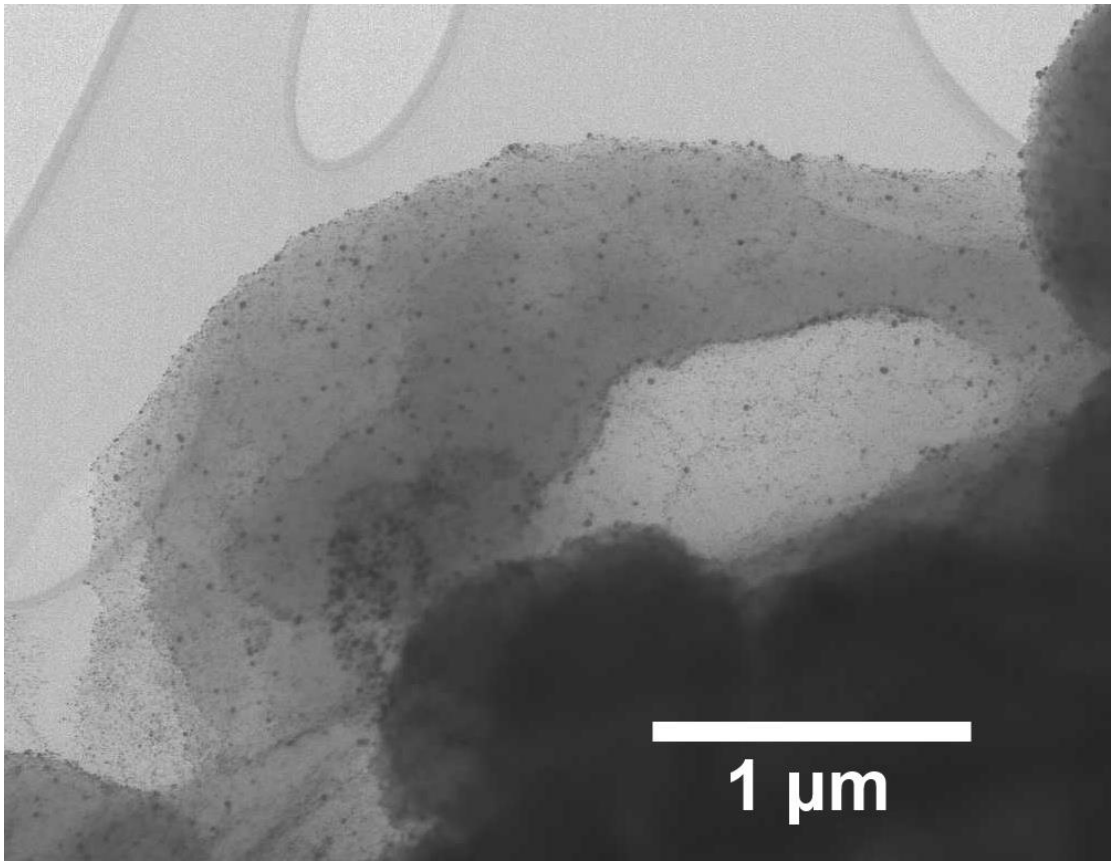

Figure 6.7: TEM image of capsules contain gold nanoparticles.

These gold nanoparticles are used for capsules observation with SEM With focused ion beam. The inside area of the cells and capsules are able to be observed. After ion beam milling on desired area of sample, the cross section shows the z – axis of the area. With the cross section, location of capsules is

below or above the cell membrane can be directly seen. GNP provides good contrast in images taken by back scattered detector. They are very bright dots, help to distinguish capsules and other intercellular or extracellular matrix.

6.4 Magnetite nanoparticles functionalized microcapsules

Magnetite (Fe_3O_4) nanoparticles with an average size around 10 to 20 nm, stabilized with tetramethyl ammonium hydroxide, were synthesized in water according to the method presents in 4.1.3 (Massart 1981).

Fe_3O_4 nanoparticles were coated by re-suspended $CaCO_3$ particles with PLL as outmost layer into iron nanoparticles solution. Then the capsule walls were deposited with magnetite nanoparticles. Same as gold nanoparticles, the magnetite nanoparticles cannot fully cover the previous layer. Thus additional layer of PLL is formed as positively charged layer to cover the iron nanoparticles. Size of Magnetite nanoparticles were measured using Zetasizer Nano. The result shows ~80% nanoparticles with diameter around 30 nm. Zeta potential is also measured using Zetasizer Nano as -22.3 mV.

Figure 6.8 shows the TEM image of capsules with magnetite nanoparticles. Iron nanoparticles are incorporated in shell of capsule. Bottom left image of Figure 6.8 is capsules with magnetite nanoparticles suspended in deionized water, and right image is capsules with magnetite nanoparticles treated by a magnet after 3 minutes. Figure 6.8 shows capsules with magnetite nanoparticles are attracted by a magnet on the wall of the tube, not precipitate at the bottom. Magnetite nanoparticles incorporated capsules are prepared for physical treatment with epithelial cells.

Polyelectrolyte microcapsules are prepared by LbL technique. All capsules are fresh produced the same day or one day before investigation. As the

amount of substance released is increasing with time, encapsulated substances release test is performed just after capsules fabrication.

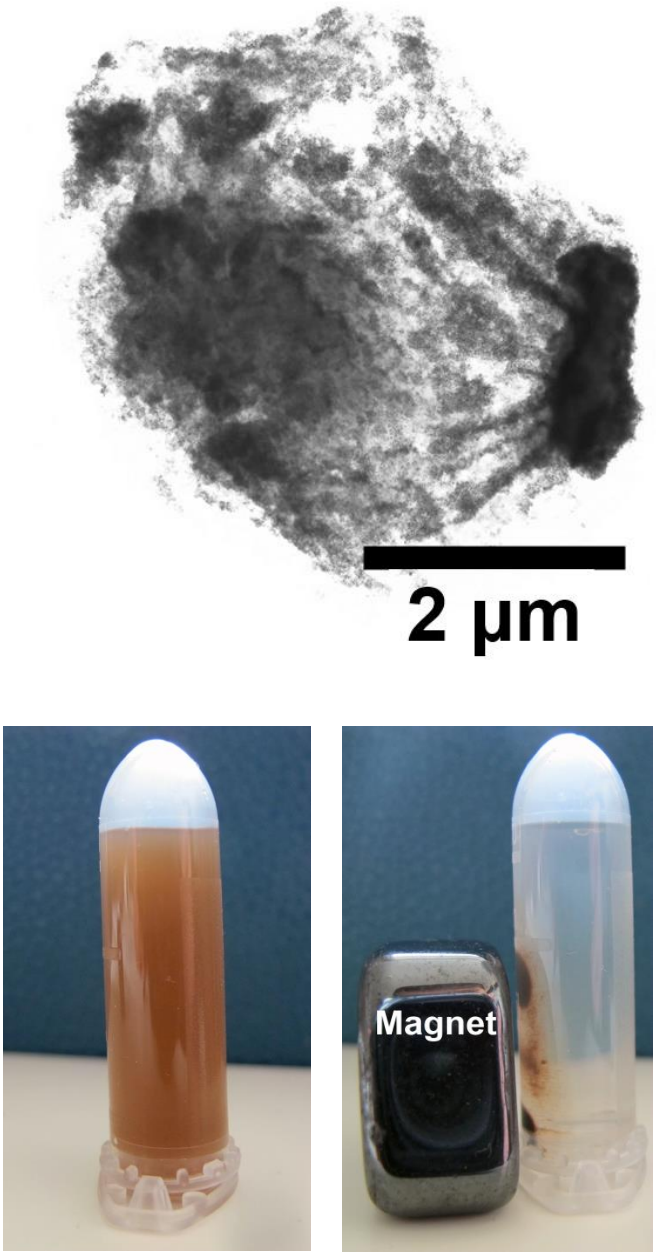

Figure 6.8: Images of capsules with magnetite nanoparticles.

Image of capsules with magnetite nanoparticles is viewed using TEM (top). Capsules with magnetite nanoparticles without (bottom left) and with (bottom right) a magnet. TEM image was taken together with Dr. Denys Usov.

7 Deliver capsules with magnetite nanoparticles to epithelial cells with physical method

Epithelium is one of the four basic types of animal tissue with functions of secretion, selective absorption, protection, trans-cellular transport and detection of sensation. As mentioned before, epithelial cells form continuous sheets by junction complex like tight junctions, desmosomes, adhering junctions and gap junctions. Thus, epithelial cells are very concentrated connect with each other like bricks in a wall result a very narrow intercellular space.

One primary function of epithelial cells is protection. As these cells cover and line all free body surfaces, create barriers between outside environment and the body. Stratified epithelial cells provide better protection of the underlying tissue even the outmost layer cells is damaged. The most interesting function of epithelial cells in drug delivery system is transportation. Epithelial cells of intestinal lining are able to transport filtered substances by active transport system which moves molecules across cell membrane against its concentration gradient.

In order to transfer materials between two different environments and maintain distinct properties on both sides of the cell, transcytosis is selectively transport of membrane bounded carrier contains materials from apical surface of the cell to basolateral surface. This transportation is for small molecules and macromolecular in nanometer range. For 4 μm diameter polyelectrolyte capsules, the internalization mechanism is unknown yet, but endocytosis is considered as the most possible reason.

The epithelial cell used in this study is Caco-2 cell line which is a continuous cell of heterogeneous human epithelial colorectal

adenocarcinoma cells. This cell line is able to form a confluent monolayer on cell culture. The monolayer contains epithelial cell with cylindrical polarized morphology, microvilli on the apical side, and tight junctions between adjacent cells. It performs as a physical and biochemical barrier which blocks ions and small molecules pass the layer (Artursson 1990). The Caco-2 cell line is also widely used in drug delivery studies as an *in vitro* model of the human small intestinal mucosa to investigate the absorption of drugs.

Magnetite nanoparticles in a carrier are able to provide external force with magnetic fields. The magnet can be placed on desired area of the sample. Thus microcapsules loaded with magnetite nanoparticles are manipulated by magnet in the area and perform a target delivery. The delivery of magnetite nanoparticles loaded carrier systems by applying a magnetic field has been performed *in vivo* (Pankhurst, Connolly et al. 2003).

7.1 Model of co-incubation of capsules with magnetite nanoparticles and epithelial cells

The monolayer of epithelial cells is provided by Dr. Maya Thanou in pharmacy department of King's College London. Capsules with magnetite nanoparticles used in this study is 8 layers biodegradable DS/PLL-FITC capsules with magnetite nanoparticles between 4^{th} and 5^{th} layer. Capsules formation is (Dextran sulfate/ Poly L lysine – $FITC)_2$/ Fe_3O_4/ (Dextran sulfate/ Poly L lysine – $FITC)_2$, and control capsules formation is $(DS/PLL\text{-}FITC)_4$. Figure 7.1 shows capsules with magnetite nanoparticles incubate with epithelial cells with a magnet at the bottom.

Most cancer cells and immune cells such as macrophages and dendritic cells are called phagocytic cells. Many researches proved these cells are able to internalize polyelectrolyte microcapsules. Caco-2 cells are colon cancer epithelia cells, also internalize capsules spontaneously.

Microcapsules internalized by breast cancer cells of the cell line MDA MB 435s has been demonstrated by Sukhorukov et al in 2005. They found approximate 70 % and 90 % of the breast cancer cells are able to adhering microcapsules within 1 and 3 hours, respectively. (Sukhorukov, Rogach et al. 2005).

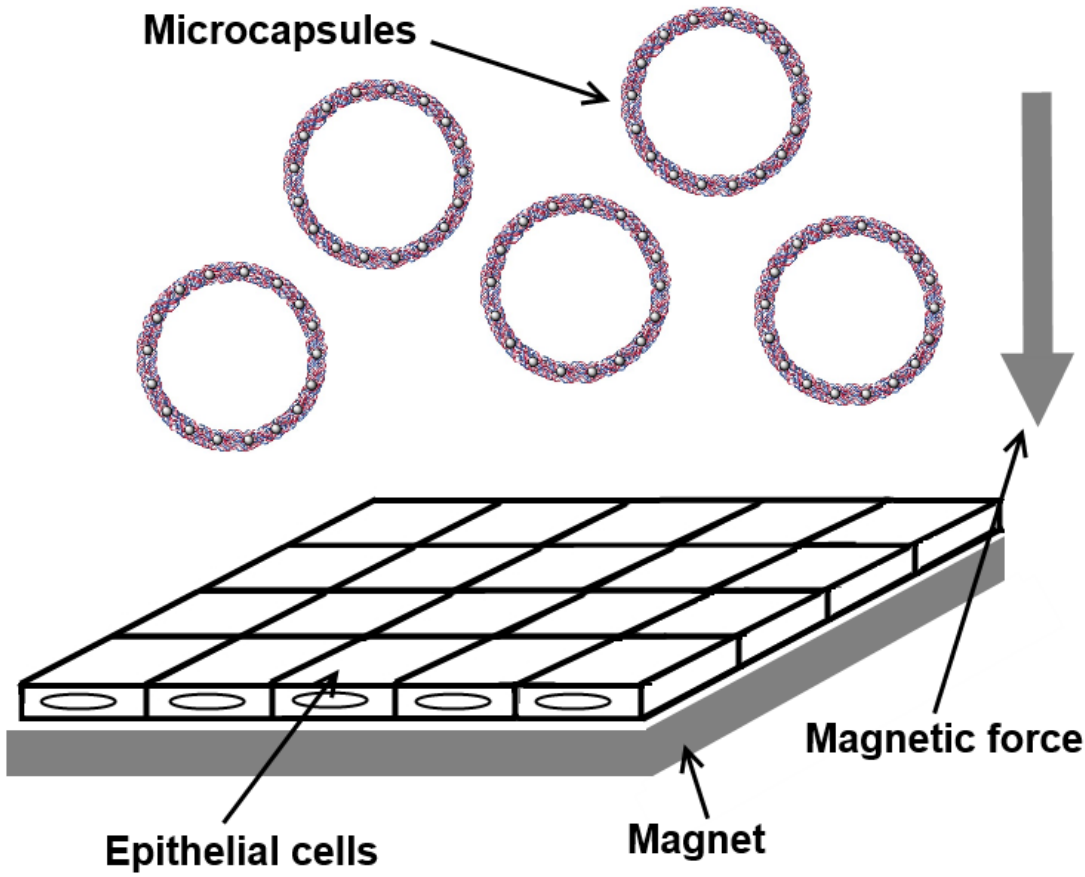

Figure 7.1: Schematic illustration of physical stimuli of capsules with magnetite nanoparticles and epithelial cells.

Capsules with magnetite nanoparticles incubate with epithelial cells with a magnet at the bottom.

Therefore, even no magnetic field applying during capsules and Caco-2 cells co-incubation, both capsules with magnetite nanoparticles and control capsules are adhered by most of the cancer cells after 1 hour. Thus, to minimize the affect caused by cancer cells natural absorption, and observer difference between samples of capsules with magnetite nanoparticles and

control capsules with Caco-2 cells, the co-incubation time is reduced from hours to few minutes.

7.2 CLSM study on capsules with magnetite nanoparticles and epithelial cells co-incubation

Same volume of capsules with magnetite nanoparticles and control capsules were premixed with same volume of culture medium in two tubes. Then the tubes of culture medium were added to the different wells with Caco-2 cells. A magnet was placed under the wells to generate magnetic field during co-incubation time. After 5 minutes, both samples were removed from the magnet and washed 3 times with culture medium to remove un-adhered capsules.

Caco-2 cells were stained with 4', 6 - diamidino - 2 - phenylindole (DAPI) at the concentration of 50 µg / ml, a nuclear stain, for 10 minutes at room temperature. After nucleus staining, cells were gently washed with culture medium and observed using CLSM. Images are taken together with Dr. Maya Thanou group (pharmacy department of King's College London).

In Figure 7.2, the co-incubation time for capsules with magnetite nanoparticles (A) and control capsules (B) with Caco-2 cells is 5 minutes. Both images show capsules (labeled with FITC) are adhered by the cells. From the enface images, the number of adhered capsules with magnetite nanoparticles is obviously more than control capsules. In bottom and right side panels at z – axis, most of capsules are located at the top of the cells. However, some of the capsules with magnetite nanoparticles are at the nucleus level and closer to the cells bottom than the control one.

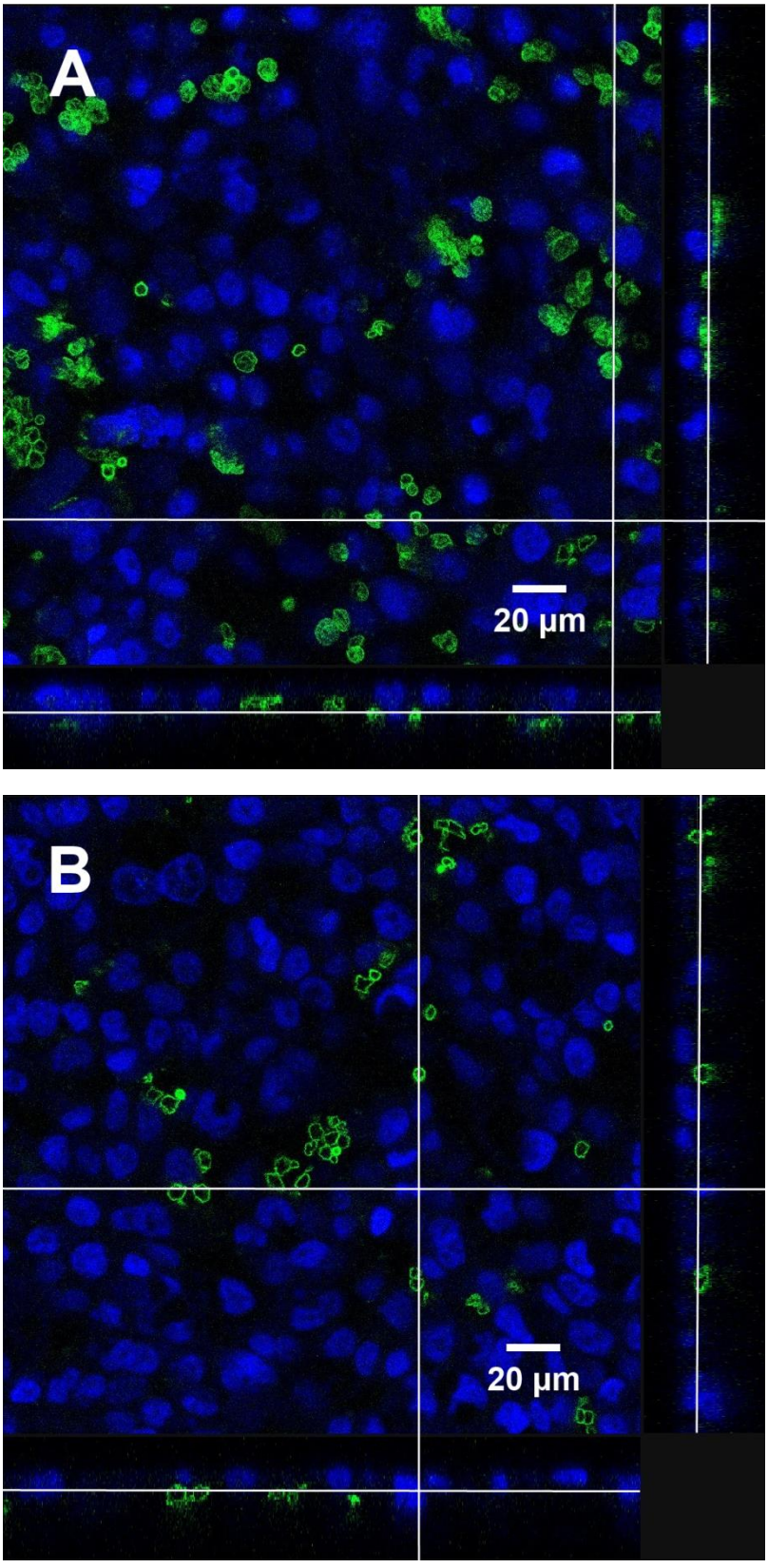

Figure 7.2: Capsules with epithelial cells after treated with magnet for 5 minutes.
Image (A) is capsules with magnetite nanoparticles, and image (B) is control capsules. The main panel shows the enface image at a given z-depth. The bottom and side panels show the x–z and y–z cross-sectional images, respectively.

All three dimensional CLSM images of epithelial cells are taken from the glass slide to the top of the cell at a series of depths with Δ z = 250 nm interval along the z - axis. The main enface panel shows the fluorescent image in the x – y cross section at a given z – location. The two smaller panels reveal the structure of the Caco-2 cells along the x – z at the bottom panel and y – z cross sections at the right side panel as indicated by dashed lines in the enface image.

Same method was using on capsules with magnetite nanoparticles and control capsules with Caco-2 cells treated by magnet for 10 minutes. Images (A) and (B) in Figure 7.3 show capsules with magnetite nanoparticles and control sample, respectively. The number of both capsules in Figure 7.3 is higher than in Figure 7.2. Long time of co-incubation of capsules / cells is increasing the number of adhered capsules.

The simple, squamous epithelial cells are quite distinctive morphologically. They are extremely thin (~ 0.2 – 0.5 μm) in the regions not including nuclei (TUMA and HUBBARD 2003). Due to limitation of cell thickness, no enough space in the cell to internalize aggregated capsules. In both Figure 7.2 and Figure 7.3, capsules with magnetite nanoparticles are more aggregated than controls. The magnetic field generated by the magnet is not homogeneous. Thus, some areas of the cells were treated with a strong magnetic field while other areas are treated with a weak one. One reason for capsules aggregation is many capsules with magnetite nanoparticles are attracted by the strong magnetic field to a limited area.

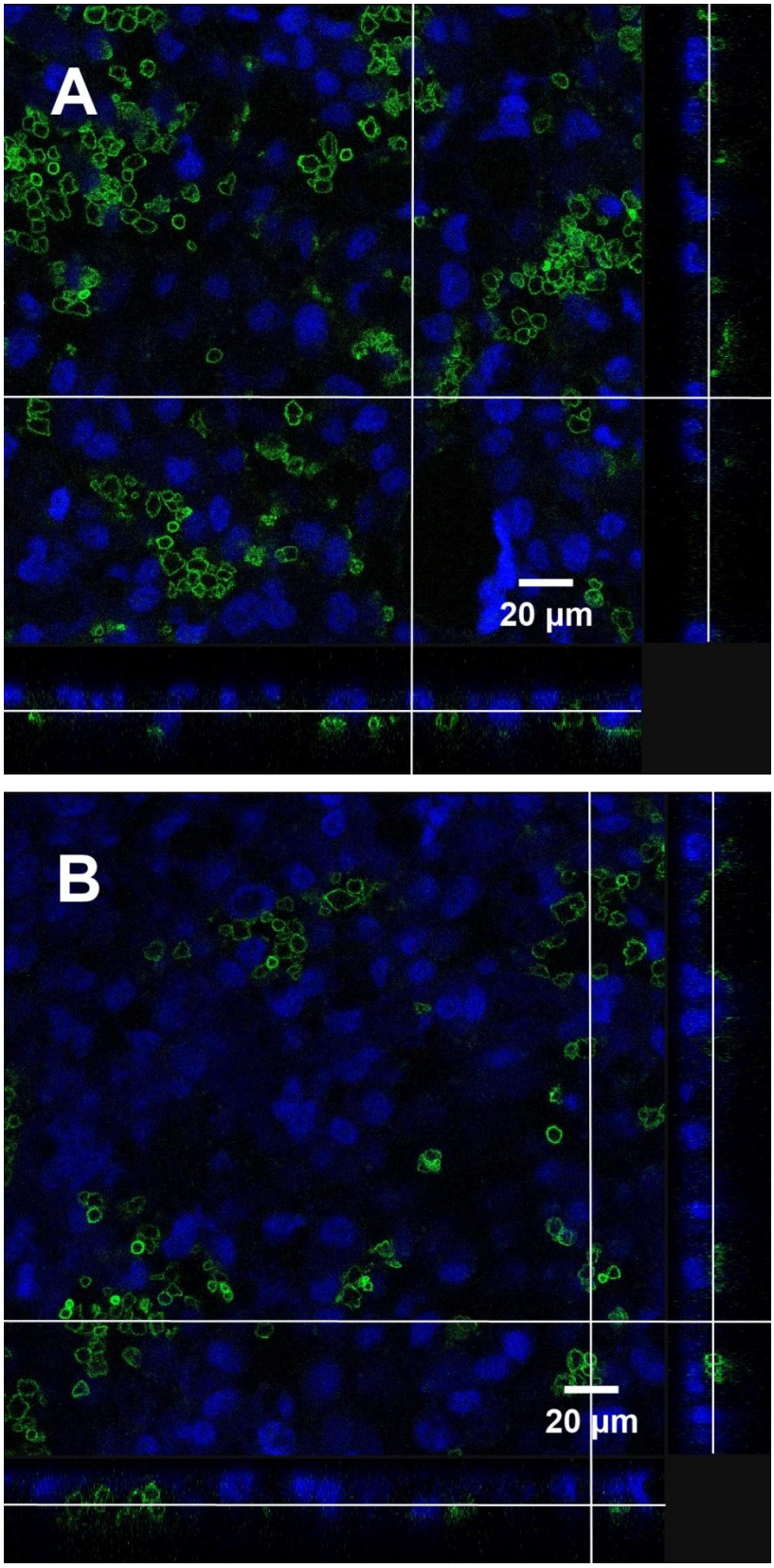

Figure 7.3: Capsules with Caco-2 cells after treated with magnet for 10 minutes.
(A) Capsules with magnetite nanoparticles and (B) control capsules. The main panel shows the enface image at a given z-depth. The bottom and side panels show the x–z and y–z cross-sectional images, respectively.

In both Figure 7.2 and 7.3, all capsules are close to the cell nucleus rather than the cell edges. Because the nuclei is the highest part of the cell, and the edge is too thin to internalize capsules with 4 μm diameter. The number of adhered capsules pre cell is summarized in Figure 7.4.

7.3 Number of adhered capsules per epithelial cell

Figure 7.4 shows the number of adhered capsules in 5 minutes and 10 minutes samples. The number of adhered capsules in capsules with magnetite nanoparticles with Caco-2 cells sample is 3 times higher than the control sample. As previous work on microcapsules with breast cancer cells, after 1 hour co-incubation of microcapsules and breast cancer cells, the number of internalized capsules per cell is around 1.4 (Sukhorukov, Rogach et al. 2005).

Number of adhered capsules in 10 minutes sample is ~1.5 times higher than 5 minutes samples. The magnet provides additional driving force attracts the capsules with magnetite nanoparticles to the bottom of the well. These capsules with magnetite nanoparticles may aggressively pass through extracellular matrix and cell membrane by damage the cells surface. Internalization of microcapsules by cells is one of primary processes for monitoring intracellular cargo transportation. Although internalization mechanism is unknown yet, phagocytosis is mostly accepting reason of these processes by scientists.

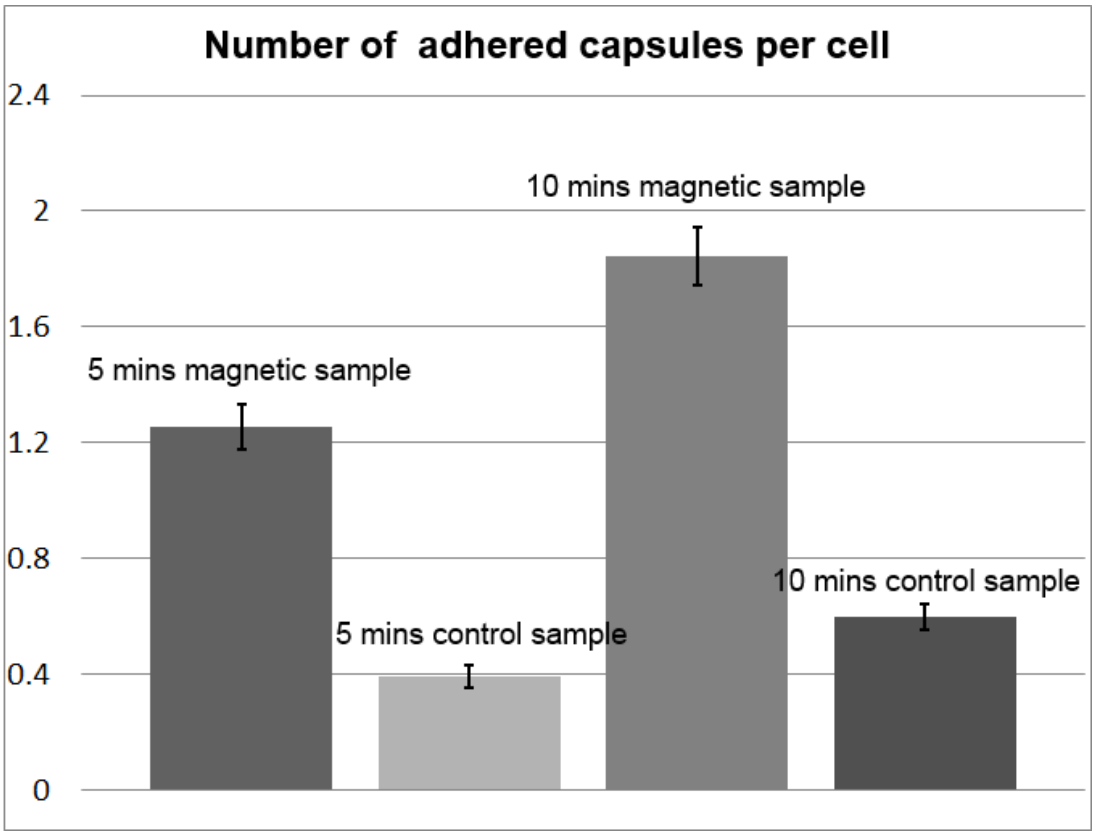

Figure 7.4: Number of adhered capsules per cell.

Every point in the results was based on 5 experimental data from five independent experiments, although, every experimental data was the averaged value based on 20 cells.

7.4 Conclusion

In this study, we demonstrate the colon cancer epithelia cells of Caco-2 internalize certain amount of capsules in few minutes. Control capsules naturally precipitate on the top of the epithelial cells. Capsules with magnetite nanoparticles are attracted by additional magnetic field to the cells. The additional driving force makes the capsules internalization more efficiency. The result is shown in our work that 1.2 and 1.8 adhered capsules per cell are observed for treat the sample at 5 and 10 minutes with magnet respectively. These numbers of capsules is 3 times higher than the control samples. Furthermore, capsules with magnetite nanoparticles are more aggregated and close to the cell bottom.

For further studies, to prove the capsules locate inside the cells, cell membrane is labeled. Another significance of this study is the magnet can be placed in any directions such as side or top of vessels. The magnetically forced uptake of capsules model is able to play an important role *in vivo*, as the blood circulation takes capsules anywhere within the body, but the highly forced magnetic field is able to force the capsules with magnetite nanoparticles to remain in the typically area for investigations.

8 Investigation of interactions between capsules and endothelial cells by biochemical stimuli

The luminal surface of blood vessels is lined by a monolayer of endothelial cells, which are in direct contact with the circulating blood. The vascular endothelial cells play significant roles in tissue homeostasis, vascular regulation, blood cell activation and migration during physiological and pathological processes (Risau 1995; Middleton, Neil et al. 1997). On the luminal surface of endothelial cells, the glycocalyx has a brush like structure that contains negatively charged matrix of proteoglycans, glycosaminoglycans and glycoproteins (Pries, Secomb et al. 2000). The thickness of the glycocalyx layer ranges between a few hundred nm and few µm (Squire, Chew et al. 2001). Neuraminidase, an enzyme that cleaves N-acetyl neuraminic acid residues of glycoproteins and targets specifically the sialic acid component of the endothelial glycocalyx is commonly used to manipulate the structure of the glycocalyx (Barker, Konopatskaya et al. 2004).

Recently, number of natural polyelectrolytes and polypeptides have been used to fabricate biodegradable microcapsules and these capsules are successfully internalized by several phagocytic cells such as most cancer cells and immune cells (Sukhorukov, Rogach et al. 2005; De Geest, Vandenbroucke et al. 2006). The mechanisms of uptake of microcapsules by living cells are not yet fully understood (De Cock, De Koker et al. 2010) and are still under investigation, but apparently the natural endocytosis of these cells is most probable reason for uptake. So far, no reports on microcapsules internalization and/or degradation by non-phagocytic cells had been published. In this paper, normal healthy cells of human umbilical vein endothelial cells (HUVECs) are used for the study of induced microcapsule entry.

This part of thesis is to investigate the role of the glycocalyx on trans-membrane movement of microcapsules *in vitro*. Microcapsules with neuraminidase and $CaCO_3$ co-precipitated templates were fabricated. The neuraminidase encapsulation efficiency and release rate were investigated. Comparison between neuraminidase loaded microcapsules and the control was carried out. We further studied the degradation rate of DS/PArg microcapsules after internalized by HUVECs.

8.1 Capsules charge affected by culture medium

In our study, microcapsules were premixed with culture medium and incubated with HUVECs, so it is likely that the charge on microcapsule outermost layer will be changed by the culture medium due to salt effects and protein adsorption. To study this effect, 4 layered PSS – PAH capsules with either PSS outmost layer or PAH outmost layer, i.e. $(PSS\text{-}PAH)_2$ and $(PAH\text{-}PSS)_2$ capsules, were mixed with culture medium for 12 hours and washed 3 times with Milli-Q water, before their zeta potentials were measured.

Figure 8.1 shows the results and their comparison to the control, i.e. before they were exposed to the cell culture medium. It is seen that for the control, zeta potentials for PAH and PSS outmost layered capsules are of +10.13 mV and -17 mV respectively. However, after 12 hours in the culture medium, their Zeta potentials have changed to -5.5 mV and -8.97 mV. Results show that sespite their initial difference in the charge property, both capsules exhibited negative charges in the cell culture medium.

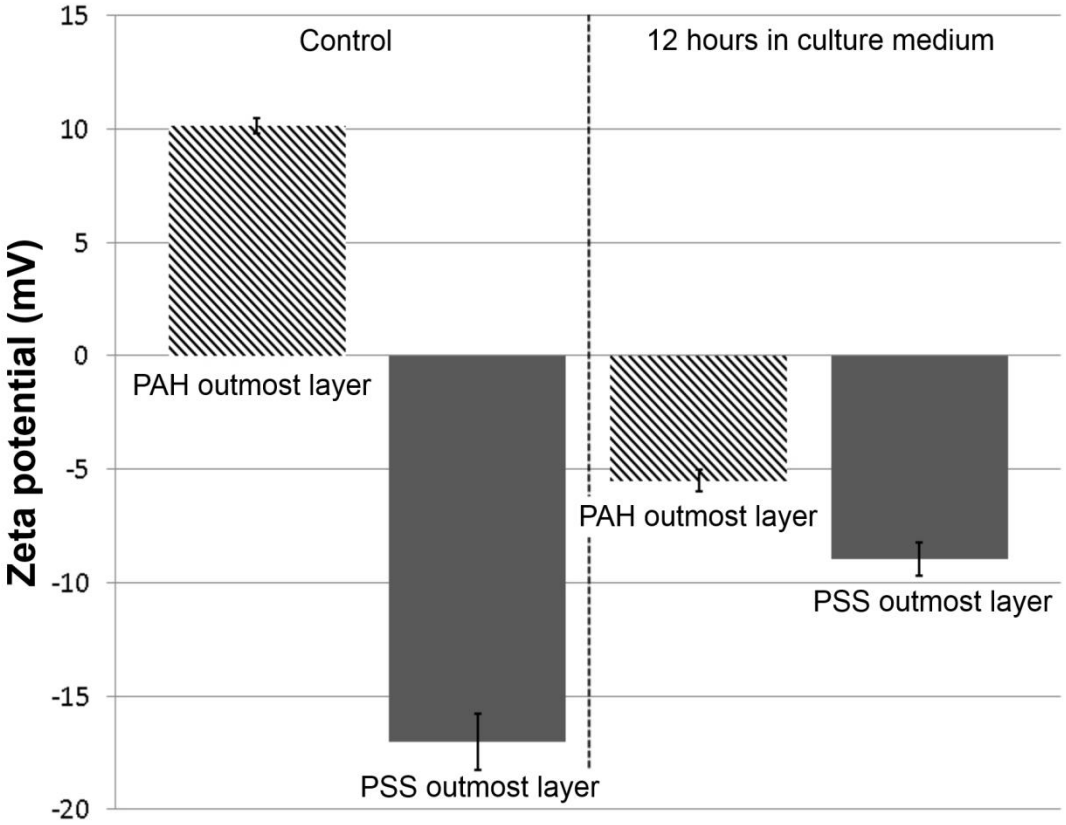

Figure 8.1: Zeta potentials of capsules affected by culture medium.

Zeta potentials of 4 layered PSS – PAH microcapsules with either PAH or PSS outmost layer after 12 hours in the cell culture medium (n = 5).

Cell culture medium contains a variety of components and growth factors for cells viability that can alter the charge property of the capsule, including salts, such as NaCl (6800 mg/L), KCl (400 mg/L) and $NaHCO_3$ (2200 mg/L). Georgieva et al studied the influence of different salts on polyelectrolyte hollow microcapsules. They reported that the surface charge of capsules changed from initially positive to negative values after 24 hours of incubation in each of the carbonate solutions (Georgieva, Dimova et al. 2005). They demonstrated that the complete charge reversal of PAH layer is caused by interaction of the

8.2 Microcapsules sterilization

One of the primary problems of study microcapsules for drug delivery to living cells is toxicity. After capsules fabrication, an autoclaving step was applied for sterilization of capsules. Capsules solution was placed into a glass tube with unsealed cover, heated to 126 ^{o}C for 30 minutes. After the solution cool to room temperature, the capsules were sterilized and ready for endothelial cells co-incubation. Thus, the viability of cells is only affected by materials of the capsules.

Capsules before autoclaving

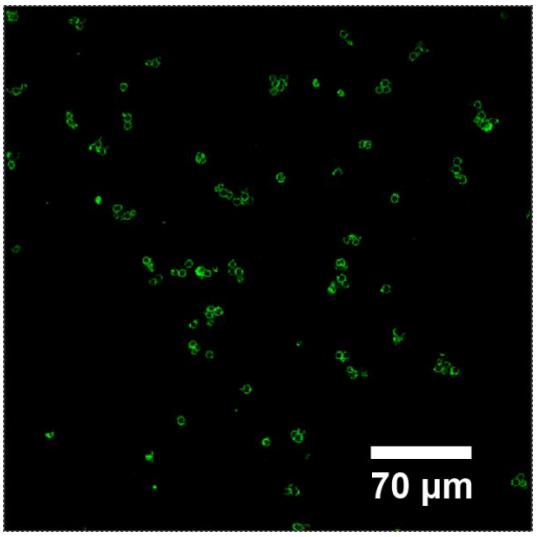

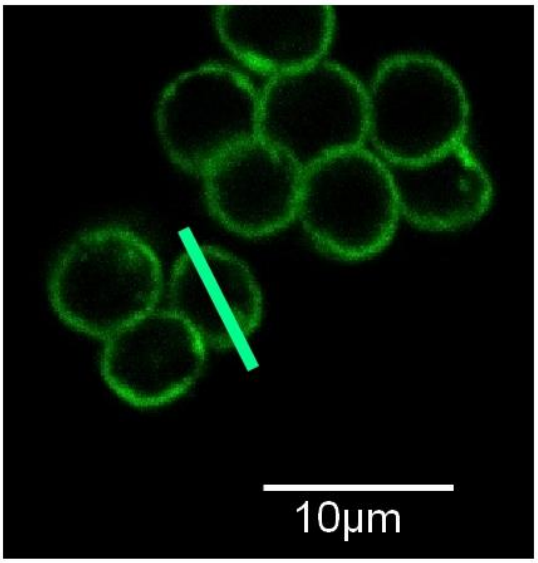

Capsules after autoclaving

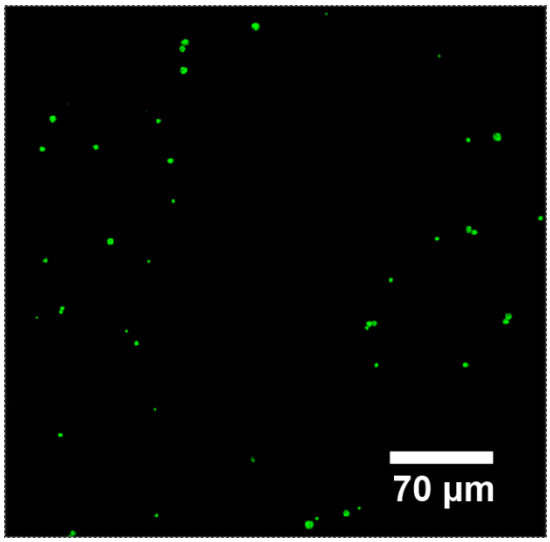

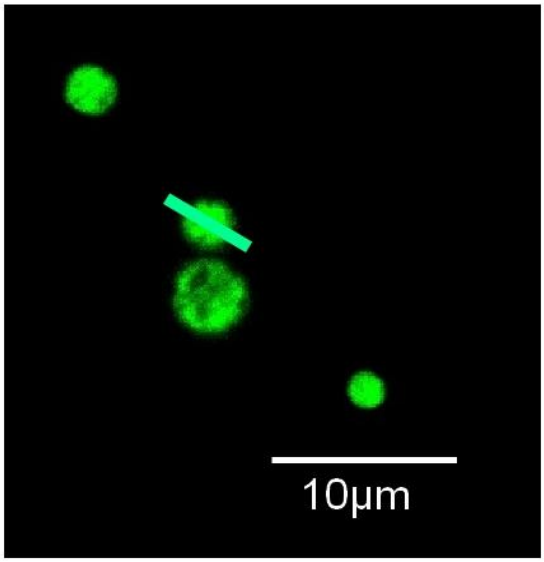

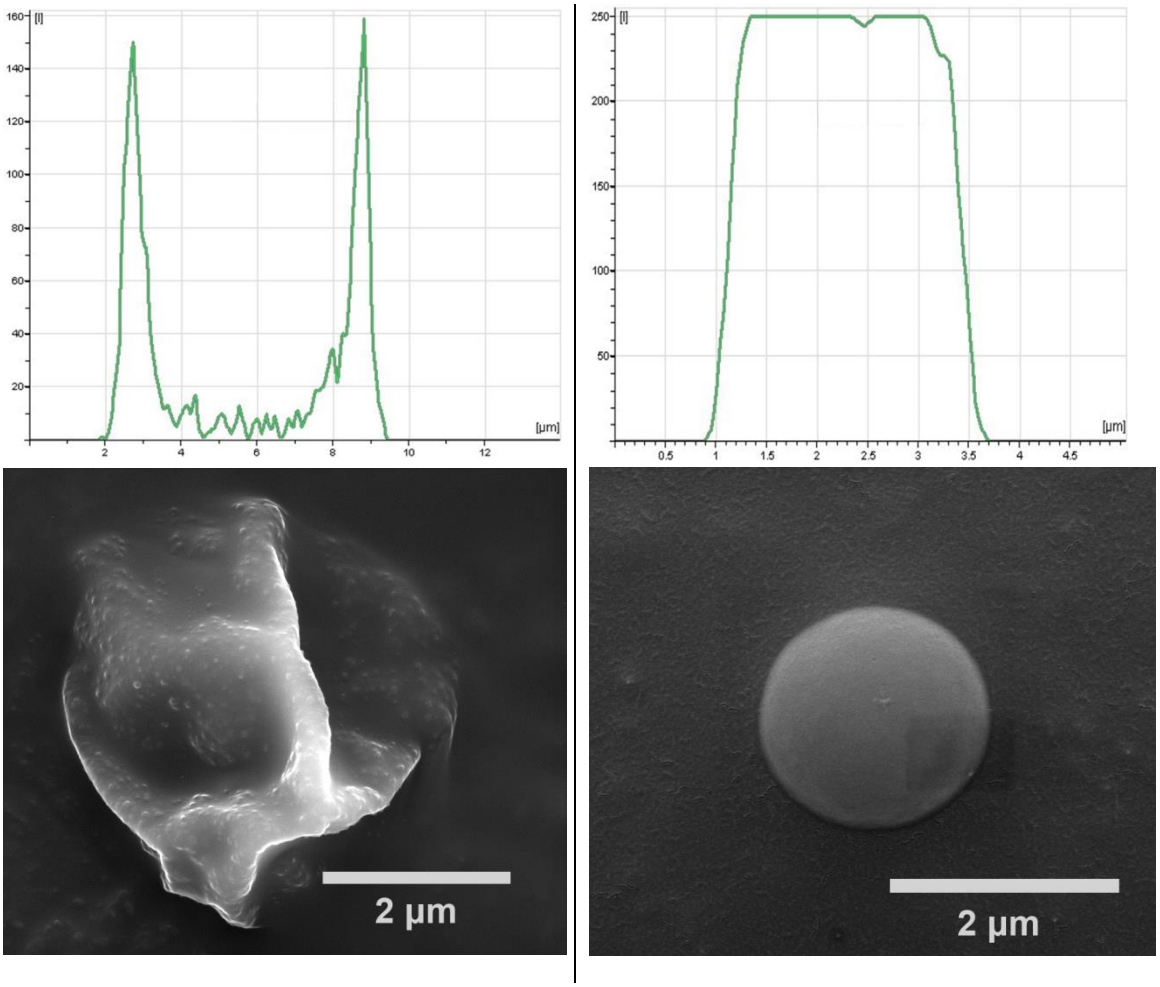

Figure 8.2: CLSM and SEM images of capsules before and after autoclaving.
Images from top to bottom are overview CLSM images, zoomed CLSM images, FITC intensity along the marked green line, and SEM images represent the capsules before (left) and after (right) autoclaving.

Figure 8.2 shows the initial 4 µm $(PSS/PAH)_3$ capsules collapse during drying to flat creased structures. The shell with thickness approximate 20 nm was not stable enough to keep the spherical shape of capsule in the dried state. Figure 8.2 shows the capsules keep their spherical shape after autoclaving, no deformations indicating a collapse were observed. Capsules size reduced from average 4 µm to 2 µm with surface became smoother, shell thickness was increased and encapsulated fluorescence dye was concentrated. The increasing mechanical stability against collapse of the capsules with decreasing diameter points to a steadily increasing wall thickness.

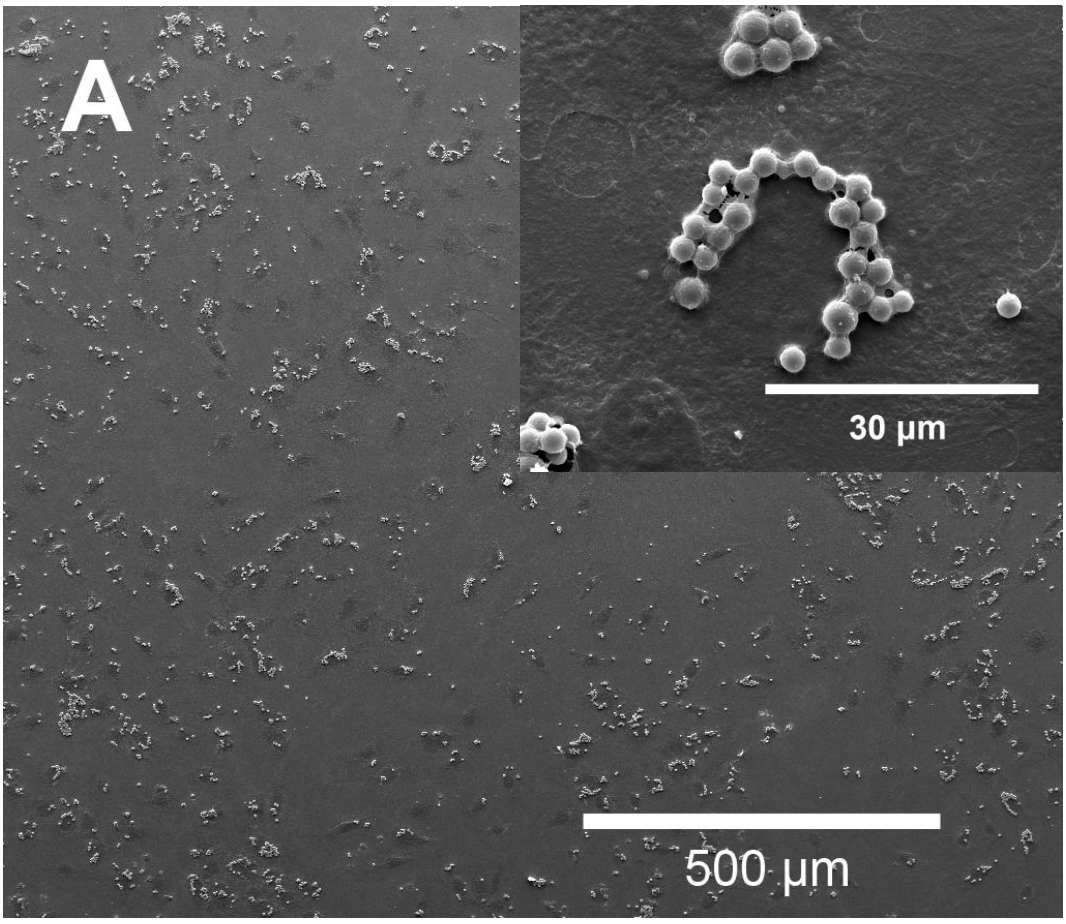
A
30 µm
500 µm

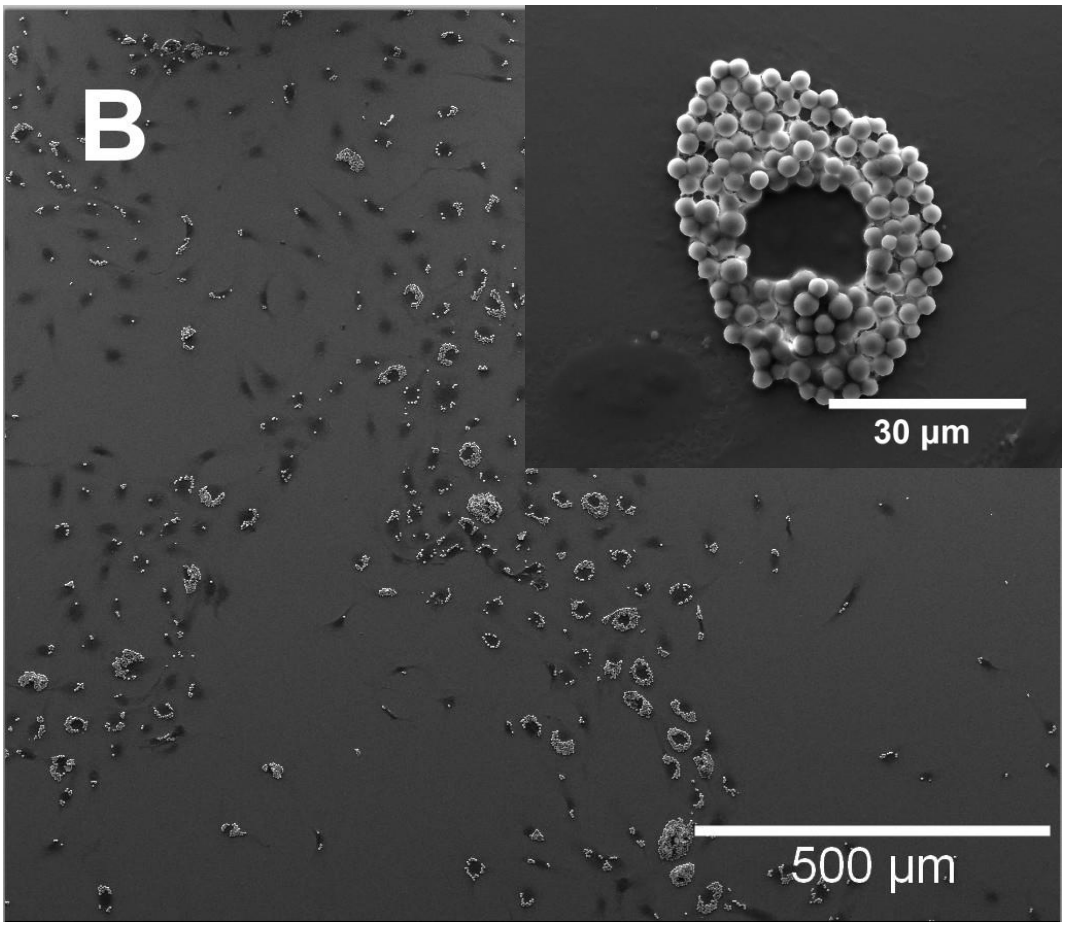
B
30 µm
500 µm

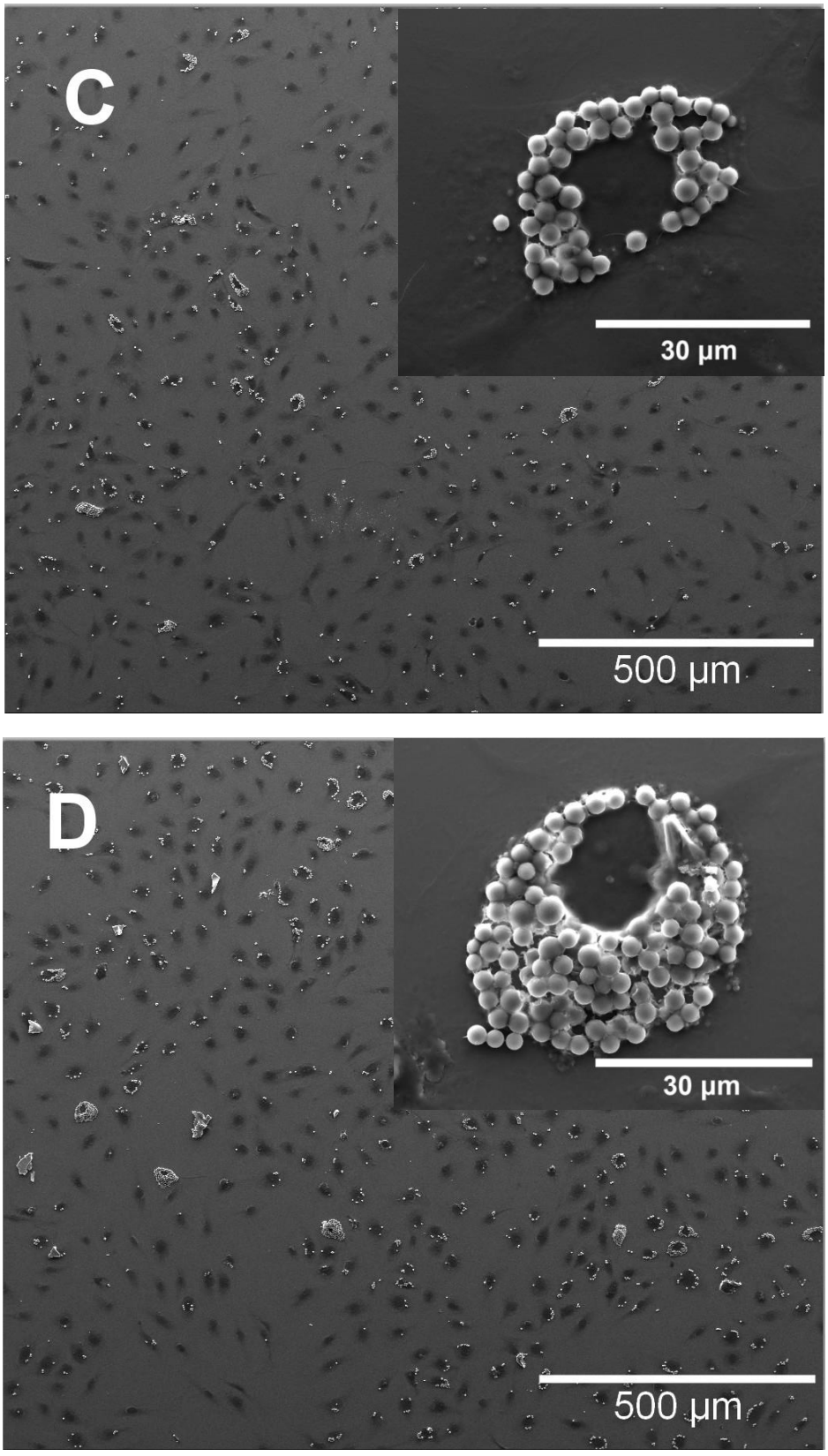

Figure 8.3: SEM images of sterilized PSS/PAH microcapsules with endothelial cells. Capsules and cells were in the incubator with cells favorite conditions after 2 (A), 4 (B), 7 (C) and 14 (D) days.

Before adding capsules into cells, capsules were diluted with cell culture medium. Number of capsules to cells ratio is 50:1. The culture medium was changed every two days during co-incubation. Therefore, the capsules in Figure 8.3 (D) were washed at least 6 times with culture medium. From Figure 8.3, the cells number is changed, old cells were died and new cells were divided. For some cells in Figure 8.2 (B), (C) and (D), large number of capsules form aggregates around cell nucleus, and capsules are covered by wax like materials, may be inter- or extra-cellular matrix.

Generally, the PSS/PAH capsules located on HUVECs are non-toxic for endothelial cells and cannot be degraded after two weeks. Endothelial cells can still survival with many capsules on the membrane l. So far, we can conclude these capsules can be adhered tightly by endothelial cells.

8.3 Encapsulation efficiency of TRICT-dextran

Encapsulation efficiency was measured with encapsulated TRICT-dextran by PerkinElmer LS55 fluorescence spectroscopy. A process of preloading was used for TRICT-dextran encapsulation. 2 mg of TRICT-dextran was mixed with 1 ml of 0.33 M $CaCl_2$ and 1 ml of 0.33 M Na_2CO_3 aqueous solutions under vigorous agitation for 15 s. After 3 times wash step with Milli-water, $CaCO_3$ micro particles containing TRITC-dextran in their pores was used as template for capsules fabrication. The capsules were synthesized under typical LbL process, template cores were dissolved while desired number of layers reached.

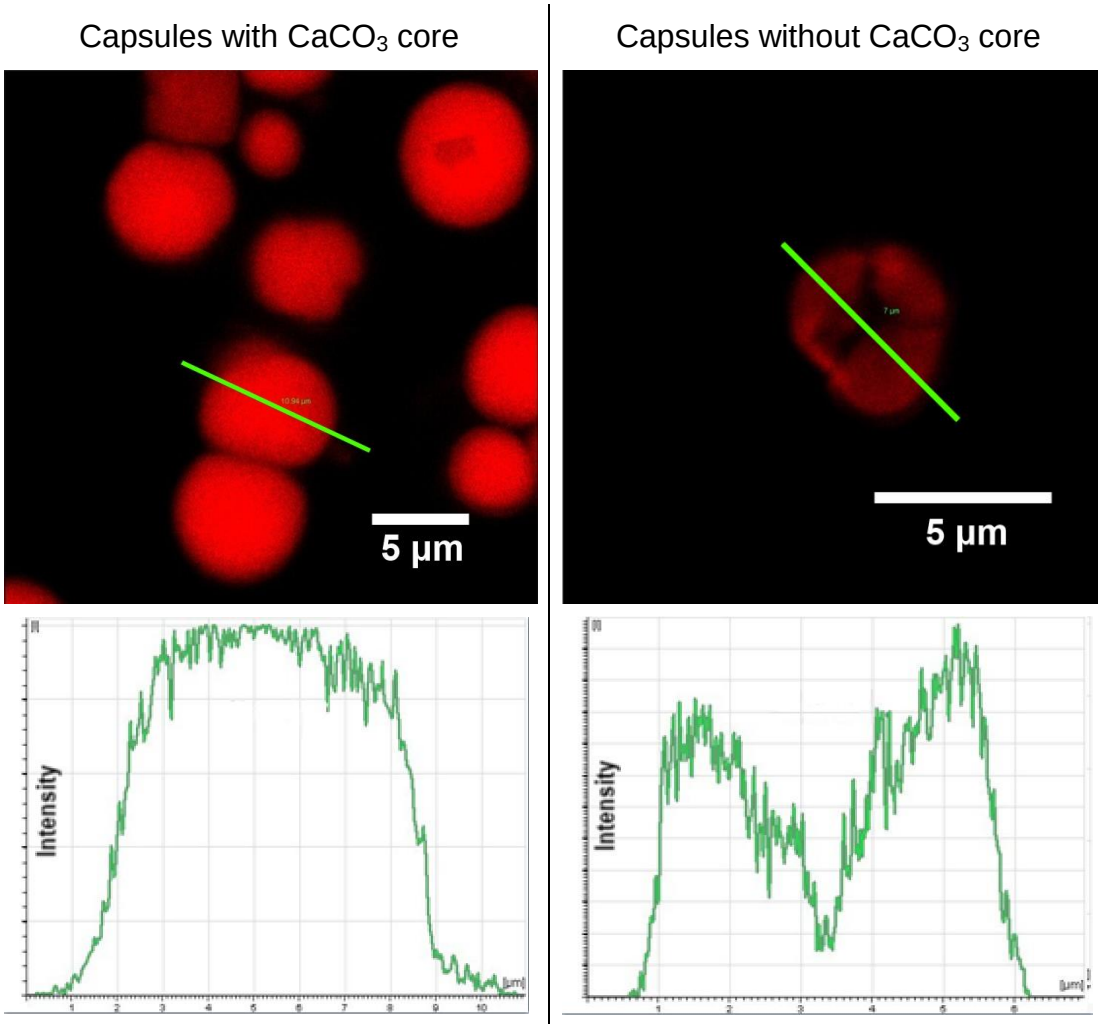

Figure 8.4: CLSM images of capsules contain TRICT-dextran

Images present TRICT-dextran in capsules before (left) and after (right) $CaCO_3$ core dissolution. The bottom is the intensity along the green drawing line through the capsules. Scale bar is 5 µm.

Supernatants centrifuged by core dissolution and washings steps, were collected for fluorescence spectroscopy measurement. The amount of TRITC-dextran encapsulated is mostly depended by the interaction between it and $CaCO_3$ in co-precipitation step. Figure 8.4 shows TRITC-dextran intensity of capsules interior is obviously reduced after core dissolution. Therefore, the encapsulated protein is rapidly released in $CaCO_3$ template decomposition step.

Control TRITC-dextran intensities with different prepared concentrations have been measured to generate the calibration curve. Once the calibration curve is generated, any samples with the same substance at the same wavelength can be calculated from the slope. The amount of TRITC-dextran lost during capsules fabrication in washing steps is very lower compare with core dissolution step. The amount of protein lost during core removing step is varied from 30% to 40% of the total amount of protein. More polyelectrolyte layers result thicker capsule shell which could keep more proteins compared with few layers capsules in core dissolution step. Encapsulation efficiency of neuraminidase enzyme used in the following section is tested.

8.4 Encapsulation efficiency and release rate of neuraminidase

Polyelectrolyte capsules are not completely sealed for proteins. Protein release occurs according to capsule wall composition (She, Wang et al. 2012). In our study, microcapsules, $(PSS/PAH)_2$, had 4 layers. 4 mg of neuraminidase was co-precipitate with $CaCO_3$ microparticles. 0.836 mg of neuraminidase remained in the glass beaker with uncollected particles. During polyelectrolytes absorbing and capsule washing steps, there was negligible amount of neuraminidase losses, and its concentration in the supernatants was too low to be detected by UV−Vis Spectroscopy. 1.56 mg of neuraminidase was lost in the $CaCO_3$ template decomposition step, called burst release. Therefore, approximately 21% and 39% of the neuraminidase were lost in the core co-precipitation and the dissolution steps respectively, leaving 40% of the neuraminidase in capsules. Total number of capsules was determined using haemocytometer counting chambers, and they were estimated to be $(7.8 \pm 0.3) \times 10^7$. The amount of neuraminidase in a single microcapsule was therefore estimated to be ~20 pico-gram.

To investigate the release rate of neuraminidase from $(PSS/PAH)_2$ microcapsules, all microcapsules were placed in 2 ml Milli-Q water at room temperature. The supernatant was collected after 2, 24 and 72 hrs, and the surrounding water was fully refreshed at each time point. The concentration of neuraminidase in the collected supernatant was determined by UV-Vis spectrometer. Figure 8.5 shows the release rates of neuraminidase from $(PSS/PAH)_2$ microcapsules. It is seen that in the first 2 hours, neuraminidase was released at 12.82 µg/h, but the value decreased to 10.36 µg/h over the next 22 hours and then to 8.64 µg/h over the following 48 hours. Protein encapsulation and release have been studied by a number of groups (Antipov, Sukhorukov et al. 2001; De Geest, Sanders et al. 2007; She, Antipina et al. 2010). Our results are consistent to their findings that the release rate of proteins from polyelectrolyte microcapsules over the first hours is significantly higher than that over the following hours.

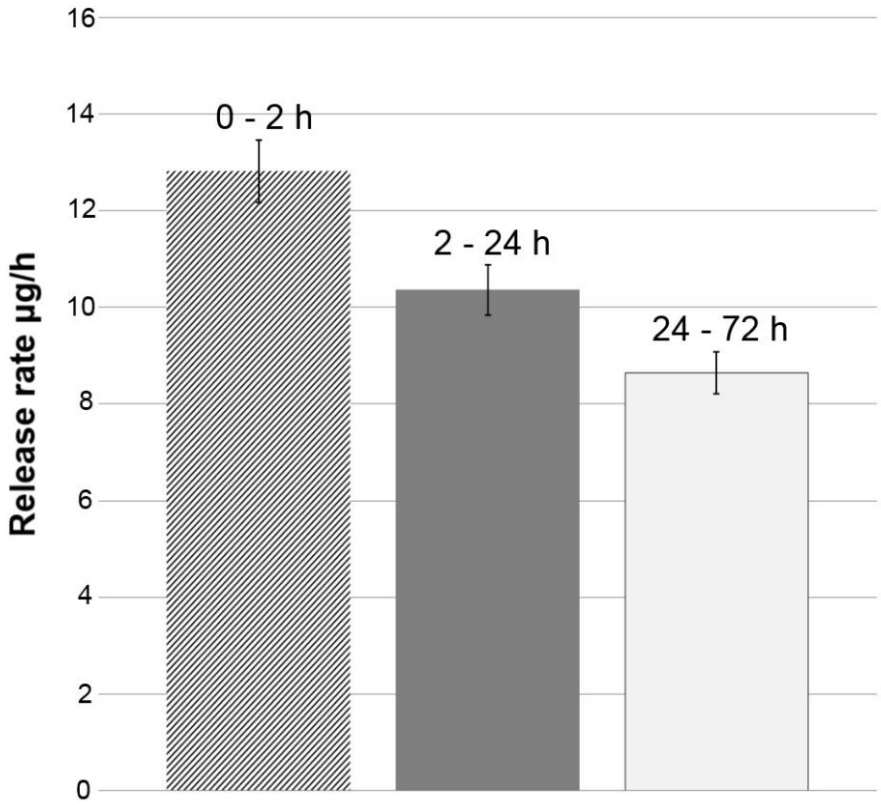

Figure 8.5: Neuraminidase release rate.
Release rate from $(PSS/PAH)_2$ microcapsules at room temperature (number of experiments, n = 5).

8.5 Samples preparation

Capsules preparation is introduced in the above section of chapter 6. HUVECs (primary pooled) were purchased from Lonza (Lonza Cologne AG, Germany). They were thawed and cultured in the M199 medium (Gibco) in collagen type I-coated flasks (5 μg/ml) at 37 ^{o}C and 5% CO_2. The culture medium contains 10 % foetal bovine serum, EC growth factor-β (1 ng/ml), EC growth supplement from bovine neural extract (3 μg/ml), thymidine (1.25 μg/ml), heparin (10 μg/ml), 100 U/ml penicillin, 100 mg/ml streptomycin (all supplements are from Sigma Aldrich). The medium was changed every 2 days. After reaching 80% confluence, HUVECs were treated with 0.25% trypsin containing 0.02% ethylenediaminetetraacetic acid (EDTA; Sigma Aldrich) and cells were split and seeded on collagen type I-coated glass slide. (Bai and Wang 2012).

8.6 Cleavage of the glycocalyx by neuraminidase

The process of a neuraminidase loaded microcapsule entering a vascular endothelial cell is represented in a schematic drawing in Figure 8.6. Figure 8.6 (A) shows microcapsule is added in culture medium and incubated with endothelial cells; Figure 8.6 (B) shows capsule comes to contact with the endothelial membrane. Neuraminidase released from the capsule cleaves the endothelial glycocalyx; Figure 8.6 (C) shows capsule is internalized by the endothelial cell.

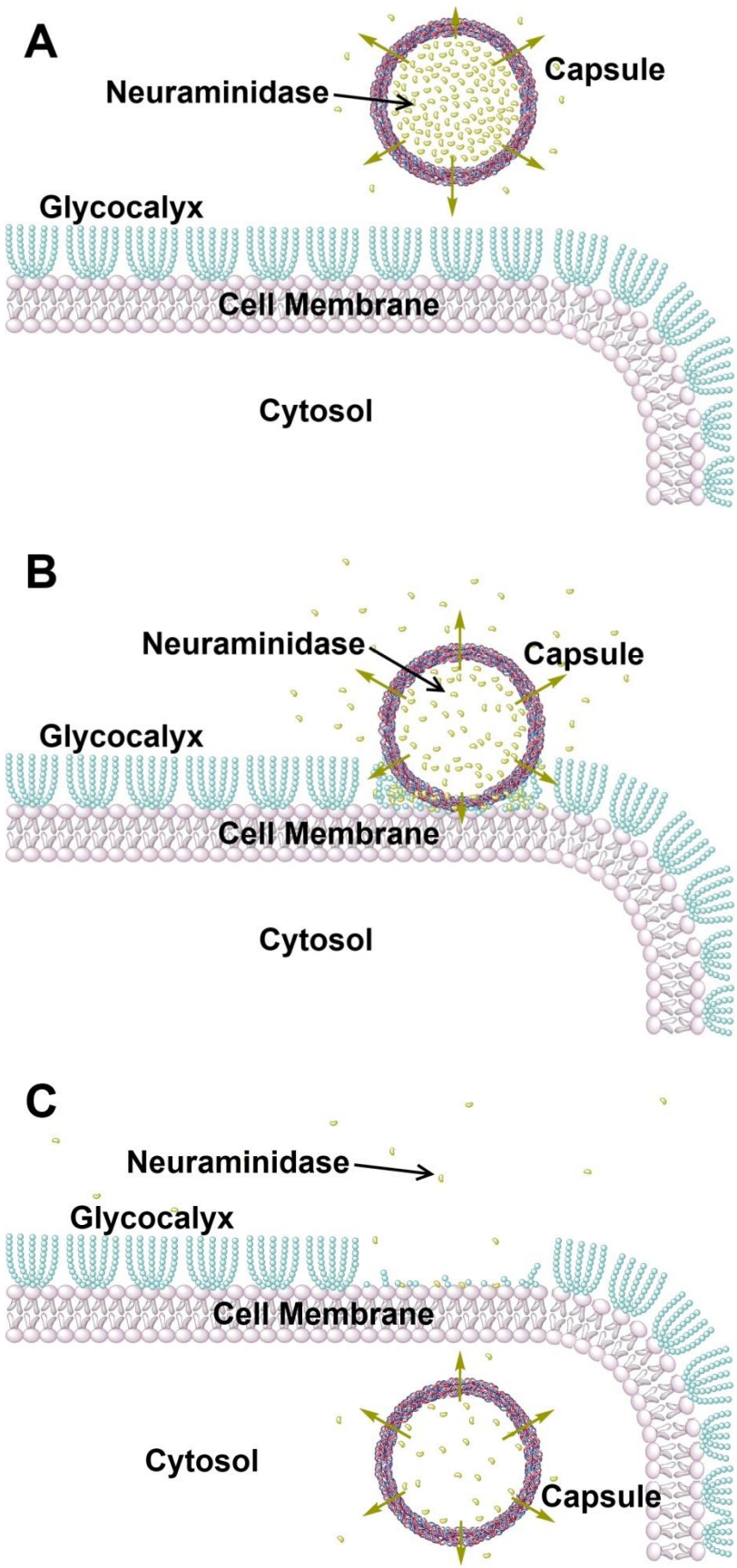

Figure 8.6: Schematic illustration of the uptake of a neuraminidase-loaded microcapsule by a vascular endothelial cell.

HUVECs on cover slips were stained as following: wheat germ agglutinin (WGA-FITC) was used to bind to N-acetly-D-glucosamine and sialic acid component of the glycocalyx; the endothelial cytoplasm was stained by Cell Tracker Red CMTPX and cell nucleuses were stained using Hoechst 33342. Samples were briefly washed 3 times using the serum free M199 medium before each staining step. WGA-FITC and Cell Tracker Red were applied to live cells for 15 min at 37 ^{o}C before Hoechst 33342 was applied for 10 min. Cells were washed and immersed in culture medium contain 10% serum immediately after staining, and were kept in the culture medium with serum during CLSM observation.

For neuraminidase treated samples, they were prepared according to the protocol by Barker et al (Barker, Konopatskaya et al. 2004) as we performed in previous studies (Bai and Wang 2012; Bai and Wang 2013). HUVECs samples were gently washed with serum free M199 medium twice before they were incubated with 1 mg/ml neuraminidase medium for 10 min at 37 ^{o}C. They were then stained and observed under the CLSM.

Different enzymes are able to cleave different components of the glycocalyx. The technique and protocol of enzyme treatments have been studied in a number of previous investigations (Barker, Konopatskaya et al. 2004). In this work, we first establish that neuraminidase abolishes the glycocalyx layer on our cultured endothelial cells. Then we investigate interaction between microcapsules and HUVECs with and without the glycocalyx layer. Finally, we study interaction between neuraminidase-loaded microcapsules and HUVECs that have the glycocalyx layer.

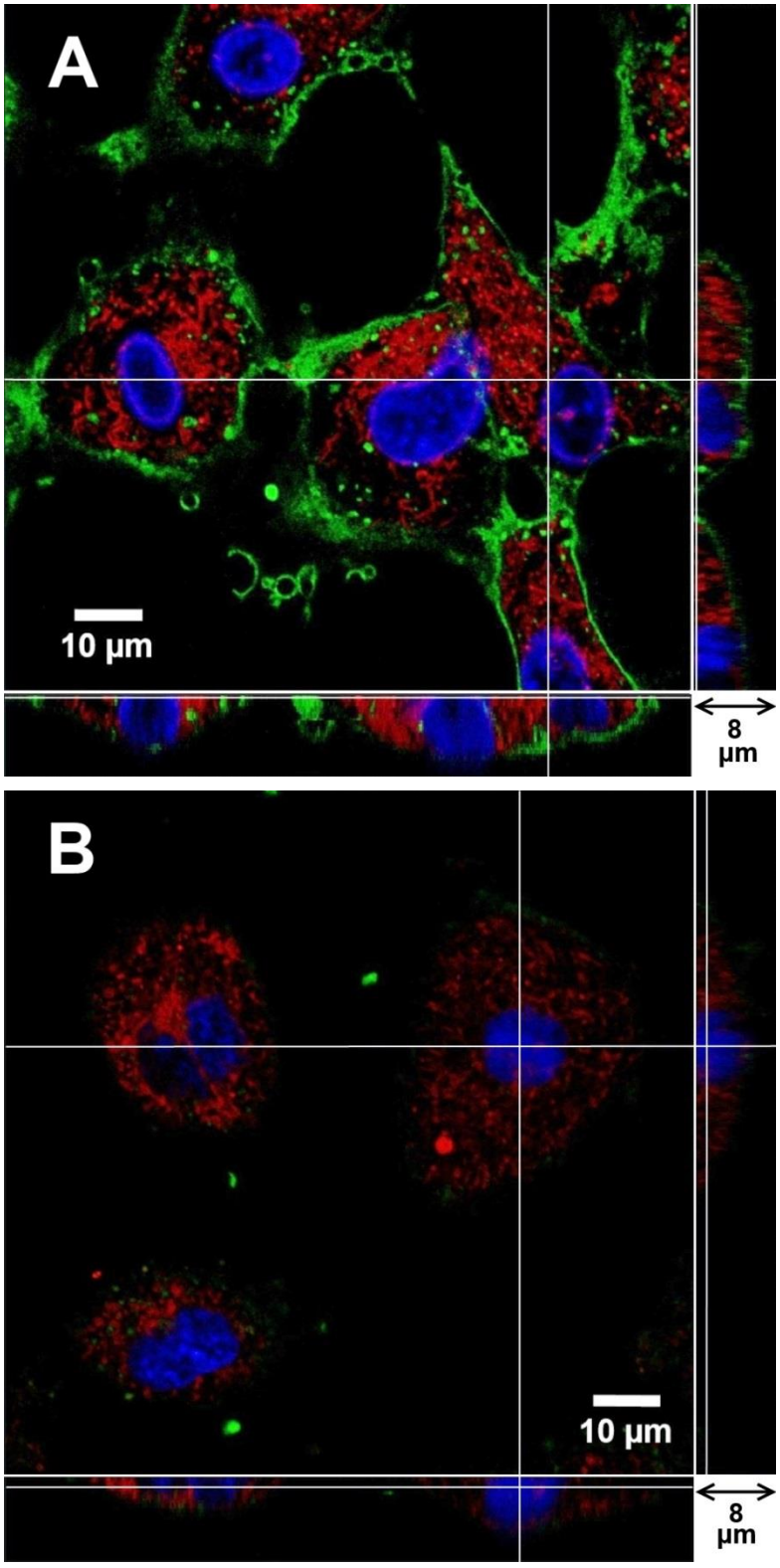

Figure 8.7: Three dimensional CLSM images of HUVECs.

(A) Control, (B) Neuraminidase treated. The main panel shows the enface image at a given z-depth. The bottom and side panels show the x–z and y–z cross-sectional images, respectively. Scale bar in the main panel = 10 µm, and scale bar in the bottom and side panels = 8 µm.

Figure 8.7 shows the three dimensional CLSM images of HUVECs from the glass slide to the top of the cell at a series of depths along the z-axis, with Δz = 250 nm. The main enface panel shows the fluorescent image in the x–y cross section at a given z-location. The two smaller panels reveal the structure along the x–z (bottom panel) and y–z cross sections (right side panel) as indicated by dashed lines in the enface image. Figure 8.7 (A) is the control, where HUVECs have been cultured for 14 days. The green-stained glycocalyx layer is seen to have a thickness of several hundred nanometers to one micrometer. It is continuous and covers the surface of the endothelium. Following neuraminidase treatment, shown in Figure 8.7 (B), there is hardly any green fluorescence in the image; giving evidence that neuraminidase cleaves away most of the glycocalyx layer from the HUVEC membrane.

Figure 8.8 shows the interaction between microcapsules and endothelial cells. Cell-viability assays *in vitro* such as MTT test reported no acute cell toxicity at moderate microcapsule concentrations (An, Kavanoor et al. 2009). In all our study, the ratio between the numbers of microcapsules and HUVECs was controlled at approximately 20:1. Further increase of the microcapsule concentration in the culture medium results in more capsules precipitated on the cell surface, which may affect cell metabolism and viability (Kirchner, Javier et al. 2005; Liu, Gao et al. 2005).

For the Control, shown in Figure 8.8 (A), HUVECs were cultured for 14 days and their membrane was covered with the glycocalyx layer. $(PSS/PAH)_2$ microcapsules with TRITC-dextran (hence red fluorescence in images) was added in the culture medium. Following 48 hours co-incubation, there were a small number of microcapsules observed in the enface image. However, a close look of the bottom and side panels in Figure 8.8 (A) revealed that these microcapsules were all on top of the endothelial glycocalyx and none had penetrated into the endothelial cells.

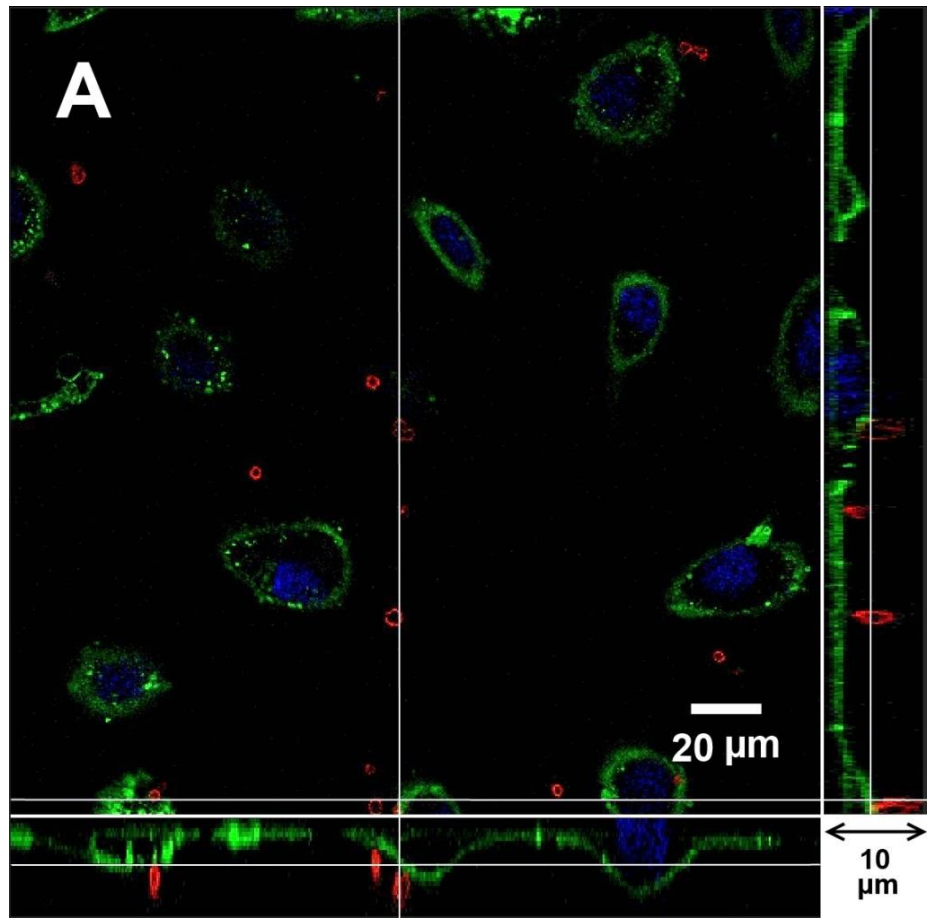
A
20 µm
10
µm

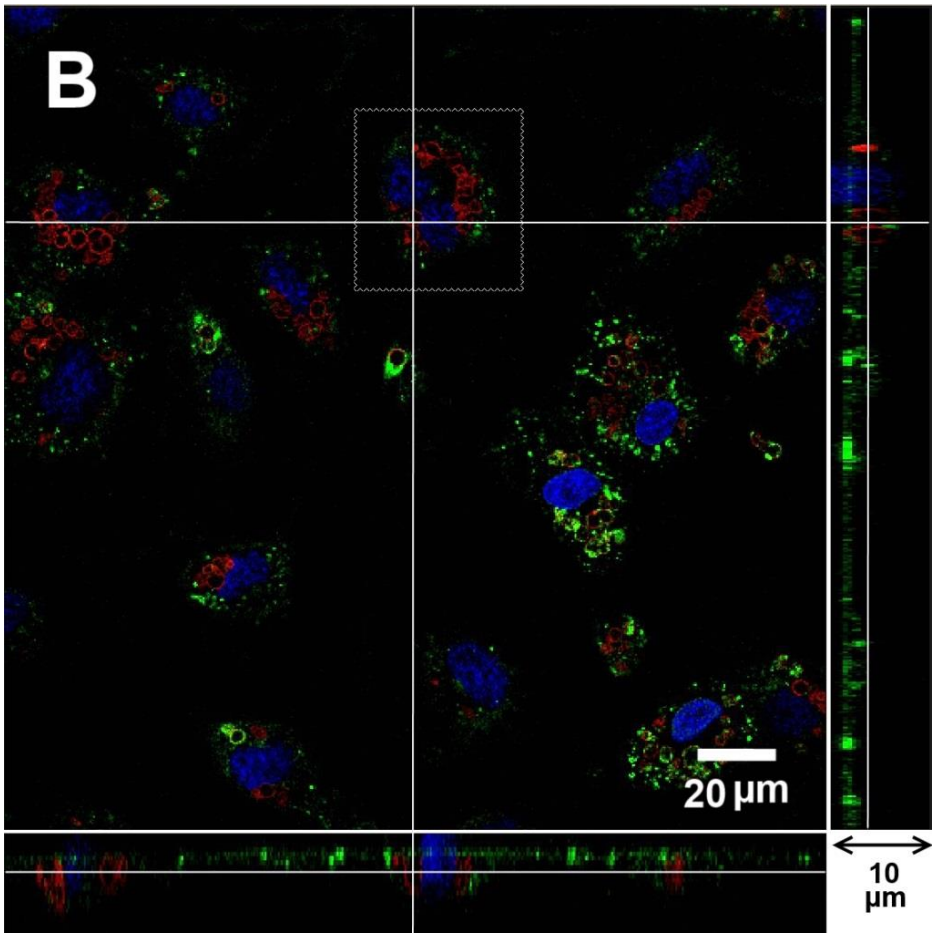
B
20 µm
10
µm

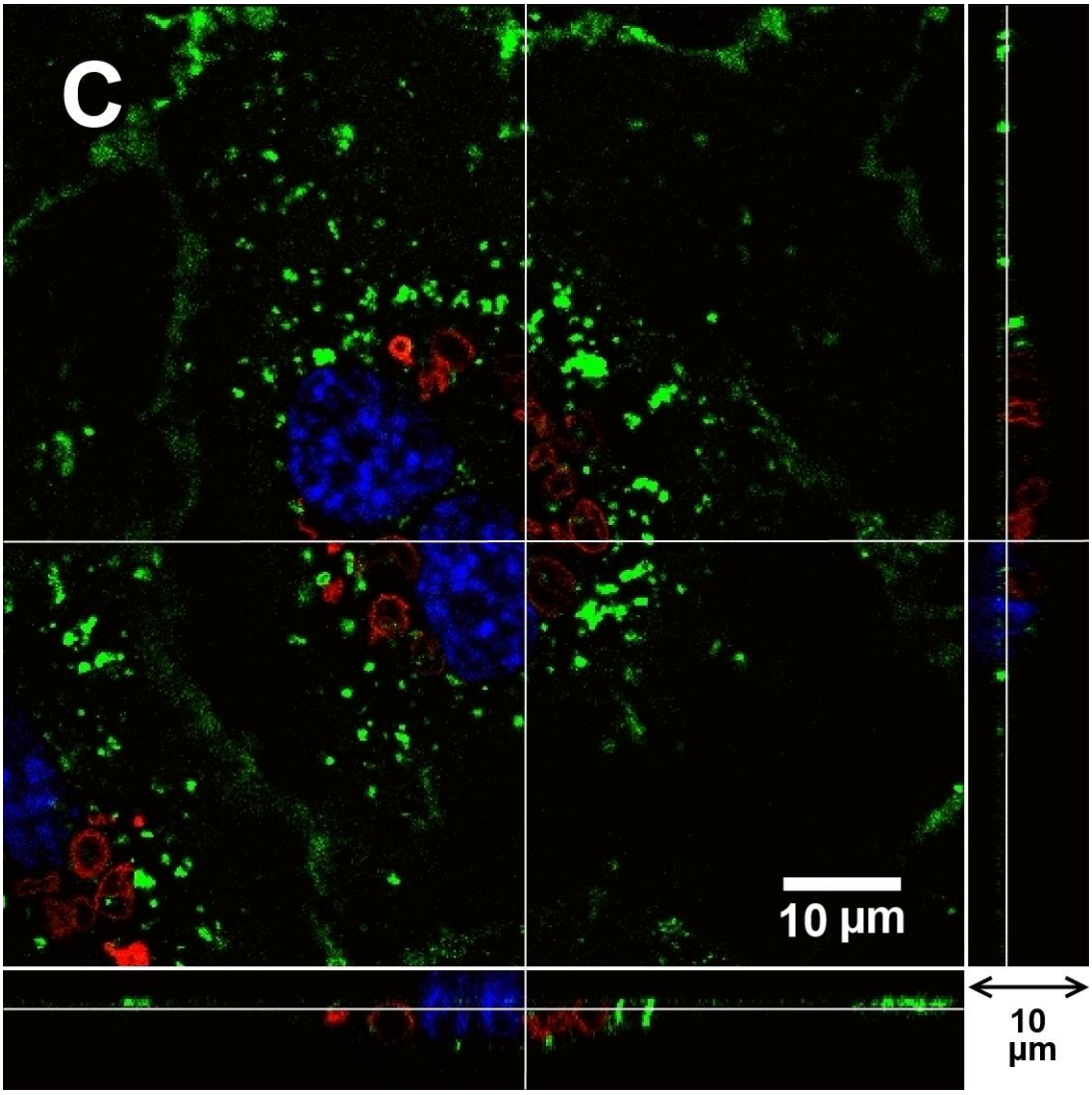

Figure 8.8: Interaction between microcapsules and endothelial cells.

(A) Control, (B) Endothelial cells were pretreated with neuraminidase and then incubated with microcapsules for 48 hrs, (C) Enlarged image of the highlighted area in B). The main panel shows the enface image at a given z-depth. The bottom and side panels show the x–z and y–z cross-sectional images, respectively.

In Figure 8.8 (B), HUVECs were pretreated with 1 mg/ml neuraminidase for 10 min at 37 ^{o}C. This abolished the glycocalyx layer on the cell membrane. $(PSS/PAH)_2$ microcapsules were added to the culture medium and incubated with the pretreated HUVECs for 48 hours. At the end of 48 hours, part of the glycocalyx layer was recovered, but it was still patchy with little sign of green staining on the membrane above the cell nucleus. Microcapsules were

observed inside the endothelial cells. This can be seen clearer in the enlarged image in Figure 8.8 (C), where red stained microcapsules clustered around cell nucleus. They were inside the cells and, in places, covered by re-grown glycocalyx layer. The x-z and y-z panels revealed that they leveled with the nucleus rather than being on top of the cell membrane, as seen in the control.

8.7 Number of capsules adhered by HUVECs

$(PSS/PAH)_2$ microcapsules were fabricated with neuraminidase as described before. They were divided equally into 20 portions and added to HUVECs with 2 ml culture medium. The number of microcapsules in each sample was estimated in the haemocytometer counting chamber. After 2 hours co-incubation, the sample was washed 3 times with the culture medium. The number of microcapsules in the supernatant was estimated by the haemocytometer counting chamber.

	total number of capsules used in experiment ($\times 10^6$).	number of capsules washed away in supernatant ($\times 10^6$).	% of capsules entered or adhered to HUVECs
Control	4.07 ± 0.08	3.88 ± 0.21	4.67%
Neuraminidase loaded capsules	3.93 ± 0.11	2.76 ± 0.17	29.77%

Table 8.1: number of capsules before and after co-incubated with HUVECs.
Neuraminidase-loaded microcapsules show a significantly increase in the number that adhere to or enter vascular endothelial cells after 2 hours in the cell culture medium (number of experiments, n = 20).

As the control, similar experiments were carried out for $(PSS/PAH)_2$ microcapsules without neuraminidase. Table 8.1 shows our data from experiments. For the control, most of the microcapsules were washed away,

and only ~5% remained in the sample. For neuraminidase-loaded microcapsules, there were significant increases and approximately 30% of microcapsules had either adhered to or entered into vascular endothelial cells. In the following study, CLSM images will be used to reveal the location of these microcapsules in relation to HUVECs.

8.8 Interaction between neuraminidase-loaded microcapsules and endothelial cells

During immuno-fluorescent staining steps, cultured HUVECs were briefly washed using the serum free M199 medium for 9 times before observed by CLSM. All microcapsules suspended in the medium should be removed. Three-dimensional CLSM images are taken from the glass slide to the top of the cell.

In Figure 8.9, the location of the microcapsules in relation to endothelial cells was observed after they were added in the cell culture medium. In the control group, shown in Figure 8.9 (A), there were far fewer capsules in the enface image, as most of the microcapsules were washed away. The bottom and side panels in Figure 8.9 (A) revealed that the remaining capsules (red) were located on the glycocalyx layer (green) outside of the endothelial cells. In contrast, for neuraminidase loaded microcapsules, shown in Figure 8.9 (B), there were clusters of capsules near the cell nucleus in the enface image. From the bottom and side panels, we can see the capsules were inside the endothelial cell and existed at the same z - level as the nucleus. The glycocalyx layer was on top, covering the microcapsules.

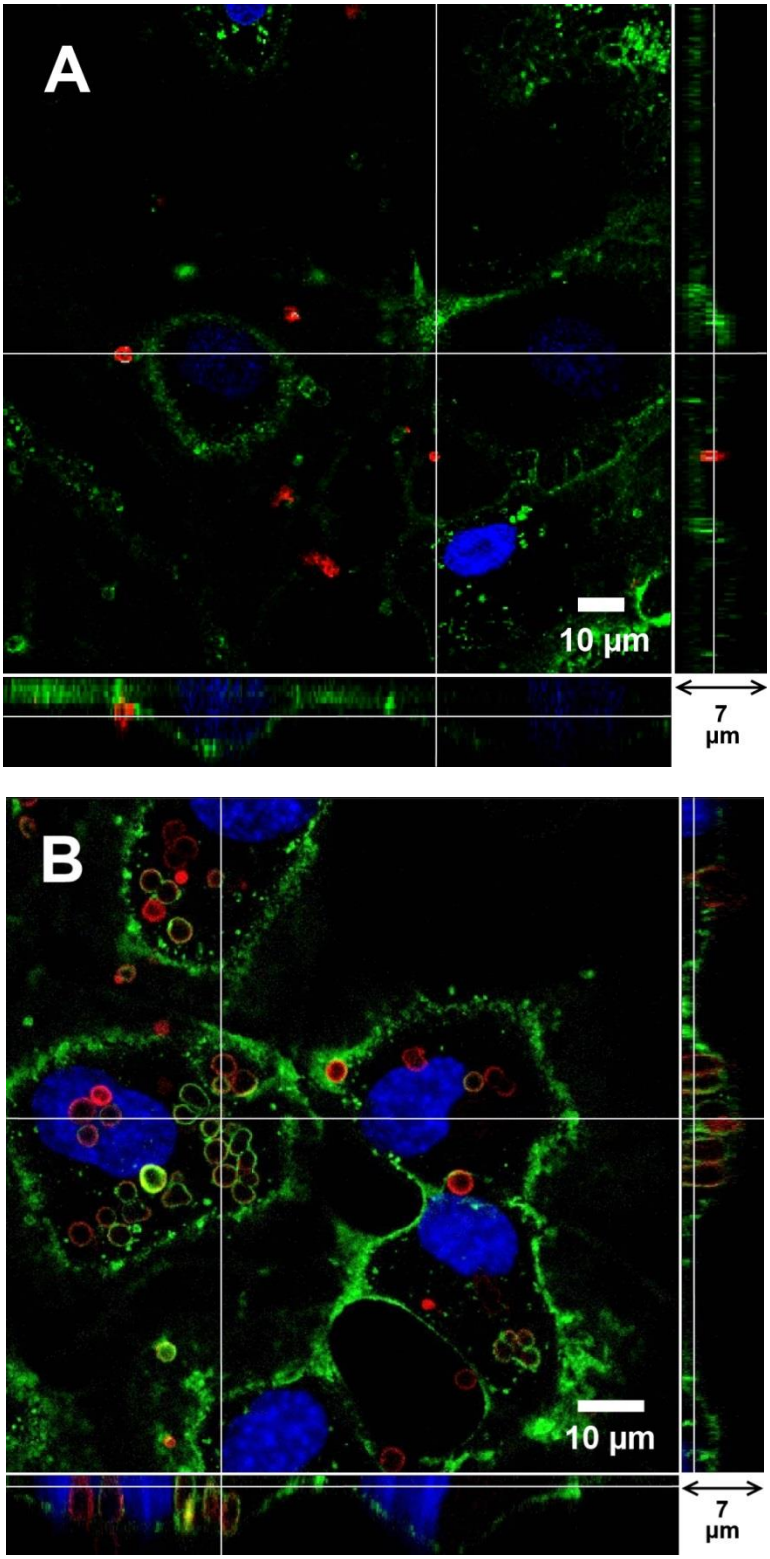

Figure 8.9: Interaction between $(PSS/PAH)_2$ capsules and HUVECs after microcapsules were added in the culture medium for 2 hours.

(A) Control capsules, (B) neuraminidase-loaded microcapsules. The main panel shows the enface image at a given z-depth. The bottom and side panels show the x–z and y–z cross-sectional images, respectively.

Note the difference between Figure 8.9 (B) and Figure 8.8 (C). Although in both studies, microcapsules were able to enter the endothelial cells, in Figure 8.8 (C), endothelial cells were pretreated with neuraminidase to abolish their entire glycocalyx layer. The green stain represented the newly synthesized glycocaly after 48 hours culture. In Figure 8.9 (B), neuraminidase loaded microcapsules came to contact with the glycocalyx layer, cleaved the glycocalyx structure in their proximity and left most of the glycocalyx layer intact, hence the green stained glycocalyx layer in Figure 8.9 (B) was well developed.

PSS/PAH/GNPs/PSS/PAH capsules contain neuraminidase in the cavity were used for SEM with FIB investigation. The capsules were incubated with endothelial cells for 2 hours. After co-incubation, the sample was fixed by immersed with 5% formaldehyde for 10 minutes and then washed with PBS buffer. After sample fixation, dehydration step was applied. Dehydration process was followed by sequentially wash the cell samples in methanol with increased concentrations at 20%, 40% and 60% for 5 minutes, 80% for 3 minutes, and 100 % methanol for 30 seconds. After the methanol removing, the samples were left in dry seal vacuum desiccator with calcium chloride anhydrous overnight.

Sample of SEM images in Figure 8.10 is tilted. Angles between the sample and horizontal plane, electron detectors, ion beam are 52^{o}, 38^{o} and 90^{o}. The milled part is 8 μm in length, 1 μm in width and 3 μm in depth. The milled part should reach the glass slide, and shows cuboid shape. But during the milling process, the sample was drifted result the final shape uncontrolled. However, the milling shape is not affecting the result.

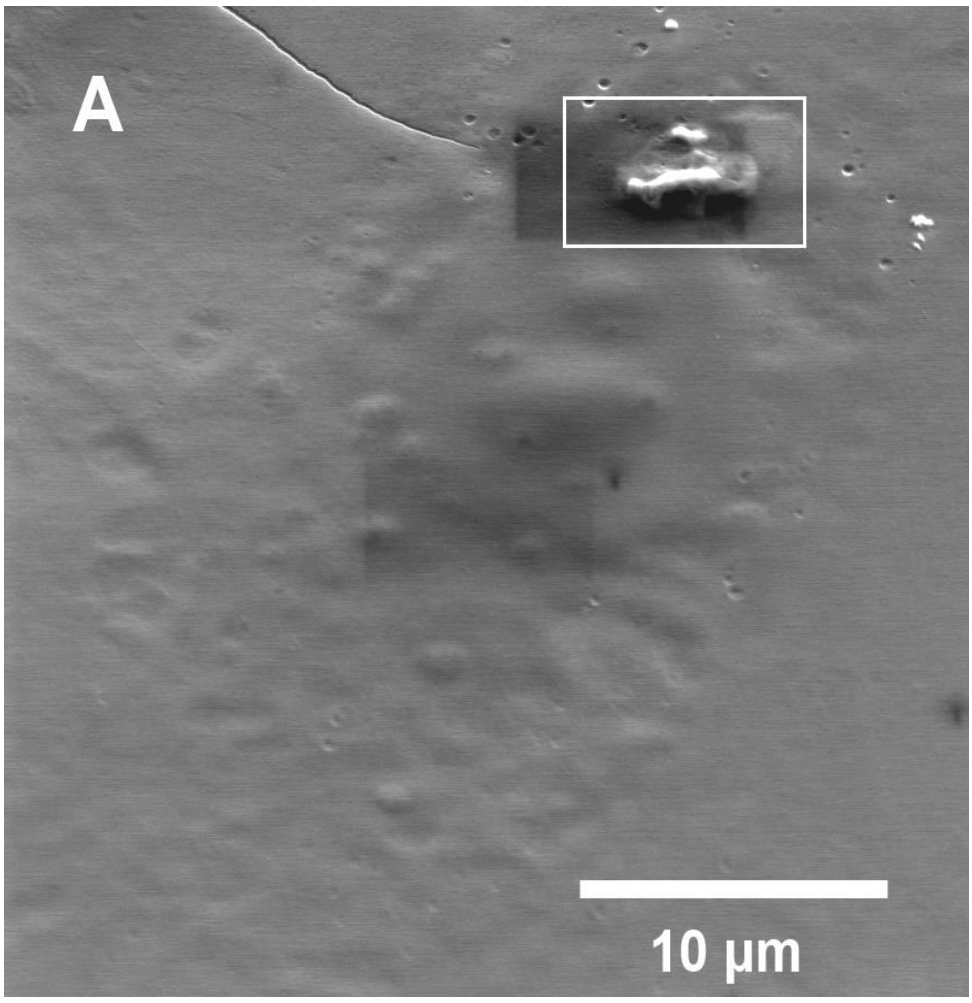
A
10 µm

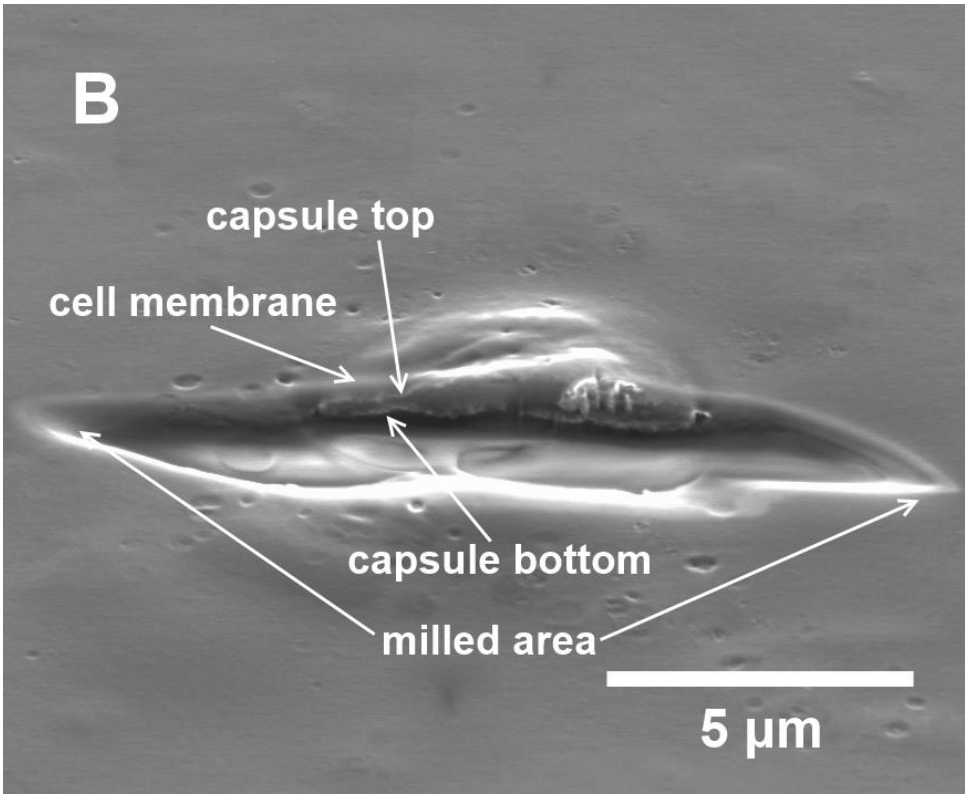
B
capsule top
cell membrane
capsule bottom
milled area
5 µm

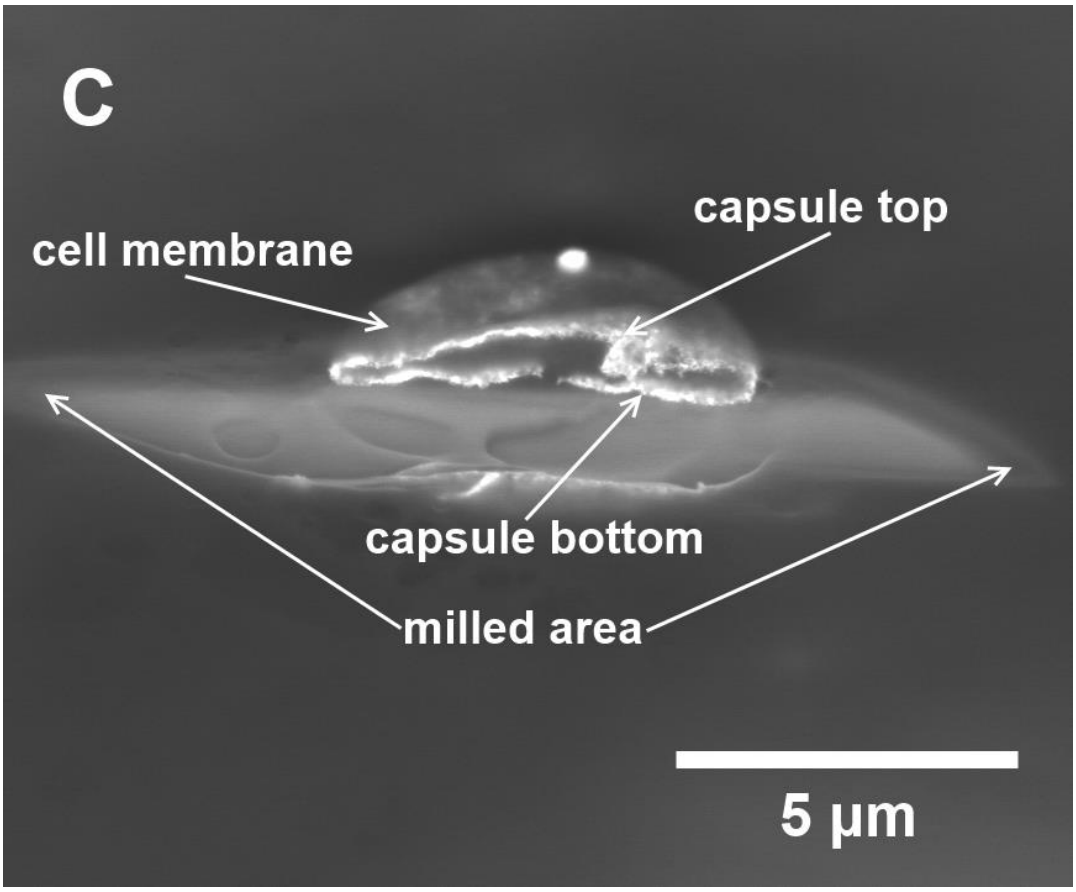

Figure 8.10: SEM with FIB images of capsule in endothelial cell.

(A) is overview of a HUVEC with a capsule; (A) and (B) are images viewed by Everhart-Thornley detector (ETD); (C) is viewed by back scattered electron detector (BSED). (B) and (C) is the area marked in A) after milling by focused ion beam, bright dots in (C) are GNPs.

Because HUVECs lost all the water in dry state, its thickness significantly drops from average 3 - 5 µm to 1 – 2 µm (even lower in the parts without nuclei). Thus, it is easier to observe the cross section and interface of the sample for single capsule in a cell. More capsules in one cell makes the interface between cell membrane and capsule shell too thin to be observed.

In Figure 8.10 (A), the cell is in dried state, a nucleus in the center of cell is still higher than the edges. The marked area in Figure 8.10 (A) is the milled part shows in Figure 8.10 (B) and (C). GNPs are shows in BSED image (C) of Figure 8.10. The GNPs prove the capsule within the milled part. In the cross

section of image Figure 8.10 (B), the top left shell of the capsule is definitely below the cell membrane. As the height of capsule increase from left to right side, the capsule's top shell beneath the cell membrane.

The bottom shell of the capsule closes to the glass slide which is a bright area with diamond shape in Figure 8.10 (B) and (C). In Figure 8.10 (C), the GNPs in the cross section were directly scanned by the detector and shows bright white colour; while GNPs on the top shell of the capsule are covered by cell membrane and shows gray colour.

Therefore, capsules functionalized with neuraminidase are able to cleave part of glycocalyx layer on the HUVECs membrane. After the glycocalyx is removed, channels that allowing the passage of capsules through the cell membrane becomes accessible. Three-dimensional CLSM images reveal that microcapsules containing neuraminidase are internalized by HUVECs, whereas microcapsules without neuraminidase are blocked by the glycocalyx layer.

8.9 Effects of time on the internalization of neuraminidase loaded microcapsules

Time required for microcapsules to pass through the cell membrane is very important in drug delivery. In the following study, we investigate the uptake of neuraminidase loaded $(PSS/PAH)_2$ microcapsules by HUVECs at different time. In Figure 8.11, CLSM images of capsules in HUVEC samples at 0.5, 1, 2, and 3 hours are shown. Equal amount of capsules were added in samples at the beginning of experiment.

At t = 0.5 hour, shown in Figure 8.11 (A), a number of microcapsules adhere to endothelial cells. Majority of these capsules were still above the glycocalyx layer, although a few has entered into the cells. In Figure 8.11 (B), at t = 1 hour, more capsules have made their way through the membrane into the cell. However, there were still many microcapsules above the endothelial glycocalyx layer. In Figure 8.11 (C), at t = 2 hours, most capsules have passed through the cell membrane with only a few capsules outside the cell. Finally, in Figure 8.11 (D), at t = 3 hours, we observe a similar pattern as that in t = 2 hours sample, without further significant change.

These results suggest that the approximate time for HUVECs to internalize neuraminidase-loaded $(PSS/PAH)_2$ microcapsules is approximately 2 hours. This time will clearly be affected by the permeability of the capsules and the amount of neuraminidase encapsulated in them.

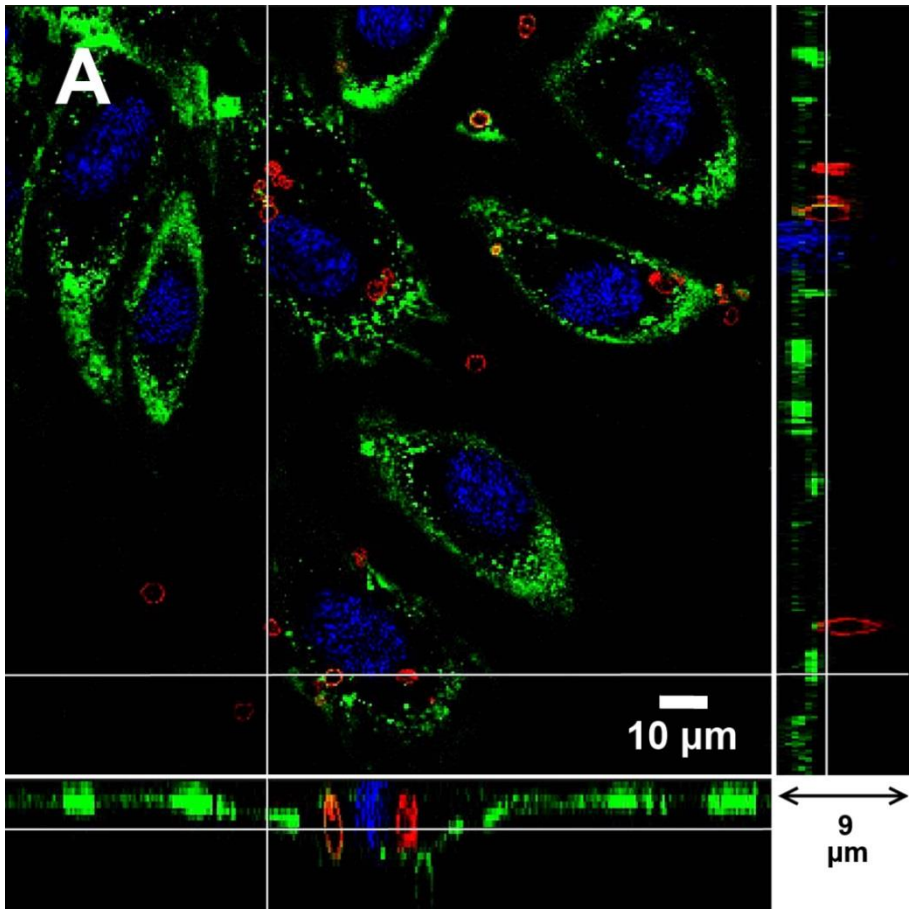
A
10 µm
9
µm

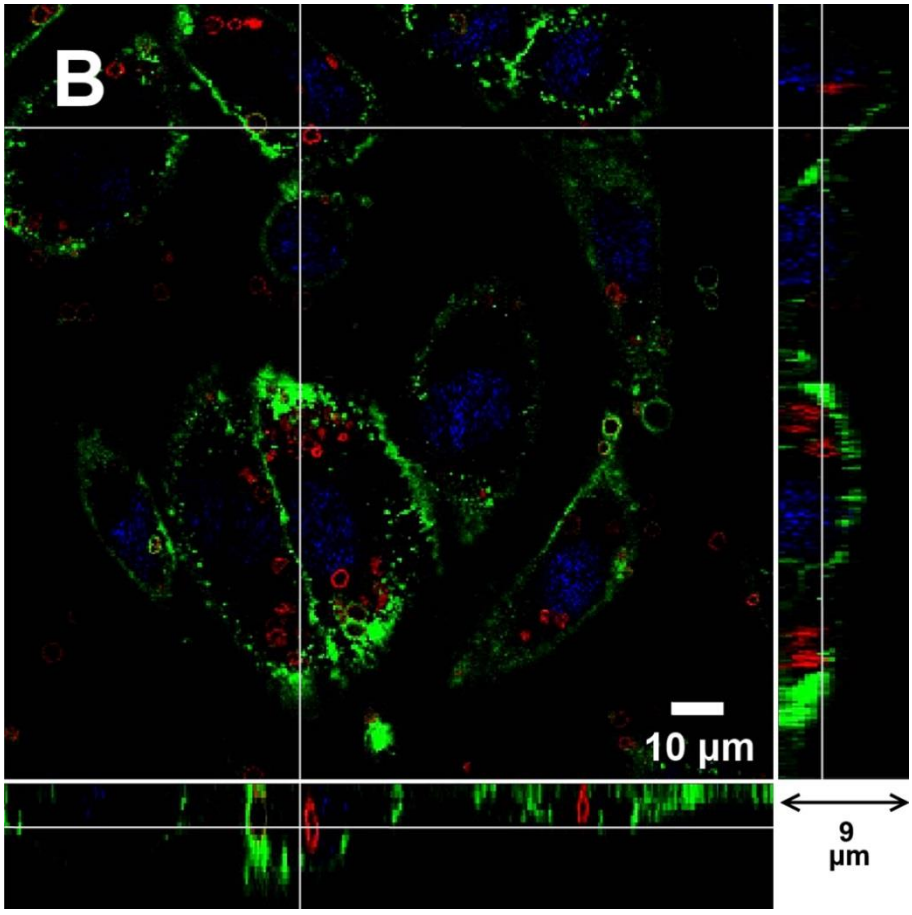
B
10 µm
9
µm

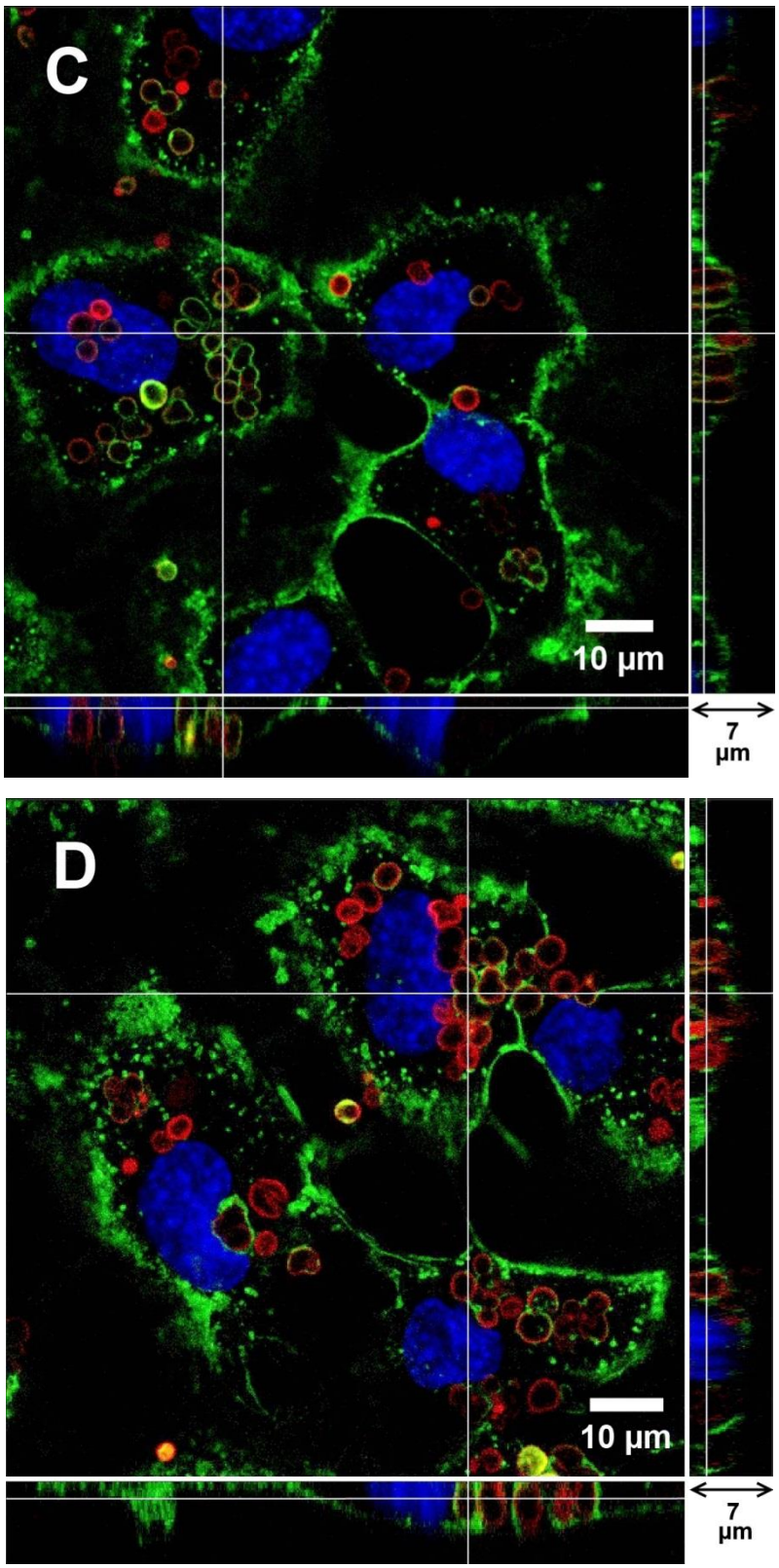

Figure 8.11: CLSM images of neuraminidase-loaded $(PSS/PAH)_2$ microcapsules in HUVEC samples at different time points.

(A) t = 0.5 hour; (B) t = 1 hour; (C) t = 2 hours and (D) t = 3 hours. The main panel shows the enface image at a given z-depth. The bottom and side panels show the x–z and y–z cross-sectional images respectively.

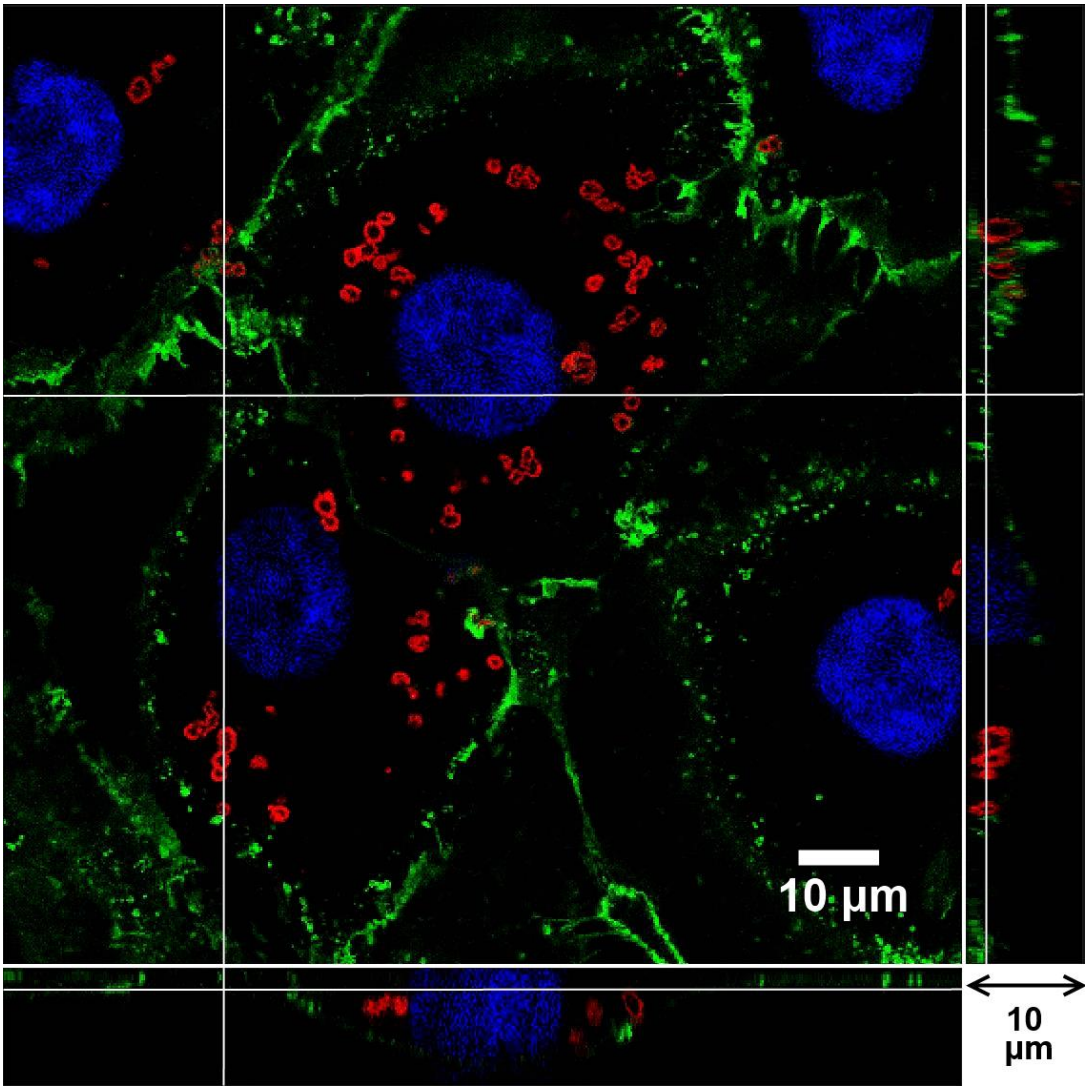

Figure 8.12: $(PSS/PAH)_2$ capsules with neuraminidase are incubated with cells after 7 days. Culture medium was changed every 2 days. The main panel shows the enface image at a given z-depth. The bottom and side panels show the x–z and y–z cross-sectional images, respectively.

$(PSS/PAH)_2$ capsules are known as non-biodegradable. Stability of neuraminidase loaded microcapsules after their internalization by HUVECs was investigated in the following study. HUVEC samples containing $(PSS/PAH)_2$ capsules in their cytoplasma were cultured for 7 days. At the end of day 7, cells showed no difference to the control group, i.e. HUVECs cultured for the same length of time without capsules inside. In Figure 8.12, we can see that $(PSS/PAH)_2$ capsules retained their circular shape and

integrity. The capsules remained in cytoplasm, which can be seen in the bottom and side panels.

8.10 Neuraminidase loaded biodegradable DS/PArg capsules

Although $(PSS/PAH)_2$ microcapsules have excellent biocompatibility and can be functionalized with neuraminidase to enter vascular endothelial cells, they are not biodegradable. In drug delivery systems for therapeutic purposes and medical applications, the drug carrier needs not only be biocompatible but also biodegradable over a reasonable period of time under physiological conditions. Polyelectrolytes microcapsules made of natural polysaccharides and polypeptides are known to be biodegradable, and once in phagocytic cells, they can degrade within hours (Rivera-Gil, De Koker et al. 2009).

De Geest et al developed polyelectrolyte microcapsules that could be degraded by intracellular proteases or hydrolytic enzymes (De Geest, Vandenbroucke et al. 2006). The dextran sulfate/poly-L-arginine (DS/PArg) microcapsules were susceptible to enzymatic degradation and gradual disintegrated over 60 hours after internalized by VERO-1 cancer cells. De Koker reported these microcapsules could also be degraded after incubated with bone-marrow-derived dendritic cells, and proposed macro-pinocytosis as the mechanism of uptake of capsules by the cells (De Koker, De Geest et al. 2007; De Koker, De Geest et al. 2009). Here we use the same composition to make $(DS/PArg)_2$ microcapsules and explore the capsule fate in the non- phagocytic HUVECs.

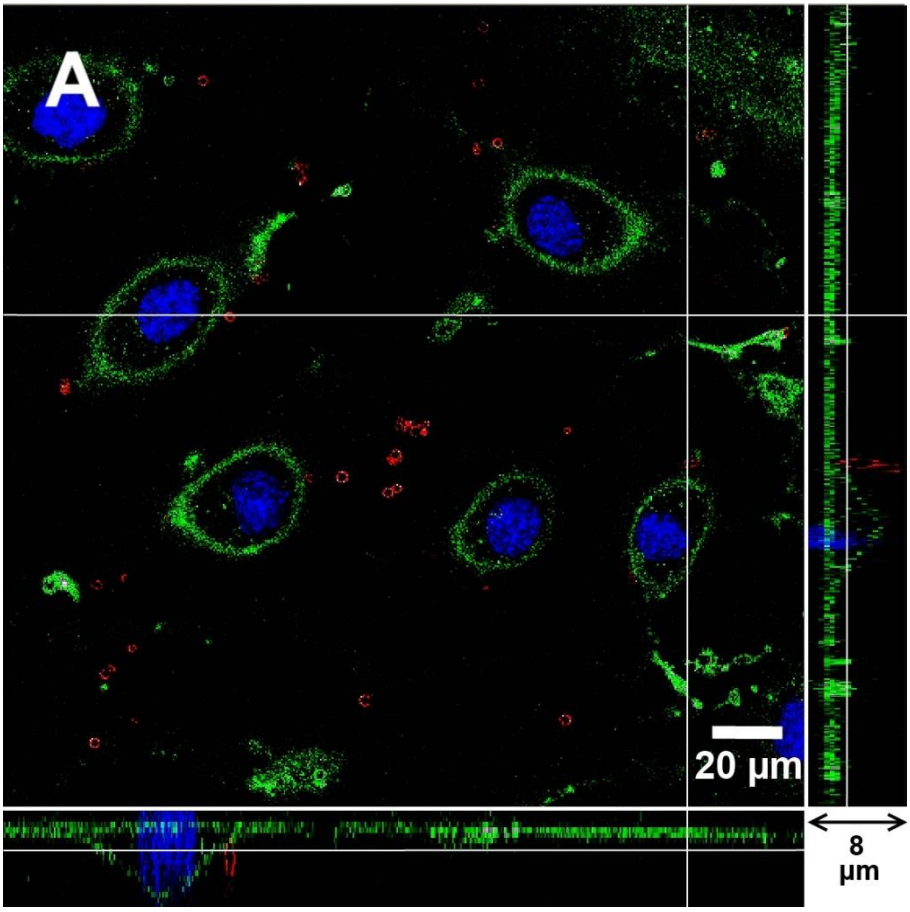
A
20 µm
8
µm

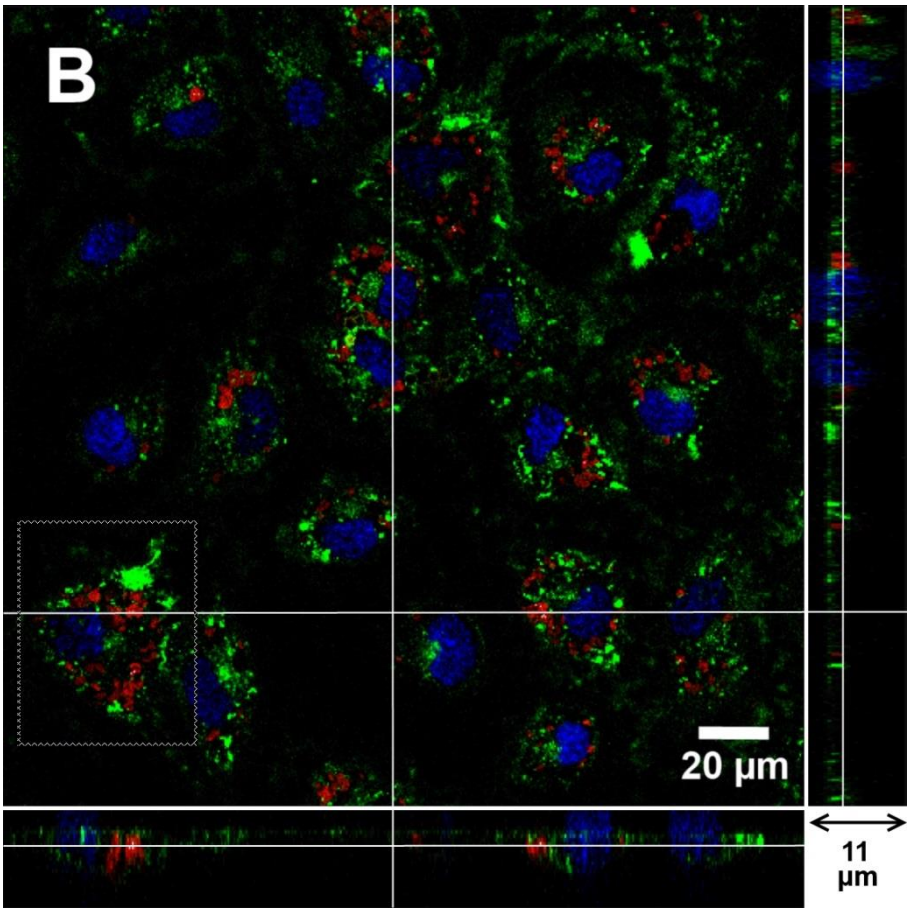
B
20 µm
11
µm

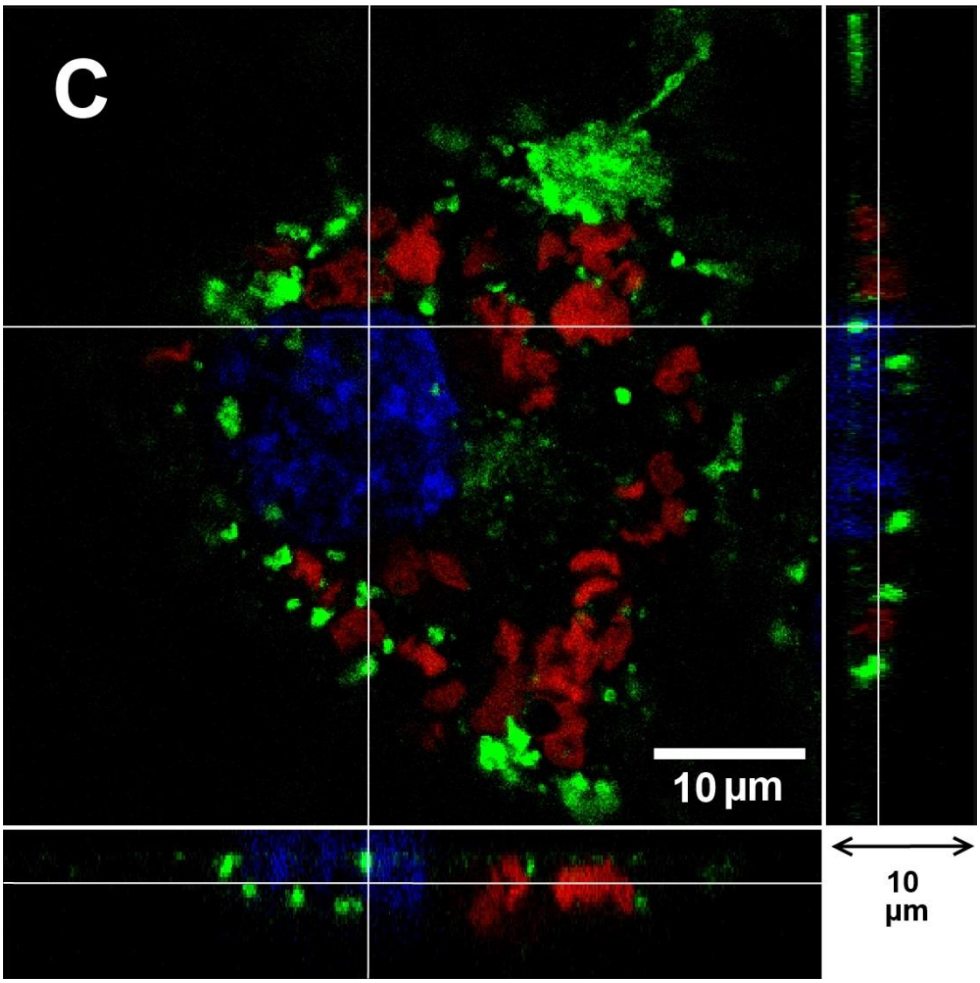

Figure 8.13: Interaction between $(DS/PArg)_2$ microcapsules and HUVECs after 48 hours co-incubation..

(A) Control, capsules were seen on top of the glycocalyx layer, (B) Endothelial cells were pretreated with neuraminidase, and capsules were seen inside the cells clustered around the nucleus, (C) zoomed in view of the area highlighted in (B). The main panel shows the enface image at a given z-depth. The bottom and side panels show the x–z and y–z cross-sectional images respectively.

Same experiments presented above on $(PSS/PAH)_2$ microcapsules were carried out on biodegradable $(DS/PArg)_2$ microcapsules. Firstly, we establish the interaction between $(DS/PArg)_2$ microcapsules and HUVECs with and without the glycocalyx layer. Figure 8.13 shows the results after $(DS/PArg)_2$ microcapsules were added in HUVEC samples for 48 hours. For the control group, in Figure 8.13 (A), HUVECs have a well-developed glycocalyx layer, and $(DS/PArg)_2$ microcapsules are observed on top of the glycocalyx outside

the endothelial cells. For neuraminidase pretreated HUVECs, in Figure 8.13 (B), clusters of $(DS/PArg)_2$ microcapsules were observed near nucleus of endothelial cells. The green stain represents newly synthesized glycocalyx in the 48 hour period. The bottom and side panels reveal these microcapsules are at the same z- location as the nucleus of the cell, and in places, they were underneath the glycocalyx layer. A close up view is presented in Figure 8.13 (C), where the location of the microcapsules inside the endothelial cells can be seen more clearly.

Internalization of neuraminidase loaded $(DS/PArg)_2$ microcapsules at different time points are studied at t = 0.5 hour, 1 hour, 2 hour, and 3 hours. As seen in Figure 8.14, the number of internalized microcapsules increases with time. By t = 2 hours, there are a large of number of capsules inside HUVECs, clustering in cytoplasma around nucleus. As time increases to t = 3 hours, there is a further increase of capsules inside HUVECs, but the increase is less significant. A quantitative measure of the number of capsules in endothelial cells at different time is given below in Figure 8.15.

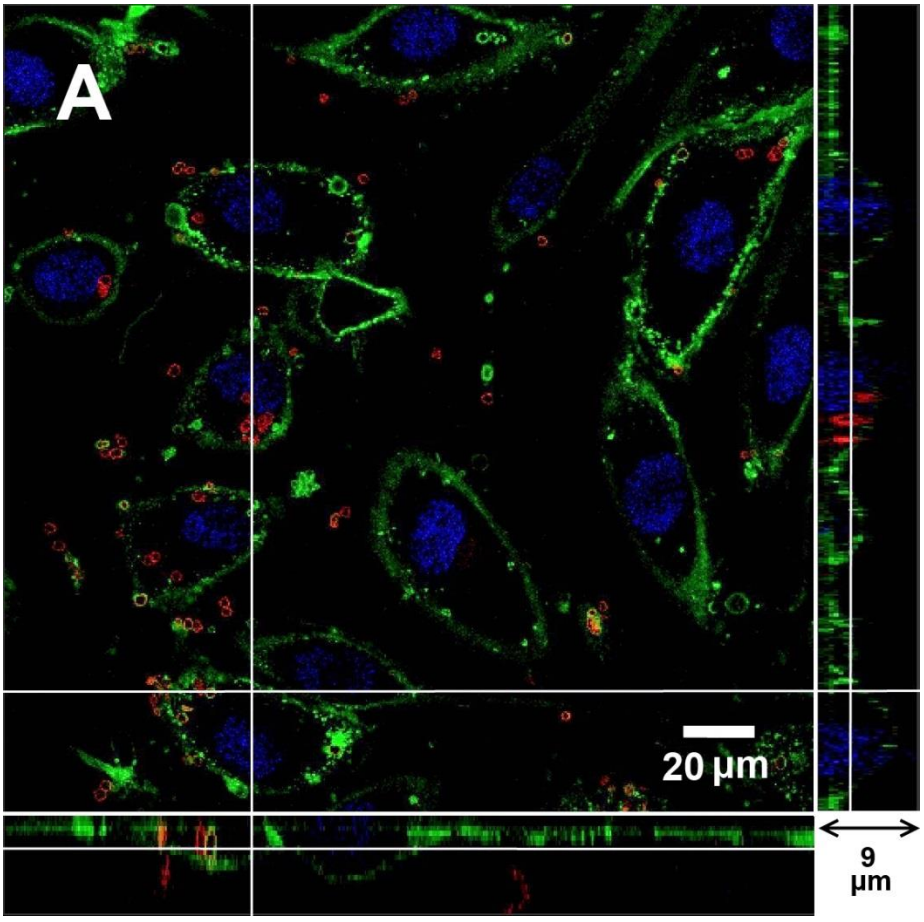
A
20 µm
9
µm

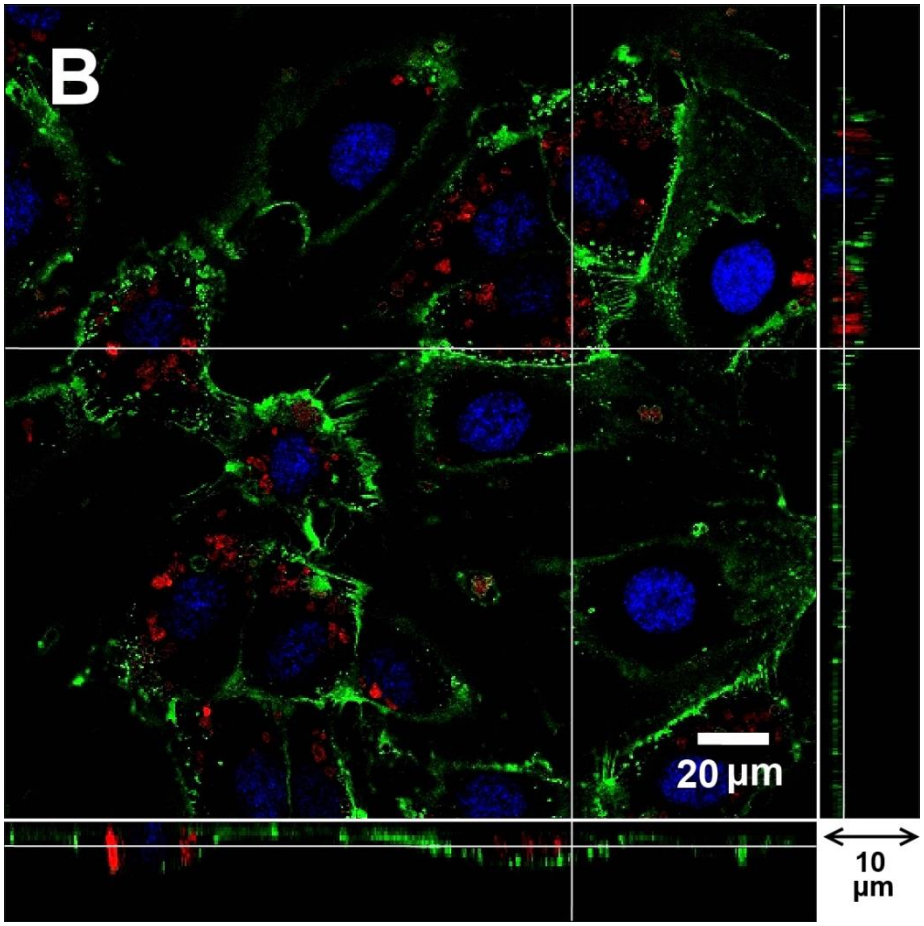
B
20 µm
10
µm

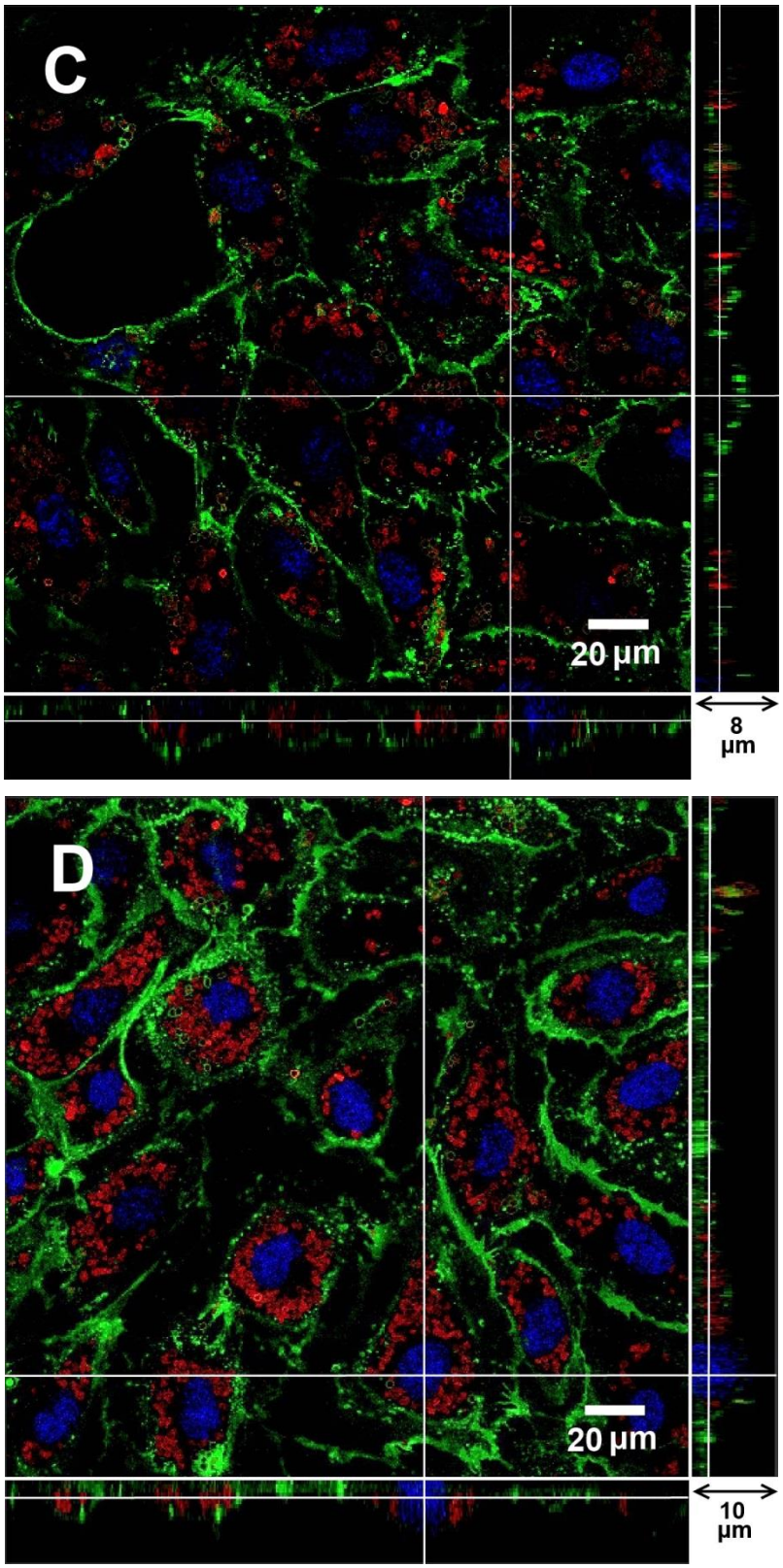

Figure 8.14: Internalization of neuraminidase-loaded $(DS/PArg)_2$ microcapsules after they were added in HUVEC culture medium for different length of time.
(A) t = 0.5 hour, (B) t = 1 hour, (C) t = 2 hour and (D) t = 3 hours. The main panel shows the enface image at a given z-depth. The bottom and side panels show the x–z and y–z cross-sectional images respectively.

Figure 8.15 shows the relationship between the number of internalized capsules and the time after they are added in HUVEC samples. For both $(PSS/PAH)_2$ and $(DS/PArg)_2$ capsules, their presence in endothelial cells was not uniform. There are cells that take in many capsules, while the neighboring cells have few capsules in them.

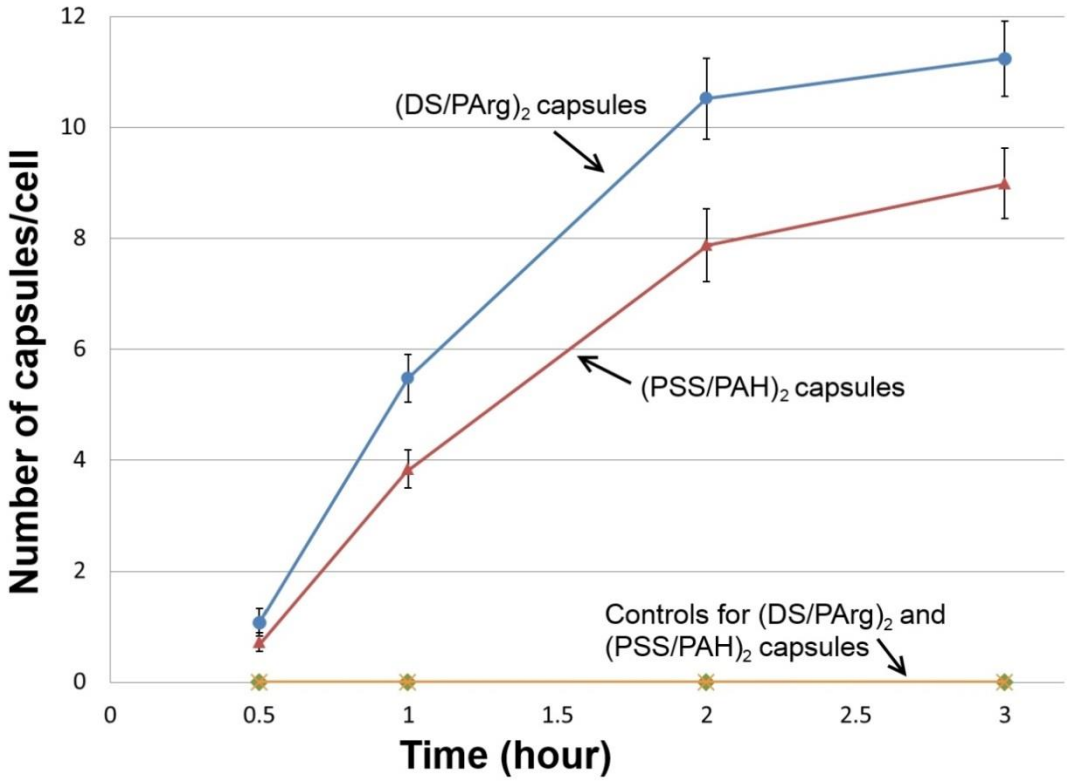

Figure 8.15: Number of internalized capsules per cell increases with time following their addition into HUVEC samples.

Every point in the results was based on 5 experimental data from five independent experiments, although, every experimental data was the averaged value based on 20 cells..

In our study, we chose two sampling areas randomly in an experiment, with approximately 20 cells being examined. The average number of capsules in a cell in an experiment is recorded. The experiment was repeated five times for each time point. For both $(PSS/PAH)_2$ and $(DS/PArg)_2$ capsules, the number inside the cell increases with the time. The increase in number is faster at earlier time (i.e. up to t = 1 hour) and slows down after 2 hours. Higher

number of biodegradable $(DS/PArg)_2$ capsules are observed in cells than $(PSS/PAH)_2$ capsules at all given time points. The results support the hypotheses that neuraminidase-loaded microcapsules release the enzyme to cleave the glycocalyx in the proximity of the capsules, leading to their internalization in vascular endothelial cells.

8.11 Degradation of $(DS/PArg)_2$ capsules in HUVECs

Most cancer cells and immune cells are phagocytic cells such as macrophages and dendritic cells are able to internalize capsules (De Cock, De Koker et al. 2010). *In vitro* and *in vivo* studies on cellular uptake of capsules and degradable capsules are able to be degraded at physiological pH or destroyed by endogenous enzymes have been recently published. Polyelectrolyte microcapsules formed by and enzymatically or hydrolytically degradable polycation could spontaneously degrade in several types of cell (De Geest, Vandenbroucke et al. 2006; De Koker, De Geest et al. 2007; De Koker, Naessens et al. 2010).

To investigate the degradation of $(DS/PArg)_2$ capsules after their internalization in HUVECs, we studied samples at different days. Figure 8.16 shows that $(DS/PArg)_2$ capsules gradually disintegrate between 3 days and 7 days. After 1 day in endothelial cells, as shown in Figure 8.16 (A), capsules retain their circular shape and integrity. By 3 days, some of the capsules start to change their shape to discontinuous and patchy circle. By the end of 5 days, in Figure 8.16 (C), most of the capsules have disintegrated to pieces and hardly any intact capsules can be seen inside endothelial cells. By the end of 7 days, as seen in Figure 8.16 (D), microcapsules have completely degraded into pieces, with the red coloured polyelectrolytes clouds and dots spread in the entire cytoplasm.

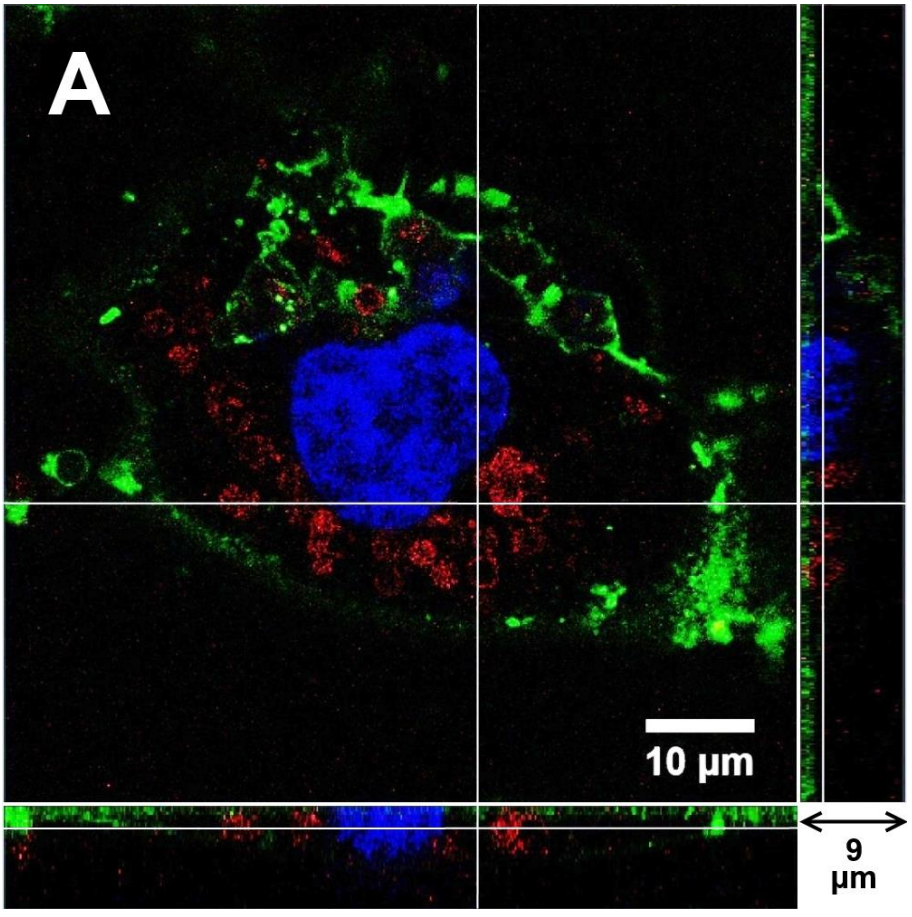
A
10 µm
9
µm

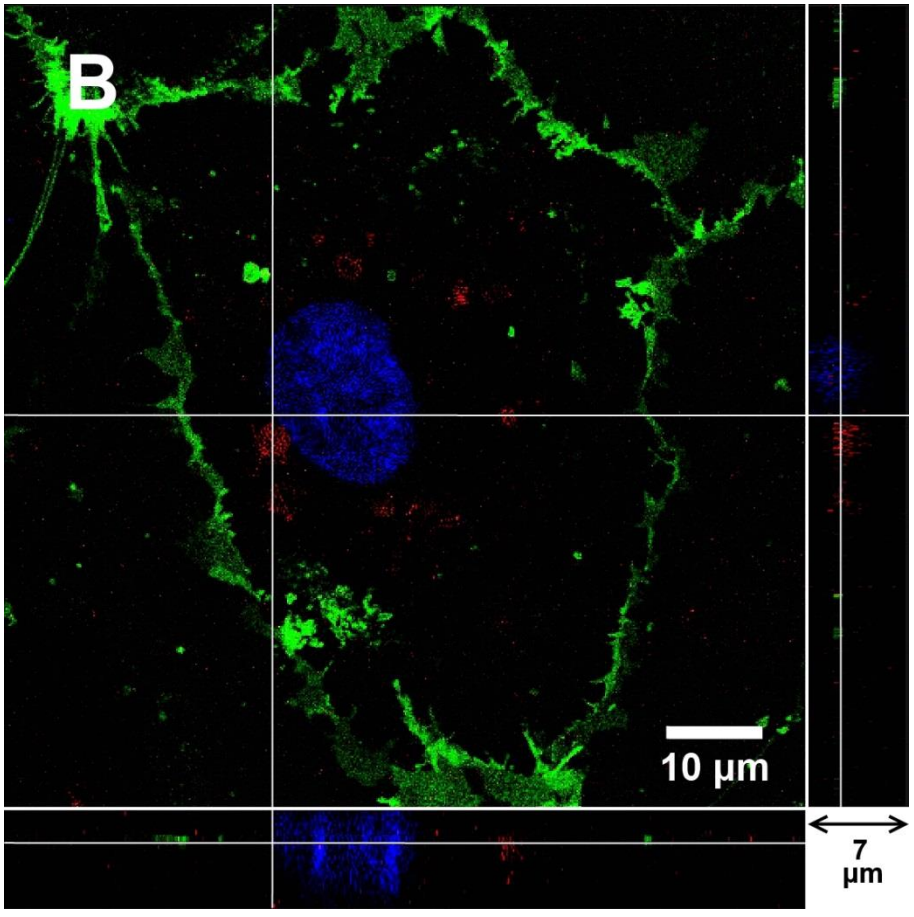
B
10 µm
7
µm

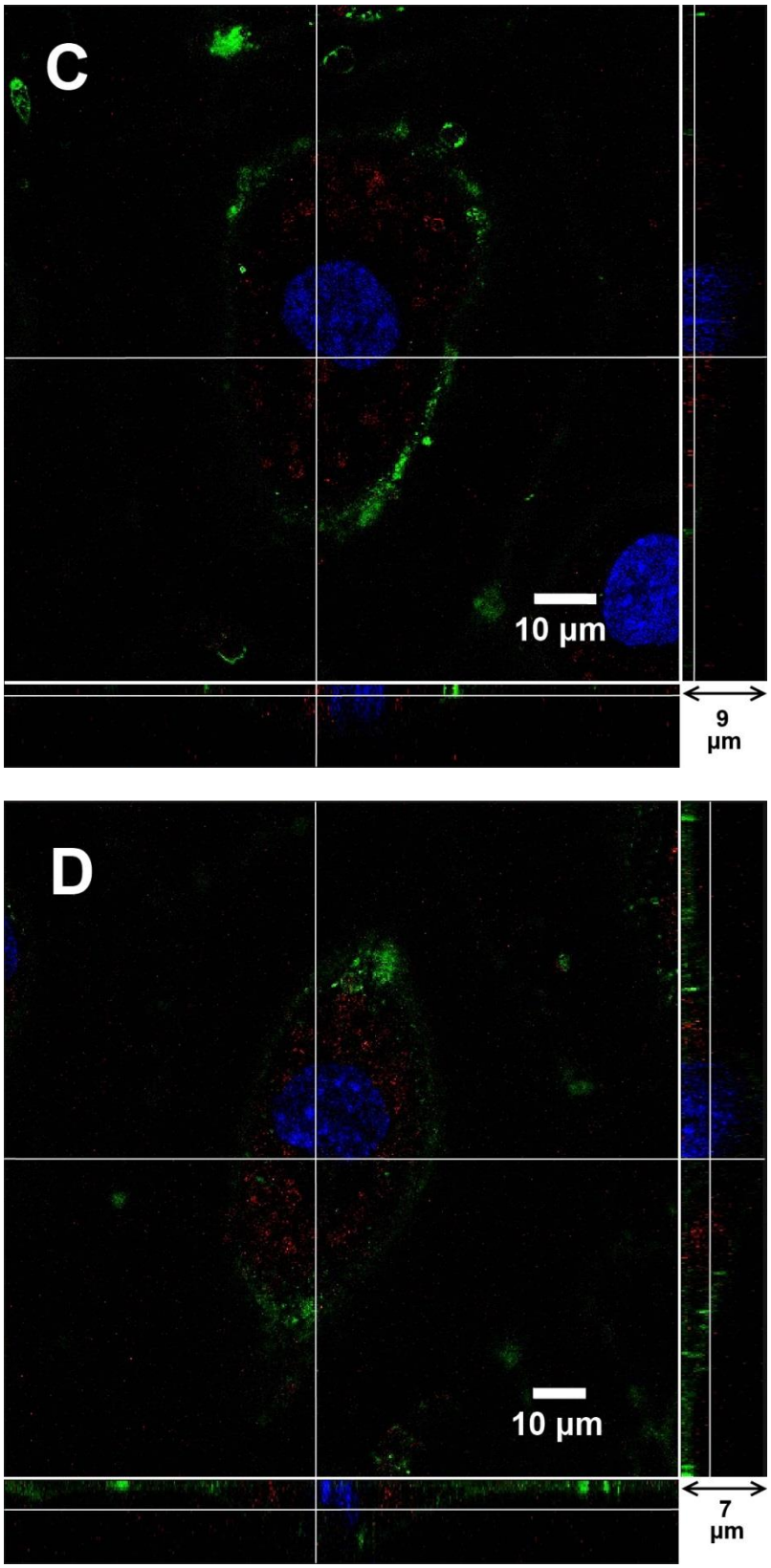

Figure 8.16: $(DS/PArg)_2$ microcapsules at different days inside endothelial cells
(A) 1 day, (B) 3 days, (C) 5 days and (D) 7 days. The main panel shows the enface image at a given z-depth. The bottom and side panels show the x–z and y–z cross-sectional images respectively.

Further studies on biodegradable DS/PArg microcapsules contain neuraminidase were performed with SEM. Back scattered electron detector w used for GNPs loaded DS/PArg capsules imaging. Thus, the formation of sample used in SEM studies is DS/PArg/GNPs/DS/PArg with neuraminidase in capsules cavity. The GNPs in capsules shell is not affect cell viability and interactions between microcapsules and HUVECs.

Figure 8.17 shows biodegradable DS/PArg capsules with GNPs in the shell and neuraminidase in cavity are incubated with endothelial cells after 7 days. Everhart Thornley detector (ETD) images on the left side, and back scattered electron detector (BSED) images on the right side. Figure 8.17 (A) shows several capsules are on the top of the cell in region B, while few capsules are under the cell membrane in region C. Some of the capsules in Figure 8.17 (B) are still have same morphology with SEM image of capsules after fabrication.

Figure 8.17 (C) shows the surface of capsules is smoother than Figure 8.17 (B). GNPs shows in BSED of Figure 8.17 (B) are brighter and densely formed with capsule shape; while in Figure 8.17 (C) are not firmed by capsule and diffused in a larger region than capsule size. The cross section in Figure 8.17 (B) shows capsules partially in the cell, and in Figure 8.17 (C) shows capsules are in the cell.

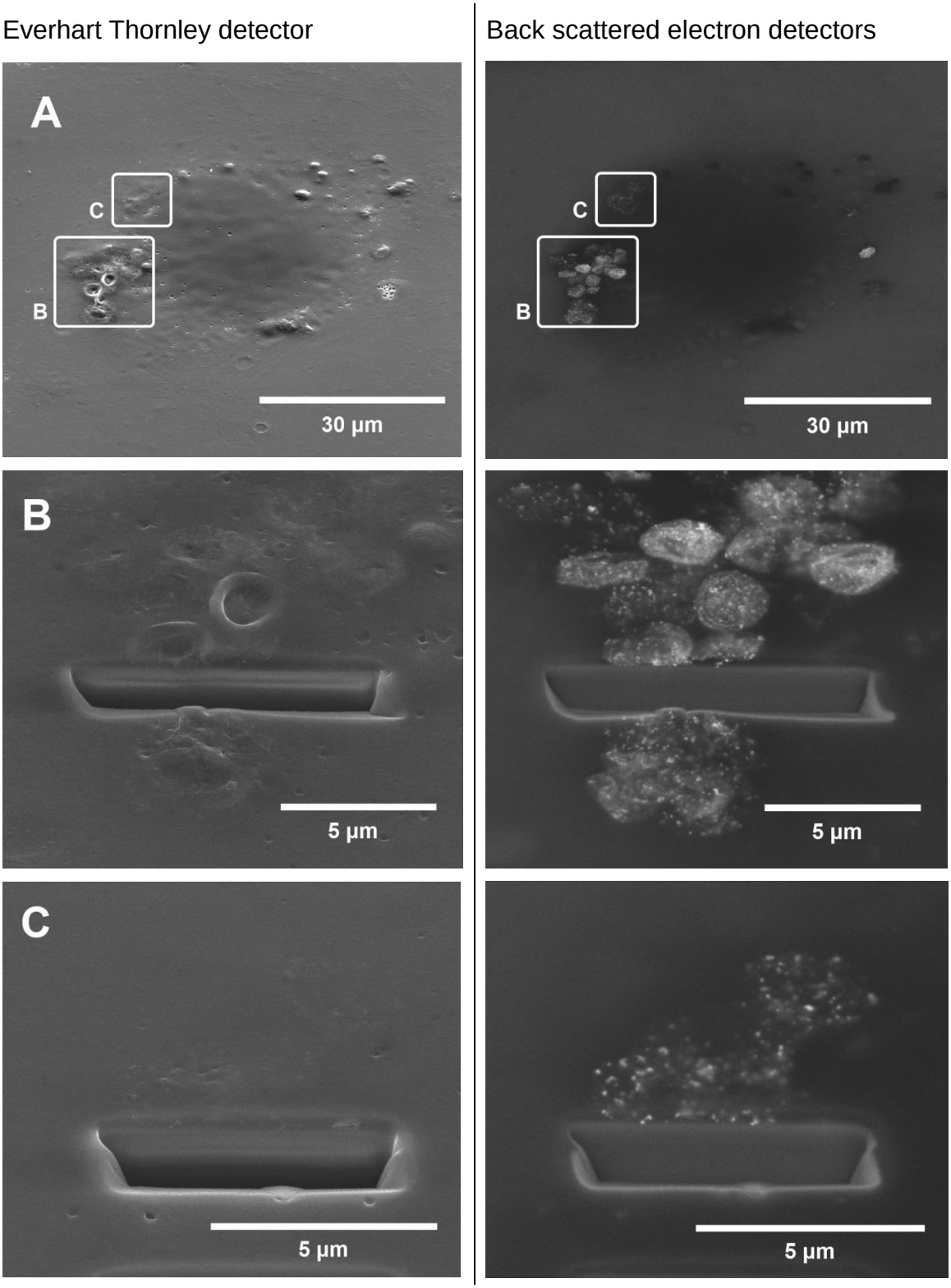

Figure 8.17: $(DS/PArg)_2$ capsules with GNPs in the shell and neuraminidase in cavity are incubated with endothelial cells after 7 days.

All images are tilt 52 degree. Images of (B) and (C) are zoomed in part of image (A) after focused ion beam etching. Images on the left side were viewed using Everhart Thornley detector and on the right side were viewed using back scattered electron detectors.

In Figure 8.17, capsules with concentrated GNPs in the shell are considered as not degraded, while capsules with GNPs in a widespread area are considered as degraded. Some capsules are not internalized by HUVECs even with neuraminidase. One possible reason is the space inside the cell is occupied by internalized capsules, and no enough space for other capsules. Also neuraminidase encapsulation cannot make sure each capsule contain certain amount of enzyme with working concentration. However, SEM images serve as another evidence to insure the neuraminidase capsules are able to pass through the HUVECs membrane, and not significantly affect the cell biological activity for weeks.

8.12 Transfection of HUVECs with neuraminidase loaded microcapsules

The process of delivery nucleic acids into cells is called transfection. A successful transfection of eukaryotic cells requires transient holes opening in the cell membrane, and transfers the carried cargo inside. Usually, transfection is performed by non-viral methods and cells are eukaryotic. DNA can be delivered into the cell nucleus either using physical process or designed carriers that deliver the genes into the cells and generate expression of the gene (Azzam and Domb 2004). Generally, eukaryotic cells can be transfected by three common methods which are physical, viral, and chemical methods.

Some physical methods are more toxic for several kinds of cells and always under certain conditions and carried by specialized equipment (Villemejane and Mir 2009). Viral method has high efficiency for gene transfection, but may cause insertional mutagenesis, immunogenicity. Furthermore, there is size limitation of used genes with this method. Chemical method is well used in many experiments, compare with other two methods, it is simple, cheap and low side effect (Douglas 2008).

Because free DNA molecules are rejected by the cell membrane, vehicles are able to provide protection and transportation. DNAs are encapsulated in microcapsules, and then the capsules are delivered into cells. DNAs are released from the capsules inside the cell is the main objective of the transfection study. This transfection method with DNA plasmids is non-viral delivery.

Neuraminidase loaded $(DS/PArg)_2$ microcapsules were prepared with same method in above section. Amount of 100 µl DNA plasmid was encapsulated using neuraminidase in $CaCO_3$ core particles co-precipitation

step. The final concentration of DNA in $CaCO_3$ solution is 0.05 mg/ml. These capsules were premixed with culture medium and then incubated with HUVECs. DNA plasmid was prepared by Dr. David Gould (Bone and Joint Research Unit, Barts and The London, Queen Mary's School of Medicine and Dentistry, University of London).

To compare transfection efficiency between capsules contain DNA and commonly transfection protocols, a commercial transfection reagent Fugene 6 is used as control (Hunt, Currie et al. 2010). Because amount of DNA lost during capsules fabrication is difficult to be measured, same amount of DNA plasmid were used in capsules fabrication and Fugene 6. The volume ratio of Fugene 6 to DNA plasmid is 3: 1, and Fugene 6 plus DNA plasmid to the culture medium is 1: 10. Fugene 6 was mixed with serum free medium M199, the solution was vortexed for 5 second and then incubate for 5 minutes. A certain amount of DNA plasmid was added to solution of Fugene 6 transfection reagent and M199. Then the final mixed solution was incubated for 15 minutes. After that, the final mixture was added to endothelial cells.

To deliver DNA into cells for expression of GFP, capsules have to pass cells membrane and deliver the plasmid DNA to the nucleus where gene transcripted. Capsules are not labeled with any fluorescent dyes, as any fluorescence may overlap with the fluorescence that generated by the cell. Samples were observed using CLSM after 12 hours, and 1, 2, 3, 5 days.

For all samples, very few of transfected cells can be observed, and the intensity of green fluorescence is weak. As obvious degradation of $(DS/PArg)_2$ capsules occurs after 3 days, the encapsulated DNA plasmids are released by during the period. Samples are observed before 3 days, may be not have sufficient time to express the fluorescent protein. Furthermore, the fluorescent proteins may be not remaining stable after 5 days. In Figure 8.18, the green fluorescent proteins in Fugene 6 sample distribute all around

cytoplasm region; while in capsules sample, GFPs have strong intensity in small area.

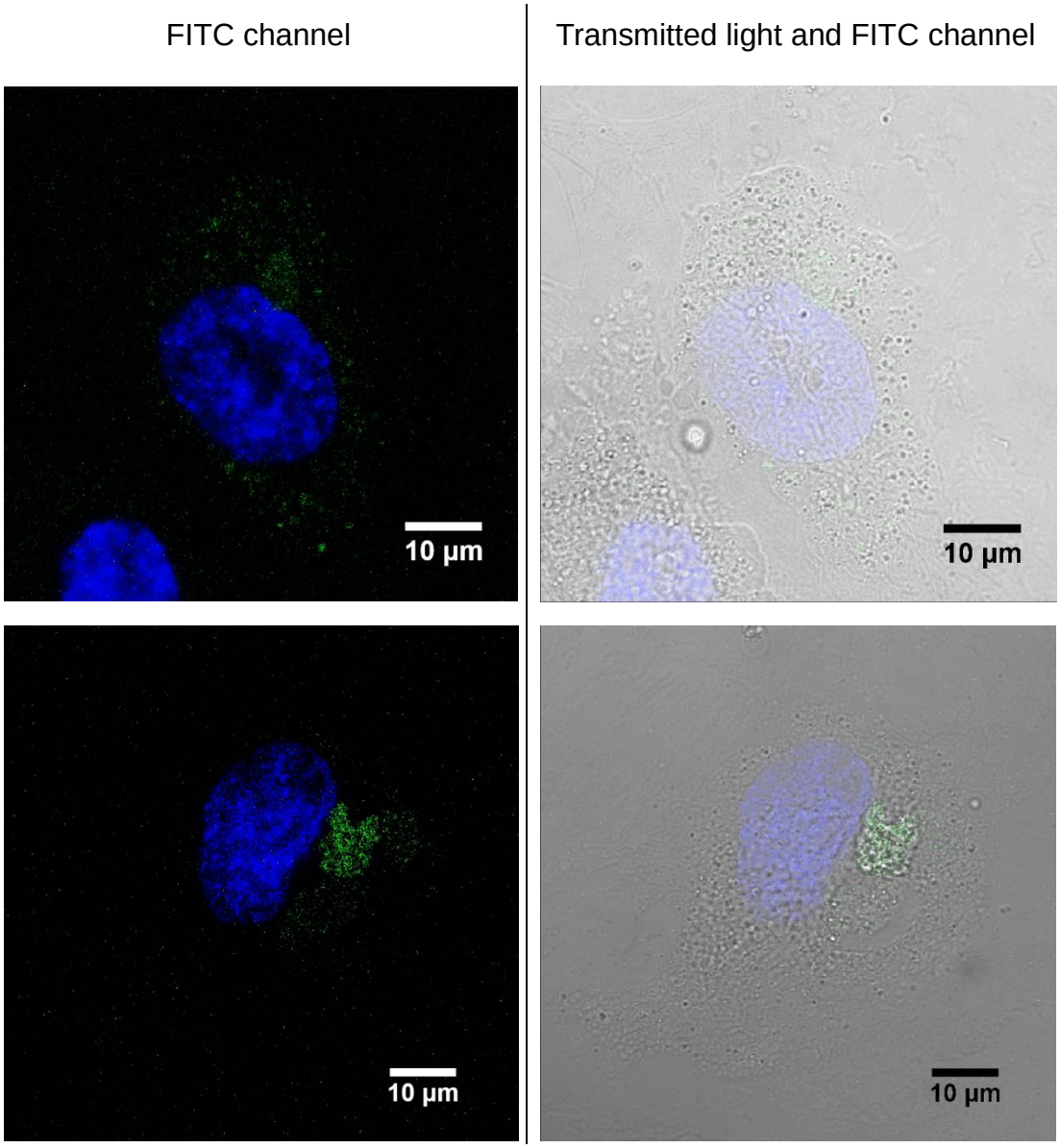

Figure 8.18: CLSM images of transfected endothelial cell observed after 72 hours co-incubation.

Top images are HUVECs with commercial reagent Fugene 6; bottom images are HUVEC with capsules contain neuraminidase and DNA plasmids.

Summarized from 5 samples of neuraminidase + DNA plasmid capsules with HUVECs, sample of 3 days has highest number of cell with GFP expression. In the 3 days sample, the cells with green fluorescent protein

shows in bottom images of Figure 8.18 are very few. For control sample of HUVECs with commercial transfection reagent Fugene 6 after 3 days, cells in top images of Figure 8.18 are also very few. For samples of both capsules and Fugene 6 at 1, 2 and 5 days, the transfection efficiencies are even lower. In sample at 12 hours, GFP expression cannot be observed.

The problem of low transfection efficiency of HUVECs is because these cells are primary cells. The primary cells are more difficult to transfect, as they are more susceptible to toxic agents and able to degrade exogenous nucleic acids in the cytoplasm (van Beijnum, van der Linden et al. 2008). Michelle et al studied 9 commercially available chemical transfection reagents work with primary HUVECs. GFP expression of total cells is less than 10 % in most reagents samples after 24 hours co-incubation time. After 48 hours co-incubation time, GFP expressions in these samples are still less than 10 %. The highest GFP expression sample is using Lipofectamine LTX reagent, but up to 40 % cells of the sample are died (Hunt, Currie et al. 2010). Because low transfection efficiency on HUVECs, the non-viral method of delivery DNA plasmid with neuraminidase loaded capsule does not compete with commercial reagents method.

8.13 Conclusions

In this work, we studied interactions between $(PSS/PAH)_2$ and $(DS/PArg)_2$ microcapsules and vascular endothelial cells *in vitro*. We first established that these capsules will be blocked by the endothelial glycocalyx layer and cannot penetrate through the cell membrane into endothelial cells. When the glycocaly layer is abolished by neuraminidase, the pretreat endothelial cells are accessible by both $(PSS/PAH)_2$ and $(DS/PArg)_2$ capsules. Although the mechanisms involved in the uptake of capsules by endothelial cells are not yet fully understood, the endothelial glycocalyx layer plays an important role in the internalization of these capsules.

To minimize destruction of the endothelial glycocalyx layer while achieving cross cell membrane transport of the capsules, we encapsulated neuraminidase inside $(PSS/PAH)_2$ and $(DS/PArg)_2$ capsules. By controlling the permeability of capsules to neuraminidase, we achieve gradual release of the enzyme through the porous membrane of the capsule. The neuraminidase molecules surrounding the capsules work as clippers to cleave the glycocalyx layer to open a channel for the capsule to go through. Neuraminidase-loaded capsules can pass through the endothelial cell membrane and remain in cytoplasm for many days with no apparent effect on cell viability. Of the two capsules studied, $(DS/PArg)_2$ ones are biodegradable, This makes them an even more appropriate candidate as drug delivery carries.

The novelty of the current study lies in the fact that we demonstrated the effect of the endothelial glycocalyx in the interaction between microcapsules and endothelial cells. Furthermore, we functionalized microcapsules by loading them with an enzyme to enable them to pass through the glycocalyx layer and achieve cell internalization. Results from our study show that

microcapsules can be functionalized to work as delivery carriers not only into phagocytic cells but also into other types of normal healthy cells. Vascular endothelial cells are chosen in this study due to the fact that these cells have the primary function of being the ‘barrier’ between the circulating blood and the tissue. Large particles, such as proteins and microcapsules, are not permeable through the endothelial cell lining *in vivo*. In conclusion, we have fabricated microcapsules that have the high potential to act as drug delivery carriers with the ability to pass through the endothelium barrier of blood vessels into surrounding tissues.

9. General Conclusion

There are growing interests in the past decades in micro sized vehicles with the function of storing, targeting and controlled release of substances. However, delivering desired drugs by micro containers to live cells is a challenging topic in material science. Various drug delivery systems have been developed with particular biomedical applications. They deliver a defined quantity of a therapeutic payload to a specific target site or tissue, at a controlled release rate, with or without externally trigger mechanism, such as ultrasound or light. Micro sized capsules with controlled delivery and release to designated sites have been introduced as potential drug containing vesicles.

The Layer-by-Layer (LbL) technique based on the sequential adsorption of oppositely charged polymers on a charged substrate has been developed to construct these microcapsules. Oppositely charged proteins and polyelectrolytes are sequentially absorbed onto a charged template by electrostatic attraction, resulting in complex formation between polyanions and polycations of defined thickness. Empty capsules can be obtained after decomposing the template. The size and morphology of the microcapsules, the polyelectrolytes and thickness of the shell, the permeability as well as the release activation mechanism can be controlled with the Layer-by-Layer method.

The present work starts with microcapsules fabrication and functionalization. Biocompatible $CaCO_3$ particles with porosity, uniform and almost spherical shape are used as template cores. Fluorescent dyes, neuraminidase and DNA plasmids are encapsulated by $CaCO_3$ co-precipitation method also called pre-loading. Gold nanoparticles and magnetite nanoparticles are coated as a capsule layer in the shell.

The main research outcome of the thesis is making a further step on drug delivery system with microcapsules *in vitro*. Investigating interactions between epithelial cells (Caco-2 cell line) and capsules with magnetite nanoparticles is performed with physical method. Epithelial cells are incubated with iron nanoparticles functionalized capsules with a magnet. Magnet provides magnetic field as an extra driving force attracts capsules with magnetite nanoparticles toward to epithelial cells. The number of internalized capsules with magnetite nanoparticles by epithelial cells is 3 times higher than control capsules. After magnet treatment for 10 minutes, 1.8 adhered capsules with magnetite nanoparticles per cell are observed with CLSM.

Investigating interactions between non-phagocytic cell of HUVECs and capsules is performed with biochemical stimuli. Neuraminidase encapsulated $(PSS/PAH)_2$ and $(DS/PArg)_2$ capsules as well as control capsules are prepared for the experiments. Capsules are first mixed with culture medium then added to HUVECs. The glycocalyx layer on cell membrane shows negative charge, thus capsules outmost layer is prepared with positive charge. However, the culture medium changes the surface charge of microcapsules to negative. Therefore, capsules cannot adhere with HUVECs by electrostatic attraction between ions of opposite charge.

Toxicity of capsules is studied before neuraminidase encapsulation. Capsules are sterilized using autoclaving process. These capsules are incubated with cells for up to 14 days. Comparing SEM images of co-incubation time of 2, 4, 7, 14 days samples, cells viability are not obviously affected by these capsules. Most capsules are dispersed in a circle shape around cell nucleus.

After pretreat HUVECs with neuraminidase, control capsules are observed under the glycocalyx layer. Therefore, HUVECs are able to internalize

capsules without the glycocalyx layer. After neuraminidase encapsulation and capsules fabrication, ~40% of neuraminidase added for $CaCO_3$ co-precipitation is remaining in the entire hollow capsules. The release rate of neuraminidase loaded $(PSS/PAH)_2$ capsules is 12μg/h in first 2 hours. The amount of released enzyme in the 2 hours is sufficient to cleave glycocalyx around capsules. After 2 hours co-incubation, images of CLSM show ~4 neuraminidase loaded capsules are internalized per cell, while no control capsule can be observed in the cell. Images taken from SEM with focused ion beam shows neuraminidase loaded capsules below cell membrane at the cross section of the milled area.

Synthetic $(PSS/PAH)_2$ capsules are not degraded after 7 days internalized by HUVECs. Biodegradable capsules of $(DS/PArg)_2$ are used to study the degradation of HUVECs. After 3 days of $(DS/PArg)_2$ capsules internalized by cells, capsules shape are changed and turned into segments. After 7 days, the internalized capsules became polymer pieces and dispersed widely in cell cytoplasm region. Images from SEM with focused ion beam also show similar result. Neuraminidase loaded DS/PArg capsule are used as a vehicle to deliver DNA plasmids into HUVECs. After 48 hours co-incubation, number of cells with GFP expression is very few. The non-viral transfection method with capsules does not compete with commercial reagents method.

In summary, this work has provided a detailed analysis of deliver polyelectrolyte multilayer capsules into normal healthy human umbilical vein endothelial cells. Glycocalyx of HUVECs is essential barrier for substance absorption. These neuraminidase loaded microcapsules may able to apply to other non-immune and non-phagocytic types of cell. Neuraminidase loaded microcapsules are able to pass the membrane of endothelial cells, and may penetrate the cell layer. As endothelial cells cover the interior of capillary, capsules may diffuse into tissues or organs. Therefore, these multifunctional

microcapsules have huge potentials in drugs encapsulation and delivery system. Although the reason for capsules internalization by cells is not fully understand yet, the results presented in this thesis contribute a step in field of microcapsules with cells investigation.

Reference:

Adalsteinsson, T., W. F. Dong, et al. (2004). "Diffusion of 77 000 g/mol dextran in submicron polyelectrolyte capsule dispersions measured using PFG-NMR." The Journal of Physical Chemistry B **108**(52): 20056-20063.

Ahrens, H., K. Büscher, et al. (2004). Poly (styrene sulfonate) self‐organization: electrostatic and secondary interactions, Wiley Online Library.

An, Z., K. Kavanoor, et al. (2009). "Polyelectrolyte microcapsule interactions with cells in two-and three-dimensional culture." Colloids and Surfaces B: Biointerfaces **70**(1): 114-123.

An, Z., H. Möhwald, et al. (2006). "pH controlled permeability of lipid/protein biomimetic microcapsules." Biomacromolecules **7**(2): 580-585.

Antipov, A. A., D. Shchukin, et al. (2003). "Carbonate microparticles for hollow polyelectrolyte capsules fabrication." Colloids and Surfaces A: Physicochemical and Engineering Aspects **224**(1-3): 175-183.

Antipov, A. A., G. B. Sukhorukov, et al. (2001). "Sustained release properties of polyelectrolyte multilayer capsules." The Journal of Physical Chemistry B **105**(12): 2281-2284.

Antipov, A. A., G. B. Sukhorukov, et al. (2002). "Polyelectrolyte multilayer capsule permeability control." Colloids and Surfaces A: Physicochemical and Engineering Aspects **198**: 535-541.

Ariga, K., Y. Lvov, et al. (1997). "Assembling alternate dye-polyion molecular films by electrostatic layer-by-layer adsorption." Journal of the American Chemical Society **119**(9): 2224-2231.

Artursson, P. (1990). "Epithelial transport of drugs in cell culture. I: A model for studying the passive diffusion of drugs over intestinal absorbtive (Caco‐2) cells." Journal of pharmaceutical sciences **79**(6): 476-482.

Azzam, T. and A. J. Domb (2004). "Current developments in gene transfection agents." Current drug delivery **1**(2): 165-193.

Bédard, M., A. G. Skirtach, et al. (2007). "Optically driven encapsulation using novel polymeric hollow shells containing an azobenzene polymer." Macromolecular rapid communications **28**(15): 1517-1521.

Bai, K. and W. Wang (2012). "Spatio-temporal development of the endothelial

glycocalyx layer and its mechanical property in vitro." Journal of The Royal Society Interface.

Bai, K. and W. Wang (2013). "Shear stress-induced redistribution of the glycocalyx on endothelial cells in vitro." Biomechanics and modeling in mechanobiology: 1-9.

Bakeev, K., V. Izumrudov, et al. (1992). "Kinetics and mechanism of interpolyelectrolyte exchange and addition reactions." Macromolecules **25**(17): 4249-4254.

Barker, A. L., O. Konopatskaya, et al. (2004). "Observation and characterisation of the glycocalyx of viable human endothelial cells using confocal laser scanning microscopy." Physical Chemistry Chemical Physics **6**(5): 1006-1011.

Baur, J. W., S. Kim, et al. (1998). "Thin‐film light‐emitting devices based on sequentially adsorbed multilayers of water‐soluble poly (p‐phenylene) s." Advanced materials **10**(17): 1452-1455.

Bédard, M. F., D. Braun, et al. (2008). "Toward self-assembly of nanoparticles on polymeric microshells: near-IR release and permeability." ACS nano **2**(9): 1807-1816.

Bedard, M. F., B. G. De Geest, et al. (2009). "Direction specific release from giant microgel-templated polyelectrolyte microcontainers." Soft Matter **5**(20): 3927-3931.

Bedard, M. F., A. Munoz-Javier, et al. (2009). "On the mechanical stability of polymeric microcontainers functionalized with nanoparticles." Soft Matter **5**(1): 148-155.

Beltran, S., H. H. Hooper, et al. (1991). "Monte Carlo study of polyelectrolyte adsorption: isolated chains on a planar charged surface." Macromolecules **24**(11): 3178-3184.

Bertrand, P., A. Jonas, et al. (2000). "Ultrathin polymer coatings by complexation of polyelectrolytes at interfaces: suitable materials, structure and properties." Macromolecular rapid communications **21**(7): 319-348.

Biesheuvel, P. M. and M. A. C. Stuart (2004a). "Cylindrical cell model for the electrostatic free energy of polyelectrolyte complexes." Langmuir **20**(11): 4764-4770.

Biesheuvel, P. M. and M. A. C. Stuart (2004b). "Electrostatic free energy of weakly charged macromolecules in solution and intermacromolecular complexes consisting of oppositely charged polymers." Langmuir **20**(7): 2785-2791.

Bolze, J., B. Peng, et al. (2002). "Formation and Growth of Amorphous Colloidal CaCO3 Precursor Particles as Detected by Time-Resolved SAXS." Langmuir **18**(22): 8364-8369.

Borodina, T., E. Markvicheva, et al. (2007). "Controlled Release of DNA from Self‐Degrading Microcapsules." Macromolecular rapid communications **28**(18‐19): 1894-1899.

Burke, S. E. and C. J. Barrett (2004). "Controlling the physicochemical properties of weak polyelectrolyte multilayer films through acid/base equilibria." Pure and applied chemistry **76**(7): 1387-1398.

Cant, N. E., K. Critchley, et al. (2003). "Surface functionalisation for the self-assembly of nanoparticle/polymer multilayer films." Thin solid films **426**(1): 31-39.

Carey, D. J. (1997). "Syndecans: multifunctional cell-surface co-receptors." Biochemical Journal **327**(Pt 1): 1.

Caruso, F., R. A. Caruso, et al. (1998). "Nanoengineering of inorganic and hybrid hollow spheres by colloidal templating." Science **282**(5391): 1111-1114.

Caruso, F., D. N. Furlong, et al. (1998). "Characterization of polyelectrolyte-protein multilayer films by atomic force microscopy, scanning electron microscopy, and Fourier transform infrared reflection-absorption spectroscopy." Langmuir **14**(16): 4559-4565.

Cassidy, J. T., G. W. Jourdian, et al. (1965). "The Sialic Acids: VI. PURIFICATION AND PROPERTIES OF SIALIDASE FROM CLOSTRIDIUM PERFRINGENS." Journal of Biological Chemistry **240**(9): 3501-3506.

Chang, T. (1964). "Semipermeable microcapsules." Science **146**(3643): 524.

Cheong, I. W., J. S. Shin, et al. (2004). "Preparation of monodisperse melamine-formaldehyde microspheres via dispersed polycondensation." Macromolecular Research **12**(2): 225-232.

Chiarelli, P. A., M. S. Johal, et al. (2001). "Controlled Fabrication of Polyelectrolyte Multilayer Thin Films Using Spin‐Assembly." Advanced materials **13**(15): 1167-1171.

Choi, J. and M. F. Rubner (2005). "Influence of the degree of ionization on weak polyelectrolyte multilayer assembly." Macromolecules **38**(1): 116-124.

Colman, P. M. (1994). "Influenza virus neuraminidase: structure, antibodies, and inhibitors." Protein Science **3**(10): 1687-1696.

Connal, L. A., C. R. Kinnane, et al. (2009). "Stabilization and Functionalization of Polymer Multilayers and Capsules via Thiol− Ene Click Chemistry." Chemistry of materials **21**(4): 576-578.

Cordeiro, A. L., M. Coelho, et al. (2004). "Effect of shear stress on adhering polyelectrolyte capsules." Journal of colloid and interface science **280**(1): 68-75.

Cremer, C. and T. Cremer (1974). "Considerations on a laser-scanning-microscope with high resolution and depth of field." Microscopica acta: 31-44.

Cundall, R., J. Lawton, et al. (1979). "Polyelectrolyte complexes, 1. The effect of pH and ionic strength on the stoichiometry of model polycation—polyanion complexes." Die Makromolekulare Chemie **180**(12): 2913-2922.

Déjugnat, C. and G. B. Sukhorukov (2004). "pH-responsive properties of hollow polyelectrolyte microcapsules templated on various cores." Langmuir **20**(17): 7265-7269.

Dalecki, D. (2004). "Mechanical bioeffects of ultrasound." Annu. Rev. Biomed. Eng. **6**: 229-248.

Dautzenberg, H. (1997). "Polyelectrolyte complex formation in highly aggregating systems. 1. Effect of salt: polyelectrolyte complex formation in the presence of NaCl." Macromolecules **30**(25): 7810-7815.

Dautzenberg, H. and G. Rother (2004). "Response of Polyelectrolyte Complexes to Subsequent Addition of Sodium Chloride: Time‐Dependent Static Light Scattering Studies." Macromolecular Chemistry and Physics **205**(1): 114-121.

De Cock, L. J., S. De Koker, et al. (2010). "Polymeric multilayer capsules in drug delivery." Angewandte Chemie International Edition **49**(39): 6954-6973.

De Geest, B., C. Dejugnat, et al. (2006). "Layer-by-layer coating of degradable microgels for pulsed drug delivery." Journal of controlled release **116**(2): 159-169.

De Geest, B. G., M. J. McShane, et al. (2008). "Microcapsules ejecting nanosized

species into the environment." Journal of the American Chemical Society **130**(44): 14480-14482.

De Geest, B. G., N. N. Sanders, et al. (2007). "Release mechanisms for polyelectrolyte capsules." Chem. Soc. Rev. **36**(4): 636-649.

De Geest, B. G., G. B. Sukhorukov, et al. (2009). "The pros and cons of polyelectrolyte capsules in drug delivery."

De Geest, B. G., W. Van Camp, et al. (2008). "Biodegradable microcapsules designed via 'click'chemistry." Chemical Communications(2): 190-192.

De Geest, B. G., W. Van Camp, et al. (2008). "Degradable multilayer films and hollow capsules via a 'click'strategy." Macromolecular rapid communications **29**(12‐13): 1111-1118.

De Geest, B. G., R. E. Vandenbroucke, et al. (2006). "Intracellularly degradable polyelectrolyte microcapsules." Advanced materials **18**(8): 1005-1009.

De Koker, S., B. G. De Geest, et al. (2007). "In vivo cellular uptake, degradation, and biocompatibility of polyelectrolyte microcapsules." Advanced Functional Materials **17**(18): 3754-3763.

De Koker, S., B. G. De Geest, et al. (2009). "Polyelectrolyte Microcapsules as Antigen Delivery Vehicles To Dendritic Cells: Uptake, Processing, and Cross‐Presentation of Encapsulated Antigens." Angewandte Chemie **121**(45): 8637-8641.

De Koker, S., B. N. Lambrecht, et al. (2011). "Designing polymeric particles for antigen delivery." Chemical Society Reviews **40**(1): 320-339.

De Koker, S., T. Naessens, et al. (2010). "Biodegradable polyelectrolyte microcapsules: antigen delivery tools with Th17 skewing activity after pulmonary delivery." The journal of immunology **184**(1): 203-211.

Decher, G. (1997). "Fuzzy nanoassemblies: toward layered polymeric multicomposites." Science **277**(5330): 1232.

Decher, G. and J. Hong (1991b). "Buildup of ultrathin multilayer films by a self‐assembly process: II. Consecutive adsorption of anionic and cationic bipolar amphiphiles and polyelectrolytes on charged surfaces." Berichte der Bunsengesellschaft für physikalische Chemie **95**(11): 1430-1434.

Decher, G., J. Hong, et al. (1992). "Buildup of ultrathin multilayer films by a self-assembly process: III. Consecutively alternating adsorption of anionic

and cationic polyelectrolytes on charged surfaces." Thin solid films **210**: 831-835.

Decher, G. and J. D. Hong (1991a). Buildup of ultrathin multilayer films by a self‐assembly process, 1 consecutive adsorption of anionic and cationic bipolar amphiphiles on charged surfaces, Wiley Online Library.

Decher, G. and J. B. Schlenoff (2003). Multilayer thin films, Wiley Online Library.

Deurs, B., K. Roepstorff, et al. (2003). "Caveolae: anchored, multifunctional platforms in the lipid ocean." Trends in cell biology **13**(2): 92-100.

Donath, E., G. B. Sukhorukov, et al. (1998). "Novel hollow polymer shells by colloid‐templated assembly of polyelectrolytes." Angewandte Chemie International Edition **37**(16): 2201-2205.

Dong, W. F., J. K. Ferri, et al. (2005). "Influence of shell structure on stability, integrity, and mesh size of polyelectrolyte capsules: mechanism and strategy for improved preparation." Chemistry of materials **17**(10): 2603-2611.

Douglas, K. L. (2008). "Toward Development of Artificial Viruses for Gene Therapy: A Comparative Evaluation of Viral and Non‐viral Transfection." Biotechnology progress **24**(4): 871-883.

Dragan, E. S. and S. Schwarz (2004). "Polyelectrolyte complexes. VII. Complex nanoparticles based on poly (sodium 2‐acrylamido‐2‐methylpropanesulfonate) tailored by the titrant addition rate." Journal of Polymer Science Part A: Polymer Chemistry **42**(20): 5244-5252.

Dreja, M., I. T. Kim, et al. (2000). "Multilayered supermolecular structures self-assembled from polyelectrolytes and cyclodextrin host–guest complexes." Journal of Materials Chemistry **10**(3): 603-605.

Dubas, S. T. and J. B. Schlenoff (1999). "Factors controlling the growth of polyelectrolyte multilayers." Macromolecules **32**(24): 8153-8160.

Dubas, S. T. and J. B. Schlenoff (2001). "Polyelectrolyte multilayers containing a weak polyacid: construction and deconstruction." Macromolecules **34**(11): 3736-3740.

Dubas, S. T. and J. B. Schlenoff (2001). "Swelling and smoothing of polyelectrolyte multilayers by salt." Langmuir **17**(25): 7725-7727.

Estrela-Lopis, I., S. Leporatti, et al. (2002). "SANS studies of polyelectrolyte multilayers on colloidal templates." Langmuir **18**(21): 7861-7866.

Everhart, T. and R. Thornley (1960). "Wide-band detector for micro-microampere low-energy electron currents." Journal of scientific instruments **37**(7): 246.

Farhat, T., G. Yassin, et al. (1999). "Water and ion pairing in polyelectrolyte multilayers." Langmuir **15**(20): 6621-6623.

Fernandes, P. A. L., G. Tzvetkov, et al. (2008). "Quantitative analysis of scanning transmission X-ray microscopy images of gas-filled PVA-based microballoons." Langmuir **24**(23): 13677-13682.

Fleer, G. J. (1993). Polymers at interfaces, Springer.

Fransson, L. Å., M. Belting, et al. (2004). "Novel aspects of glypican glycobiology." Cellular and molecular life sciences **61**(9): 1016-1024.

Fuoss, R. M. and G. I. Cathers (1947). "Polyelectrolytes. I. Picrates of 4‐vinylpyridine‐styrene copolymers." Journal of Polymer Science **2**(1): 12-15.

Fuster, M. M. and J. D. Esko (2005). "The sweet and sour of cancer: glycans as novel therapeutic targets." Nature Reviews Cancer **5**(7): 526-542.

Gao, C., E. Donath, et al. (2002). "Spontaneous Deposition of Water‐Soluble Substances into Microcapsules: Phenomenon, Mechanism, and Application." Angewandte Chemie **114**(20): 3943-3947.

Gao, C., S. Leporatti, et al. (2003). "Swelling and shrinking of polyelectrolyte microcapsules in response to changes in temperature and ionic strength." Chemistry-A European Journal **9**(4): 915-920.

Gao, C., S. Moya, et al. (2002). "Melamine formaldehyde core decomposition as the key step controlling capsule integrity: optimizing the polyelectrolyte capsule fabrication." Macromolecular Chemistry and Physics **203**(7): 953-960.

Gao, G., S. Moya, et al. (2001). "The decomposition process of melamine formaldehyde cores: the key step in the fabrication of ultrathin polyelectrolyte multilayer capsules." Macromolecular Materials and Engineering **286**(6): 355-361.

Gao, M., C. Lesser, et al. (2000). "Electroluminescence of different colors from polycation/CdTe nanocrystal self-assembled films." Journal of Applied Physics **87**: 2297.

Geary, R. L., N. Koyama, et al. (1995). "Failure of heparin to inhibit intimal hyperplasia in injured baboon arteries: the role of heparin-sensitive and-insensitive pathways in the stimulation of smooth muscle cell migration

and proliferation." Circulation **91**(12): 2972-2981.

Gedanken, A. (2008). "Preparation and properties of proteinaceous microspheres made sonochemically." Chemistry-A European Journal **14**(13): 3840-3853.

Georgieva, R., R. Dimova, et al. (2005). "Influence of different salts on micro-sized polyelectrolyte hollow capsules." J. Mater. Chem. **15**(40): 4301-4310.

Georgieva, R., S. Moya, et al. (2000). "Conductance and capacitance of polyelectrolyte and lipid-polyelectrolyte composite capsules as measured by electrorotation." Langmuir **16**(17): 7075-7081.

Glinel, K., A. Moussa, et al. (2002). "Influence of polyelectrolyte charge density on the formation of multilayers of strong polyelectrolytes at low ionic strength." Langmuir **18**(4): 1408-1412.

Gopinadhan, M., H. Ahrens, et al. (2005). "Approaching the precipitation temperature of the deposition solution and the effects on the internal order of polyelectrolyte multilayers." Macromolecules **38**(12): 5228-5235.

Gorin, D. A., S. A. Portnov, et al. (2008). "Magnetic/gold nanoparticle functionalized biocompatible microcapsules with sensitivity to laser irradiation." Physical Chemistry Chemical Physics **10**(45): 6899-6905.

Gouda, E., M. Aly, et al. (2011). "Molecular Study On Avian Viral Influenza (h5n1) Neuraminidase Gene In Egypt."

Guldi, D. M., C. Luo, et al. (2002). "Photoactive nanowires in fullerene-ferrocene dyad polyelectrolyte multilayers." Nano Letters **2**(7): 775-780.

H. Dautzenberg, W. J., J. Kötz, B. Philipp, C. Seidel, D. Stscherbina (Eds.), Ed. (1994). Polyelectrolytes: Formation, Characterization and Application. Munich, Hanser Publishers.

Hermanson, G. T. (1996). Bioconjugate techniques, Academic press.

Hiller, J. A., J. D. Mendelsohn, et al. (2002). "Reversibly erasable nanoporous anti-reflection coatings from polyelectrolyte multilayers." Nature Materials **1**(1): 59-63.

Hiller, J. A. and M. F. Rubner (2003). "Reversible molecular memory and pH-switchable swelling transitions in polyelectrolyte multilayers." Macromolecules **36**(11): 4078-4083.

Hunt, M. A., M. J. Currie, et al. (2010). "Optimizing transfection of primary human

umbilical vein endothelial cells using commercially available chemical transfection reagents." Journal of biomolecular techniques: JBT **21**(2): 66.

Hunter, R. J. (1981). Zeta potential in colloid science. New York, Academic Press.

Ihrcke, N. S., L. E. Wrenshall, et al. (1993). "Role of heparan sulfate in immune system-blood vessel interactions." Immunology today **14**(10): 500-505.

Iler, R. (1966). "Multilayers of colloidal particles." Journal of colloid and interface science **21**(6): 569-594.

Instruments, M. (2004). "Zetasizer nano series user manual." MAN0317.

Itoh, Y., M. Matsusaki, et al. (2004). "Preparation of biodegradable hollow nanocapsules by silica template method." Chemistry Letters **33**(12): 1552-1553.

Izquierdo, A., S. Ono, et al. (2005). "Dipping versus spraying: Exploring the deposition conditions for speeding up layer-by-layer assembly." Langmuir **21**(16): 7558-7567.

Jaber, J. A. and J. B. Schlenoff (2005). "Polyelectrolyte multilayers with reversible thermal responsivity." Macromolecules **38**(4): 1300-1306.

Jackson, R. L., S. J. Busch, et al. (1991). "Glycosaminoglycans: molecular properties, protein interactions, and role in physiological processes." Physiological Reviews **71**(2): 481-539.

Jin, W., A. Toutianoush, et al. (2005). "Size-and charge-selective transport of aromatic compounds across polyelectrolyte multilayer membranes." Applied surface science **246**(4): 444-450.

Jung, B. D., J. D. Hong, et al. (2002). "Photochromic hollow shells: photoisomerization of azobenzene polyionene in solution, in multilayer assemblies on planar and spherical surfaces." Colloids and Surfaces A: Physicochemical and Engineering Aspects **198**: 483-489.

Kügler, R., J. Schmitt, et al. (2002). "The swelling behavior of polyelectrolyte multilayers in air of different relative humidity and in water." Macromolecular Chemistry and Physics **203**(2): 413-419.

Köhler, K. (2006). Temperature-Induced Rearrangements of Polyelectrolyte Multilayer Capsules: Mechanisms and Applications. Max-Planck-Institut. Germany.

Köhler, K. and G. B. Sukhorukov (2007). "Heat treatment of polyelectrolyte multilayer capsules: a versatile method for encapsulation." Advanced Functional Materials **17**(13): 2053-2061.

Kabanov, V. (2003). "Fundamentals of polyelectrolyte complexes in solution and the bulk." Multilayer Thin Films: 47-86.

Kabanov, V. and A. Zezin (1984). "Soluble interpolymeric complexes as a new class of synthetic polyelectrolytes." Pure and applied chemistry **56**(3): 343-354.

Katchalsky, A. and P. Spitnik (1947). "Potentiometric titrations of polymethacrylic acid." Journal of Polymer Science **2**(4): 432-446.

Kern, W. (1970). "Cleaning solutions based on hydrogen peroxide for use in silicon semiconductor technology." RCA review **31**: 187-206.

Kim, B. Y. and M. L. Bruening (2003). "pH-dependent growth and morphology of multilayer dendrimer/poly (acrylic acid) films." Langmuir **19**(1): 94-99.

Kirchner, C., A. M. Javier, et al. (2005). "Cytotoxicity of nanoparticle-loaded polymer capsules." Talanta **67**(3): 486-491.

Kiriy, A., J. Yu, et al. (2006). "Interpolyelectrolyte complexes: a single-molecule insight." Langmuir **22**(4): 1800-1803.

Klitzing, R. and H. Moehwald (1995). "Proton concentration profile in ultrathin polyelectrolyte films." Langmuir **11**(9): 3554-3559.

Klitzing, R. V. and H. Möhwald (1996). "Transport through ultrathin polyelectrolyte films." Thin solid films **284**: 352-356.

Kotov, N. A. (1999). "Layer-by-layer self-assembly: The contribution of hydrophobic interactions." Nanostructured Materials **12**(5-8): 789-796.

Krasemann, L. and B. Tieke (1999). "Composite membranes with ultrathin separation layer prepared by self-assembly of polyelectrolytes." Materials Science and Engineering: C **8**: 513-518.

Krasemann, L. and B. Tieke (2000). "Highly Efficient Composite Membranes for Ethanol‐Water Pervaporation." Chemical engineering & technology **23**(3): 211-213.

Krasemann, L. and B. Tieke (2000). "Selective ion transport across self-assembled alternating multilayers of cationic and anionic polyelectrolytes." Langmuir **16**(2): 287-290.

Kreft, O., A. M. Javier, et al. (2007). "Polymer microcapsules as mobile local pH-sensors." J. Mater. Chem. **17**(42): 4471-4476.

Kreft, O., A. G. Skirtach, et al. (2007). "Remote control of bioreactions in multicompartment capsules." Advanced materials **19**(20): 3142-3145.

Kurth, D. G., M. Schütte, et al. (2002). "Metallo-supramolecular polyelectrolyte multilayers with cobalt (II): preparation and properties." Colloids and Surfaces A: Physicochemical and Engineering Aspects **198**: 633-643.

Lösche, M., J. Schmitt, et al. (1998). "Detailed structure of molecularly thin polyelectrolyte multilayer films on solid substrates as revealed by neutron reflectometry." Macromolecules **31**(25): 8893-8906.

Ladam, G., P. Schaad, et al. (2000). "In situ determination of the structural properties of initially deposited polyelectrolyte multilayers." Langmuir **16**(3): 1249-1255.

Lakowicz, J. R. (2006). Principles of Fluorescence Spectroscopy, Springer.

Langer, R. and D. A. Tirrell (2004). "Designing materials for biology and medicine." Nature **428**(6982): 487-492.

Laschewsky, A., E. Wischerhoff, et al. (1997). "Polyelectrolyte multilayer assemblies containing nonlinear optical dyes." Macromolecules **30**(26): 8304-8309.

Lavalle, P., C. Picart, et al. (2004). "Modeling the Buildup of Polyelectrolyte Multilayer Films Having Exponential Growth x." The Journal of Physical Chemistry B **108**(2): 635-648.

Lenahan, K. M., Y. X. Wang, et al. (1998). "Novel Polymer Dyes for Nonlinear Optical Applications Using Ionic Self‐Assembled Monolayer Technology." Advanced materials **10**(11): 853-855.

Li, C., K. Mitamura, et al. (2003). "Electrostatic layer-by-layer assembly of poly (amido amine) dendrimer/conducting sulfonated polyaniline: structure and properties of multilayer films." Macromolecules **36**(26): 9957-9965.

Li, J., L. F. Brown, et al. (1997). "Macrophage-dependent regulation of syndecan gene expression." Circulation research **81**(5): 785-796.

Lipowsky, H. H. (2005). "Microvascular rheology and hemodynamics." Microcirculation **12**(1): 5-15.

Liu, X., C. Gao, et al. (2005). "Multilayer Microcapsules as Anti‐Cancer Drug Delivery Vehicle: Deposition, Sustained Release, and in vitro Bioactivity."

Macromolecular bioscience **5**(12): 1209-1219.

Lu, C., H. Möhwald, et al. (2007). "Plasmon resonance tunable by deaggregation of gold nanoparticles in multilayers." The Journal of Physical Chemistry C **111**(27): 10082-10087.

Luft, J. (1966). "Fine structure of capillary and endocapillary layer as revealed by ruthenium red." Microcirc Symp Fed Proc **25**: 1773–1783.

Lulevich, V. V., I. L. Radtchenko, et al. (2003). "Mechanical properties of polyelectrolyte microcapsules filled with a neutral polymer." Macromolecules **36**(8): 2832-2837.

Lvov, Y., K. Ariga, et al. (1995). "Assembly of multicomponent protein films by means of electrostatic layer-by-layer adsorption." Journal of the American Chemical Society **117**(22): 6117-6123.

Lvov, Y., K. Ariga, et al. (1994). "Layer-by-layer assembly of alternate protein/polyion ultrathin films." Chemistry Letters **23**(12): 2323-2326.

Lvov, Y., G. Decher, et al. (1993). "Assembly, structural characterization, and thermal behavior of layer-by-layer deposited ultrathin films of poly (vinyl sulfate) and poly (allylamine)." Langmuir **9**(2): 481-486.

Lvov, Y., G. Decher, et al. (1993). "Assembly of thin films by means of successive deposition of alternate layers of DNA and poly (allylamine)." Macromolecules **26**(20): 5396-5399.

Müller, M., S. Heinen, et al. (2001). Stimulation and binding properties of polyelectrolyte multilayers verified by ATR‐FTIR spectroscopy, Wiley Online Library.

Mamedov, A. A., N. A. Kotov, et al. (2002). "Molecular design of strong single-wall carbon nanotube/polyelectrolyte multilayer composites." Nature Materials **1**(3): 190-194.

Manning, G. S. (1978). "The molecular theory of polyelectrolyte solutions with applications to the electrostatic properties of polynucleotides." Q. Rev. Biophys **11**(2): 179-246.

Marieb, E. N. and K. Hoehn (2007). Human anatomy and physiology, Pearson Education.

Massart, R. (1981). "Preparation of aqueous magnetic liquids in alkaline and acidic media." Magnetics, IEEE Transactions on **17**(2): 1247-1248.

McAloney, R. A., V. Dudnik, et al. (2003). "Kinetics of salt-induced annealing of a polyelectrolyte multilayer film morphology." Langmuir **19**(9): 3947-3952.

McAloney, R. A., M. Sinyor, et al. (2001). "Atomic force microscopy studies of salt effects on polyelectrolyte multilayer film morphology." Langmuir **17**(21): 6655-6663.

Mendelsohn, J., C. Barrett, et al. (2000). "Fabrication of microporous thin films from polyelectrolyte multilayers." Langmuir **16**(11): 5017-5023.

Michaels, A. S. (1965). "Polyelectrolyte complexes." Industrial & Engineering Chemistry **57**(10): 32-40.

Michaels, A. S. and R. G. Miekka (1961). "Polycation-polyanion complexes: Preparation and properties of poly-(vinylbenzyltrimethylammonium) poly-(styrenesulfonate)." The Journal of Physical Chemistry **65**(10): 1765-1773.

Middleton, J., S. Neil, et al. (1997). "Transcytosis and surface presentation of IL-8 by venular endothelial cells." Cell **91**(3): 385-395.

Minsky, M. (1961). Microscopy apparatus, Google Patents.

Moya, S., L. Dähne, et al. (2001). "Polyelectrolyte multilayer capsules templated on biological cells: core oxidation influences layer chemistry." Colloids and Surfaces A: Physicochemical and Engineering Aspects **183**: 27-40.

Moya, S., E. Donath, et al. (2000). "Lipid coating on polyelectrolyte surface modified colloidal particles and polyelectrolyte capsules." Macromolecules **33**(12): 4538-4544.

Muñoz Javier, A., O. Kreft, et al. (2008). "Uptake of Colloidal Polyelectrolyte‐Coated Particles and Polyelectrolyte Multilayer Capsules by Living Cells." Advanced materials **20**(22): 4281-4287.

Murdoch, A. D., G. Dodge, et al. (1992). "Primary structure of the human heparan sulfate proteoglycan from basement membrane (HSPG2/perlecan). A chimeric molecule with multiple domains homologous to the low density lipoprotein receptor, laminin, neural cell adhesion molecules, and epidermal growth factor." Journal of Biological Chemistry **267**(12): 8544.

N. S. Claxton, T. J. F., M. W. Davidson (2006). Laser Scanning Confocal Microscopy.

Neu, B., A. Voigt, et al. (2001). "Biological cells as templates for hollow microcapsules." Journal of microencapsulation **18**(3): 385-395.

Neuman, K. C. and S. M. Block (2004). "Optical trapping." Review of scientific instruments **75**(9): 2787-2809.

Olivier, B. and C. Sorensen (1990). "Evolution of the cluster size distribution during slow colloid aggregation." Journal of colloid and interface science **134**(1): 139-146.

Olson BJ, M. J. (2007). Current Protocols in Protein Science, John Wiley & Sons, Inc**:** 3.4.1 - 3.4.29.

Onda, M., Y. Lvov, et al. (1996). "Sequential actions of glucose oxidase and peroxidase in molecular films assembled by layer‐by‐layer alternate adsorption." Biotechnology and bioengineering **51**(2): 163-167.

Otakar Söhnel, J. G. (1992). Precipitation: basic principles and industrial applications. Oxford, Butterworth-Heinemann.

P. Lavalle, V. V., N. Jessel, G. Decher, J.-C. Voegel, P. J. Mesini, P. Schaaf (2004). "Direct Evidence for Vertical Diffusion and Exchange Processes of Polyanions and Polycations in Polyelectrolyte Multilayer Films." Macromolecules **37**: 1159.

Pankhurst, Q. A., J. Connolly, et al. (2003). "Applications of magnetic nanoparticles in biomedicine." Journal of physics D: Applied physics **36**(13): R167.

Pavlov, A. M., V. Saez, et al. (2011). "Controlled protein release from microcapsules with composite shells using high frequency ultrasound—potential for in vivo medical use." Soft Matter **7**(9): 4341-4347.

Pavlov, A. M., A. V. Sapelkin, et al. (2011). "Neuron cells uptake of polymeric microcapsules and subsequent intracellular release." Macromolecular bioscience **11**(6): 848-854.

Petrov, A. I., D. V. Volodkin, et al. (2005). "Protein—Calcium Carbonate Coprecipitation: A Tool for Protein Encapsulation." Biotechnology progress **21**(3): 918-925.

Peyratout, C. S. and L. Dähne (2004). "Tailor‐Made Polyelectrolyte Microcapsules: From Multilayers to Smart Containers." Angewandte Chemie International Edition **43**(29): 3762-3783.

Philipp, B., H. Dautzenberg, K. J. Linow, J. Koetz and W. Dawydoff (1989). "Polyelectrolyte complexes - recent developments and open problems." Prog. Polym. Sci. **14**(1): 91-172.

Picart, C., P. Lavalle, et al. (2001). "Buildup mechanism for poly (L-lysine)/hyaluronic acid films onto a solid surface." Langmuir **17**(23): 7414-7424.

Pontes, R., M. Raposo, et al. (1999). "Non‐Equilibrium Adsorbed Polymer Layers via Hydrogen Bonding." physica status solidi (a) **173**(1): 41-50.

Poptoshev, E., B. Schoeler, et al. (2004). "Influence of solvent quality on the growth of polyelectrolyte multilayers." Langmuir **20**(3): 829-834.

Porcel, C., P. Lavalle, et al. (2006). "From exponential to linear growth in polyelectrolyte multilayers." Langmuir **22**(9): 4376-4383.

Presta, M., M. Statuto, et al. (1992). "Structure-function relationship of basic fibroblast growth factor: site-directed mutagenesis of a putative heparin-binding and receptor-binding region." Biochemical and biophysical research communications **185**(3): 1098-1107.

Pries, A., T. Secomb, et al. (2000). "The endothelial surface layer." Pflügers Archiv European Journal of Physiology **440**(5): 653-666.

Prouty, M., Z. Lu, et al. (2007). "Layer-by-Layer Engineered Nanoparticles for Sustained Release of Phor21-CG (ala) Anticancer Peptide." Journal of Biomedical Nanotechnology **3**(2): 184-189.

R. v. Klitzing, R. S. (2002). Handbook of Polyelectrolytes and Their Application. Los Angeles, American Scientific Publishers.

Raines, E. W. and R. Ross (1992). "Compartmentalization of PDGF on extracellular binding sites dependent on exon-6-encoded sequences." The Journal of cell biology **116**(2): 533-543.

Rapraeger, A., M. Jalkanen, et al. (1985). "The cell surface proteoglycan from mouse mammary epithelial cells bears chondroitin sulfate and heparan sulfate glycosaminoglycans." Journal of Biological Chemistry **260**(20): 11046-11052.

Regine v. Klitzing*, a. and H. Möhwald (1996). "A realistic diffusion model for ultrathin polyelectrolyte films." Macromolecules **29**(21): 6901-6906.

Reitsma, S., D. W. Slaaf, et al. (2007). "The endothelial glycocalyx: composition, functions, and visualization." Pflügers Archiv European Journal of Physiology **454**(3): 345-359.

Reyntjens, S. and R. Puers (2001). "A review of focused ion beam applications in microsystem technology." Journal of Micromechanics and Microengineering

11: 287.

Risau, W. (1995). "Differentiation of endothelium." The FASEB journal **9**(10): 926-933.

Rivera-Gil, P., S. De Koker, et al. (2009). "Intracellular processing of proteins mediated by biodegradable polyelectrolyte capsules." Nano Letters **9**(12): 4398-4402.

Rosenberg, R., N. Shworak, et al. (1997). "Heparan sulfate proteoglycans of the cardiovascular system. Specific structures emerge but how is synthesis regulated?" Journal of Clinical Investigation **99**(9): 2062.

Rouse, J. H. and P. T. Lillehei (2003). "Electrostatic assembly of polymer/single walled carbon nanotube multilayer films." Nano Letters **3**(1): 59-62.

Russel, W. B., W. Russel, et al. (1992). Colloidal dispersions, Cambridge Univ Pr.

Ruths, J., F. Essler, et al. (2000). "Polyelectrolytes I: polyanion/polycation multilayers at the air/monolayer/water interface as elements for quantitative polymer adsorption studies and preparation of hetero-superlattices on solid surfaces." Langmuir **16**(23): 8871-8878.

Salomäki, M., P. Tervasmäki, et al. (2004). "The Hofmeister anion effect and the growth of polyelectrolyte multilayers." Langmuir **20**(9): 3679-3683.

Salomäki, M., I. A. Vinokurov, et al. (2005). "Effect of temperature on the buildup of polyelectrolyte multilayers." Langmuir **21**(24): 11232-11240.

Saremi, F., E. Maassen, et al. (1995). "Self-assembled alternating multilayers built-up from diacetylene bolaamphiphiles and poly (allylamine hydrochloride): polymerization properties, structure, and morphology." Langmuir **11**(4): 1068-1071.

Saremi, F., B. Tieke, et al. (1997). "Organized multilayers of polydiacetylenes prepared by electrostatic self-assembly." Supramolecular Science **4**(3-4): 471-477.

Satcher, R., C. F. Dewey Jr, et al. (1997). "Mechanical remodeling of the endothelial surface and actin cytoskeleton induced by fluid flow." Microcirculation **4**(4): 439-453.

Schlenoff, J. B. and S. T. Dubas (2001). "Mechanism of polyelectrolyte multilayer growth: charge overcompensation and distribution." Macromolecules **34**(3): 592-598.

Schlenoff, J. B., S. T. Dubas, et al. (2000). "Sprayed polyelectrolyte multilayers." Langmuir **16**(26): 9968-9969.

Schlenoff, J. B., H. Ly, et al. (1998). "Charge and mass balance in polyelectrolyte multilayers." Journal of the American Chemical Society **120**(30): 7626-7634.

Schneider, G. and G. Decher (2004). "From functional core/shell nanoparticles prepared via layer-by-layer deposition to empty nanospheres." Nano Letters **4**(10): 1833-1839.

Schoeler, B., G. Kumaraswamy, et al. (2002). "Investigation of the influence of polyelectrolyte charge density on the growth of multilayer thin films prepared by the layer-by-layer technique." Macromolecules **35**(3): 889-897.

Schoeler, B., E. Poptoshev, et al. (2003). "Growth of multilayer films of fixed and variable charge density polyelectrolytes: Effect of mutual charge and secondary interactions." Macromolecules **36**(14): 5258-5264.

Segarini PR, R. D., Seyedin SM (1989). "Binding of transforming growth factor-beta to cell surface proteins varies with cell type." Mol Endocrinol **Feb;3(2)**: 261.

Seog, J., D. Dean, et al. (2005). "Nanomechanics of opposing glycosaminoglycan macromolecules." Journal of biomechanics **38**(9): 1789-1797.

Shchukin, D. G., K. Köhler, et al. (2005). "Gas‐Filled Polyelectrolyte Capsules." Angewandte Chemie International Edition **44**(21): 3310-3314.

She, Z., M. N. Antipina, et al. (2010). "Mechanism of protein release from polyelectrolyte multilayer microcapsules." Biomacromolecules **11**(5): 1241-1247.

She, Z., C. Wang, et al. (2012). "Encapsulation of Basic Fibroblast Growth Factor by Polyelectrolyte Multilayer Microcapsules and Its Controlled Release for Enhancing Cell Proliferation." Biomacromolecules **13**(7): 2174-2180.

Shenoy, D. B., A. A. Antipov, et al. (2003). "Layer-by-layer engineering of biocompatible, decomposable core-shell structures." Biomacromolecules **4**(2): 265-272.

Shenoy, D. B. and G. B. Sukhorukov (2005). "Microgel‐Based Engineered Nanostructures and Their Applicability with Template‐Directed Layer‐by‐Layer Polyelectrolyte Assembly in Protein Encapsulation." Macromolecular bioscience **5**(5): 451-458.

Shiratori, S. S. and M. F. Rubner (2000). "pH-dependent thickness behavior of

sequentially adsorbed layers of weak polyelectrolytes." Macromolecules **33**(11): 4213-4219.

Skirtach, A. G., C. Dejugnat, et al. (2005). "The role of metal nanoparticles in remote release of encapsulated materials." Nano Letters **5**(7): 1371-1377.

Skirtach, A. G., P. Karageorgiev, et al. (2008). "Reversibly permeable nanomembranes of polymeric microcapsules." Journal of the American Chemical Society **130**(35): 11572-11573.

Smith, P., R. I. Krohn, et al. (1985). "Measurement of protein using bicinchoninic acid." Analytical biochemistry **150**(1): 76.

Squire, J. M., M. Chew, et al. (2001). "Quasi-periodic substructure in the microvessel endothelial glycocalyx: a possible explanation for molecular filtering?" Journal of structural biology **136**(3): 239-255.

Steitz, R., W. Jaeger, et al. (2001). "Influence of charge density and ionic strength on the multilayer formation of strong polyelectrolytes." Langmuir **17**(15): 4471-4474.

Steitz, R., V. Leiner, et al. (2000). "Influence of the ionic strength on the structure of polyelectrolyte films at the solid/liquid interface." Colloids and Surfaces A: Physicochemical and Engineering Aspects **163**(1): 63-70.

Steitz, R., V. Leiner, et al. (2002). "Temperature-induced changes in polyelectrolyte films at the solid-liquid interface." Applied Physics A: Materials Science & Processing **74**: 519-521.

Stockton, W. and M. Rubner (1997). "Molecular-level processing of conjugated polymers. 4. Layer-by-layer manipulation of polyaniline via hydrogen-bonding interactions." Macromolecules **30**(9): 2717-2725.

Sui, Z., D. Salloum, et al. (2003). "Effect of molecular weight on the construction of polyelectrolyte multilayers: Stripping versus sticking." Langmuir **19**(6): 2491-2495.

Sukhishvili, S. A., E. Kharlampieva, et al. (2006). "Where polyelectrolyte multilayers and polyelectrolyte complexes meet." Macromolecules **39**(26): 8873-8881.

Sukhorukov, G., H. Möhwald, et al. (1996). "Assembly of polyelectrolyte multilayer films by consecutively alternating adsorption of polynucleotides and polycations." Thin solid films **284**: 220-223.

Sukhorukov, G. B., M. Brumen, et al. (1999). "Hollow polyelectrolyte shells:

exclusion of polymers and donnan equilibrium." The Journal of Physical Chemistry B **103**(31): 6434-6440.

Sukhorukov, G. B., E. Donath, et al. (1998). "Stepwise polyelectrolyte assembly on particle surfaces: a novel approach to colloid design." Polymers for Advanced Technologies **9**(10‐11): 759-767.

Sukhorukov, G. B., E. Donath, et al. (1998). "Layer-by-layer self assembly of polyelectrolytes on colloidal particles." Colloids and Surfaces A: Physicochemical and Engineering Aspects **137**(1-3): 253-266.

Sukhorukov, G. B., A. L. Rogach, et al. (2007). "Multifunctionalized polymer microcapsules: novel tools for biological and pharmacological applications." Small **3**(6): 944-955.

Sukhorukov, G. B., A. L. Rogach, et al. (2005). "Nanoengineered Polymer Capsules: Tools for Detection, Controlled Delivery, and Site‐Specific Manipulation." Small **1**(2): 194-200.

Sukhorukov, G. B., J. Schmitt, et al. (1996). "Reversible swelling of polyanion/polycation multilayer films in solutions of different ionic strength." Berichte der Bunsengesellschaft für physikalische Chemie **100**(6): 948-953.

Sukhorukov, G. B., D. G. Shchukin, et al. (2004). "Comparative analysis of hollow and filled polyelectrolyte microcapsules templated on melamine formaldehyde and carbonate cores." Macromolecular Chemistry and Physics **205**(4): 530-535.

Sukhorukov, G. B., D. V. Volodkin, et al. (2004). "Porous calcium carbonate microparticles as templates for encapsulation of bioactive compounds." J. Mater. Chem. **14**(14): 2073-2081.

Tan, H. L., J. Meredith, et al. (2003). "Temperature dependence of polyelectrolyte multilayer assembly." Langmuir **19**(22): 9311-9314.

Tarbell, J. M. and M. Pahakis (2006). "Mechanotransduction and the glycocalyx." Journal of internal medicine **259**(4): 339-350.

Telford, A. M., B. T. Pham, et al. (2013). "Micron‐sized polystyrene particles by surfactant‐free emulsion polymerization in air: Synthesis and mechanism." Journal of Polymer Science Part A: Polymer Chemistry **51**(19): 3997-4002.

Thünemann, A. F., M. Müller, et al. (2004). "Polyelectrolyte complexes." Polyelectrolytes with Defined Molecular Architecture II: 19-33.

Tiourina, O., I. Radtchenko, et al. (2002). "Artificial cell based on lipid hollow polyelectrolyte microcapsules: Channel reconstruction and membrane potential measurement." Journal of Membrane Biology **190**(1): 9-16.

Tong, W., W. Dong, et al. (2005). "Charge-controlled permeability of polyelectrolyte microcapsules." The Journal of Physical Chemistry B **109**(27): 13159-13165.

Tong, W., C. Gao, et al. (2005). "Manipulating the properties of polyelectrolyte microcapsules by glutaraldehyde cross-linking." Chemistry of materials **17**(18): 4610-4616.

Tsuchida, E. a. K. A. (1982). "Interactions between macromolecules in solution and intermacromolecular complexes." Advances in Polymer Science **45**: 1-130.

TUMA, P. L. and A. L. HUBBARD (2003). "Transcytosis: Crossing Cellular Barriers." Physiological Reviews **83**(3): 871-932.

v. Klitzing, R. and B. Tieke (2004). "Polyelectrolyte membranes." Polyelectrolytes with Defined Molecular Architecture I: 177-210.

van Beijnum, J. R., E. van der Linden, et al. (2008). "Angiogenic profiling and comparison of immortalized endothelial cells for functional genomics." Experimental cell research **314**(2): 264-272.

van den Berg, B. M., H. Vink, et al. (2003). "The Endothelial Glycocalyx Protects Against Myocardial Edema." Circulation research **92**(6): 592-594.

van Haaren, P. M. A., E. VanBavel, et al. (2005). "Charge modification of the endothelial surface layer modulates the permeability barrier of isolated rat mesenteric small arteries." American Journal of Physiology-Heart and Circulatory Physiology **289**(6): H2503-H2507.

Vanerek, A. and T. Van De Ven (2006). "Coacervate complex formation between cationic polyacrylamide and anionic sulfonated kraft lignin." Colloids and Surfaces A: Physicochemical and Engineering Aspects **273**(1): 55-62.

Varcoe, J. S. (2001). Clinical biochemistry, techniques and instrumentation : a practical course. Singapore, World Scientific Publishing Co. Pte. Ltd.

Varghese, J. N., J. L. McKimm‐Breschkin, et al. (1992). "The structure of the complex between influenza virus neuraminidase and sialic acid, the viral receptor." Proteins: Structure, Function, and Bioinformatics **14**(3): 327-332.

Varki, A., R. D. Cummings, et al. (2009). "I-type lectins."

Vergaro, V., F. Scarlino, et al. (2011). "Drug-loaded polyelectrolyte microcapsules for sustained targeting of cancer cells." Advanced drug delivery reviews.

Villemejane, J. and L. M. Mir (2009). "Physical methods of nucleic acid transfer: general concepts and applications." British journal of pharmacology **157**(2): 207-219.

Voigt, A., H. Lichtenfeld, et al. (1999). "Membrane filtration for microencapsulation and microcapsules fabrication by layer-by-layer polyelectrolyte adsorption." Industrial & engineering chemistry research **38**(10): 4037-4043.

Volodkin, D. V., N. I. Larionova, et al. (2004). "Protein encapsulation via porous CaCO3 microparticles templating." Biomacromolecules **5**(5): 1962-1972.

Volodkin, D. V., A. I. Petrov, et al. (2004). "Matrix polyelectrolyte microcapsules: new system for macromolecule encapsulation." Langmuir **20**(8): 3398-3406.

Wang, L., Z. Wang, et al. (1997). "A new approach for the fabrication of an alternating multilayer film of poly (4 - vinylpyridine) and poly (acrylic acid) based on hydrogen bonding." Macromolecular rapid communications **18**(6): 509-514.

Wang, Y., V. Bansal, et al. (2008). "Templated synthesis of single-component polymer capsules and their application in drug delivery." Nano Letters **8**(6): 1741-1745.

Webb, R. H. (1996). "Confocal optical microscopy." Reports on Progress in Physics **59**: 427.

Weinbaum, S., X. Zhang, et al. (2003). "Mechanotransduction and flow across the endothelial glycocalyx." Proceedings of the National Academy of Sciences **100**(13): 7988.

Werner, C., U. König, et al. (1999). "Electrokinetic surface characterization of biomedical polymers—a survey." Colloids and Surfaces A: Physicochemical and Engineering Aspects **159**(2): 519-529.

William, K. J. and W. J. Krause (2005). Krause's essential human histology for medical students, Universal-Publishers. com.

Wong, J. E., F. Rehfeldt, et al. (2004). "Swelling behavior of polyelectrolyte multilayers in saturated water vapor." Macromolecules **37**(19): 7285-7289.

Yoneda, A. and J. R. Couchman (2003). "Regulation of cytoskeletal organization by syndecan transmembrane proteoglycans." Matrix biology **22**(1): 25-33.

Yoo, D., S. S. Shiratori, et al. (1998). "Controlling bilayer composition and surface wettability of sequentially adsorbed multilayers of weak polyelectrolytes." Macromolecules **31**(13): 4309-4318.

Zebli, B., A. S. Susha, et al. (2005). "Magnetic targeting and cellular uptake of polymer microcapsules simultaneously functionalized with magnetic and luminescent nanocrystals." Langmuir **21**(10): 4262-4265.

Zhai, L., A. J. Nolte, et al. (2004). "pH-gated porosity transitions of polyelectrolyte multilayers in confined geometries and their application as tunable Bragg reflectors." Macromolecules **37**(16): 6113-6123.

Zhang, S., Y. Zhou, et al. (2013). "Fabrication of uniform "smart" magnetic microcapsules and their controlled release of sodium salicylate." Journal of Materials Chemistry B **1**(34): 4331-4337.